Master's thesis

NTNU
Norwegian University of Science and Technology
Faculty of Natural Sciences
Department of Biotechnology and Food Science

Fredrikke Kjærnsmo

Explorations of *in vitro* models for new understanding of the host-material response

Master's thesis in Chemical Engineering and Biotechnology
Supervisor: Anne Mari Rokstad
July 2020

NTNU
Norwegian University of
Science and Technology

Fredrikke Kjærnsmo

Explorations of *in vitro* models for new understanding of the host-material response

Master's thesis in Chemical Engineering and Biotechnology
Supervisor: Anne Mari Rokstad
July 2020

Norwegian University of Science and Technology
Faculty of Natural Sciences
Department of Biotechnology and Food Science

NTNU
Norwegian University of
Science and Technology

Preface

This master thesis is a part of the master degree program Chemical Engineering and Biotechnology with a specialization within biotechnology at the Norwegian University of Science and Technology, NTNU. The laboratory work was conducted at the Department of Clinical and Molecular Medicine during the spring semester 2020. The thesis is partly a continuation of previous work from my specialization project from autumn 2019.

This year has been different, and Covid-19 has been responsible. It has been challenging to cover the initial aims of the study, but with some adjustments the project was possible to finalize, even though we did not get time to do everything we wanted.

I would like to thank my supervisor, Researcher Anne Mari Rokstad, for introducing me to the field of biomaterials and immunology. Thank you for letting me take a part in your research. You have been very supportive through the semester both during the laboratory work and the writing process, and have always been available for discussions and questions. Thank you, senior engineer Liv Ryan, for training and guidance in the lab. Thank you for being supportive and helpful during the laboratory work and your help by conducting experiments. I would also like to thank Berit L. Strand for being my supervisor at the Department of Biotechnology.

Fredrikke Kjærnsmo Trondheim, July 1, 2020

Abstract

Cell encapsulation technology employs biomaterials for transplantation of cells and shows promise as a therapeutic option for the treatment of diabetes type 1. The field has come far in the development of microspheres for transplantation, but the development of low-inflammatory biomaterials has shown to be demanding, and the search for a fibrosis free microsphere is still ongoing. Additionally, knowledge about the biomaterials' ability to avoid or develop fibrosis is missing and needs to be further explored. In the search for a better bio(in)compatibility understanding and a predictive *in vitro* model for evaluation of biomaterials, alginate microspheres, different types of soluble alginate, and cholesterol crystals (CC) were investigated in two distinct procedures to illuminate alternative explanations that cause fibrosis.

The human whole blood (WB) model has shown its value in the prediction of microspheres' inflammatory potential. Based on the knowledge obtained from the WB model, a new long-term *in vitro* experimental (L-IVE) model in 2D and 3D was developed as an attempt for better prediction of long-term overgrowth studies, by keeping mechanisms essential for activation. The phenomenon of trained immunity has been described as the innate immunity's ability to adapt when exposed to stimuli, which results in a long-term activation that provides broad non-specific protection upon reinfection. This ability has been investigated for being a contributing factor to the pathogenesis of fibrosis. Different types of soluble alginate and CC were investigated in their ability to induce training.

Three different alginate microspheres, three different types of soluble alginate, and CC were incubated in a L-IVE model in 2D and 3D with peripheral blood mononuclear cells (PBMCs) for 14 days, while supernatants were harvested at selected time points for cytokine analyzation by Bio-plex Multiplex technology. Alginate microspheres were able to induce trends of cytokine release observed in the WB model, where the step of the opsonization of microspheres showed to be an essential contributor. Induction of cytokines by soluble alginates showed in some cases to be concentration-dependent. Microbead SA and soluble SA induced relatively high levels of cytokines central in the foreign body response. However, soluble SA did also induce partly high levels of anti-inflammatory IL-10 and IL-1ra. The 2D and 3D model showed various responses. The cytokine secretion induced by the microspheres and CC tended to be more elevated following the 3D conditions as compared to the 2D cultivation. Soluble alginates were observed to induce the highest levels of cytokines in 2D, which could be a result of polystyrene promoting cell-adherence. The microspheres were observed to induce the highest levels of the pro-inflammatory cytokines TNF, IL-1β, and IL-6, as well as, the chemokine GRO-α in 3D.

Four different soluble alginates and CC were investigated for inducing training in human monocytes by analyzation of cytokines describing a trained phenotype. None of the conditions showed a specific training effect after restimulation with LPS, including the positive control β-glucan. However, SA contributed to maintain an elevated background stimulation five days after wash-out for the inflammatory cytokines TNF, IL-1β, and IL-6 under complement-free conditions. Further, SA and HM were observed to be influenced by the presence of complement in the culture medium. SA induced a presumable tolerance effect of TNF, IL-1β, and IL-6.

In conclusion, microspheres and soluble alginates induced interesting trends that should be further investigated for a better understanding of mechanisms driving fibrosis. Investigation of monocyte maturing to

macrophages can provide extensive information to the search. Further studies of trained immunity should be performed before it is possible to conclude whether soluble alginates and CC are able to induce training of human monocytes.

Sammendrag

Celleinnkapslingteknologi benytter biomaterialer for transplantasjon av celler og viser potensiale som et terapeutisk alternativ til behandling av diabetes type 1. Fagfeltet har kommet langt i utviklingen av kapsler for transplantasjon, men utviklingen av lav-inflammatoriske biomaterialer er krevende, og søket etter en fibrosefri kapsel pågår. I tillegg mangler kunnskap om biomaterialers evne til å unngå eller utvikle fibrose og må utforskes ytterligere. I søken etter en bedre bio(in)kompatibilitetsforståelse og en prediktiv *in vitro* modell for evaluering av biomaterialer ble alginatkapsler, forskjellige typer løselig alginat, og kolesterolkrystaller (KK) undersøkt i to forskjellige prosedyrer for å belyse alternative forklaringer på forårsaket fibrose.

Fullblodsmodellen har vist sin verdi ved å predikere det inflammatoriske potensiale til kapsler. Basert på kunnskap fra fullblodsmodellen ble en ny langtids- *in vitro* eksperimentel (L-IVE) modell i 2D og 3D utviklet som et forsøk på å kunne bedre predikasjonen av overvekst-studier ved å beholde essensielle mekanismer for aktivering. Fenomenet "trent immunitet" har blitt beskrevet som det medfødte immunforsvarets evne til tilpasning når det blir utsatt for stimuli, noe som resulterer i en langvarig aktivering som gir bred ikke-spesifikk beskyttelse ved reinfeksjon. Denne evnen er undersøkt for å være en medvirkende faktor til patogenesen av fibrose. Ulike typer løselig alginat og KK ble undersøkt med hensyn til deres evne til å indusere trening.

Tre forskjellige alginatkapsler, tre forskjellige typer løselig alginat og KK ble inkubert i en L-IVE modell i 2D og 3D med perifere mononukleære blodceller (PBMC) i 14 dager, mens supernatanter ble høstet ved utvalgte tidspunkter for cytokinanalyse med Bio-Plex Multiplex-teknologi. Alginatkapslene induserte trender for cytokinfrigjøring observert i fullblodsmodellen, der trinnet med opsonisering av kapsler viste seg å være en viktig medvirkende faktor. Mengde cytokiner indusert av de løselige alginatene viste i noen tilfeller å være konsentrasjonsavhenging. SA-kapsel og løselig SA induserte relativt høye nivåer av cytokiner sentralt i fremmedlegeme-respons. Men, løselig SA induserte også delvis høye nivåer av anti-inflammatorisk IL-10 og IL-1ra. 2D- og 3D-modellen viste forskjellige responser. Løselige alginater ble observert til å indusere høyest nivåer av cytokiner i 2D, noe som kan være et resultat av polystyren som fremmer celleadhesjon. Kapslene induserte de høyeste nivåene av de pro-inflammatoriske cytokinene TNF, IL-1β, og IL-6, samt kjemokinet GRO-α i 3D.

Fire forskjellige løselige alginater og KK ble undersøkt i deres evne til å indusere trening i humane monocytter ved analyse av cytokiner tilknyttet en trent fenotype. Ingen av betingelsene viste en spesifikk treningseffekt etter re-stimulering med LPS, inkludert den positive kontrollen β-glukan. SA bidro imidlertid til å opprettholde en forhøyet bakgrunnstimulering fem dager etter utvasking, av de inflammatoriske cytokinene TNF, IL-1β, og IL-6 under komplementfrie forhold. Videre ble SA og HM observert til å være påvirket av tilstedeværelsen av komplement i kulturmediet. SA induserte en antatt toleranseeffekt av TNF, IL-1β og IL-6.

Avslutningsvis induserte kapslene og løselige alginater interessante trender som bør undersøkes videre for bedre forståelse av mekanismer som driver fibrose. Undersøkelse av monocyttmodning til makrofager kan gi omfattende informasjon til søket. Ytterligere studier av trent immunitet bør utføres før det er mulig å konkludere om løselige alginater og KK er i stand til å indusere trening av humane monocytter.

Abbrevations

- 2D - 2-dimensional
- 3D - 3-dimensional
- A - Alginate microbead
- AP - Alginate-poly-L-lysine microcapsule
- BCG - Bacillus Calmette-Guérin
- CC - Cholesterol Crystals
- CCR2 - C-C chemokine receptor 2
- CR3 - Complement receptor 3 (CD11b/CD18)
- CSF1R - Colony-stimulating factor 1 receptor
- DAMP - Damage associated molecular pattern
- DC - Dendritic cell
- ECM - Extracellular matrix
- FACS - Fluorescence-activated cell sorting
- FBGC - Foreign body giant cell
- FX - Factor X
- FXII - Factor XII
- G - α-L-guluronic acid
- GRO-α - Growth-regulated oncogene-α
- h.i. - Heat-inactivated
- H3K4me(3) - (Tri)methylation of lysine unit 4 on histone 3
- H3K36 - Lysine unit 36 on histone 3
- H3K27Ac - Acetylation of lysine 27 on histone 3
- HBSS - Hanks buffered salt solution
- HSC - Hematopoietic stem cell
- iC3b - inactivated C3b
- IFN - Interferon
- IgG - Immunoglobulin G
- IgM - Immunoglobulin M

- IL - Interleukin
- ILC - Innate lymphoid cell
- LPS - Lipopolysaccharide
- L-IVE - Long-term *in vitro* experimental model
- M - β-D-mannuronic acid
- M-CSF - Macrophage colony-stimulating factor
- M1 - Classically activated macrophage
- M2 - Alternatively activated macrophage
- MBL - Mannose-binding lectin
- MCP-1 - Monocyte Chemoattractant Protein-1
- NK cell - Natural killer cell
- oxLDL - Oxidized low-density lipoprotein
- PAMP - Patter recognition molecular patterns
- PBMC - Peripheral blood mononuclear cell
- PBS - Phosphate-buffered saline
- PDGF - Platelet-derived growth factor
- PMN - Polymorphonuclear cell
- PLL - Poly-L-lysine
- PRR - Pattern recognition receptor
- RPMI - Roswell Park Memorial insitute
- SA - Sulfated alginate microbead/ Sulfated alginate
- TAM - Trondheim alginate microcapsule
- TCC - Terminal complement complex
- TF - Tissue factor
- TGF-β - Transforming growth factor-β
- TLR - Toll-like receptor
- TNF - Tumour necrosis factor
- VEGF - Vascular endothelial growth factor
- WB - Whole blood model

Contents

1 Introduction

1.1 Background

1.1.1 Cell encapsulation technology

Biomaterials are constructed to interact with biological systems and are widely used in biomedical applications to enhance or replace a natural function. Their chemical structure can be of different materials, both from nature and synthesized, and their application may range from serving as a hip implant to be used for transplantation[1]. WHO defines transplantation as "the transfer of human cells, tissues or organs from a donor to a recipient with the aim of restoring functions in the body"[2]. However, intending to restore functions, a major obstacle is the risk of immune rejection of the foreign tissue, making immunosuppressive drugs a requirement. Using immunosuppressants over time can cause side effects, such as losing resistance to infections, anemia, and an increased risk of malignancies[3, 4]. Providing biomaterials for transplantation of encapsulated cells reduces the need for immunosuppressants, and the side effects can be avoided.

In cell encapsulation technology, cells are immobilized within a biocompatible, semipermeable membrane that allows free diffusion of nutrients, oxygen, and metabolic waste. This technology can be employed in cell transplantation where the encapsulated cells secrete a therapeutic product *in vivo*. By being semipermeable, the membrane can be impermeable to larger molecules, such as cells and other components of the host's immune system, making it protect the transplanted cells. Thereby, the membrane provides immunoisolation and can prevent a rejection reaction of the transplanted cells, so that immunosuppressive drugs are not needed[3, 5, 6]. Figure 1.1.1 shows the principle of immunoisolating cells into a semipermeable membrane.

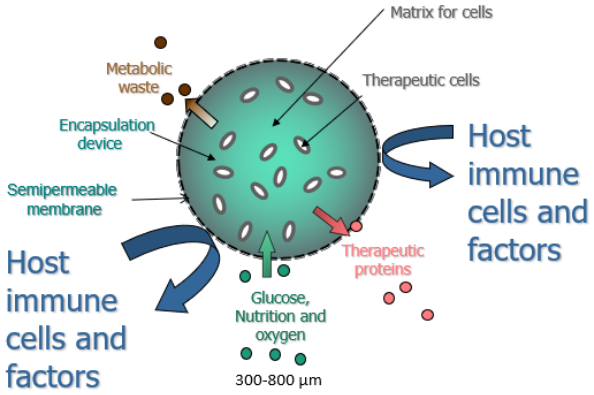

Figure 1.1.1: Illustration of cell encapsulation. The semipermeable membrane allows free diffusion of nutrients, oxygen, metabolic waste and secretion of a therapeutic product. Simultaneously, it ensures exclusion of host immune cells and factors. Adapted with permission from A. M. Rokstad.

Lim and Sun proposed in 1980 a novel microencapsulation procedure for transplantation of pancreatic islets that could be a therapeutic option for the treatment of diabetes type 1[7]. Since then, the focus has been to develop a device that provides a safe and applicable cell therapy in diabetes treatment[8]. By encapsulating pancreatic islets, the therapeutic product secreted is insulin. This is produced in response to the glucose

level in blood and is thereby able to regulate the blood glucose of the patient. Even though the transplanted cells are protected from immune attack, the biomaterial that comprises the semipermeable membrane is not.

1.1.2 Biocompatibility

Biocompatibility and biotolerability is an absolute requirement for making cell encapsulation therapy possible. A biocompatibility manifesto was published in 2011, where definitions of biocompatibility and biotolerability for the 21. century were proposed. Biocompatibility is "the ability of a material to locally trigger and guide non-fibrotic wound healing, reconstruction, and tissue integration", while biotolerability is "the ability of a material to reside in the body for long periods of time with only low degrees of inflammatory reaction"[9]. The degree of biocompatibility and biotolerability will vary with the purpose of the biomaterial, its chemical structure, and the implantation site. As a prosthesis material, the activation of inflammatory response leading to overgrowth of fibrotic tissue will not necessarily affect its function, but can rather provide a firm adhesion of the material without causing harm. In cases with microspheres as the biomaterial, overgrowth will impair its function. The fibrotic tissue will reduce the free diffusion of the semipermeable membrane and prevent the encapsulated cells from interacting with the surroundings. This may result in necrosis, and the transplanted cells lose their therapeutic effect. For cell encapsulation, the goal is to develop microspheres of biomaterials being biotolerable and further show the ability to promote a fibrosis free surface[10]. Of note, there is not necessarily that a low-inflammatory material is fibrosis free, as is shown by Ca/Ba beads of alginate that promote low inflammation[11, 12] but promotes fibrosis in the most challenging rodent models (C57/BL6 mice)[13] and monkeys[14]. The interaction between the biomaterial and the encapsulated cells must also be taken into account so that the biomaterial itself does not create a toxic milieu for the cells[15].

1.2 Material host-response

In the defense against microorganisms and foreign components, the innate immune system is fundamental. Its ability to distinguish between self- and non-self relies on collaboration between effector proteins of the complement and coagulation system, and immune cells, such as natural killer (NK) cells, polymorphonuclear cells (PMNs) and monocytes[16]. Proteins in serum and on the surface of host cells, especially soluble and surface regulators of the complement, tightly regulate these systems, and contact with foreign surfaces, such as microorganisms or biomaterials that lack these regulators, will easily activate the cascades leading to inflammation and/or homeostasis[8, 10].

1.2.1 The complement system

The complement system consists of about 50 serum and cell membrane proteins that, together with other molecules from both the innate and adaptive immune system, work to eliminate pathogens, dying cells, and immune complexes from the body. Most of the proteins are synthesized in the liver by hepatocytes and make up approximately 15% of the globulin fraction in plasma. Complement proteins circulate the blood as inactive precursors, zymogens, and are activated by sequential cleavage[17]. This leads to the generation of effector molecules that, in different ways, participate in the elimination of microbes. As complement proteins activated early in the cascade can result in the formation of a large number of effector molecules, the system is capable of a high amplification of the response[18]. In inflammation, the complement system can be initiated

through three major pathways, the classical, lectin, and alternative pathway, all leading to the formation of the enzyme complex, C3 convertase, that cleaves the most abundant complement protein C3. The classical pathway can be initiated by the formation of an antigen-antibody complex, where antibodies of the activating complex must be of the immunoglobulin M (IgM) or G (IgG) isotype. Formation of antigen-antibody complex allows the involvement of the complement protein C1 consisting of C1q, C1r, and C1s, which are essential for further activation. The lectin pathway is initiated through pattern recognition receptors (PRRs), like Mannose-binding lectin (MBL), a lectin receptor that circulates blood and extracellular fluids and binds to carbohydrates, such as mannose found on microbial cell surfaces. The alternative pathway can be initiated by several factors, most importantly, through spontaneous hydrolysis of C3[17]. Initiation of the complement system by biomaterials are mainly through either the classical pathway or the alternative pathway[19]. The formation of C3 convertase results in C3 cleaved into the anaphylatoxin C3a, which recruits leukocytes to the site of inflammation, and C3b, which together with inactivated C3b (iC3b), mediates phagocytosis by phagocytic cells through complement receptors 1 and 3 (CR1 and CR3). C3b is also involved in the assembly of the C5 convertase together with C3 convertase, which cleave C5 to the anaphylatoxin C5a and C5b. C5b induces the formation of the terminal complement complex (TCC), which, when membrane-bound, functions as a pore in the microbe's cell wall. This causes free diffusion of ions and water that results in osmotic instability and eventually lysis[17]. Regulators of the complement are essential for host cells to avoid activation of the complement and thereby avoid cell lysis. As foreign surfaces, such as microorganisms and biomaterials, lack these regulators, the complement becomes activated. C1 esterase inhibits several proteases of the classical and lectin pathway[20]. Factor H, on the other hand, controls activation of the alternative pathway, either by removing Bb from the C3 convertase (C3bBb) or being a cofactor for the degradation of C3b[20]. Biomaterials may also take advantage of these regulators by lowering the activation of the complement. For example, Arlov et al. observed factor H on the surface of low-inflammatory sulfated alginate microspheres, suggesting that biomaterials are able to bind factor H, thereby lowering the activation of complement through the alternative pathway, contributing to reduce the inflammatory response[21].

1.2.2 The coagulation sytsem

Like the complement system, the coagulation system contains zymogens circulating the blood activated sequentially by proteolytic cleavage. The cascade can be initiated through two pathways, the intrinsic and the extrinsic pathway, that converge into the common pathway, and lead to the formation of fibrin, resulting in a blood clot[8, 22]. The fibrin clot is meant to prevent blood loss from damaged vascular tissue. However, coagulation can also be a response to infection where the fibrin network can trap bacteria and protect the host by controlling the pathogen by reducing its spread[23, 24].

The intrinsic pathway is activated through contact with negatively charged surfaces, that could be a biomaterial. The pathway becomes activated when plasma factor XII (FXII) is exposed to a negatively charged surface, which activates other plasma factors, including factor X (FX), responsible for the formation of thrombin from prothrombin, further resulting in blood clot[22, 25].

The extrinsic pathway is activated through tissue factor (TF), a transmembrane glycoprotein expressed by extravascular cells that surround blood vessels. Leukocytes, such as monocytes and macrophages, also express TF after stimulation by inflammatory cytokines, such as tumor necrosis factor (TNF) and interleukin-1 (IL-

1), suggesting that these cells also are involved in blood coagulation[26, 27]. Activation through TF leads eventually to the activation of FX, resulting in blood clot formation[22].

1.2.3 Protein adsorption to surface

When implanted biomaterials encounter blood, proteins found in plasma, such as immunoglobulins (IgG), fibrinogen, complement proteins (C1, C3, and C4), coagulation proteins (FXII) and human serum albumin, will adhere to the surface of the biomaterial forming a protein layer called a provisional matrix[19, 28]. Determined by the biomaterials' surface properties, this protein layer will further determine the activation of complement, coagulation, platelets, and immune cells, thereby being essential for a further immune response[19]. Plasma proteins adsorbed to the surface of the biomaterial can cause a conformational change and make them "contact-activated". This applies to molecules like fibrinogen, FXII, IgG, and C3[16, 29]. Contact-activated fibrinogen can bind platelets, and FXII initiates the coagulation cascade through the intrinsic pathway[16]. C3's conformational change can mimic C3b, leading to activation through the alternative pathway, while hexamers of IgG adsorbed to the surface of the biomaterial can bind C1q that results in C1 assembly and thereby activation of the classical pathway[19, 28, 30]. Formation of C3b from the proteolytic cleavage by C3 convertase will result in more deposition of C3b, and will further cause an amplification of the cascade through the alternative pathway[11]. The generated anaphylatoxins C3a and C5a of the complement system will recruit immune cells to the site of inflammation, while C3b and iC3b facilitate the binding and activation of the recruited cells to the foreign surface. Factors of the coagulation system, such as thrombin, FXIIa, and FXa, can generate C3a and C5a without the complement being activated. Additionally, C5a has the ability to upregulate the expression of active TF on endothelial cells and circulating polymorphonuclear leukocytes[29, 31, 32]. These events show a crosstalk between the two systems during inflammation. Formation of thrombin, initiated by adsorbed FXII, activates platelets, which further release mediators of the coagulation cascade and other mediators, such as cytokines, contributing to the inflammation response[19, 33].Figure 1.2.1 shows a simple illustration of protein adsorption to biomaterial surface following complement activation and recruitment of leukocytes.

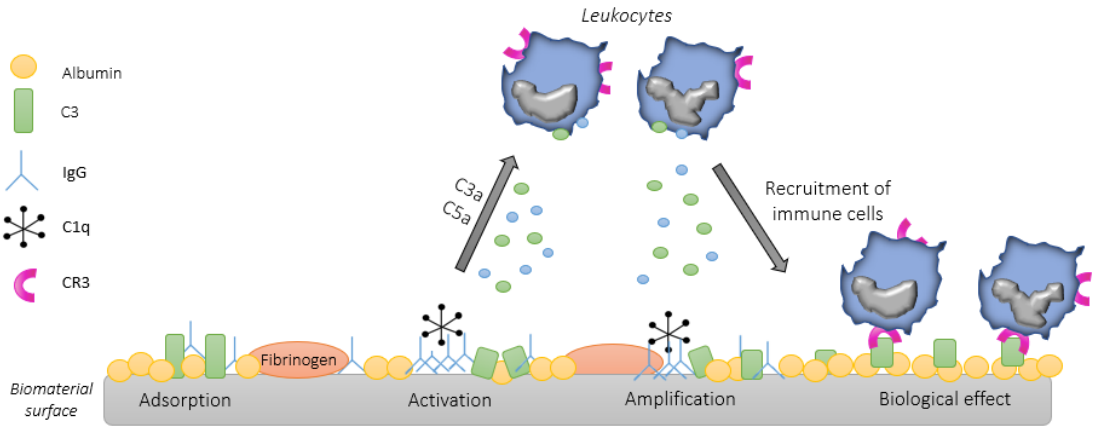

Figure 1.2.1: A schematic illustration of protein adsorption, complement activation, and recruitment of leukocytes induced by a biomaterial surface. Upon blood exposure, plasma proteins, such as albumin, C3, fibrinogen, and IgG, will adhere to the surface and form a protein film. Interaction between surface and some proteins (e.g., C3 and IgG) may cause a surface-induced conformational change of the protein resulting in activation of the complement system. Generated C3a and C5a recruit and activate leukocytes, while C3b binds to the surface and amplifies the cascade through the alternative pathway. The recruited leukocytes can bind to adsorbed iC3b via CD11b of CR3, which will further initiate the inflammatory response. Based on illustration from [28, 29].

The amount of adsorbed proteins to the biomaterial and the activation of the immune response are tightly connected, where the surface properties of the material are a major influencing factor. Biomaterials with free groups of NH_3 and OH influence the activity of complement. These chemical groups are essential for the covalent binding of C3b and are therefore regarded as possible activators of the complement[28]. Experiments based on a whole blood model, where biomaterials are incubated in whole blood, have shown that polycation containing microspheres are capable of inducing inflammatory cytokines, while alginate microbeads do not induce activation of the corresponding cytokines[11, 12]. Further, the induction of inflammatory cytokines by alginate microspheres has been connected to the microspheres' ability to activate complement, meaning that the release of some cytokines, such as IL-1β, TNF, IL-6, happens in a complement-dependent manner[34]. This may be explained by electrostatic interactions reflecting a protein's affinity for a biomaterial. Alginate is rich in carboxyl groups and is at physiological pH negatively charged. Several complement proteins have pI below physiological pH, making them also negatively charged at physiological pH and will thereby have a lower affinity for the alginate microbeads[11]. Additionally, the polycation microcapsule contains NH_3-groups, making it a potential binding site for C3b that will further initiate complement activation. As a wish to avoid complement activation, strategies to create more tolerable biomaterials are developed. These include: modulation of surface chemistry with CH_3 and COOH avoiding binding of C3b etc.; modulation of surface topography in, where smoother surfaces have been shown to decrease complement activation; and incorporation of bioactive molecules, for example, anti-inflammatory drugs, which will not necessarily inhibit complement activation but can inhibit inflammatory cell activation and promote resolution of inflammation[19, 29].

1.2.4 Cellular players and pattern recognition responses

Pattern recognition receptors (PRRs) are an important part of the immune system by detecting the presence of pathogen-associated molecular patterns (PAMPs) or damage-associated molecular patterns (DAMPs) and activate immune cells to clear out an infection[17]. Adsorbed proteins to biomaterials can be recognized as PAMPs by PRRs on cells, such as polymorphonuclear leukocytes (neutrophils, granulocytes) and monocytes, and promote cell adhesion to the surface of the biomaterial. Binding of PAMPs through PRRs can activate transcription factors that initiate the production of genes essential for the innate immune response, such as antimicrobials and cytokines. By remaining attached to the biomaterial, the cells can secrete various immunoregulatory signals that will recruit more immune cells to the site of inflammation, activate them, and continue the inflammatory response[19].

1.2.5 Effector molecules

Cytokines work as signaling molecules that stimulate intracellular cascades such as activation, proliferation, differentiation, cytokine release, and apoptosis[17, 35]. Cytokines are divided into subgroups based on their function. Pro-inflammatory cytokines ensure the up-regulation of the immune response, anti-inflammatory cytokines contribute to control pro-inflammatory cytokines, and chemokines are heparin-binding cytokines with a chemotactic activity that recruit and activate leukocytes to the site of inflammation, like where a biomaterial is implanted[36, 37]. Table 1.2.1 shows an overview of the cytokines emphasized in this study and are listed along with their cell source and main activity in the inflammatory response. IL-1β, TNF, and IL-6 are pro-inflammatory cytokines that act on blood vessels to increase vascular permeability for recruiting and activation of leukocytes and lymphocytes[17]. IL-8 is a pro-inflammatory chemokine that recruits neutrophils from blood to the site of infection for clearing of infection and amplifying the response. Monocyte-chemoattractant protein-1 (MCP-1) is a chemokine recruiting monocytes to the site of inflammation. This recruitment is probably dependent on interaction through MCP-1 and the C-C chemokine receptor 2 (CCR2), because mice lacking CCR2 have shown to be deficient in monocyte infiltration at sites of infection[37]. GRO-α is also a chemokine recruiting and activating neutrophils at the site of inflammation[38]. Chemokine's recruitment of leukocytes to the site of inflammation is an early phase of the dynamic process of wound healing. Dysregulation of the inflammatory response and the wound healing process can result in fibrosis. Research has shown that some chemokines play a role in the pathogenesis of fibrosis diseases[37]. For example, MCP-1 has been connected to liver fibrosis, where CCR2 deficient mice did not show the development of liver fibrosis[37]. IL-10 and IL-1ra are anti-inflammatory molecules working to regulate the pro-inflammatory response by preventing the immune system from responding in excess and thereby causing damage [39]. IL-10 inhibits macrophage and monocyte activation and further the production and release of pro-inflammatory cytokines[17, 40]. IL-1ra works as a competitive inhibitor of IL-1β and IL-1α by binding to the same cellular receptors and thereby dampening activation through the pro-inflammatory cytokines[41]. Macrophage colony-stimulating factor (M-CSF) is a growth factor that promotes macrophage growth, differentiation, activation, and survival through the colony-stimulating factor 1 receptor (CSF1R). This signaling is up-regulated in several diseases, such as rheumatoid arthritis and arteriosclerosis, and may contribute to the development of the diseases[42]. For example, inhibition of CSF1R led to complete loss of fibrosis, suggesting that secretion of M-CSF that causes accumulation of macrophages at the site of

inflammation contributes to the development of fibrosis[43].

Table 1.2.1: An overview of the cytokines investigated in this study with associated cell source and activity.

Cytokines	Cell source	Cytokine activity	References
IL−1 β	Macrophages, monocytes, dendritic cells, NK cells, epithelial and endothelial cells, fibroblasts	Proinflammatory: induces local inflammation and systemic effects such as fever, upregulates adhesion to vascular endothelium	[17, 40]
IL-6	Macrophages, monocytes, some T-cells and B-cells, endothelial cells, fibroblasts	Proinflammatory: T- and B-cell growth factor, induces inflammation	[17, 40]
IL-8 (CXCL8)	Macrophages, monocytes, granulocytes, lymphocytes, epithelial and endothelial cells, fibroblasts	Pro-inflammatory chemokine: recruits and activates neutrophils, angiogenic activity	[17, 40]
IL-10	Macrophages, monocytes, dendritic cells, activated subsets of CD4+ and CD8+ T cells	Anti-inflammatory: inhibits macrophage and monocyte activation, and release of proinflammatory cytokines. Enhance B-cell proliferation	[17, 40]
IL-1ra	Macrophages, monocytes	Anti-inflammatory: Competitive inhibitor of IL-1β and IL-1α	[41]
MCP-1 (CCL2)	Macrophages, monocytes	Monocyte chemoattractant	[40]
TNF	Macrophages, monocytes, T-cell, neutrophils, NK cells	Pro-inflammatory: activates antigen-presenting cells and monocytes/macrophages	[17, 40]
PDGF	Macrophages, platelets	Erythropoiesis, angiogenesis, cell proliferation	[44]
VEGF	Macrophages, neutrophils, platelets	Growth factor: Angiogenic, increases vascular permeability	[40]
M-CSF	Monocytes, lymphocytes, fibroblasts	Growth factor: macrophage growth, differentiation, activation and survival	[17, 41]
GRO-α (CXCL1)	Macrophages, neutrophils	Chemokine: Recruits and activates neutrophils and basophils	[38, 45]

1.2.6 Foreign body response

When a biomaterial is perceived as foreign by surface activation of proteins, a foreign body response is initiated. After the formation of the provisional matrix, neutrophils and monocytes migrate to the site of implantation in response to chemokines and the anaphylatoxins C3a and C5a, where their interaction

with surface-adsorbed proteins induce cell activation[46]. Activation of monocytes causes differentiation into macrophages, and as the inflammation is unresolved, macrophages accumulate, and the inflammation enters the phase of chronic inflammation. A prolonged presence of macrophages accompanied by secretion of chemoattractant signals and cytokines contribute to the formation of granulation tissue, a foreign body response, which results in encapsulation of the biomaterial. Through the deposition of extracellular matrix (ECM) and expansion of the vasculature by angiogenesis lead to the formation of foreign body giant cells (FBGCs) through fusion of an IL-4-induced subset of adherent macrophages[46–48]. The further fusion of adherent macrophages and FBGCs characterize the foreign body reaction. In this phase, macrophages and FBGCs release degrading mediators, such as reactive oxygen intermediates, enzymes, and acids, in an attempt to destroy the foreign substance. Again, the biomaterials surface properties will be a determining factor of its susceptibility to attack. Adherent macrophages can also secrete fibrogenic factors stimulating fibrogenesis by fibroblasts, resulting in the accumulation of fibrotic tissue and the development of a fibrotic capsule around the biomaterial. For a microsphere, the fibrosis will reduce its in- and outflux and further impair its function as a biomedical device[48]. The initiated microenvironment in the form of adsorbed proteins, cytokine release, and activation of leukocytes caused by the implanted biomaterial becomes crucial in determining the resolution of inflammation and, thereby, reflecting the biomaterials biotolerability.

1.2.7 Monocytes and macrophages as essential players

Hematopoiesis describes the process where hematopoietic stem cells (HSCs) differentiate into mature blood cells. All mature blood cells are derivatives from HSCs and can be divided into two lineages: myeloid and lymphoid. The myeloid lineage gives rise to red blood cells, platelets, and white blood cells, including granulocytes, monocytes, macrophages, and some dendritic cell (DC) populations. These white blood cells are a part of the innate immune system and are the first to respond to an infection. The lymphoid lineage can differentiate into white blood cells like B-cells, T-cells, innate lymphoid cells (ILCs), and specific DC populations, where especially B-cells and T-cells are important in the regulation of the adaptive immune response[17].

Earlier, it was believed that monocytes were immature, homogeneous blood cells giving rise to macrophages and DCs[49]. However, not all macrophages are a product of differentiated blood monocytes. Kupffer cells in the liver, microglia cells in the brain, and Langerhans cells in the skin are examples of resident macrophages that are seeded embryonically and show a self-renewal capacity like stem cells[49–51]. These resident macrophages are functionally different from blood-borne monocytes recruited during inflammation[49]. Macrophages in the dermis and the gut, on the other hand, are blood-derived monocytes[50]. As the cell repertoire of monocytes and macrophages expands, an understanding of their role in inflammation and tissue repair is required. This can, among other things, contribute to explain chronic inflammation and fibrosis caused by tissue damage[50].

In response to inflammation or infection, blood monocytes are recruited and migrate into tissues, where they can differentiate into macrophages or DCs[50, 51]. The macrophages can differentiate into different subsets depending on the pathogens and cytokines expressed in the microenvironment, and display various phenotypes[51–53]. Classically activated macrophages (M1) dominate the early phases of inflammation and possess a pro-inflammatory phenotype with pathogen destruction abilities, increased phagocytosis and antigen processing, and secretion of antimicrobial molecules, pro-inflammatory cytokines, (such as TNF, IL-1β, IL-6, and IL-12) and the chemokine CXCL10[50–53]. Macrophages are polarized in this direction through recognition of PAMPs, such as lipopolysaccharide (LPS); DAMPs, such as released intracellular proteins; as well as stimulation of the secreted T helper 1 cytokine Interferon-γ (IFN-γ)[51–53].

Alternatively activated macrophages (M2) possesses a wound-healing phenotype and dominates the later phases of inflammation related to resolution and tissue repair. They secrete vascular endothelial growth factor (VEGF), transforming growth factor-β (TGF-β), and IL-10, and promote tissue formation and remodeling with activities such as angiogenesis [50, 52, 53]. Macrophages polarize in this direction in response to, among other things, the T helper 2 cytokines IL-4 and IL-13, and anti-inflammatory IL-10. M1 and M2 macrophages are the best characterized phenotypes, each representing an endpoint of a macrophage polarization spectrum. This means that in response to different stimuli, the activated macrophages can polarize and give rise to phenotypes somewhere in-between these endpoints[53], and reflects macrophages plasticity. In an attempt to explore the scope of the spectrum, four subsets of M2 have been identified in response to different specific inducing agents, where they display an M2-like phenotype[52]. Activation and induction of genes related to the specific responses are likely to be outcomes of epigenetic regulation. In the absence of specific inducers, the gene transcription is restrained by repressors, and in case of stimulation, the repressors release making gene transcription possible[53]. Thereby, due to epigenetic regulation, the macrophage phenotype can be shaped as a response to changes in the microenvironment. Figure 1.2.2 shows an overview of macrophage differentiation into the two endpoints of the macrophage polarization spectrum.

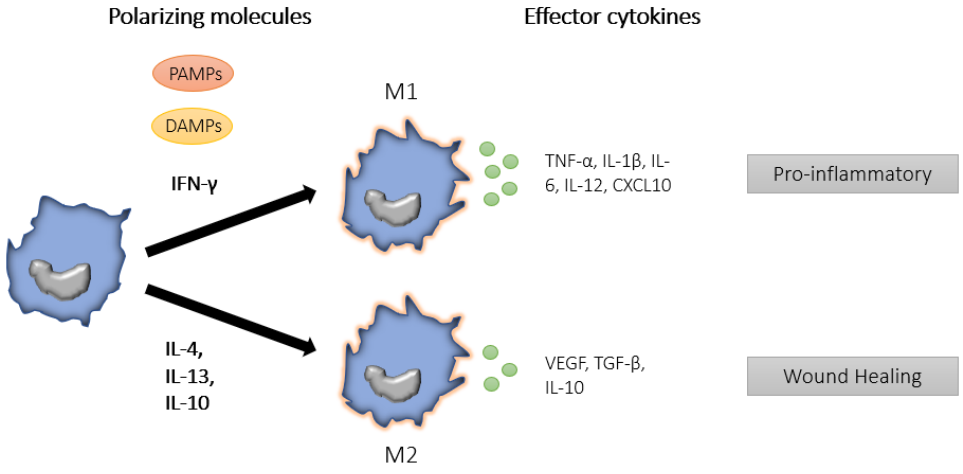

Figure 1.2.2: An overview of macrophage differentiation into the two overall subgroups: classically activated macrophages (M1) and alternatively activated macrophages (M2). Different cytokines or molecules guide the polarization towards a pro-inflammatory or wound healing phenotype. The subsets have specific activities connected to the subsets among secreting different effector cytokines.

During an infection, the body is dependent on a fast recruitment of myeloid cells to solve the injury. This requires a constant generation and mobilization of bone marrow cells. A severe infection can result in emergency hematopoiesis resulting in an alternative production, for example, by producing a higher number of monocytes, which in turn lowers the production of lymphocytes, leaving the monocytes in an altered activated state in higher numbers than usual for several weeks. The phenomenon of altered activated monocytes has been termed "trained immunity". Activation of HSCs by specific cytokines, such as IFN-γ and IL-1β, produced by immune or non-immune cells, can have an important role in the induction of the long-lasting effects[49]. For example, these long-lasting effects caused by trained immunity have been hypothesized to be the cause of non-resolving inflammation connected to atherosclerosis[54]. Non-resolving inflammation is a significant contributor to the pathogenesis of chronic diseases[55]. A main cause is persistent inflammatory stimuli caused by exogenous components, such as bacteria or viruses, non-degradable particles, and foreign food antigens[55]. These components can, for example, disturb the polarization process of macrophages, which is fundamental in wound healing and thereby cause persistent inflammation[52]. A microsphere can also be such a component of disturbance, where the cause of persistent inflammation can lead to fibrotic overgrowth of the surface, and further impairment of its function. For example, Doloff et al. investigated the type and number of cells on and around implanted alginate spheres[43]. Analysis by fluorescence-activated cell sorting (FACS) on day 1 after implantation showed the presence of immature blood monocytes, while on day 4 and 7 the subset was disappeared. Instead, a subset of macrophages was increased in number, which suggests that the macrophages later responsible for the fibrotic overgrowth induced by the biomaterial is of blood monocyte origin[43]. However, Vegas et al. have shown that it is possible to make biomaterials that reduce the foreign body reaction in rodents and non-human primates for at least six months[56]. Knowledge about the interaction between biomaterial and macrophages becomes, therefore, essential in the discovery of materials that can reduce the foreign body response.

1.2.8 Trained immunity in monocytes

The immune system has evolved to protect or limit infection of multicellular organisms caused by potential harmful endogenous or exogenous components. The immune system is dependent on cells, molecules, and pathways, forming a dynamic and interconnected network to function. Classically, the immune system is divided into the two arms of innate and adaptive immunity. Innate immunity is viewed as primitive and non-specific with no immunological memory, but in return, provides a quick response encountering danger components. Adaptive immunity is considered giving a more specific response in battling infections and possesses immunological memory, but is slower in its action. However, even though the immune system contains cells, molecules, and pathways, which are in the broader term and for simplicity divided into two systems, these arms are interconnected, and some immune cells play a dual role by providing a function in both arms[17, 57, 58].

The fact that the innate immune system is unspecific and possesses no kind of immunological memory has been questioned over the past decade. In studies based on organisms lacking adaptive immunity, such as plants and non-vertebrates, an immune adaption upon reinfection has been observed[59]. Further research has led to observations of the phenomenon in vertebrates and humans as well, meaning that the innate immune system is able to mount a specific response after a second insult. This has been observed for

innate immune cells, such as monocytes, macrophages, and NK cells and is termed "trained immunity" or "innate immune memory"[60, 61]. Thereby, trained immunity is based on the theory that it is not only the adaptive immune system but also the innate, that has the ability to adapt when exposed to infections or vaccinations. This is achieved by up-regulation of its function over time and results in a broad non-specific immune protection to secondary infections[58, 62]. In contrast, there are also stimuli that can cause tolerance by causing a down-regulation of function when restimulated. This is called LPS-induced tolerance and is induced by LPS or other stimuli of Toll-like receptors, which is an undergroup of PRRs[62].

Epigenetic and metabolic reprogramming has been identified as the major mechanisms regulating trained immunity. These processes cause a change of the functional state of the cell and restimulation results in a long-term pro-inflammatory phenotype that displays increased response and cytokine production[63]. Epigenetic mechanisms regulate the gene expression without alterations within the DNA sequence, such as mutations and recombination, which are fundamental for adaptive immunity to provide immunological memory[64]. Instead, the regulations include DNA methylation, histone modifications, and post-translational modulations by non-coding RNA resulting in changes in the chromatin architecture[60]. Modifications of histones are catalyzed by enzymes adding or removing functional groups to amino acids, such as lysine, at the histone N-terminal tail[65]. The modifications include, among other things, methylation and acetylation, which can alter the packaging of DNA and thereby result in either activation or repression of the gene transcription. Acetylation neutralizes the positive charge of histones, causing a more relaxed chromatin, and is associated with activation of gene transcription. The effect of methylation, on the other hand, is determined by the amount of added methyl groups, as well as which lysine residue in the histone tail that is involved.[60]. Trimethylation of lysine 36 on histone 3 (H3K36) will open the chromatin structure, making the DNA more accessible for transcription. Trimethylation of lysine 27 on histone 3, on the other hand, will make the chromatin more compact and repress gene transcription[60, 65]. Resting monocytes and macrophages obtain energy through oxidative phosphorylation. In response to different inflammatory stimuli, the immune cells can rewire their metabolic processes to become activated and prepare them for host defense. Exposition to inflammatory stimuli, such as LPS, induces a metabolic rewiring from oxidative phosphorylation to aerobic glycolysis so that the cells become activated[58].

In trained immunity, the epigenetic reprogramming involves epigenetic marks like methylation and trimethylation of lysine 4 on histone 3 (H3K4me, H3K4me3) and acetylation of lysine 27 on histone 27 (H3K27Ac), which leads to an open chromatin and allows gene transcription[58]. These histone modifications have been observed at promoters for cytokines as well as promoters of glycolytic genes. The up-regulation of glycolytic genes causes the cells to undergo a metabolic rewiring from oxidative phosphorylation to aerobic glycolysis, while the up-regulation of cytokine genes increases the production of inflammatory mediators. Together, they reflect activation of the cells[57, 63, 66]. Figure 1.2.3 shows a simplified overview of the hallmarks of trained immunity.

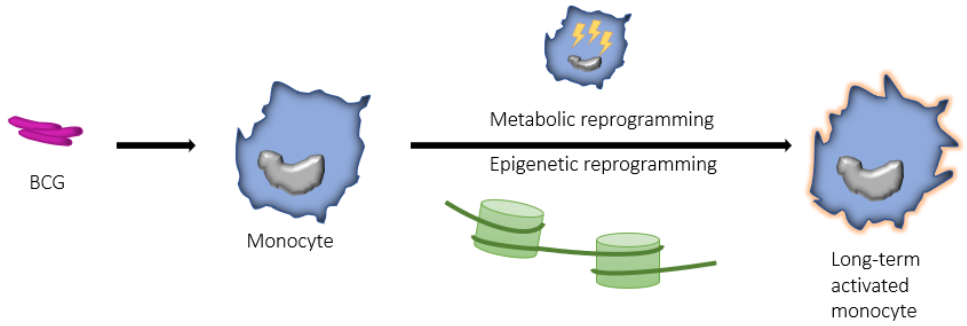

Figure 1.2.3: A simplified illustration of the hallmarks of trained immunity. Bacille Calmette-Guérin (BCG) stimulates monocytes to undergo metabolic and epigenetic reprogramming resulting in long-term activated monocytes providing protection against non-related stimuli. Inspired by drawing of Netea et al[58].

There are various types of stimuli that can induce trained immunity. Over several decades the effect of the bacillus Calmette-Guérin (BCG) vaccine has been observed. For example, studies by Garly et al. showed that childhood survival in West-Africa, areas with high mortality, was connected to vaccination with BCG, where BCG provided, in addition to the specific protection against mycobacterium, a non-specific protection[57, 67]. Studies based on mice could also confirm this effect where BCG provided a T cell-independent protection when combating secondary non-related stimuli of *Candida albicans (C.albicans)* or *Schistosoma manosi (S. manosi)*[68, 69]. These observations suggest that vaccines, such as BCG, provide protection beyond its target, and that this protection is independent of adaptive immunity.

Observations related to other types of infections have also contributed to the hypothesis that innate immunity can develop non-specific adaption. An attenuated virulent strain of *C. albicans* injected in B- and T-cell deficient mice showed protection against both the attenuated and virulent strain[70, 71]. A similar study using Rag1-deficient mice (meaning that they are not able to rearrange their antigen receptors) confirmed that the protection against reinfection was in a lymphocyte-independent manner[72]. Together, they demonstrated that the protection of reinfection was dependent on macrophages and pro-inflammatory cytokines.

Over the past years, scientists have investigated the possibility of trained immunity having a potential role in autoimmune disorders, such as rheumatoid arthritis and diabetes type 1, and inflammatory diseases such as atherosclerosis. Atherosclerosis is caused by the accumulation of lipoproteins, such as cholesterol, within the arterial wall causing decreased blood circulation due to the narrowing of the arterial cavity, resulting in a phenotype of persistent, low-grade inflammation[63, 73, 74]. Circulating monocytes are recruited to the intimal layer of the vessel wall, where they differentiate into macrophages that can further develop to foam cells that contribute to plaque formation[63]. Oxidized low-density lipoprotein (oxLDL) has been identified as a possible trigger of trained immunity in monocytes, whereas the uptake of oxLDL by macrophages results in foam cell formation. A study by Bekkering et al. showed that *in vitro* stimulation with oxLDL induced activated macrophages with a pro-inflammatory phenotype[74]. Upon restimulation with ligands of TLR2 and TLR4 (unrelated stimuli), the macrophages responded to produce TNF, IL-6, IL-8, and MCP-1: factors essential for maintaining the inflammatory environment in atherosclerosis[57, 63, 74]. At gene

transcription level Bekkering et al. also observed up-regulation of mRNA of *il-6, tnf, il-8,* and *mcp-1* in trained monocytes compared to untrained control. This up-regulation could be connected to epigenetic reprogramming of histones (H3K4me3) in the promoter regions of these genes since the training effect was prevented in controls with inhibitors of histone methyltransferases[74]. A therapeutic option in such diseases where training is a cause of the pathogenesis can be through inhibition of the training effect[57].

Trained immunity has also been investigated for playing a role in chronic inflammation resulting in fibrosis, such as systemic sclerosis. A study by Jeljeli et al. showed that trained immunity modulates inflammation-induced fibrosis[75]. They observed that BCG-training of macrophages intensifies the disease in a mouse model by comparing BCG and low-dose LPS stimulation on macrophage phenotype, cytokine production, and chromatin and metabolic modifications. For example, cytokine measurement showed overproduction of pro-inflammatory cytokines relevant in the activation of fibroblast in the synthesis of ECM. However, low-dose LPS stimulation showed the opposite effect and can indicate that development of therapeutic options for targeting training in autoimmune and inflammatory diseases is possible[75].

β-glucan

β-glucans are naturally occurring polysaccharides found as primary cell wall components in yeast, fungi (*C. ablicans*, etc.), some bacteria, and cereal grains[76]. These polysaccharides are PAMPs recognized by PRRs on innate immune cells and are the best characterized stimuli in the induction of trained immunity in monocytes[76, 77]. Many PRRs can bind β-glucans from different sources, but purified 1-3,1-6-β-glucan has been shown to induce epigenetic and metabolic rewiring primarily through the surface receptor dectin-1 expressed by dendritic cells, monocytes, macrophages, and neutrophils[66, 76, 77]. This is a different signaling pathway than the one induced by BCG, but both results in the same epigenetic changes[58]. Figure 1.2.4 shows an illustration of the signaling pathways resulting in training induced by β-glucan and BCG.

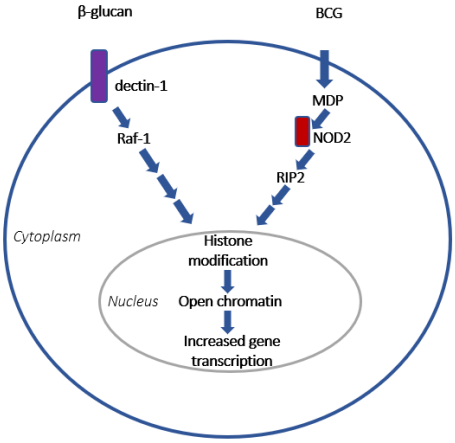

Figure 1.2.4: A simplified illustration of signaling pathways for training induced by β-glucan and BCG. β-glucan and BCG use different signaling pathways to induce training, but both pathways result in the same epigenetic changes within the chromatin. Based on schematic representation made by van der Meer et al.[57]

Leonhardt et al. investigated the effect of β-glucan on monocyte differentiation by comparing β-glucan-trained monocytes with, among other things, classically (M1) and alternatively (M2) activated macrophages[77]. Normally, monocytes circulate the body for about 24 hours before they undergo spontaneous apoptosis in the absence of external survival signals like cytokines and microbial products[78]. However, the study showed that β-glucan inhibited spontaneous apoptosis of monocytes in the absence of stimulating differential factors, such as M-CSF, and further stimulated differentiation of monocytes into macrophages[77]. Simultaneously, the β-glucan-trained cells expressed a phenotype related to both M1- and M2-like macrophages. The cells showed similarities with M2 by the types of surface markers expressed and the secretion of anti-inflammatory IL-10, but the secretion of pro-inflammatory cytokines as a response to LPS is traits related to M1[77]. This reflects the plasticity of macrophage differentiation in response to a specific microenvironment and that the differentiated subgroup may contribute in both M1-like and M2-like immunoregulatory processes.

To study the training effect of monocytes *in vitro*, Bekkering et al. have tried to determine the optional conditions for an experimental protocol by using β-glucan, BCG, and oxLDL, which are the most explored inducers of training[60]. By looking at training period, resting time, and restimulation with non-related stimuli, such as LPS, they concluded that training induce increased pro-inflammatory cytokine production, which is dependent on both training time and resting time before restimulation. Increased training time gave the best observations of the training effect, where 24 h was the most optimal compared to 2 h and 4 h. Resting time was compared for 24 h, 3 days, and 6 days. 6 days gave the best outcome, suggesting that the cells need time for epigenetic and metabolic rewiring before they have the potential of becoming long-term activated upon restimulation[60]. Their study is useful for developing similar protocols to further investigate the training effect of monocytes with different kinds of stimuli.

1.3 Material of study

1.3.1 Alginate

Alginate is a biopolymer frequently used as a biomaterial in biomedical applications due to several favorable properties. In addition to being regarded as one of the most biocompatible and nontoxic materials, alginate can form excellent gels and is easy to modify under cell-friendly conditions. An advantage compared to other biopolymers is that encapsulation of cells can be performed at room temperature at physiological pH, resulting in higher viability of the enclosed cells[15, 79].

Alginate is a naturally occurring polysaccharide mainly found as a structural component of brown algae, such as *Laminaria hyperborea*. Alginate can also be produced by some bacteria, like species of *Azotobacter* and *Pseudonomas*. Extracted alginate from seaweed contains impurities like polyphenols, endotoxins, and proteins, making purification necessary for biomedical use. The polymer consists of the two monomers (1-4)-linked β-D-mannuronic acid (M) and α-L-guluronic acid (G). Variation in composition and sequential arrangement results in the formation of three different blocks: consecutive G residues (G-block), consecutive M residues (M-block), and alternating MG residues (MG-block). The length and content of these blocks, as well as the M/G ratio, varies depending on the source of isolation. This will further influence the biological and physical properties of the polymer[15, 80, 81].

Alginate has the ability to form hydrogels in the presence of divalent cations, where the increased affinity for different divalent ions is Mn < Zn, Ni, Co < Ca < Sr < Ba < Cd < Cu < Pb[82]. Interaction with divalent ions results in the formation of junction zones and ionic cross-linking between G-blocks of two polymer chains. This is called the egg-box model, and the cross-linking results in gel formation[15, 81]. Although G-blocks are believed to be the main structural component in the formation of gels, studies have shown that MG-blocks also have the ability to form junction zones, and a direct involvement in the alginate gel network[83]. The properties of the gel will, therefore, be influenced by both the types of alginate and the divalent cation(s) used for cross-linking. Figure 1.3.1 shows the chemical structure of alginate.

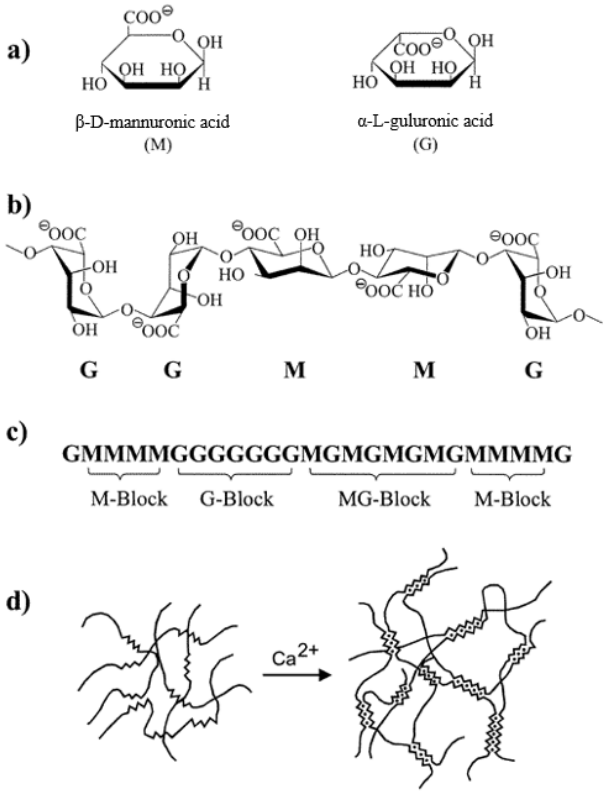

Figure 1.3.1: a) shows the monomers of alginate: (1-4)-linked β-D-mannuronic acid (M) and linked α-L-guluronic acid (G); b) shows the polymeric structure of alginate; c) shows the sequential arrangement of the different blocks; d) shows gelation of alginate with calcium resulting in formation of "egg-box" structure. Adapted from [84] with some modifications.

Alginate's excellent gelling properties can be exploited in cell encapsulation technology. By mixing sodium alginate with noncytotoxic concentrations of certain divalent cations, the cross-linking will result in a three-dimensional shape with viable cells embedded in noncytotoxic conditions[3]. For a long time, calcium has been the divalent ion of choice for cross-linking in microencapsulation since it is already present in body fluids. However, calcium can cause osmotic swelling of the capsules that lead to increased permeability, destabilization, and eventually rupture of the gel. This is explained by Ca^{2+}'s higher affinity towards some chelating agents, such as phosphate and citrate, as well as an interchange between Ca^{2+} and the non-gelling

ions Na^{+} and Mg^{2+} within the membrane[15, 83]. The addition of a polycation layer, such as Poly-L-lysine (PLL), can increase the stability, but this coat has shown to be the main component responsible for fibrotic overgrowth[15, 83].

The leakage of calcium has led to the exploration of other gelling ions in the formation of microspheres, and both strontium and barium have been investigated in the further development of microspheres. In theory, Sr^{2+} and Ba^{2+} ions have a higher affinity for G-rich alginate, but barium is considered toxic in high doses. A mixture of calcium and barium as gelling ions has led to the development of the Trondheim Alginate Microcapsule (TAM), more commonly named as the Ca/Ba Bead. The beads are gelled with a solution of 1 mM barium ions and 50 mM calcium ions, where even the low concentration of barium have shown to have an impact on the gel strength and the stability of the microsphere[8, 85, 86].

Several free hydroxyl and carboxyl groups are present along the glucose backbone of alginate. This makes the polymer susceptible to chemical modifications to alter the physicochemical properties, such as solubility and hydrophobicity. Chemical modifications can be performed through various techniques like sulfation, oxidation, or grafting. Sulfation involves chemical modification of the hydroxyl groups. Sulfated alginate has shown to be hemocompatible due to its similarity to heparin, which is widely used as an anticoagulant[87].

β-glucan and alginate have in common being naturally occurring polysaccharides. Many developed microspheres consist of an alginate core gelled with calcium. Whereas β-glucan induce stimulation through dectin-1, alginate has also been investigated for its immunostimulating properties. Since alginate can vary in composition, its sequential arrangement will decide which receptors that are involved in cell activation. Otterlei et al. demonstrated that high-M (85% M) and poly-M (99% M) were able to stimulate human monocytes to induce a TNF production similar to LPS, while G-blocks did not show such activity. This showed that alginate may also represent PAMPs like LPS, and result in activation of cells.[88]. Flo et al. further investigated poly-M and, based on their results, suggested that cell activation happened through the PRRs TLR2 and TLR4[89]. Even though G-blocks were not able to induce effects seen for poly-M, it cannot be concluded that high-G alginate is not a potent inducer of cell activation and cytokine secretion. Yamamoto et al. have looked at the induction of cytokine secretion from murine macrophages by alginate oligomers (<10 repetitive units), where G-oligomers were observed to have an ability to induce cytokine secretion (but levels were less than for M-oligomers)[90]. Even though alginate used in microbead formation has a high G content making the gel more stable, microbeads can get destabilized in the form of calcium leakage, further causing leakage of alginate. If such leakage can cause an inflammatory response, it could be a contributor to the fibrotic overgrowth. More importantly, if such leakage causes training of monocytes, the monocytes become long-term activated and can cause non-resolving inflammation, leading to the formation of fibrotic tissue around the microsphere.

1.3.2 Cholesterol crystals

Cholesterol is an organic compound which, among other things, is an important component of cellular membranes, and participate in the transport of fatty acids in the body[91, 92]. Accumulation of cholesterol within the arterial wall is a hallmark of the pathogenesis of atherosclerosis. As cholesterol accumulates within the arterial wall and contributes to plaque formation, cholesterol may crystallize. The cholesterol crystals (CC) are sharp-edged, reflecting the potential to penetrate biological membranes and thereby cause plaque

rupture. Plaque rupture can cause luminal thrombosis and further cause myocardial infraction and stroke[92]. CC have been reported to induce complement-dependent cytokine release[93] by activating complement via the classical pathway with amplification via the alternative pathway. The cytokine release was shown to be in a complement-dependent manner, where inhibition of C3 resulted in a >90% reduction of cytokines like TNF, IL-6, IL-8, and MCP-1. The fact that complement and coagulation can cross-talk, CC have been investigated for their potential in activating the coagulation cascade. Gravastrand et al. have shown that CC can induce coagulation activation by complement-dependent expression of monocytic tissue factor[94].

oxLDL has been identified as a possible trigger for trained immunity connected to atherosclerosis[74]. Since CC have showed to induce activation of complement and coagulation and are endogenous components contributing to atherosclerosis, their inflammatory potential could be further explored. Investigating their ability to induce trained immunity can contribute to a better understanding of atherosclerosis, and the development of a clinic strategy for treatment. As some of the inflammatory potential also is understood, including CC as positive controls in experiments can also contribute to explore and describe other danger components' ability to trigger an inflammatory response.

1.4 *In vitro* models

1.4.1 The human whole blood model

Blood contains proteins and cells of the immune system, and it can be used as an incubation solution for microspheres to study their biocompatibility. In 2002 Mollnes et al. developed a lepirudin-based whole blood model of inflammation to study the role of complement in inflammation induced by *Escherichia coli* (*E. coli*)[95]. Based on this model, Rokstad et al. have introduced a whole blood assay that analyzes the initial inflammatory potential of different microspheres, making it possible to distinguish them in their ability to activate the immune response. The assay cannot tell us whether a microsphere is biocompatible or not, but it can provide information about inflammatory differences that are not possible to reveal in an overgrowth study in animals. These combined strategies are used as tools to develop biomaterials with a high degree of biotolerability (without cellular overgrowth) and safety, to achieve functional microencapsulated pancreatic islets implantation.

The whole blood assay uses fresh, human whole blood together with an anticoagulant. Using an anticoagulant can affect the intercommunication between the effector systems of complement and coagulation; therefore, it is essential to use an anticoagulant that affects as few effector molecules as possible. Lepirudin is a specific thrombin inhibitor, blocking the formation of thrombin from prothrombin, and has no impact on the coagulation cascade upstream thrombin, nor the complement system[8, 95]. By incubating microspheres in anticoagulated whole blood, they can be evaluated *in vitro* under identical conditions. Activation of the complement and coagulation system, leukocytes, and cytokines can further be analyzed and indicate a microsphere's capability to trigger an inflammatory response.

Several microspheres have been tested in the whole blood model to explore their inflammatory potential, for example TAM (Ca/Ba Beads and further designated as A) beads and capsules of alginate coated with poly-L-lysine (AP)[11, 12]. AP has shown to initiate inflammatory responses during the 4 hours of incubation in the whole blood model, as well as being covered in fibrotic tissue after implantation. A, on the other

hand, has shown to have a low inflammatory potential, suggesting that it is perceived as inert. However, this microsphere did not do it well in overgrowth studies in non-human primates[14] and with variable outcome in rodents depending on the models used mice[8]. Microbeads have further been developed to investigate if it is possible to make microspheres that induce an even lower response than A in the whole blood assay, and not being susceptible to fibrotic overgrowth. For example, Vegas and Bochenek et al. have shown that it is possible to develop materials that stay fibrosis free for at least six months in rodents and non-human primates[56]. As A and AP have shown opposite effects in *in vitro* studies, they can be used as negative and positive control microspheres, respectively. Of note, unpublished data by the Trondheim group in a rodent model of fibrosis (C57/BL6) exploring a modified A bead containing sulfated alginate (SA bead) has also shown to be fibrosis free after 2-14 weeks intraperitoneal transplantation (Coron and Kjedsbu et al.). By exploring these materials in parallel *in vitro* models would contribute to increased understanding of the relations between the *in vivo* outcome and the contributing factors that can be explored by *in vitro* model systems.

Figure 1.4.1 shows my own unpublished data from whole blood experiments conducted during my specialization project in autumn 2019. 11 novel microbeads were tested for their ability to induce inflammation, where the figure below show the outcome of the ones depict for further testing in the present work in longitudinal *in vitro* studies. The alginate bead containing sulfated alginate, SA, showed in several cases to be low-inflammatory in the whole blood model, as well as, not being susceptible to fibrotic overgrowth in rodents. However, induction of prothrombin and VEGF were surprisingly high compared to A and AP, suggesting that sulfate influences their induction. This was further explored in this work, but is presented in Figure A.1.1 in Appendix A on page i due to conflicting results compared to those shown in Figure 1.4.1, and lack of time to further investigate. While the SA bead show reduced complement protein TCC and overall lower cytokine induction (with exception of VEGF), the differences between the A and SA bead are still minor. Still, these beads show very different outcome of fibrosis in the C57BL/6 mice model. An *in vitro* model that could distinguish between these bead types and predict the *in vivo* outcome would be representing a step-forward for the field of biomaterial development.

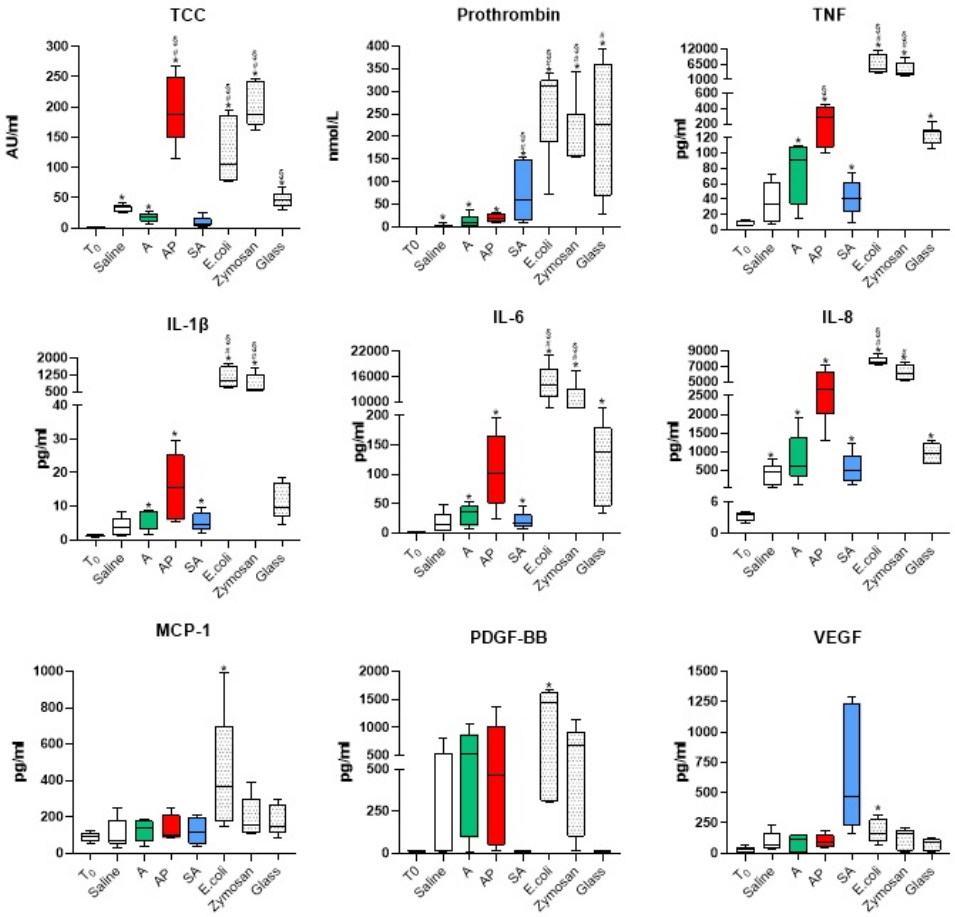

Figure 1.4.1: Terminal complement complex (TCC), prothrombin, and selected cytokines in plasma from anticoagulated whole blood after 240 minutes incubation of alginate microspheres. Induced by T_0 and negative control saline (white); negative control bead A (green); SA-bead (blue); positive control microcapsule (red); and positive controls of *E. coli*, Zymosan and glass (black spotted). Data are expressed in min to max box plot with median value of five donors. Significant values are given as $P<0.05$ compared to T_0 (*), saline (#), and A (§).

1.4.2 2D and 3D cultivation

Cell culturing is used to grow cells in an artificial environment and is a valuable tool to reveal biophysical and biomolecular mechanisms that explain cell behavior *in vivo*[96, 97]. Experimental models based on cell culturing have for over a century been conducted in 2D and have advanced the understanding behind cellular responses. Traditional *in vitro* cell culturing is based on cell-adherence to a surface, typically of glass or polystyrene, which provides mechanical support for the cell, and creates a monolayer of cells[97]. When cells grow in a monolayer, they have unlimited access to the medium's content, such as nutrients and oxygen[98].

2D culturing has its limitation by causing changes in cell morphology, disturbances in the interaction network between extracellular and cellular environments, and loss of diverse phenotype[98]. 3D culturing aims to provide environmental conditions more like *in vivo* by, among other things, allow interaction with surrounding cells, which can be fundamental for cell behavior. By allowing cell-to-cell contact, cells can aggregate and

form cell clusters, creating a gradient of nutrient access and waste buildup[97]. Models of 3D culturing can be divided into several groups based on its preparation type: suspension cultures on non-adherent plates, cultures in concentrated medium or gel-like substances, or cultures on scaffold[98]. In cell cultures on scaffold, cells can migrate within a scaffold made of, for example, alginate. The scaffold mimic *in vivo* conditions by providing attachment sites contributing to mechanical support and allow cells to grow in 3D[99]. Suspension cultures on non-adherent plates allow cells to interact with other components in the suspension[98], for example, by incubating biomaterials together with cells to observe their interaction. The human whole blood model is based on 3D culturing by incubating microspheres in whole blood in non-adherent vials of polypropylene. Using non-adherent and low activating vials, the inflammatory response induced by the biomaterial can be observed and be of a more reliable character due to low background activation and by providing culturing conditions more like *in vivo*. Figure 1.4.2 shows a schematic representation of 2D monolayer cell culturing and 3D cell culturing in suspension.

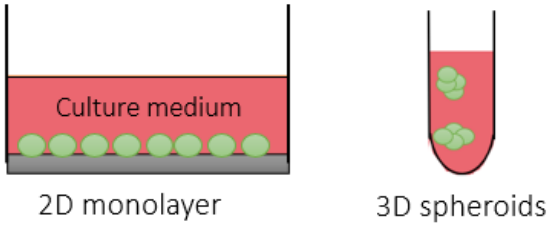

Figure 1.4.2: A schematic representation of 2D and 3D cell culturing. In 2D cell culturing, the cells adhere to the surface of the plate constructing a monolayer. In 3D suspension culturing, the cells are cultered in a non-adherent material making the cells cluster in spheroids and allows cell-to-cell interaction like *in vivo*. Based on drawing by Edmondson et al.[100]

1.4.3 Development of a long-term *in vitro* model

In microencapsulation technology, there is still a search for a microsphere being biotolerable. Several microspheres tested in the whole blood model show promise by being low-activators of the initial inflammatory responses[11]. However, the same microspheres after transplantation in non-human primates are susceptible to fibrotic overgrowth[14], which impairs the function of the membrane and is a result of an undesirable inflammatory response causing chronic inflammation. This contributes to reflect the limitation of the whole blood model to predict the long-term outcome of fibrosis. The conflicting results address that we do not necessarily have a prerequisite to predict if the microspheres are low-inflammatory or not only based on the whole blood model as an inflammatory response may be amplified after 4 hours. It is an excellent model for the prediction of initial inflammatory responses and allows weeding out the early activating microspheres so that those of more potential can further be tested in long-term studies. But, to get an improved and more comprehensive understanding of the inflammatory responses after 4 hours, a new model based on long-term *in vitro* incubation is needed. By employing knowledge obtained from the whole blood model, and keeping mechanisms essential for activation, the model can provide a better prediction of long-term overgrowth studies.

An approach is to incubate the microspheres for two weeks while screening for chosen cytokines at selected time points. This may provide a more comprehensive picture of the inflammatory responses that the microspheres initiate over time. The major differences from the human whole blood model will be incubation conditions in form of time and milieu. In the human whole blood model, the microspheres are, as earlier described, incubated in anticoagulated whole blood for 4 hours. To avoid disturbance of the intercommunication between effector molecules, Lepirudin is used as an anticoagulant, which only impairs the latest steps of the coagulation cascade: the formation of thrombin. In the long-term *in vitro* experimental model, the microspheres are incubated in culture medium supplemented with heat-inactivated serum and peripheral blood mononuclear cells (PBMCs). Using serum and PBMCs as incubation conditions excludes coagulation proteins, red blood cells and platelets. Heat-inactivation of serum contributes to inactivate complement proteins and prevents lysis of cells mediated by complement in the cell culture. However, to still maintain the opsonization effect of complement and to mimic the impact of other proteins that might adsorb over longer times, as during transplantation, a 24-hour step with incubation of microspheres in active serum can be included in studies of solid materials. This step might serve to maintain one of the advantages provided in the human whole blood model, and the long-term *in vitro* experimental model will maintain one of the important activation steps leading to cytokine release. Together, the new model will provide conditions for studying the response of leukocytes to the foreign material without amplification through the coagulation- and partly the complement system. The cytokine release can provide information about how the cells interact with microspheres over time, and depending on the choice factors to study, could serve to increase the understanding of monocytes' and macrophages' contribution to both induce inflammation or the material's impact on avoiding fibrosis.

3D culturing is better at mimicking *in vivo* conditions, and the long-term *in vitro* model should, therefore, be performed in a 3D experimental model. However, using 2D culturing as well can enlighten similarities and differences in cell behavior between the models. Figure 1.4.3 shows a simplified illustration of a possible experimental procedure of long-term incubation of microspheres and soluble alginate. The thought of using different types of soluble alginate in the model is to investigate if a possible leakage of alginate from the microspheres can contribute to the inflammatory response. Microspheres and soluble alginate are incubated with PBMCs in 2D by using polystyrene cell culture plates and in 3D by polypropylene vials. Supernatants are then collected at selected time points and analyzed, for example, by multiplex to investigate cytokine induction. These results combined with results of the human whole blood model, such as shown in Figure 1.4.1, can contribute in the understanding of biomaterials ability to develop or avoid fibrosis.

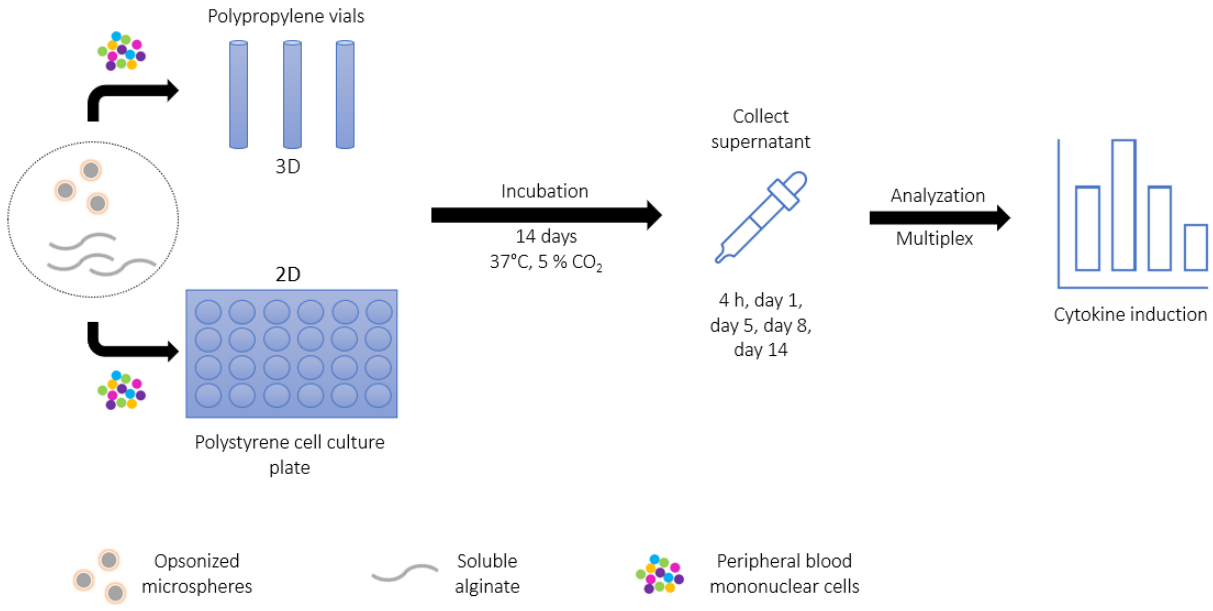

Figure 1.4.3: Illustration of an experimental procedure of a long-term *in vitro* model of microspheres and soluble alginate. Microspheres and solube alginate are incubated with PBMCs in a 2D and 3D experimental model over a period of 14 days. Supernatants are collected at selected time points for cytokine analyzation with multiplex.

1.5 Aims of the study

A long-term *in vitro* experimental model that take into account the beneficial effects of the human whole blood providing the possibility of materials surface activation, could add a new aspect to long-term *in vitro* evaluations. Additionally, an advantage with the human whole blood model is the increased contact between cells and materials that is obtained by a dynamic system (and 3 dimensions), and by use of low-reacting incubation tubes of polypropylene. Another aspect that is unexplored are the possible training effects of alginate and cholesterol crystals. The aims of the current study was therefore:

- establish a long term *in vitro* model of PBMCs taking into account the importance of protein absorption/surface opsonization
- compare the cultivation conditions in 2D and 3D to secretion patterns of selected cytokines
- explore if soluble alginates and cholesterol crystals are inducers of trained immunity

2 Materials and methods

2.1 The alginate microspheres and soluble alginates

In this study, three different empty alginate microspheres were tested in a long-term *in vitro* experimental model in an attempt to develop a system design for a broader evaluation of their inflammatory potential. The microspheres were made by Abba Elizabeth Coron and Joachim Kjedsbu in the period between July 2018 and June 2019 at the Department of Biotechnology (IBT) at the Norwegian University of Science and Technology (NTNU). Table 2.1.1 shows an overview of the composition of each microsphere, and the formation procedures described in previous work are cited.

Table 2.1.1: An overview of the type of microspheres used in the study. w/v shows the weight to volume for each microsphere given in percent; alginate solution describes the type of alginate(s) used in the formation of each microsphere; gelling solution describes concentration and type of gelling ion(s) used; coat shows the addition of polycation; the last column shows where to find the description of the formation process.

Microsphere	w/v [%]	Alginate solution [w/w]	Gelling solution	Coat	Formation description
A	1.8	UPLVG	50 mM $CaCl_2$ + 1 mM $BaCl_2$		[12, 101]
AP	1.8	UPLVG	50 mM $CaCl_2$	0.1 % PLL	[12, 101]
SA	1.8	20% SA (UPMVG, DS=0.8), 80% UPLVG	50 mM $CaCl_2$ + 1 mM $BaCl_2$		[21]

A contains G-rich alginate and is gelled with a mixture of calcium and barium. AP contains G-rich alginate and is gelled with calcium and coated with 0.1% Poly-L-Lysine. The SA-bead contains a mixture of 20% sulfated G-rich alginate with a sulfation degree (DS) of 0.8 and 80% G-rich alginate, which is gelled with a mixture of calcium and barium.

The microspheres were aliquoted and washed before use. A solution of microbeads solved in NaCl (12 mL, sterile 0.9%, B. Braun, Melsungen, Germany) were aliquoted by transferring 1 mL of suspension to 10 sterile Eppendorf tubes giving a concentration of approximately 0.5 mL microbeads in a total volume of 1.2 mL NaCl. Further, new aliquots were made by washing the microspheres twice with NaCl and dilute them in a total volume of 5.5 mL NaCl, before transferring 500 µL of suspension to 10 sterile Nunc vials of polypropylene (1.8 µL, Nunc A/S, Denmark). Supernatant (400 µL) was removed giving approximately 50 µL microspheres in a total volume of 100 µL NaCl.

Four different soluble alginates were investigated to explore potential inflammatory effects from alginate leakage. Two of the soluble alginates as used in the formation of the three microspheres. Table 2.1.2 elaborate the type of alginate both used in the formation of microspheres and soluble alginate solutions. Pronova UPLVG, UPMVG, and UPLVG were purchased from FMC Biopolymer AS (Novamatrix, Norway). Poly-M was from samples made of*Pseudonomas aeruginosa (P. aeruginosa*) at IBT at NTNU as described in [102].

Table 2.1.2: Type of alginates used in the formation of solutions and microspheres, where the abbreviation is explained in comment. M_w represents the molecular weight given in kilodaltons, G represents the fraction of guluronic acid given in percent.

Name	Batch no.	M_w [kDa]	G [%]	Comment
Pronova UPLVG	BP-0907-02	237.0	68	Ultra Pure, Low Viscosity, high G
Pronova UPMVG	FP-505-01	235.0	66	Ultra Pure, Medium Viscosity, high G
Pronova UPLVM	FP-701-06	235.0	45	Ultra Pure, Low Viscosity, high M
Poly-M	-	243.7	6	high M

The four soluble alginate solutions consisted of UPLVG, UPLVM (LVM), UPMVG with a sulfatation degree of 0.8 (SA), and PolyM (HM). The solutions were prepared by dissolving 180 mg of alginate in sterilized water (10 mL) under constant stirring (4°C) giving a concentration of 1.8 w/v %. The solutions were sterile filtered (50 mL, Nalgene^{TM} Rapid-Flow^{TM} Conical Tube Filter, 0.2 µL aPES membrane, Thermo Fisher, 564-0020) before use.

2.2 Long-term *in vitro* experimental model

A long-term *in vitro* experimental model was conducted to further investigate the differences in activation of inflammation of microspheres and soluble alginate types over a period of 14 days. The microspheres and soluble alginates were incubated with peripheral blood mononuclear cells (PBMCs) and serum-containing culture medium. The culture medium used was Roswell Park Memorial Institute (RPMI) 1640 (Sigma Aldrich, St. Louis, MO, USA R8758) supplemented with gentamicin (0.02 µg/mL, sanofi-aventis Norge AS, Lysaker, Norway, 453130), glutamine (0.3%, GLUTAMAX I, Life Technologies Europe BV, Netherlands, 35050038), and 2-30%(depending on the experiment) heat-inactivated (h.i.) A+ serum (made locally from blood donors at St. Olavs hospital). The incubation was assessed in two different layouts with PBMCs from the same donor: in vials of polypropylene (1.6 mL, Corning Incorporated, Salt Lake City, UT, USA, 4411) and on flat-bottom cell culturing plates with 24 wells of polystyrene (3.4 mL, Corning Incorporated, Kennebunk, ME, USA, 3524). The experiment was in total conducted four times with PBMCs from four different donors.

2.2.1 Opsonization of micropsheres

Before long-term incubation, the microspheres were opsonized by incubation (37°C, 24 h) with human A+ serum (500 µL) and sterile Dulbecco's phosphate-buffered saline modified with $MgCl_2$ and $CaCl_2$ (100 µL, Sigma Aldrich, St. Louis, MO, USA, D8662) under constant rotation. After 24 hours, the supernatant (approximately 650 µL) was replaced by RPMI (500 µL).

2.2.2 Isolation of Periheral Blood Mononuclear Cells

PBMCs were isolated from human A+ buffy coats donated from healthy volunteers at the blood bank of St. Olavs Hospital in Trondheim. Sterile Dulbecco's phosphate-buffered saline (DPBS, 100 ml, Sigma Aldrich, St. Louis, MO, USA, D8537) and Lymphoprep^{TM} (50 mL, Alere Technologies AS, Oslo, Norway, 1116508)

were preheated (37°C). Buffy coat (A+) was diluted approximately 1:5 in DPBS in a T75 flask (75 cm^2, Corning Incorporated, Oneonta, NY 13820 USA, 430641U). The solution was aliqouted in four tubes (50 mL, Sarstedt AG & Co. KG, Nümbrecht, Germany, 62.547.254) giving a volume of approximately 35 mL in each tube. Preheated Lymphoprep^{TM} (10 mL) was added carefully to the bottom of each tube with a pipette. The tubes were centrifuged (1800 rpm, 25 min), and the layer of mononuclear cells were removed with a pipette and split into two 50 mL tubes. The tubes were centrifuged (2000 rpm, 10 min), decanted, and the pellets were resuspended in preheated Hanks buffered salt solution (HBSS, 1 mL, Sigma Aldrich, St. Louis, MO, USA, H9269), before more HBSS was added (19 mL). The tubes were centrifuged (800 rpm, 8 min), and the washing procedure with HBSS was repeated twice. After the third wash, the pellets were resuspended in HBSS (1 mL) and transferred to one tube. HBSS was added to approximately 20 mL. 20 µL was withdrawn from the solution and added to Isoton water (10 mL, ISOTON II Diluent, Beckman Coulter Inc., CA, USA, 8448011) with two drops of Zap-oglobin (Nerliens Meszansky A.S, Oslo, Norway, 7546138) for cell counting, while the tube was centrifuged (800 rpm, 8 min) and decanted. The cell pellet was resuspended in RPMI.

2.2.3 Experimental layout

The long-term incubation model was in total conducted four times. Results from pilot studies led to some experimental differences between the setups. All experiments were performed in 2D and 3D.

Experiment 1

Figure 2.2.1 shows a simplification of the experimental layout of experiment 1.

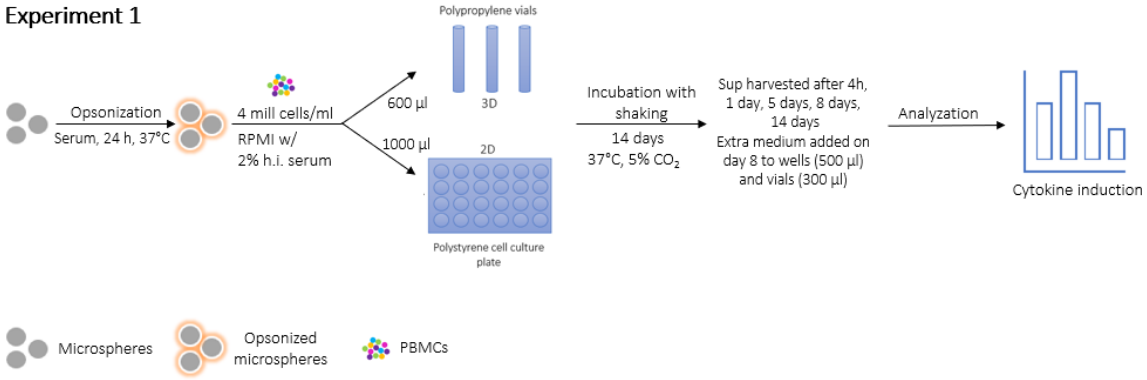

Figure 2.2.1: Illustration of the experimental setup of experiment 1 of the long-term *in vitro* experimental model.

The cell pellet from isolation of PBMCs was diluted in RPMI supplemented with 2% h.i. A+ serum, so that an addition of 0.1 mL gave an concentration of 4 million cells/mL. Due to incorrect calculations, the conditions of 2D had an final concentration of 7 million cells per milliliter. The 2D model had a total volume of 1000 µL and the 3D model had a total volume of 600 µL. The experimental layout consisted of 8 different condition: 2 medium controls, LPS (100 ng/mL, Invivogen, *E. coli* 0111-B4), cholesterol crystals (CC) (500 µg/mL, made from ultrapure cholesterol as earlier described in [93], Sigma Aldrich, C3045), opsonized

cholesterol crystals (CC ops) (500 µg/mL), A (50 µL), AP (50 µL) and SA (50 µL).

Supernatant from each condition was harvested (200 µL) at selected time points for cytokine analyzation by multiplex. The sampling time points were chosen to be after 4 hours, 1 day, 5 days, 8 days, and 14 days. In 2D, supernatants were harvested from the same well for each condition at the selected time points. In 3D, supernatants were harvested from a new vial for each condition at the selected time points. A simple illustration of the setups is shown in Figure B.1.1 in Appendix B on page xi. Supernatant (200 µL) was centrifuged (1000 g, 5 min, 4 °C) and 170 µL was frozen down (-20 °C) for further analyzation by multiplex.

On day 8, extra medium (500 µL RPMI w/ 2% h.i. A+ serum) was added to conditions of the 2D culture. Due to evaporation, extra medium (300 µL) was added to the vials for harvesting at day 14 in the 3D culture model.

Experiment 2

Figure 2.2.2 shows a simplification of the experimental layout of experiment 2.

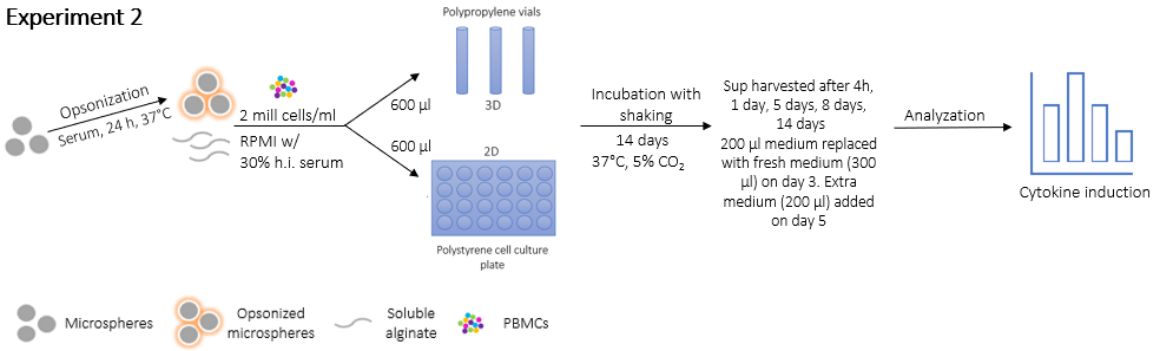

Figure 2.2.2: Illustration of the experimental setup of experiment 2 of the long-term *in vitro* experimental model.

Soluble alginates of UPLVG, LVM, SA, and HM with different concentrations (1500, 750, and 375 µg/mL) were added as conditions in experiment 2. CC ops was removed as condition. The concentration of PBMCs was reduced, and the concentration of serum was increased. The total volume of the 2D model was reduced so that the total volume of the two models were equal. Microspheres and soluble alginates, in total 15 conditions, were incubated with 2 million cells/mL in RPMI supplemented with 30% h.i. serum for 14 days. In 2D, supernatants were harvested from the same well for each condition at the selected time points. Harvested supernatant was replaced with fresh medium (200 µL). In 3D, supernatants were harvested from a new vial for each condition at the selected time points. A simple illustration of the setups is shown in Figure B.2.1 in Appendix B on page xii.

On day 3, 200 µL medium was replaced with fresh medium (300 µL) for all conditions. Due to evaporation, extra medium (200 µL) was added on day 5 after harvesting, both for conditions in 2D and 3D.

Experiment 3 and 4

Figure 2.2.3 shows a simplification of the experimental layout of experiment 3 and 4.

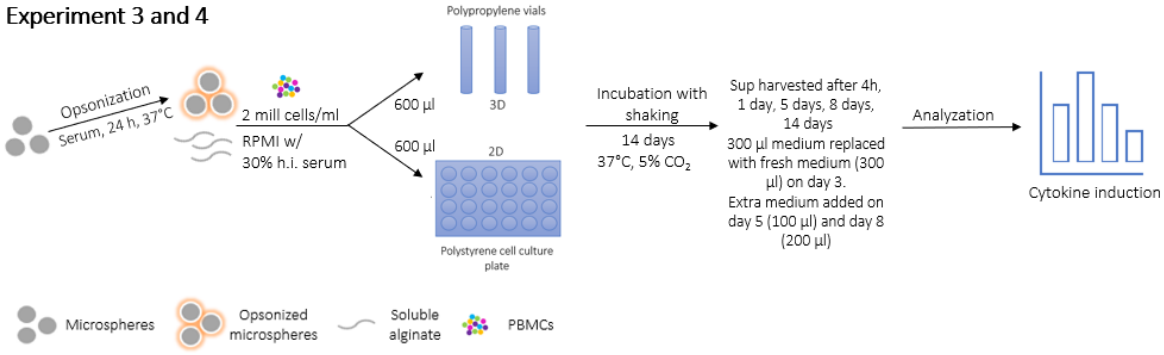

Figure 2.2.3: Illustration of the experimental setup of experiment 3 and 4 of the long-term *in vitro* experimental model.

The concentration of soluble alginates was reduced in experiment 3 and 4. Microspheres and soluble alginates (500, 100 and 10 µg/mL) were incubated with 2 million PBMCs/mL in RPMI supplemented with 30% h.i. serum for 14 days. Supernatants of the conditions LPS, CC, A, AP, and SA were harvested from the same well/vial in both 2D and 3D for each time point. Supernatants of the soluble alginates were harvested from a new well/vial for each time point. A simple illustration of the setups is shown in Figure B.3.1 in Appendix B on page xiii.

On day 3, 300 µL medium was replaced with fresh medium (300 µL) for all conditions. Due to evaporation, extra medium was added on day 5 (100 µL) and day 8 (200µL) to all conditions in both 2D and 3D.

2.3 Trained immunity

An *in vitro* experimental model of trained immunity was performed to investigate if soluble alginates and CC were able to induce trained immunity in human monocytes. The experimental model was based on Bekkering et al.'s review on optimizing a protocol for training period and resting time of monocytes before restimulation[60]. The experimental model was performed three times: experiment 1 and 2 with identical procedure, and experiment 3 with some modifications.

Experiment 1 and 2

Figure 2.3.1 shows a simplification of the experimental procedure of experiment 1 and 2.

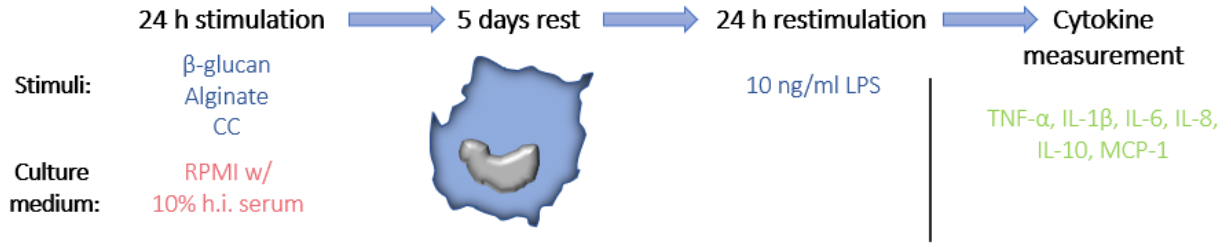

Figure 2.3.1: Experimental procedure used for training of monocytes in experiment 1 and 2. Monocytes were stimulated for 24 hours in indicated culture medium and washed, before resting for 5 days. On day 6, cells were restimulated with LPS (10 ng/mL) for 24 hours and supernatant was harvested for measurement of selected cytokines.

PBMCs were isolated like described in section 2.2.2. Cells (2 million cells/mL) diluted in RPMI supplemented with 10% serum were added to a flat-bottom 24-well plate. After incubation (37 °C, 1.5 h, 5% CO_2), adherent monocytes were selected by washing with HBSS (1 mL, 37 °C) three times. Monocytes were incubated in a total volume of 500 µL of: culture medium only, as negative control; β-glucan (10 µg/mL, SigmaAldrich, St Louis, MO, USA, G5011) as positive control; soluble alginates of UPLVG, LVM, SA and HM at different concentrations (500, 100, 10 µg/mL); and cholesterol crystals (CC) (1000 and 500 µg/mL).

After 24 hours of incubation (37 °C, 5% CO_2), the cells were washed once with HBSS (1 mL) and incubated for 5 days with RPMI. On day 3, medium (300 µL) was refreshed. After 5 days of incubation, the cells were restimulated with LPS (10 ng/mL) and incubated for 24 hours, before supernatants were harvested and frozen (-20 °C) before further cytokine analyzation. As a negative control, the cells were restimulated with RPMI after 5 days of resting, and supernatants were harvested and frozen after 24 hours of incubation.

Experiment 3

Experiment 3 followed the overall protocol as experiment 1 and 2, but with some modifications: the culture medium was now a mix between h.i. A+ serum (8%) and untreated A+ serum (2%); an additional dose of β-glucan was added (20 µg/mL); an additional stimuli of LPS was added (10 ng/mL and 1 ng/mL); and the restimulation concentration of LPS (2 ng/mL) was decreased. Figure 2.3.2 shows a simplification of the experimental procedure of experiment 3.

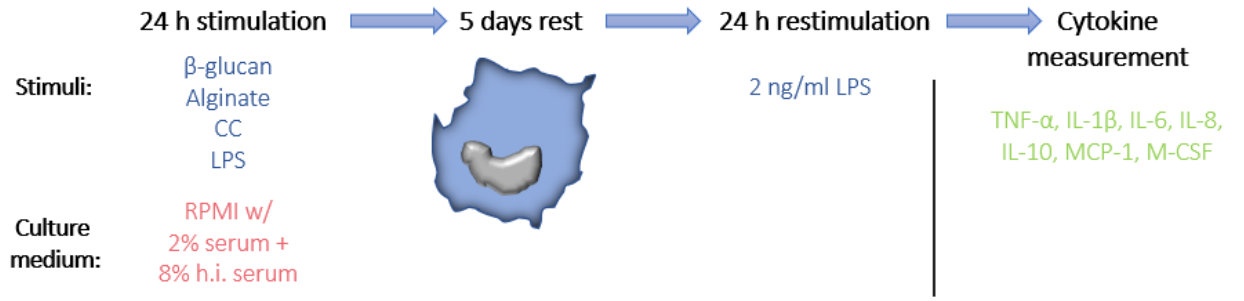

Figure 2.3.2: Experimental procedure used for training of monocytes in experiment 3. Monocytes were stimulated for 24 hours in indicated culture medium and washed, before resting for 5 days. On day 6, cells were restimulated with LPS (2 ng/mL) for 24 hours and supernatant was harvested for measurement of selected cytokines.

2.4 Multiplex

Multiplex analysis using the Bio-Plex® assays built around the Luminex xMAP technology was used to quantify the amount of various cytokines from harvested supernatants of long-term *in vitro* incubation trained immunity experiments. Multiplex techniques allow simultaneous measurement of several analytes in a single assay[103]. In the Bio-plex™ Multiplex system are fluorescently dyed magnetic microspheres with distinct color code or spectral address for each cytokine used, in order to separate between the different analytes in the suspension. The assay employs capture antibodies against the cytokine of interest that are covalently bound to the beads. Cytokine of interest will bind to the capture antibody, and after wash, a biotinylated detection antibody is added to create a sandwich-complex. Finally, a detection complex is added, phycoerythrin works as the fluorescent indicator. Biomarkers bound to the surface of the beads are measured by a flow cytometry-based plate reader that uses two lasers[104]. Figure 2.4.1 shows an illustration of the Bio-plex sandwich-immunoassay.

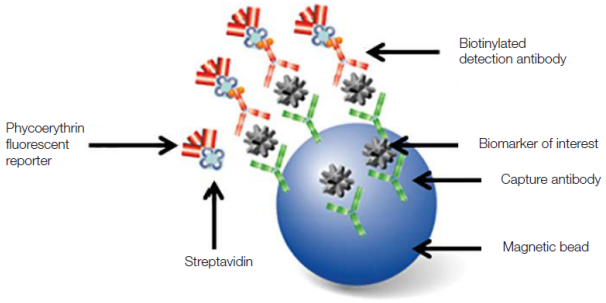

Figure 2.4.1: Illustration of Bio-plex sandwich immunoassay. The beads are coated with capture antibody, each for a specific biomarker of interest. Sample is added and the biomarker of interest, will bind to capture antibody. Biotinylated detection antibody is added and will bind to target antigen forming a sandwich complex. Detection complex is formed with addition of streptavidin-phycoerytrhin where phycoerythrin (PE) serves as a fluorescent indicator. Adapted from [104].

2.4.1 Cytokines

Plasma samples were analyzed using the multiplex assay Bio-plex™ Pro Human Cytokine Assay (Bio-Rad Laboratories, Inc.), where beads from single kits were combined to conduct the assay. This study focused on TNF (171B5026M), IL-1β (171B5001M), IL-6 (171B5006M), IL-8 (171B5008M), IL-10 (171B5010M), MCP-1 (171B5021M), M-CSF (171B6013M), GRO-α (171B6007M), and IL-1ra (171B5002M). The assay was performed in accordance with the manufacturers protocol using half amount of beads as recommended.

Diluted beads (50 µL) were added to each well of the assay plate before it was washed two times with Bio-plex wash buffer (100 µL). The plasma samples (50 µL) were added and the plate was incubated on a shaker (850 ± 50 rpm, 30 min, room temp.). The plate was washed three times (100 µL), before detection antibody solution (25 µL) was added, and the plate was incubated on shaker (850 ± 50 rpm, 30 min, room temp.) The washing procedure was repeated, and Streptavidin-PE solution was added (50 µL) before the plate was incubated on shaker (850 ± 50 rpm, 10 min, room temp.). The washing procedure was repeated, assay buffer (125 µL) was added and the plate was shaken (850 ± 50 rpm, 30 sec). The concentration of analyte bound to each bead was quantified using a Bio-Plex 200 Reader (Bio-rad Laboratories Inc.).

2.5 Ethics

The experiments were done in accordance with the Rec Central approval 2009/2245 approval for work with human whole blood or blood bank for basic experiments. The consent has been given under the prerequisite of sorting no information about the donors, an has been following these guidelines

3 Results

3.1 Long-term *in vitro* experimental model

3.1.1 Experiment 1

Pilot studies was conducted as a part of the development of the long-term *in vitro* experimental model. As a try out, microspheres were incubated with 4 million PBMCs/mL in RPMI supplemented with 2% heat inactivated (h.i.) serum for 14 days. Supernatants were harvested at selected time points: after 4 hours, 1 day, 5 days, 8 days and 14 days. Figure 3.1.1 shows the experimental layout of experiment 1. Due to incorrect calculations, the concentration of PBMCs used in the 2D culture was at 7 million cells/mL.

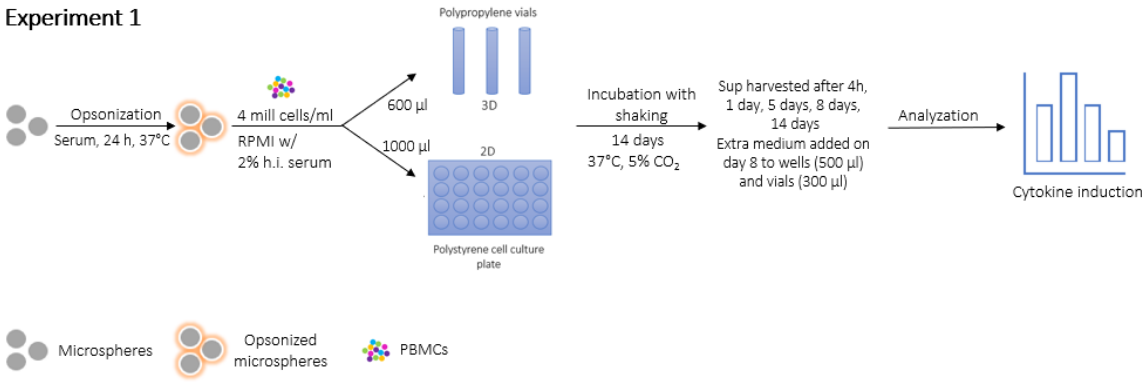

Figure 3.1.1: Shows the experimental setup of experiment 1 of the long-term *in vitro* experimental model.

The induction of several cytokines, TNF, IL-1β, IL-6, IL-8, IL-10, MCP-1, M-CSF, GRO-α, IFN-γ, IP-10, MIP-1α, IL-17A, VEGF, IL-13, TGF-β1, TGF-β2, TGF-β3, relevant for fibrosis were measured by Bio-plex from supernatants of 4 hours, 1 day, 5 days and 8 days. TNF, IL-1β, IL-6, IL-8, IL-10, MCP-1, M-CSF, and GRO-α were chosen to be tested in further experiments and are presented in the subsequent results. The rest are presented in Figures A.2.1 to A.2.9 in Appendix A on page i. The selection was based on the secreted levels induced by the different conditions compared to the medium control. Figures 3.1.2 to 3.1.9 show a comparison of the induced concentration (pg/mL) of the cytokines in 2D and 3D. The plotted data are given in Tables C.1.1 to C.1.8 in Appendix C on page xiv.

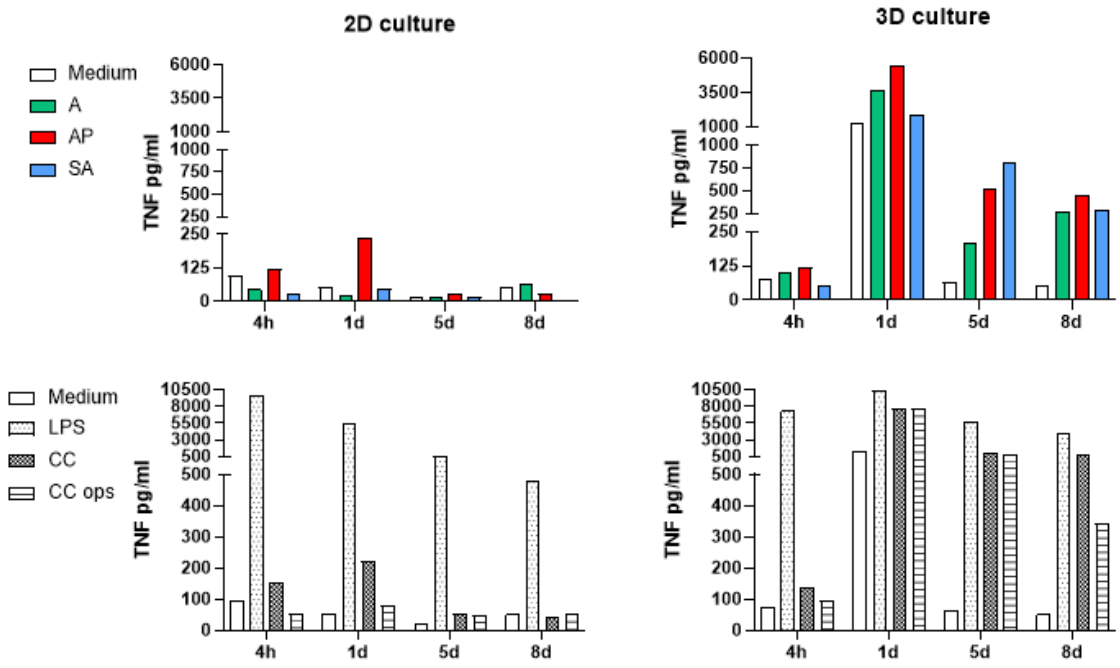

Figure 3.1.2: Comparison of the secretion of TNF in 2D and 3D culturing induced by the microspheres A (green), AP (red), and SA (blue); and the controls LPS (black spotted), CC (black squared) and opsonized CC (black striped).

The induction of TNF was observed to be higher in the 3D culture model as compared to the 2D culture for all the conditions at every time point. The level of the cytokine peaked on day 1 before decreasing at consequent time points. This was most notable for the 3D culture but could be partly observed for the 2D culture as well. The comparison between the microspheres showed that under the 2D conditions, the most prominent cytokine induction was apparent for the AP microsphere, whereas the A and SA microsphere induced lower amounts. Under the 3D conditions, the TNF induction was more comparable, but AP showed to induce the highest TNF level after 4h, day 1 and day 8. At day 5, SA induced the highest amount. For the controls, there was also observed elevated induction of TNF following incubation with CC in 3D.

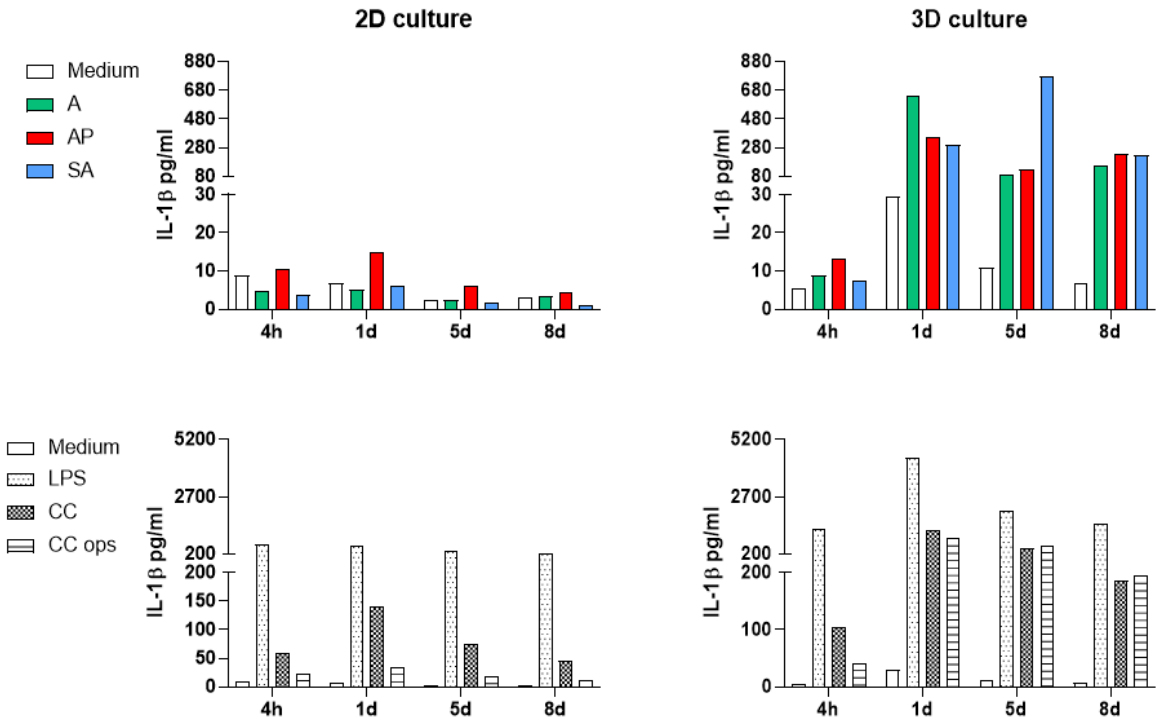

Figure 3.1.3: Comparison of the secretion of IL-1β in 2D and 3D culturing induced by the microspheres A (green), AP (red), and SA (blue); and the controls LPS (black spotted), CC (black squared) and opsonized CC (black striped).

The induction of IL-1β was higher in 3D vs. 2D for all conditions at every time point. More specific, while in the 2D condition the amounts of IL-1β were between 2-15 pg/mL, the amounts in the 3D condition reached the levels of 200-700 pg/mL. Only after 4h incubation (which is similar to the incubation time in the human whole blood model), the levels were comparable. In 3D, the amount of IL-1β found in the medium decreased after day 1, while the level amount after the addition of microspheres remained on a similar level or higher at day 5 and 8. In 2D, the level induced by the microspheres was observed to decrease at day 5 and day 8 like medium.

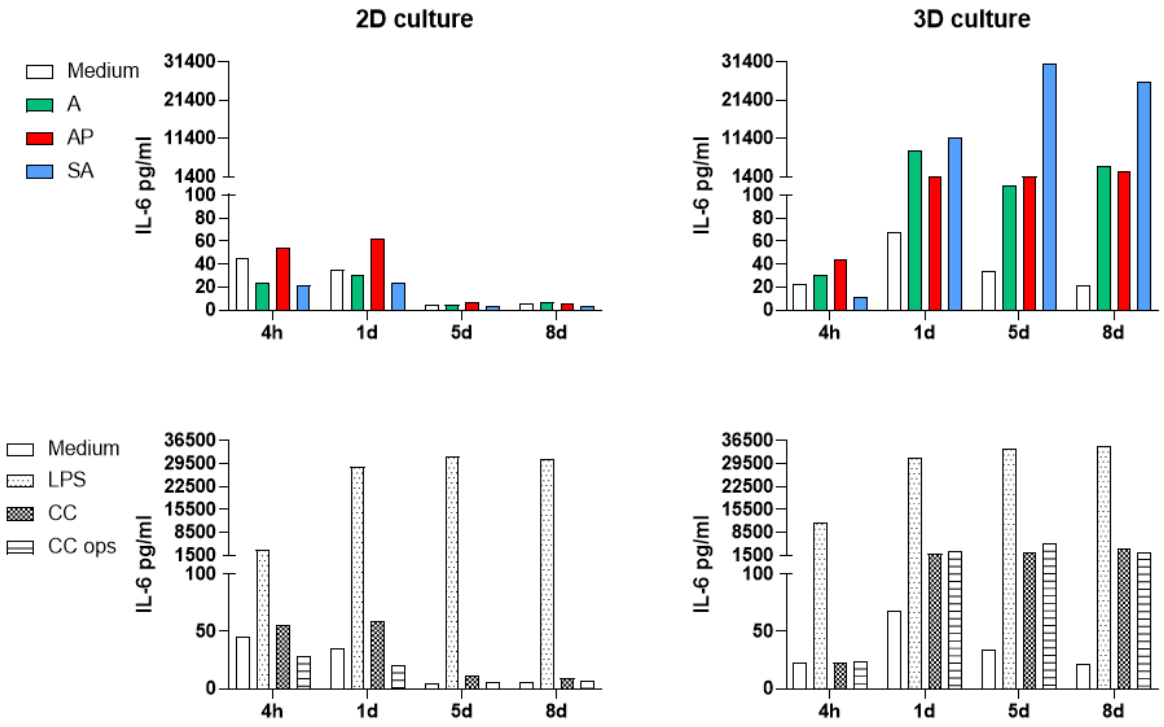

Figure 3.1.4: Comparison of the secretion of IL-6 in 2D and 3D culturing induced by the microspheres A (green), AP (red), and SA (blue); and the controls LPS (black spotted), CC (black squared) and opsonized CC (black striped).

The induction of IL-6 was also higher in the 3D culture model after day 1 for all conditions. In 2D, the level was stable from 4 hours to day 1 with the amounts measured between 20-60 pg/mL for the microspheres, and 30-60 pg/mL for the CC. Further on, the levels decreased for all conditions except for LPS. LPS also reached comparable amounts in 2D vs. 3D from day 1, peaking at around 30000 pg/mL. In 3D, the amounts of cytokines during incubation with microspheres were between 1000-30000 pg/mL from day 1, and was either stabilized or increased at the next time points. Following incubation with CC, the amounts of IL-6 were around 1500 pg/mL. SA showed at several time points to induce the highest level of IL-6. For the medium, an opposite trend was observed with decreased amounts on day 5 and 8.

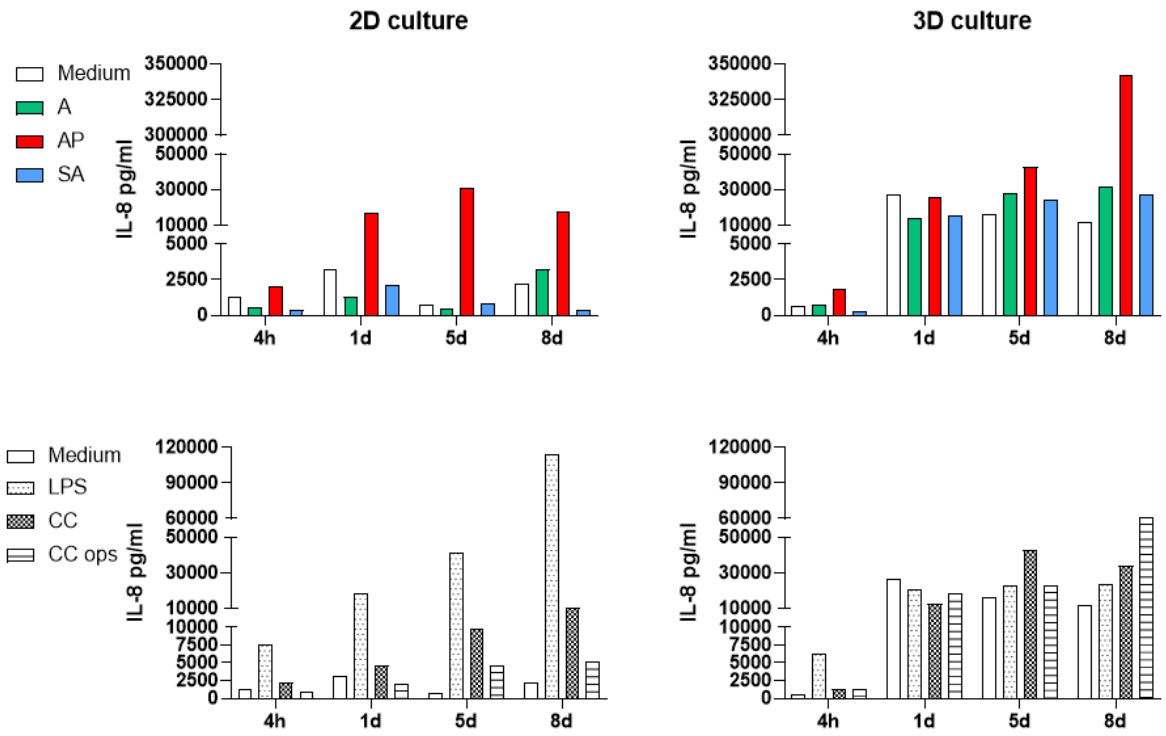

Figure 3.1.5: Comparison of the secretion of IL-8 in 2D and 3D culturing induced by the microspheres A (green), AP (red), and SA (blue); and the controls LPS (black spotted), CC (black squared) and opsonized CC (black striped).

The induction of IL-8 was observed to be higher in the 3D vs. 2D culture model for the A and SA beads from day 1, as well as the medium control (in 2D reaching amounts between 500-3500 pg/mL, in 3D reaching amounts between 10000-35000 pg/mL). AP showed a similar induction in 2D and 3D from 4 hours towards day 5, reaching amounts of 10000-30000 pg/mL in 2D, and between 25000-350000 pg/mL in 3D. LPS showed a higher induction in 2D than 3D, at day 8 reaching the amount of 114000 pg/mL in 2D vs 23000 pg/mL in 3D. For CC, the levels of IL-8 at most reached the amounts of 10000 pg/mL under 2D conditions, while under 3D between 20000 and 60000 pg/mL. In 3D, the cytokine level gradually increased or stabilized for the time points day 5-8 for the various conditions, while medium peaked at day 1 before decreasing.

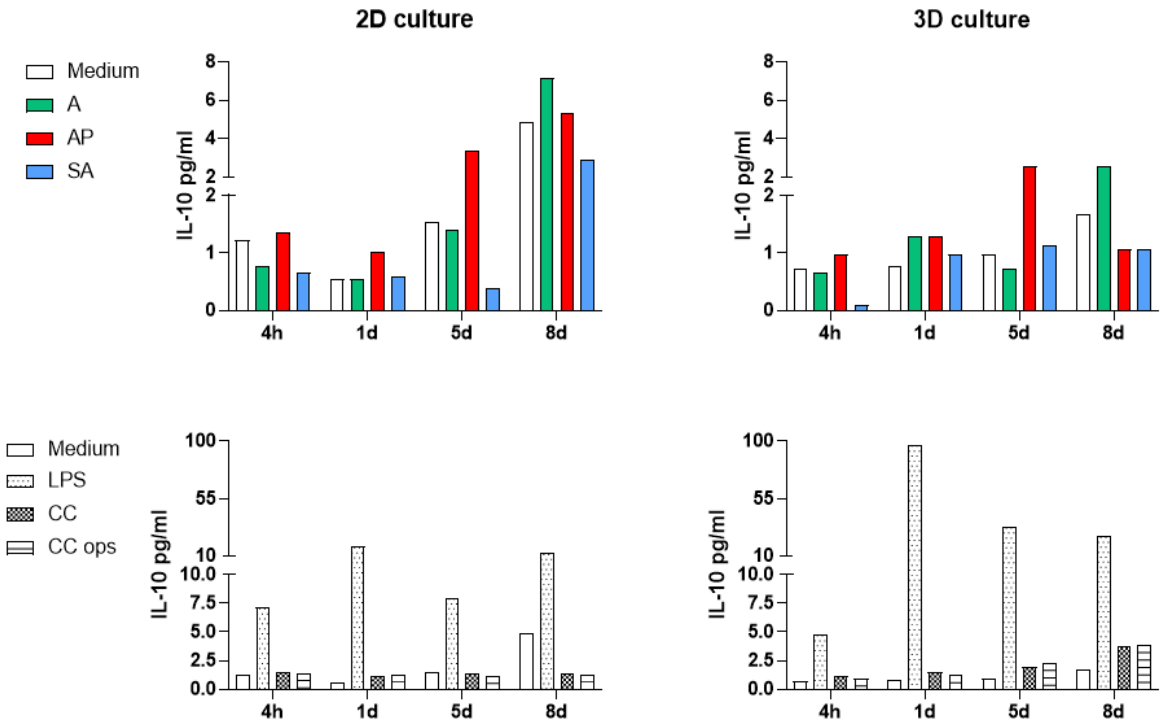

Figure 3.1.6: Comparison of the secretion of IL-10 in 2D and 3D culturing induced by the microspheres A (green), AP (red), and SA (blue); and the controls LPS (black spotted), CC (black squared) and opsonized CC (black striped).

The induction of IL-10 was observed to be higher in the 2D vs. 3D culture model and to increase with time for medium, A, AP, and SA. More specific, at day 8, the amounts of IL-10 reached in the 2D culturing conditions the amounts of 3-6 pg/mL, while between 1-2 pg/mL under 3D conditions. For LPS and CC, the tendency was the opposite, with the highest induction during the 3D condition. The induced levels were of low concentration for all conditions, thus the differences were overall small. Apart from LPS, all conditions showed a similar trend like medium and induced cytokine secretion around its level.

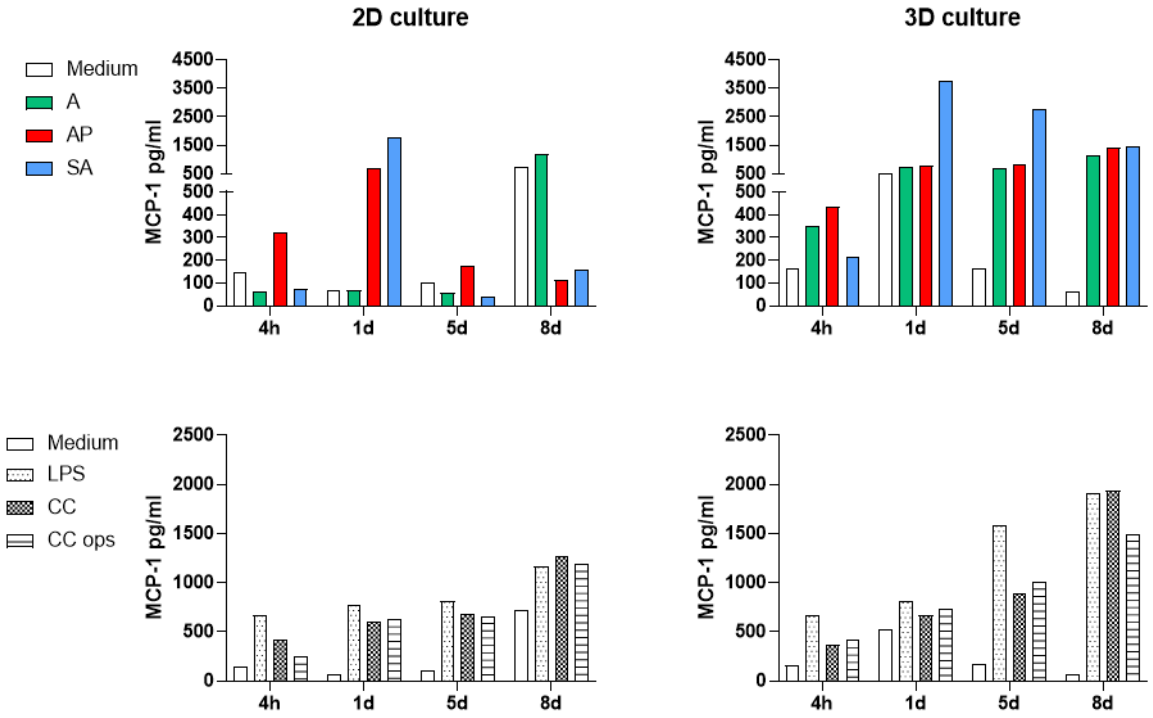

Figure 3.1.7: Comparison of the secretion of MCP-1 in 2D and 3D culturing induced by the microspheres A (green), AP (red), and SA (blue); and the controls LPS (black spotted), CC (black squared) and opsonized CC (black striped).

The induction of MCP-1 was observed to be higher in the 3D vs. 2D culture model for several conditions. More specifically, for the microspheres under 2D condition, the amounts of MCP-1 were between 40-1800 pg/mL, whereas in 3D between 300-3800 pg/mL. In 3D, peaked at day 1 before decreasing, while several other conditions showed a gradual increase for each time point. SA showed in both models to peak at day 1. For the controls, CC and LPS, only on day 5-8, there was a tendency of higher MCP-1 induction following the increase of the 3D conditions.

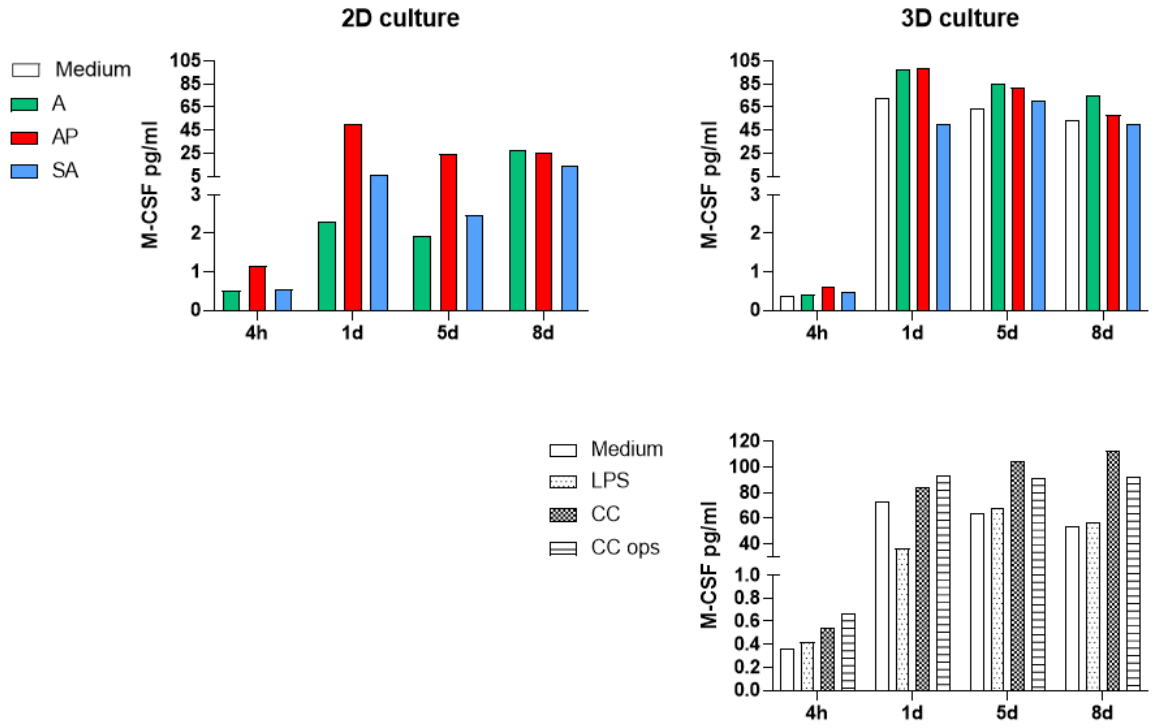

Figure 3.1.8: Comparison of the secretion of M-CSF in 2D and 3D culturing induced by the microspheres A (green), AP (red), and SA (blue); and the controls LPS (black spotted), CC (black squared) and opsonized CC (black striped).

The induced level of M-CSF was observed to be higher in the 3D vs. 2D conditions, as shown for the comparison between the microspheres. In 3D, the M-CSF induction induced by the microspheres peaked at day 1 with amounts around 50-100 pg/mL, before stabilizing or partly decreasing. In 2D, the M-CSF in most was 50 pg/mL. Several of the conditions induced a level similar to medium, as also was the case after the addition of CC or LPS under 3D cultivation conditions. The level of induced cytokine in medium, LPS, CC, and CC ops in the 2D model was not measured, so it was not possible to determine whether the microspheres gave rise to a similar level like medium control.

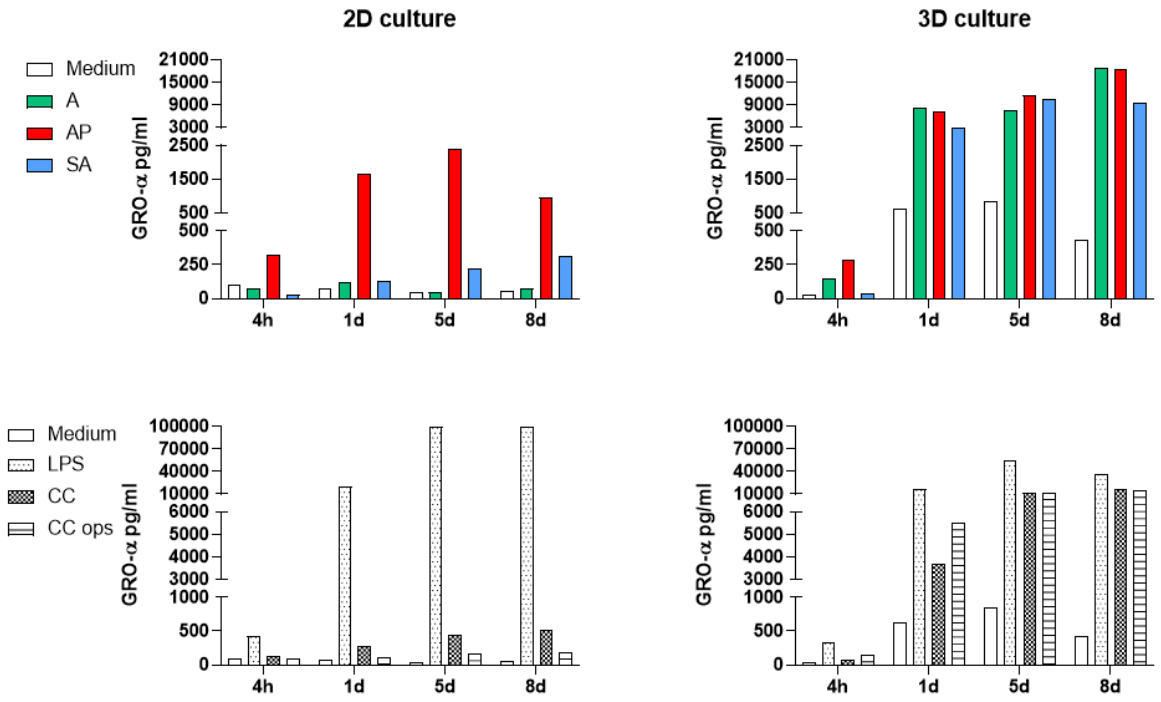

Figure 3.1.9: Comparison of the secretion of GRO-α in 2D and 3D culturing induced by the microspheres A (green), AP (red), and SA (blue); and the controls LPS (black spotted), CC (black squared) and opsonized CC (black striped).

The induced level of GRO-α was observed to be higher in the 3D vs. 2D model for several conditions. Under 2D conditions, for the medium control, A and SA, the amounts of GRO-α were between 40-300 pg/mL from day 1, while under 3D conditions, the same additives gave amounts of GRO-α between 500-19000 pg/mL. In 2D, AP showed a relatively high induction compared to the two microbeads, with amounts of GRO-α between 1500-2500 pg/mL as compared to 100-300 pg/mL by A and SA. In 3D, more comparable levels of secreted cytokine were observed for the microspheres.

Overall, several cytokines showed to be secreted at higher concentrations in the 3D culture model. In the 2D model, for some cytokines, the inflammatory potential of AP appears more distinct compare to the two microbeads. However, in the 3D model, for the same cytokines, the levels of AP are more comparable to A and SA, displaying another inflammatory potential of the microbeads than seen in 2D. Opsonized CC did not show any remarkable differences from CC, suggesting that opsonization did not have any specific effect of the induction of selected cytokines compared to CC. As a result, CC ops were removed as a condition for the next set up.

3.1.2 Experiment 2

Microspheres and soluble alginates were incubated with 2 million PBMCs/mL in RPMI supplemented with 30% h.i. serum for 14 days. Supernatants were harvested at selected time points: after 4 hours (only 3D), 1 day, 5 days, 8 days and 14 days. Figure 3.1.10 shows the experimental layout of experiment 2.

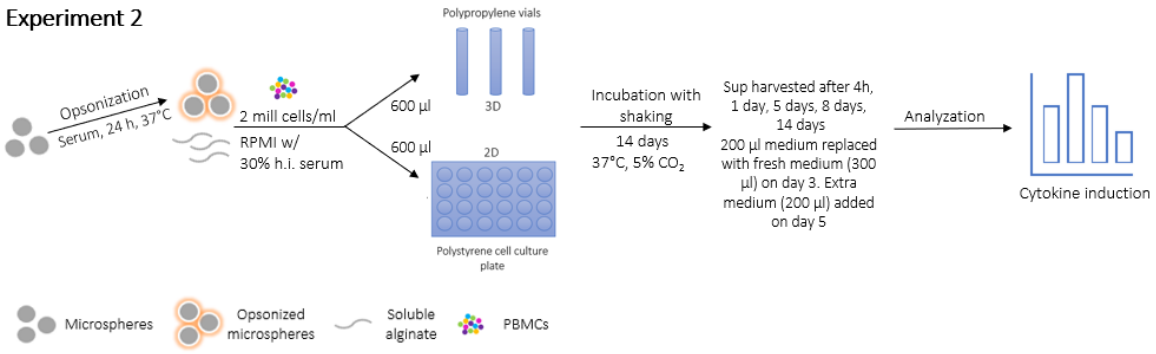

Figure 3.1.10: Shows the experimental setup of experiment 2 of the long-term *in vitro* experimental model.

The measurement of selected cytokines: TNF, IL-1β, IL-6, IL-8, IL-10, MCP-1, M-CSF, and GRO-α was based on results from experiment 1. Due to experimental error of keeping the 2D culture sterile, only supernatant from day 1 was measured. Figures 3.1.11 and 3.1.12 show a comparison of the induced concentration (pg/mL) of selected cytokines in 2D and 3D at day 1. Figures 3.1.13 to 3.1.20 show the induced concentration (pg/mL) in 3D for all time points. The plotted data are given in Tables C.1.9 to C.1.16 in Appendix C on page xvii.

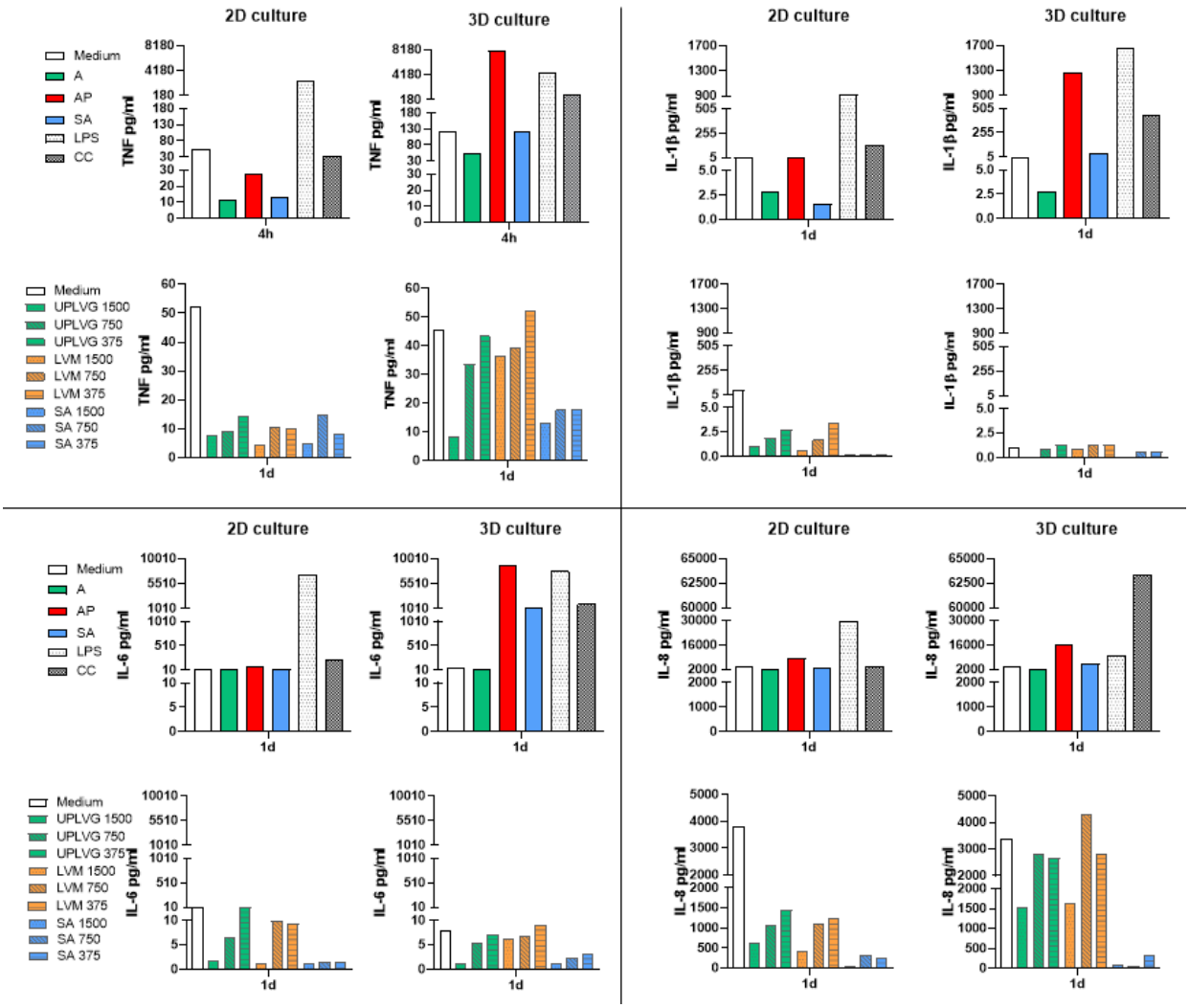

Figure 3.1.11: Comparison of secretion of selected cytokines in 2D and 3D after 1 day of culturing induced by the microspheres A (green), AP (red), and SA (blue); the soluble alginates UPLVG (G-rich alginate) (green), LVM (M-rich alginate) (orange), SA (sulfated alginate) (blue), with concentrations of 500 (spotted), 100 (diagonal lines) and 10 (straight lines) µg/mL; and the controls LPS (black spotted) and CC (black squared).

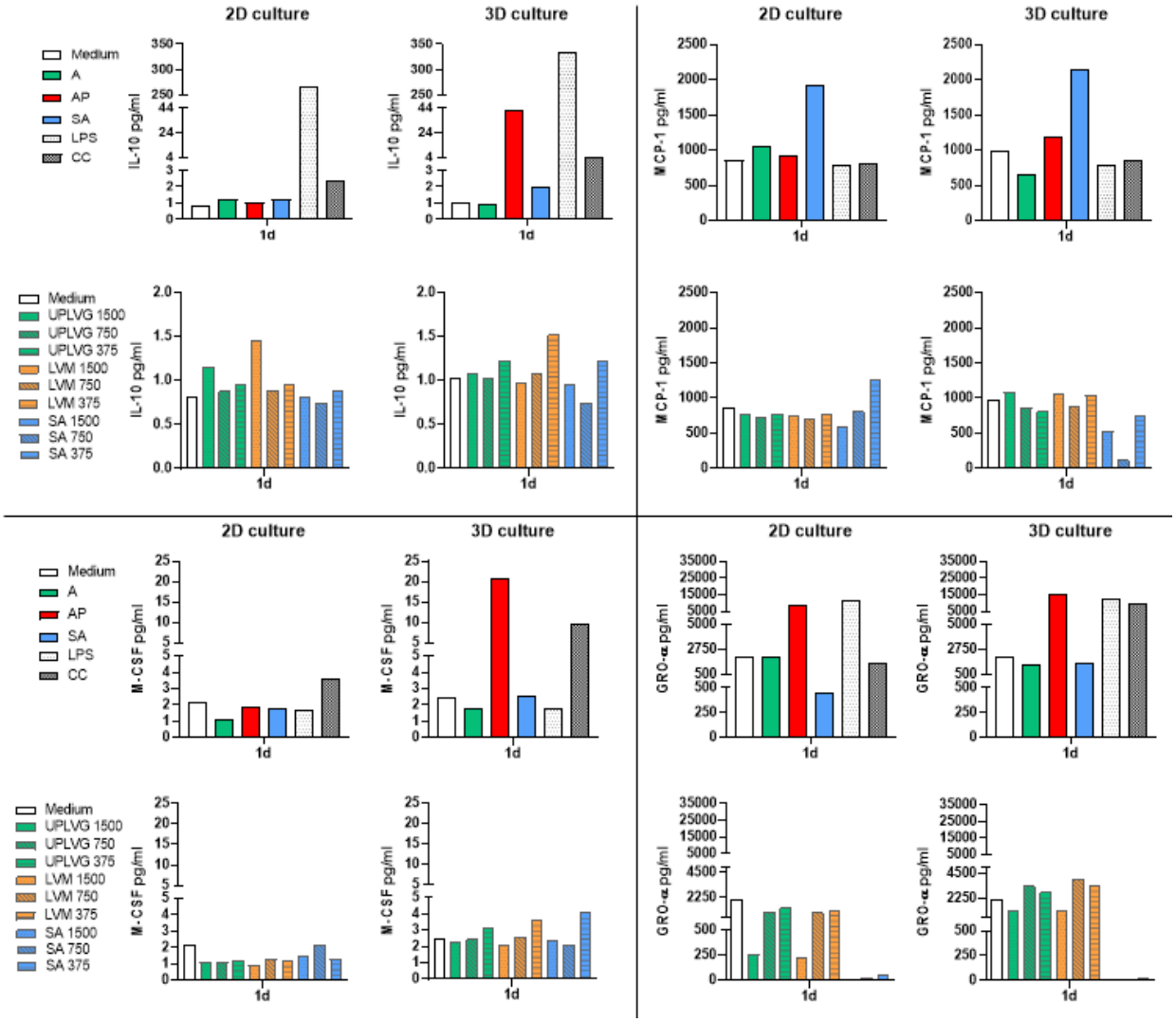

Figure 3.1.12: Comparison of the secretion of selected cytokines in 2D and 3D after 1 day of culturing induced by the microspheres A (green), AP (red), and SA (blue); the soluble alginates UPLVG (G-rich alginate) (green), LVM (M-rich alginate) (orange), SA (sulfated alginate) (blue), with concentrations of 500 (spotted), 100 (diagonal lines) and 10 (straight lines) µg/mL; and the controls LPS (black spotted) and CC (black squared).

The comparison of 2D vs. 3D on day 1, shown in Figures 3.1.11 and 3.1.12, showed that microspheres in 3D induced the highest cytokine level in several cases: TNF, IL-1β, IL-6, IL-10, MCP-1, and M-CSF. Except for MCP-1, AP showed to induce the highest concentration of the microspheres for all cytokines. SA showed to induce the highest concentration of MCP-1 in both 2D and 3D. The induction of all cytokines by LPS showed to be more or less unaffected by the 2D vs. 3D conditions. Except for MCP-1, CC induced the highest cytokine concentrations in 3D. The induction by the soluble alginates varied in 2D vs. 3D for each cytokine. The induction of TNF, IL-8, and M-CSF was higher in 3D. The induction of IL-1β, IL-6, IL-10, MCP-1, and GRO-α were more or less at the same level in 2D and 3D. Of note, all cytokines induced by the soluble alginates were, in most cases, observed to be around the level induced by medium only.

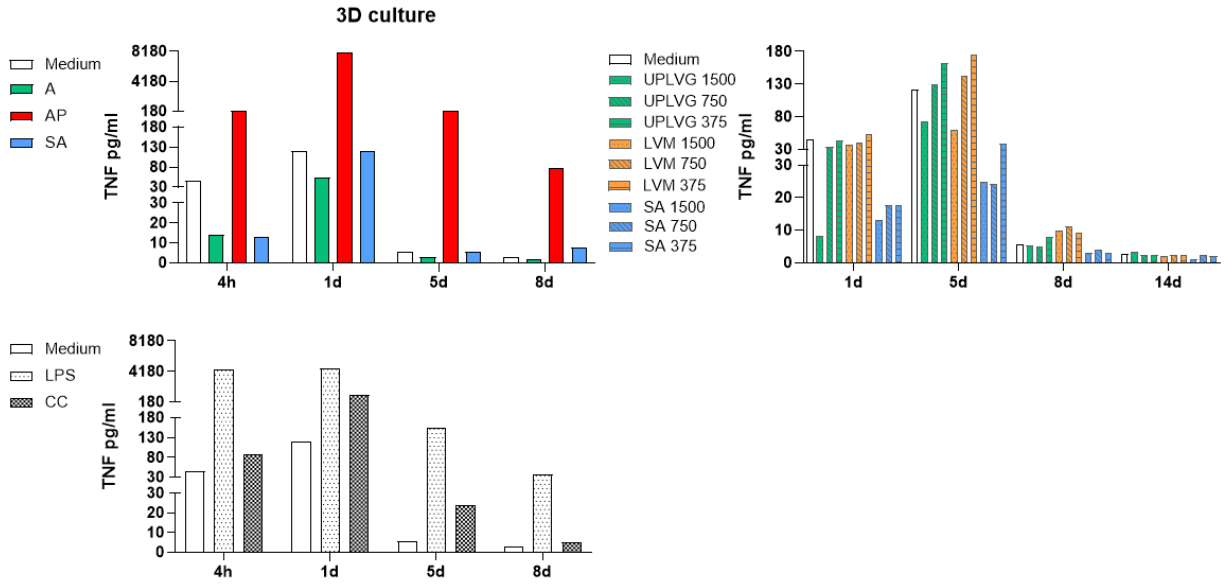

Figure 3.1.13: Secretion of TNF in 3D culturing induced by the microspheres A (green), AP (red), and SA (blue); the soluble alginates UPLVG (G-rich alginate) (green), LVM (M-rich alginate) (orange), SA (sulfated alginate) (blue), with concentrations of 500 (spotted), 100 (diagonal lines) and 10 (straight lines) µg/mL; and the controls LPS (black spotted) and CC (black squared).

The secretion of TNF peaked at day 1 for all conditions, before decreasing for the next time points. AP induced the highest amounts of TNF of the microspheres by inducing levels between 200-8000 pg/mL against 1-120 pg/mL induced by A and SA. The lowest concentrations of the soluble alginates UPLVG and LVM induced the highest TNF levels compared to SA after 4 hours and on day 1. However, the induced levels by UPLVG and LVM were not so different from the medium control. LPS and CC reached levels of 4500 and 1000 pg/mL, respectively.

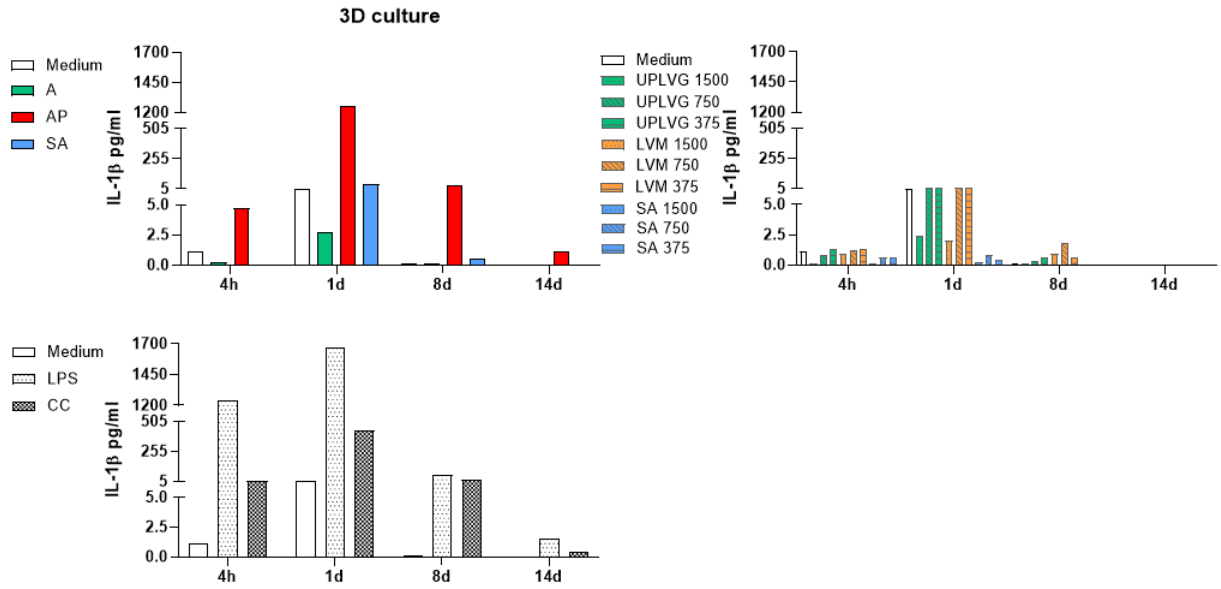

Figure 3.1.14: Secretion of IL-1β 3D culturing induced by the microspheres A (green), AP (red), and SA (blue); the soluble alginates UPLVG (G-rich alginate) (green), LVM (M-rich alginate) (orange), SA (sulfated alginate) (blue), with concentrations of 500 (spotted), 100 (diagonal lines) and 10 (straight lines) µg/mL; and the controls LPS (black spotted) and CC (black squared).

The induction of IL-1β peaked on day 1 for all conditions. AP induced a concentration of 1200 pg/mL against 2-42 pg/mg induced by A and SA. The lowest concentrations of the soluble alginates UPLVG and LVM inducted highest levels of IL-1β after 4 hours and on day 1. However, the induced levels were not so different from the medium control. LPS reached a level of 1700 pg/mL on day 1. CC showed a similar pattern like AP after 4 hours and on day 8, but on day 1, the induction by CC was a third of what was observed of AP, around 400 pg/mL.

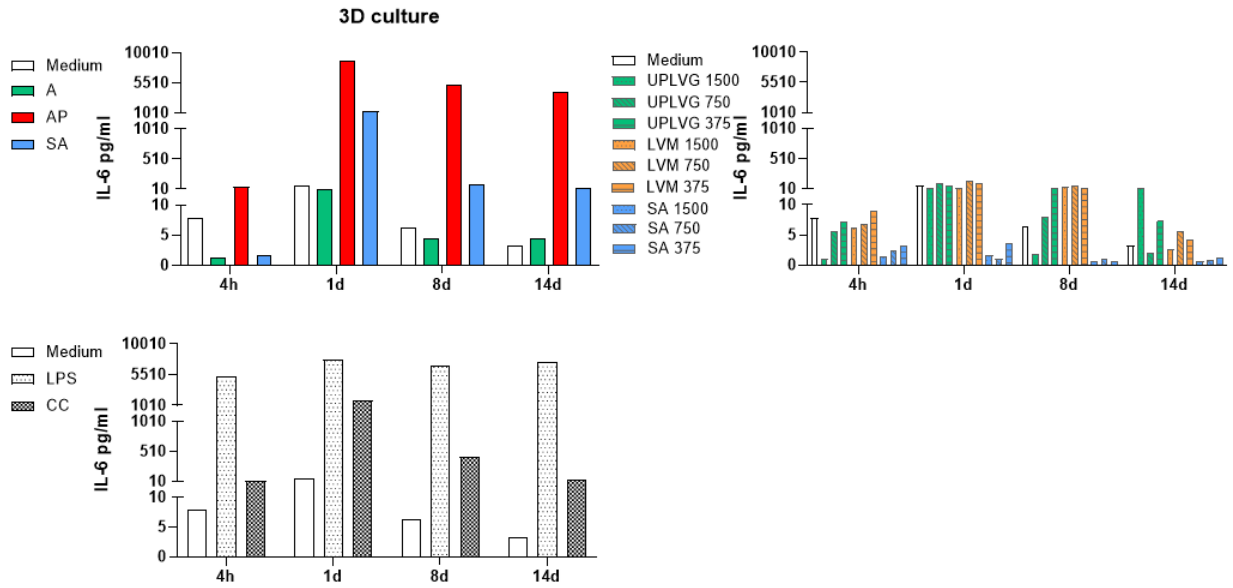

Figure 3.1.15: Secretion of IL-6 in 3D culturing induced by the microspheres A (green), AP (red), and SA (blue); the soluble alginates UPLVG (G-rich alginate) (green), LVM (M-rich alginate) (orange), SA (sulfated alginate) (blue), with concentrations of 500 (spotted), 100 (diagonal lines) and 10 (straight lines) µg/mL; and the controls LPS (black spotted) and CC (black squared).

The induction of IL-6 increased towards day 1 before decreasing for several conditions. A was relatively low compared to the other microspheres, and induced amounts around the level by the medium control. SA and AP peaked at day 1, with concentrations of IL-6 at 1200 and 8800 pg/mL, respectively. The soluble alginates of UPLVG and LVM induced higher levels than SA at every time point. LPS showed to induce a relatively stable level of IL-6 for each time point, varying between 5300-7700 pg/mL. CC reached 1700 pg/mL at day 1 before decreasing.

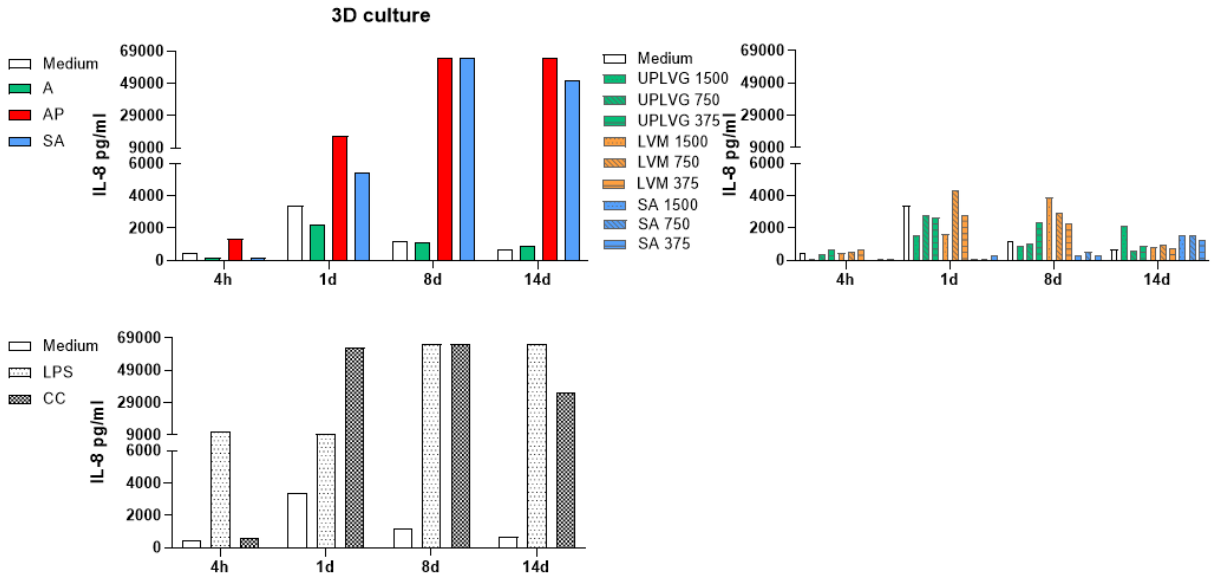

Figure 3.1.16: Secretion of IL-8 in 3D culturing induced by the microspheres A (green), AP (red) and SA (blue); the soluble alginates UPLVG (G-rich alginate) (green), LVM (M-rich alginate) (orange), SA (sulfated alginate) (blue), with concentrations of 500 (spotted), 100 (diagonal lines) and 10 (straight lines) µg/mL; and the controls LPS (black spotted) and CC (black squared).

The secretion of IL-8 increased towards day 8 for AP, SA, CC, and LPS. A peaked at day 1 together with the medium control before decreasing for the subsequent time points. The soluble alginates of UPLVG and LVM induced higher amounts of IL-8 compared to SA on day 1 and day 8. The level of IL-8 induced by SA increased for each time point from 4h towards day 14.

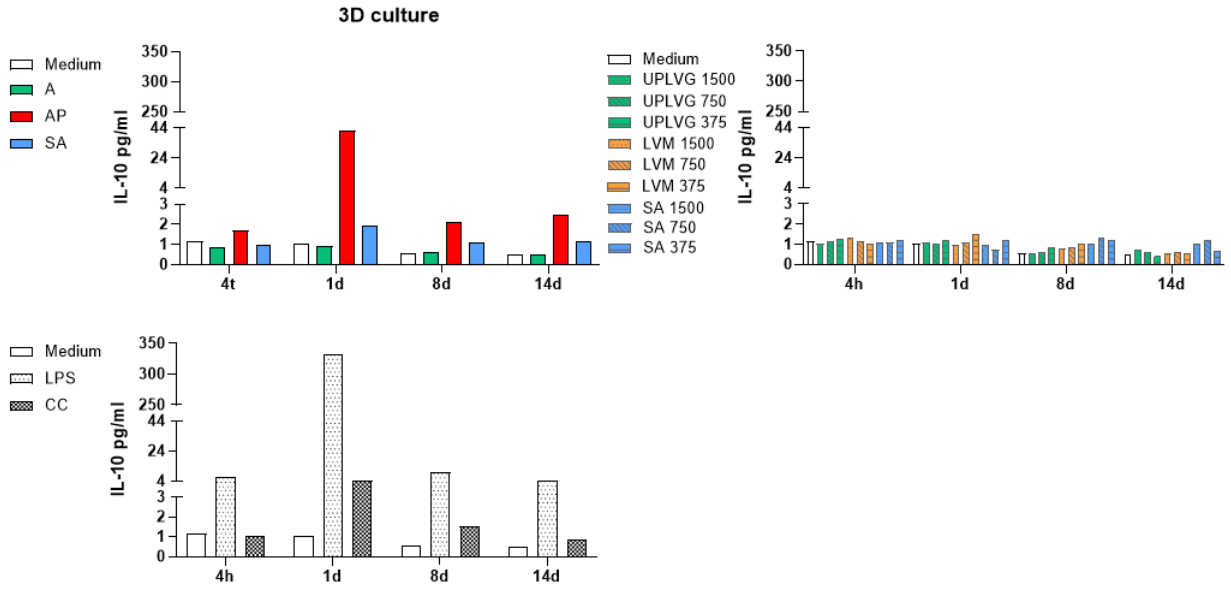

Figure 3.1.17: Secretion of IL-10 in 3D culturing induced by the microspheres A (green), AP (red), and SA (blue); the soluble alginates UPLVG (G-rich alginate) (green), LVM (M-rich alginate) (orange), SA (sulfated alginate) (blue), with concentrations of 500 (spotted), 100 (diagonal lines) and 10 (straight lines) µg/mL; and the controls LPS (black spotted) and CC (black squared).

The induction of IL-10 peaked on day 1 induced by A, AP, SA, LPS, and CC. Except for day 1, the microspheres induced a similar level of IL-10 like the medium control at concentrations between 0.5-3 pg/mL. The soluble alginates induced concentrations of IL-10 more or less like the medium control.

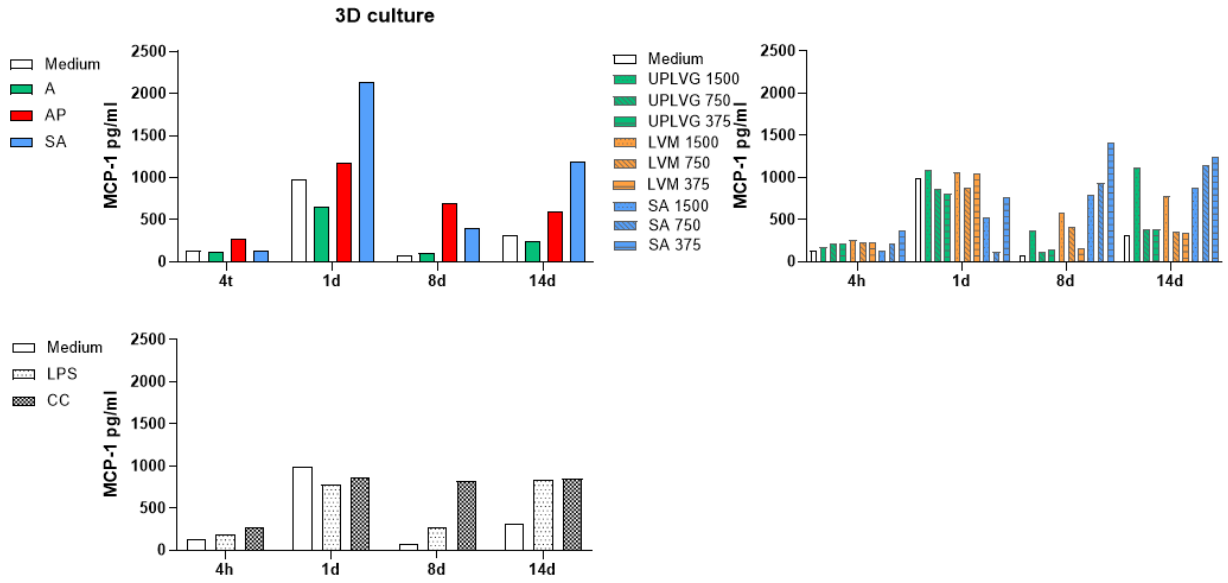

Figure 3.1.18: Secretion of MCP-1 in 3D culturing induced by the microspheres A (green), AP (red) and SA (blue); the soluble alginates UPLVG (G-rich alginate) (green), LVM (M-rich alginate) (orange), SA (sulfated alginate) (blue), with concentrations of 500 (spotted), 100 (diagonal lines) and 10 (straight lines) µg/mL; and the controls LPS (black spotted) and CC (black squared).

The induction of MCP-1 by the microspheres peaked on day 1, where SA induced the highest level at 2100 pg/mL against 600-1200 pg/mL induced by A, AP, and the medium control. The amounts of MCP-1 decreased towards day 8, but increased again towards day 14, again SA inducing the highest level. The soluble alginates UPLVG and LVM peaked together with the medium control on day 1. From day 8 and towards day 14, the induced of MCP-1 by SA became more prominent and showed a concentration-dependent induction, where the induction increased with decreasing SA concentration. The induction by LPS and CC was more or less stable from day 1, keeping a level around 800 pg/mL (except from LPS on day 8 at 250 pg/mL.

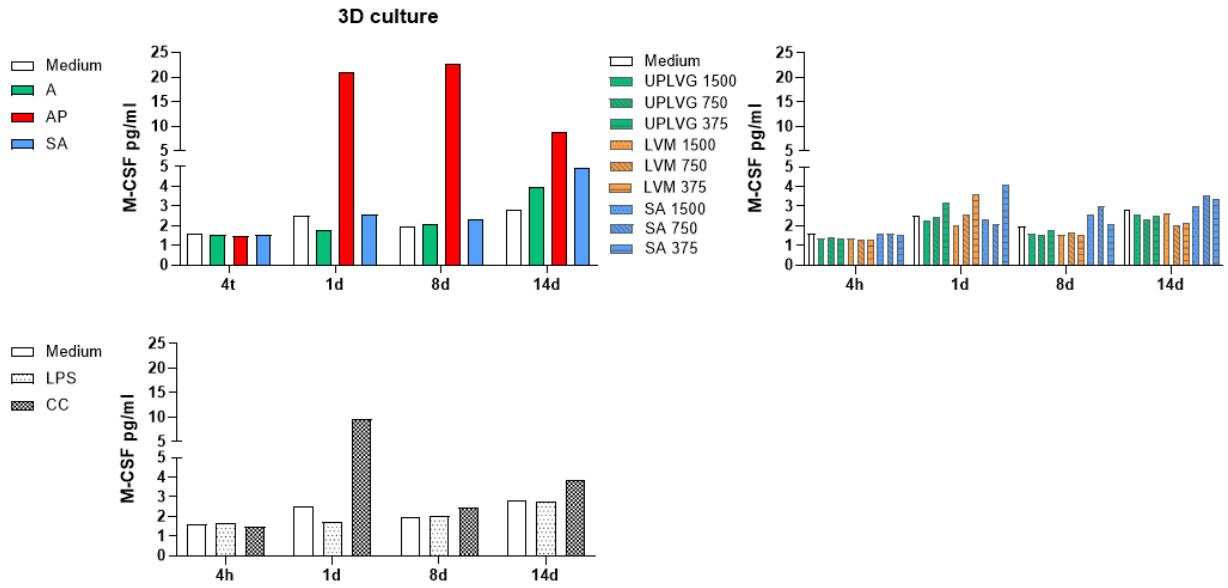

Figure 3.1.19: Secretion of M-CSF in 3D culturing induced by the microspheres A (green), AP (red), and SA (blue); the soluble alginates UPLVG (G-rich alginate) (green), LVM (M-rich alginate) (orange), SA (sulfated alginate) (blue), with concentrations of 500 (spotted), 100 (diagonal lines) and 10 (straight lines) µg/mL; and the controls LPS (black spotted) and CC (black squared).

The induction of M-CSF showed partly a pattern by increasing for each time point. This was observed for several conditions, including the medium control. AP induced higher levels of M-CSF compared to the other microspheres on day 1 and day 5, 21 vs. 1.8-2.5, and 23 vs. 2-2.3 pg/mL, respectively. The soluble alginates induced levels around the medium control, but a slight increase in induction of M-CSF by SA was observed. Except for day 1, CC and LPS showed a gradual increase like medium control towards day 14. On day 1, CC induced 4 times more M-CSF than the medium control, 2.5 vs. 10 pg/mL.

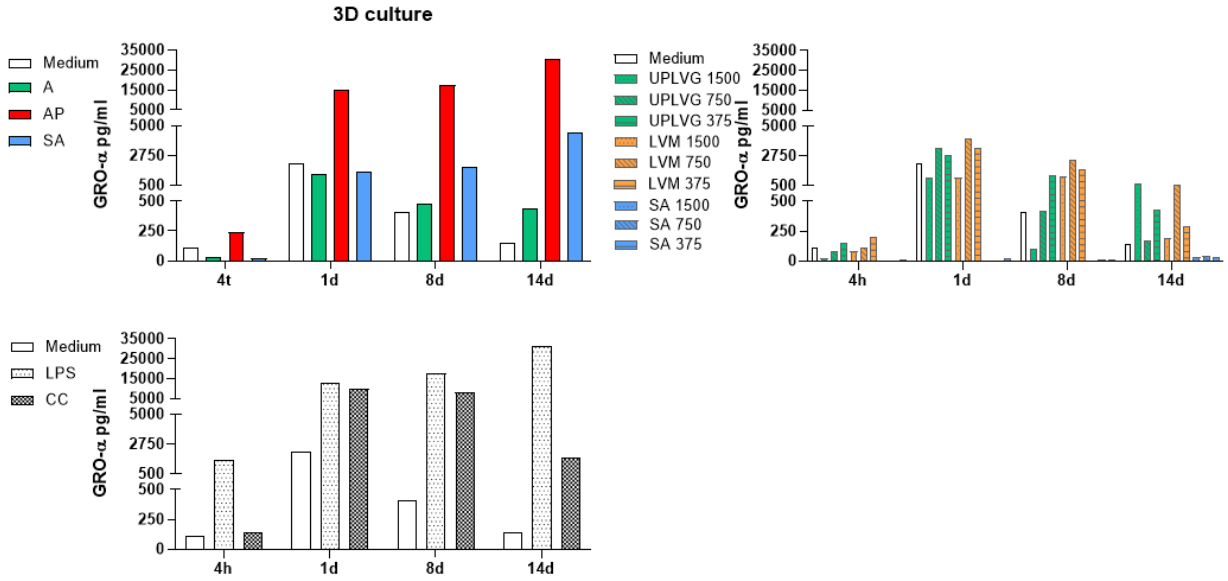

Figure 3.1.20: Secretion of GRO-α in 3D culturing induced by the microspheres A (green), AP (red), and SA (blue); the soluble alginates UPLVG (G-rich alginate) (green), LVM (M-rich alginate) (orange), SA (sulfated alginate) (blue), with concentrations of 500 (spotted), 100 (diagonal lines) and 10 (straight lines) µg/mL; and the controls LPS (black spotted) and CC (black squared).

The induction of GRO-α by AP, SA, and LPS increased for each time point. A, the medium control, the soluble alginates of UPLVG and LVM, and CC showed a different pattern by increasing towards day 1, before decreasing. AP showed a tenfold induction compared to the other microspheres on day 1 and day 8. As the soluble alginates followed more or less the induction of the medium control, SA induced low levels of GRO-α. On day 1, the medium control, UPLVG and LVM induced amounts between 1000-4000 pg/mL, while in contrast SA induced amounts from 1-20 pg/mL.

Overall, some cytokines, TNF, IL-1β, and IL-6, show a specific pattern by increasing towards day 1 before decreasing, for all conditions. The inflammatory potential of AP appears more distinct compare to the other two microbeads for the same cytokines. The soluble alginates showed in many cases to follow the medium control induction, suggesting that the addition of soluble alginate does not cause prominent differences. However, SA was observed in several cases, TNF, IL-1β, IL-6, IL-8, and GRO-α, to induce lower levels than the medium control. In contrast, SA was observed to induce higher levels of MCP-1 and M-CSF than the medium control in a partial concentration-dependence manner. CC was observed to induce levels of cytokines in a comparable picture like AP.

3.1.3 Experiment 3

Microspheres and soluble alginates were incubated with 2 million PBMCs/mL in RPMI supplemented with 30% h.i. serum for 14 days. Supernatants were harvested at selected time points: after 4 hours, 1 day, 5 days, 8 days, 14 days. Figure 3.1.21 shows the experimental layout of experiment 3 and 4.

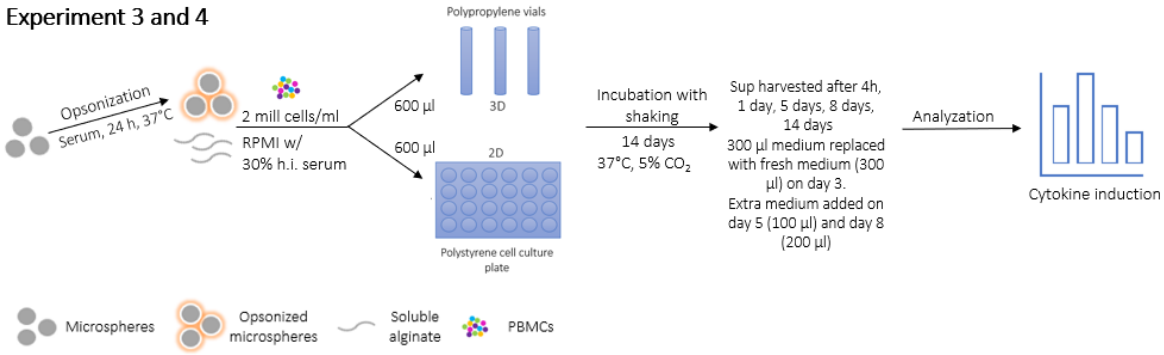

Figure 3.1.21: Shows the experimental setup of experiment 3 and 4 of the long-term *in vitro* experimental model.

The measurement of selected cytokines was based on results from experiment 1 and 2. IL-1ra was added to the cytokine selection. Figures 3.1.22 to 3.1.29 show a comparison of the induced concentration (pg/mL) of selected cytokines in 2D and 3D. The plotted data are given in Table C.1.17 to Table C.1.32 in Appendix C on page xxii. Induced levels of IL-8 were in most cases measured out of range above the standard curve, so the cytokine is not presented in results, but is shown in Figure A.2.10 in Appendix A on page viii.

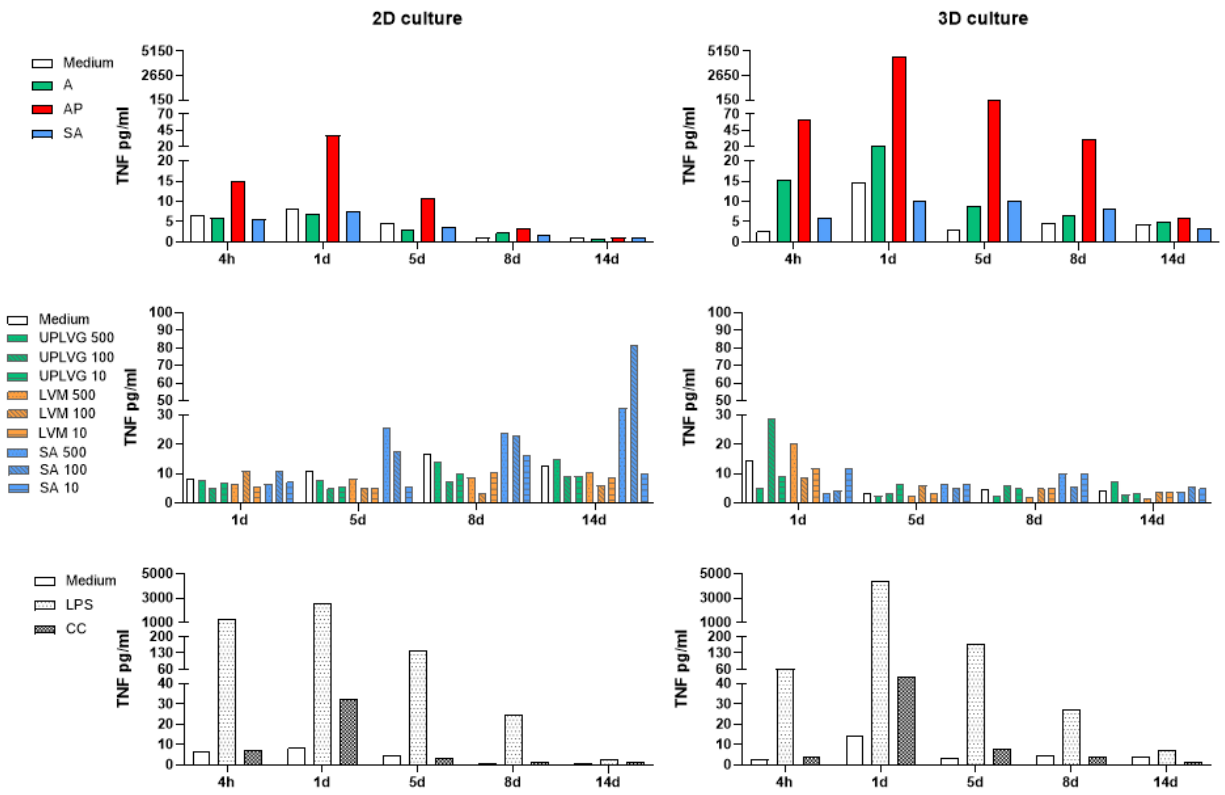

Figure 3.1.22: Comparison of the secretion of TNF in 2D and 3D culturing induced by the microspheres A (green), AP (red), and SA (blue); the soluble alginates UPLVG (G-rich alginate) (green), LVM (M-rich alginate) (orange), SA (sulfated alginate) (blue), with concentrations of 500 (spotted), 100 (diagonal lines) and 10 (straight lines) µg/mL; and the controls LPS (black spotted), CC (black squared).

The induction of TNF was observed to be higher in the 3D culture model as compared to the 2D culture for the microspheres. The induction peaked for both models at day 1, were the microspheres induced levels between 6-38 pg/mL in 2D, and 10-4500 pg/mL in 3D. The induction of TNF induced by the soluble alginates was higher in the 2D model from day 5. The induced level was observed to increase for each time point in 2D, while decreasing for each time point in 3D. SA induced prominent TNF amounts compared to the medium control, UPLVG, and LVM from day 5 in 2D. Following the incubation with CC, the amounts peaked at day 1, following a similar picture observed for the microspheres. The amounts of TNF induced by CC in 2D and 3D were of comparable character, between 1-35 pg/mg in 2D and 1-60 pg/mL in 3D.

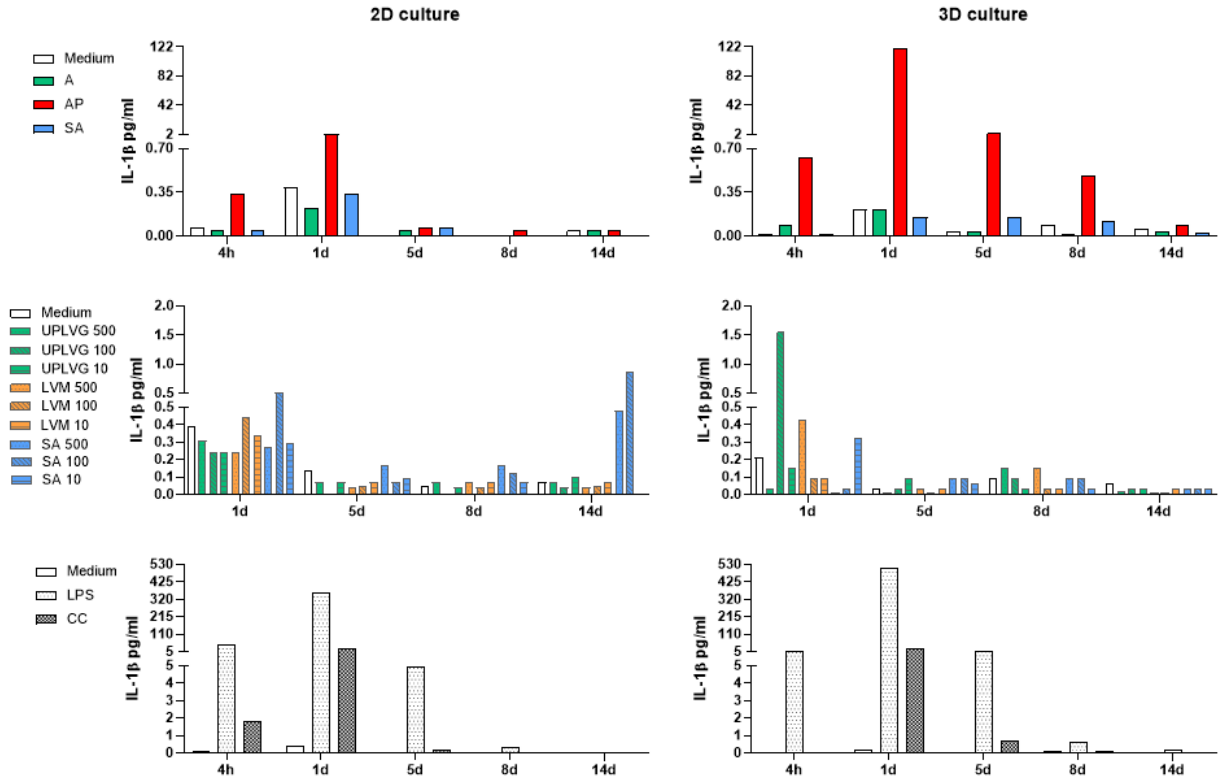

Figure 3.1.23: Comparison of the secretion of IL-1β in 2D and 3D culturing induced by the microspheres A (green), AP (red), and SA (blue); the soluble alginates UPLVG (G-rich alginate) (green), LVM (M-rich alginate) (orange), SA (sulfated alginate) (blue), with concentrations of 500 (spotted), 100 (diagonal lines) and 10 (straight lines) µg/mL; and the controls LPS (black spotted), CC (black squared).

The induction of IL-1β was higher in 3D vs. 2D for the microsphere AP. On day 1, AP induced 2 pg/mL in 2D vs. 120 pg/mL in 3D. A and SA induced similar levels in 2D vs. 3D ranging from 0.001-0.3 vs. 0.01-0.2 pg/mL. The amount IL-1β induced by the soluble alginates were higher in 2D on day 1 and day 14. On day 5 and day 8, similar levels of induced IL-1β were observed. CC and LPS peaked on day 1 and showed a comparable picture in 2D vs. 3D.

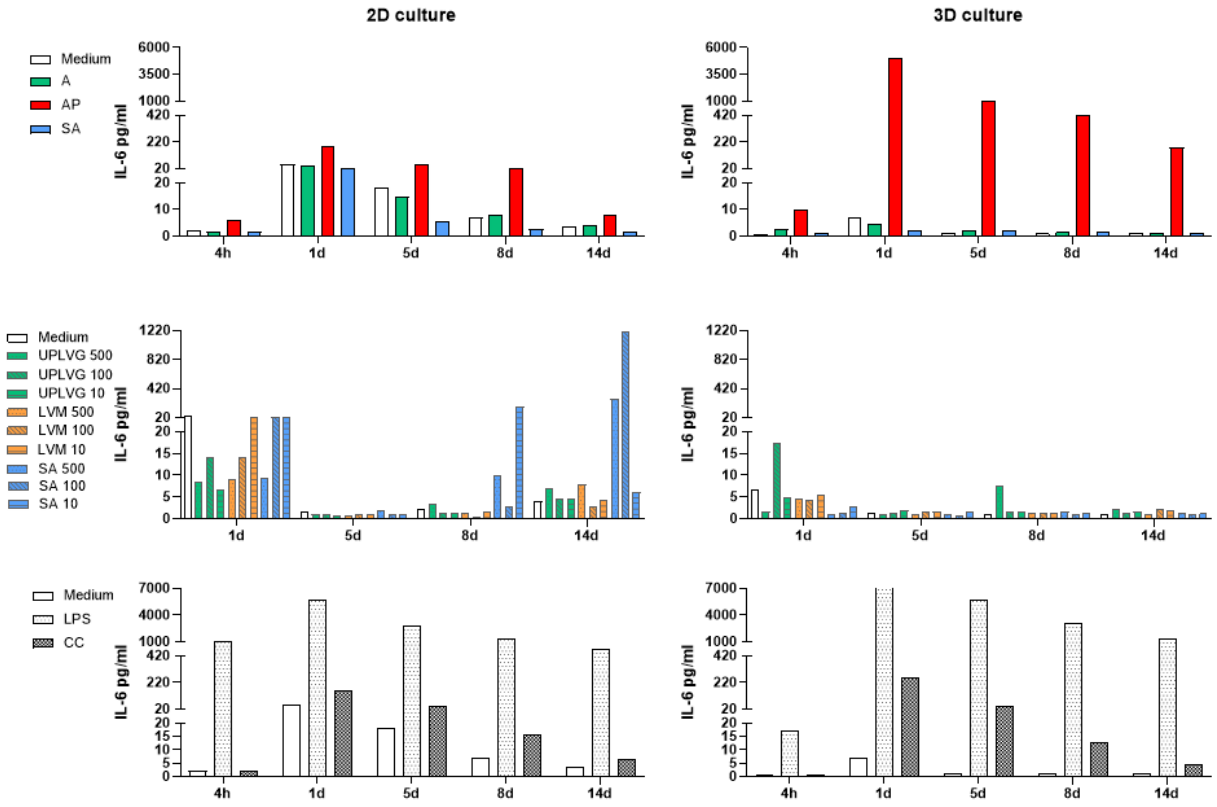

Figure 3.1.24: Comparison of the secretion of IL-6 in 2D and 3D culturing induced by the microspheres A (green), AP (red), and SA (blue); the soluble alginates UPLVG (G-rich alginate) (green), LVM (M-rich alginate) (orange), SA (sulfated alginate) (blue), with concentrations of 500 (spotted), 100 (diagonal lines) and 10 (straight lines) µg/mL; and the controls LPS (black spotted), CC (black squared).

The induction of IL-6 was higher in the 3D culture model after day 1 for the microsphere AP by ranging between 170-5000 pg/mL compared to 6-190 pg/mL in 2D. The medium control, A, and SA induced higher amounts of IL-6 in 2D than in 3D, for example on day 1: 25-50 pg/mL vs. 2-7 pg/mL. The amounts of IL-6 induced by the soluble alginates were higher in 2D on day 1 and day 14. Some concentrations of SA induced higher levels on day 8 and day 14 compared to the medium control (and UPLVG and LVM) by ranging between 170-1200 pg/mL against 1-7 pg/mL in 2D. The induction of LPS and CC peaked on day 1 and showed a comparable picture in 2D vs. 3D.

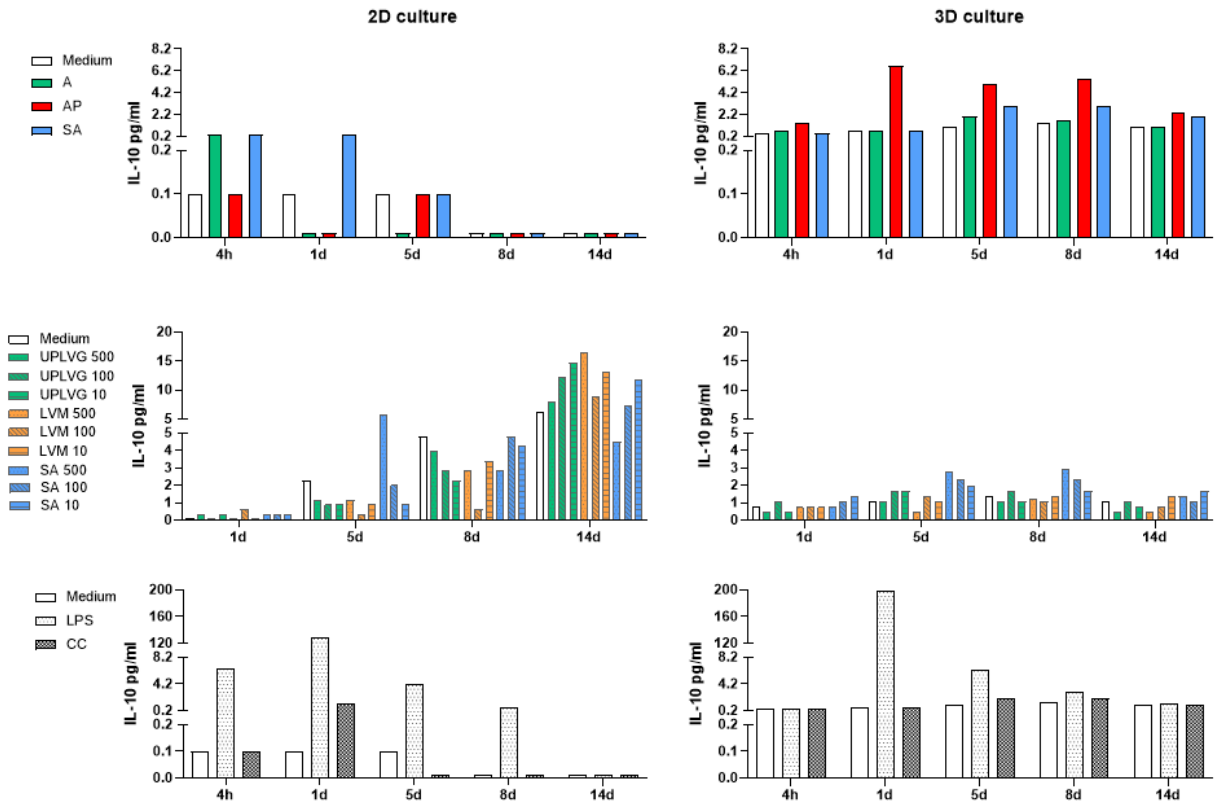

Figure 3.1.25: Comparison of the secretion of IL-10 in 2D and 3D culturing induced by the microspheres A (green), AP (red), and SA (blue); the soluble alginates UPLVG (G-rich alginate) (green), LVM (M-rich alginate) (orange), SA (sulfated alginate) (blue), with concentrations of 500 (spotted), 100 (diagonal lines) and 10 (straight lines) µg/mL; and the controls LPS (black spotted), CC (black squared).

The induction of IL-10 was observed to be higher in the 3D vs. 2D culture model for the microspheres. In 2D, the level of IL-10 decreased after day 1. In 3D, the induced level was observed to be stable around 0.40-3 pg/mL from 4 hours towards day 14. AP peaked on day 1 with a concentration around 7 pg/mL before decreasing towards the level of the medium control and the other microspheres. The induction of IL-10 induced by the soluble alginates was observed to be higher in 2D from day 5 towards day 14. This increase followed more or less the induced increase by the medium control. In 3D, IL-10 induced by UPLVG and LVM showed amounts comparable to the medium control: 0.4-1.40 vs. 0.7-1.40 pg/mL. SA showed an increase in induced IL-10 compared to the medium control, on day 5 and day 8, 2-2.8 and 1.7-3 pg/mL, where the induction increased with decreasing SA concentration. CC peaked on day 1 around the same amount of IL-10 induced in 3D for each time point. LPS showed partially the same pattern in 2D vs. 3D by increasing towards day 1 before decreasing.

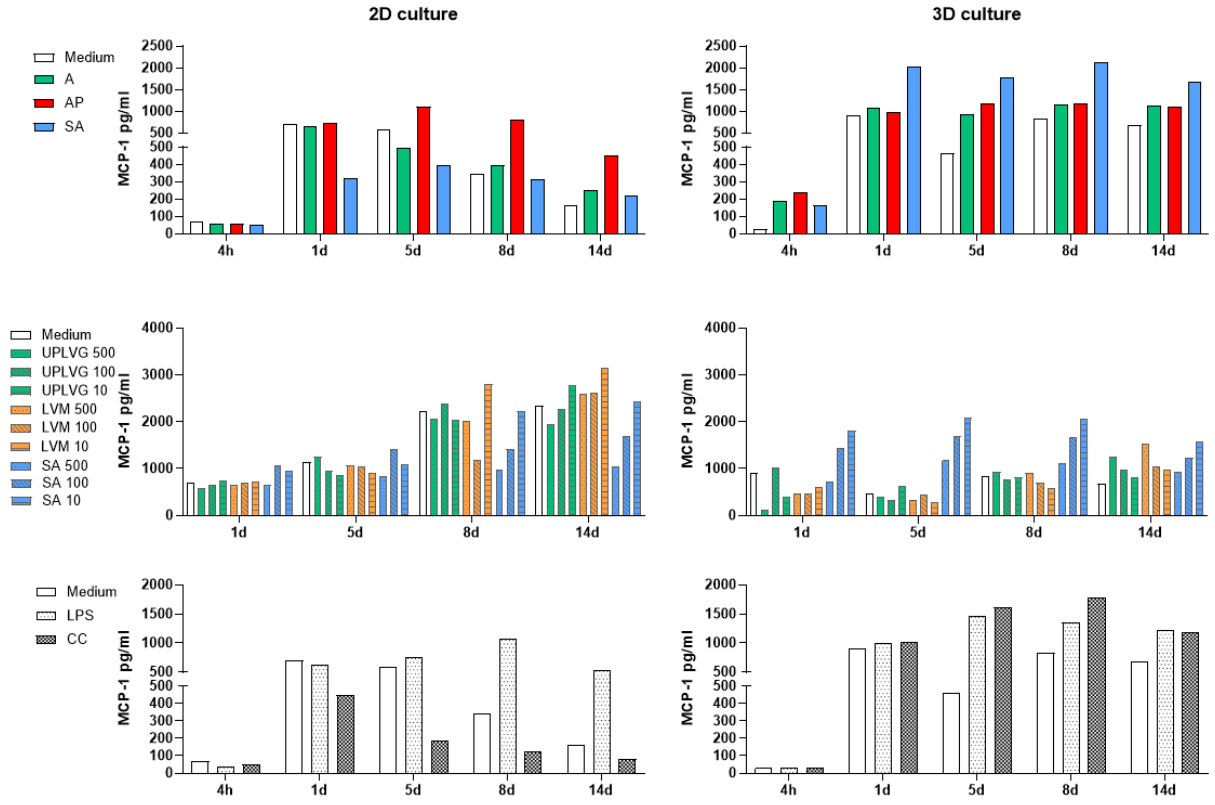

Figure 3.1.26: Comparison of the secretion of MCP-1 in 2D and 3D culturing induced by the microspheres A (green), AP (red), and SA (blue); the soluble alginates UPLVG (G-rich alginate) (green), LVM (M-rich alginate) (orange), SA (sulfated alginate) (blue), with concentrations of 500 (spotted), 100 (diagonal lines) and 10 (straight lines) µg/mL; and the controls LPS (black spotted), CC (black squared).

The induction of MCP-1 was observed to be higher in 2D vs. 3D for the microspheres. In 2D, the induced level increased towards day 1 and 5 before decreasing. A and SA induced levels of MCP-1 comparable to medium, while AP was prominent from day 5 by inducing amounts of 450-1100 pg/mL vs. 150-600 pg/mL by the medium control. In 3D, the induced level of MCP-1 was more or less stable from day 1, where A and AP were measured around the medium control: 450-900 pg/mL; and SA induced amounts above: 1600-2100 pg/mL. The induction of MCP-1 by the soluble alginates was observed to be higher in 2D for the medium control, UPLVG, and LVM from day 5, where UPLVG and LVM showed a similar induction like the medium control. SA was observed to induce lower amounts than the medium control in 2D, and lower amounts than SA in 3D. As LVM and UPLVG induced more or less similar amounts of MCP-1 like the medium control in 3D on day 1, 5, and 8, SA induced high amounts ranging from 1100-2100 pg/mL vs. 450-900 pg/mL by the medium control. The induction by SA aslo showed a concentration-dependence, where the induction of MCP-1 increased with decreasing SA concentration. CC and LPS induced higher amounts of MCP-1 in 3D.

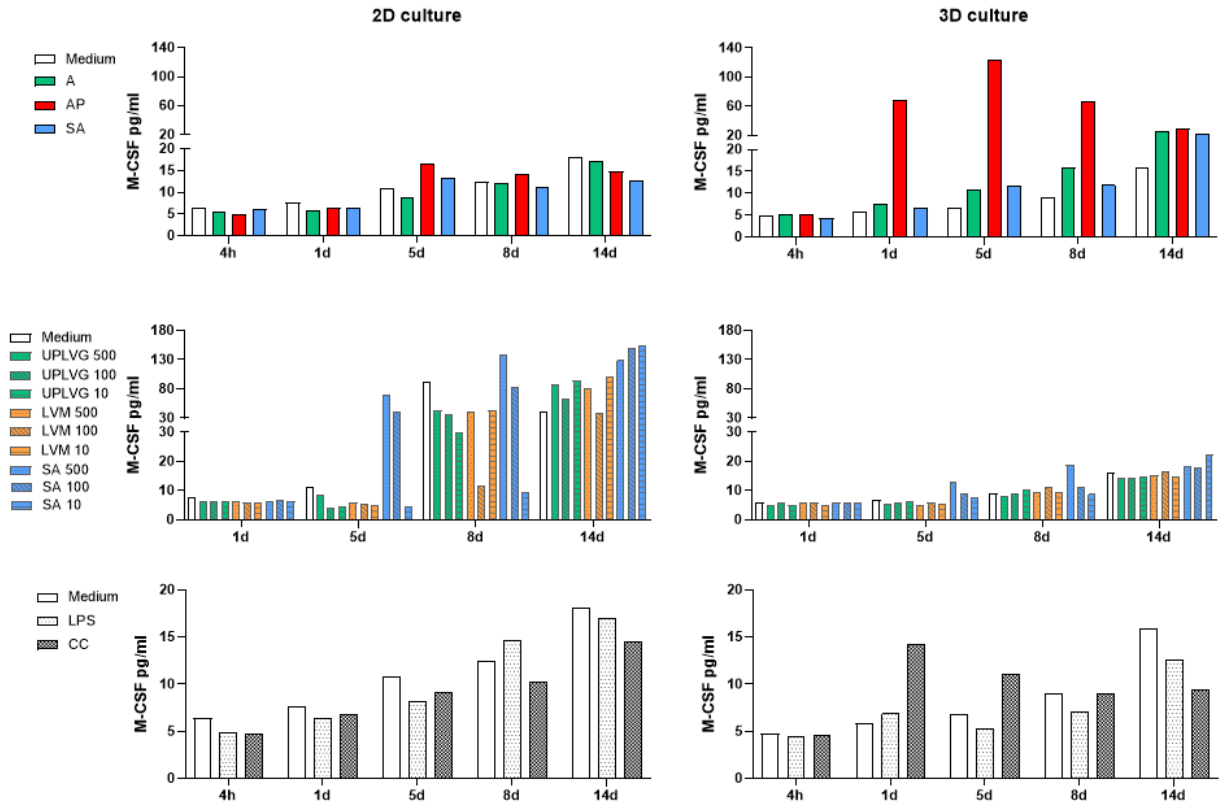

Figure 3.1.27: Comparison of the secretion of M-CSF in 2D and 3D culturing induced by the microspheres A (green), AP (red), and SA (blue); the soluble alginates UPLVG (G-rich alginate) (green), LVM (M-rich alginate) (orange), SA (sulfated alginate) (blue), with concentrations of 500 (spotted), 100 (diagonal lines) and 10 (straight lines) µg/mL; and the controls LPS (black spotted), CC (black squared).

The induced level of M-CSF by AP was observed to be higher in 3D from day 1. The medium control, A and SA showed a comparable induction by ranging from 6-18 pg/mL in 2D and 4-25 pg/mL in 3D. The soluble alginates induced higher M-CSF levels in 2D from day 8, where some concentrations of SA were prominent compared to the other conditions. In 3D, it was observed a gradual increase in the induced amounts of M-CSF form day 1 towards day 14, where UPLVG, LVM, and SA induced more or less amounts similar to the medium control. CC and LPS showed an increased induction of M-CSF in 2D from 4 hours towards day 14, together with the amounts induced by the medium control. LPS showed a similar pattern in 3D but induced lower amounts of M-CSF than in 2D. The induction of M-CSF by CC peaked on day 1 in 3D before decreasing.

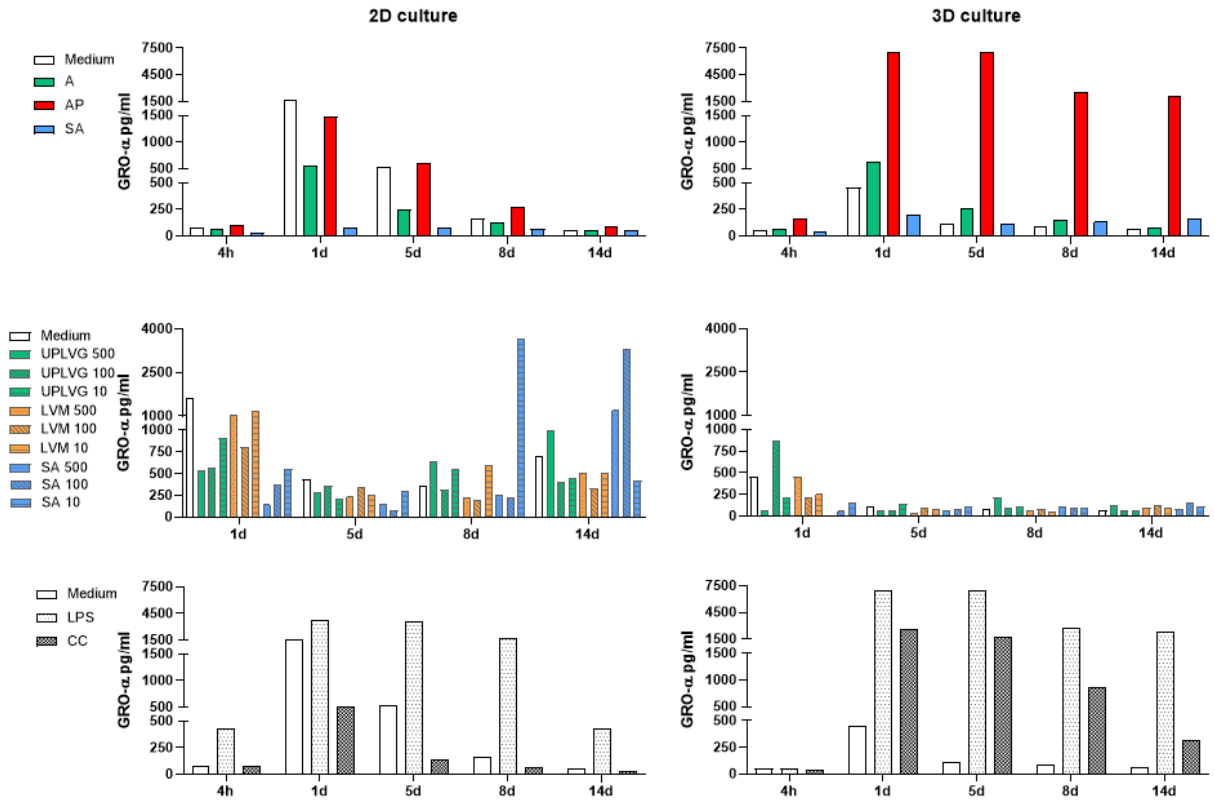

Figure 3.1.28: Comparison of the secretion of GRO-α in 2D and 3D culturing induced by the microspheres A (green), AP (red), and SA (blue); the soluble alginates UPLVG (G-rich alginate) (green), LVM (M-rich alginate) (orange), SA (sulfated alginate) (blue), with concentrations of 500 (spotted), 100 (diagonal lines) and 10 (straight lines) µg/mL; and the controls LPS (black spotted), CC (black squared).

The induction of GRO-α was observed to be higher in 3D vs. 2D for the AP microsphere, for example on day 1, the measured amount of GRO-α was 1500 pg/mL in 2D vs. 7000 pg/mL in 3D. A and SA induced similar levels in 2D vs. 3D: 50-600 vs. 60-600 pg/mL. The secretion of GRO-α induced by the soluble alginates was higher in 2D vs. 3D. In most cases, the soluble alginates induced levels like the medium control ranging from 350-1600 pg/mL, but some outliers of SA on day 8 and 14 induced amounts of 3200-3700 pg/mL. In 3D, the soluble alginates induced levels around the medium control, in the range 60-500 pg/mL. CC induced higer amounts of GROα in 3D vs. 2D, at top 2700 pg/mL compared to 500 pg/mL. LPS induced higher amounts in 3D vs. 2D, ranging from 40-2700 vs. 60-5000 pg/mL.

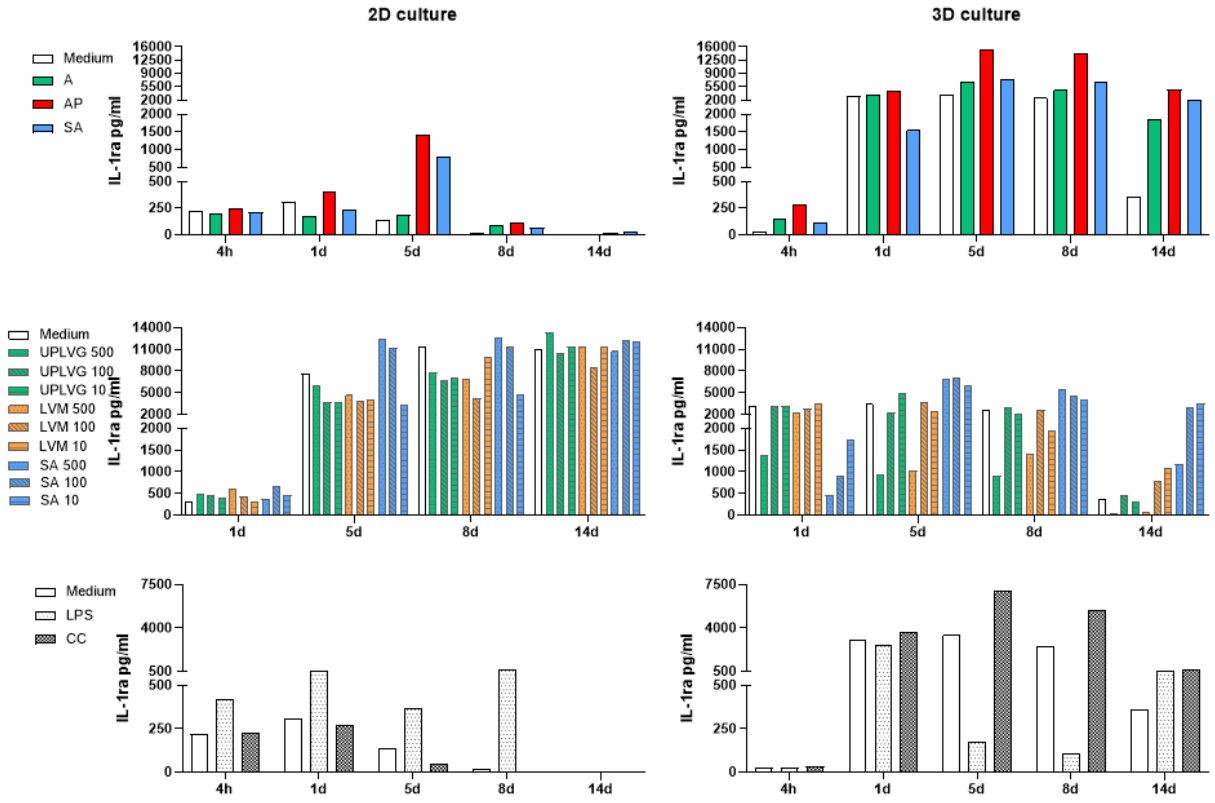

Figure 3.1.29: Comparison of the secretion of IL-1ra in 2D and 3D culturing induced by the microspheres A (green), AP (red), and SA (blue); the soluble alginates UPLVG (G-rich alginate) (green), LVM (M-rich alginate) (orange), SA (sulfated alginate) (blue), with concentrations of 500 (spotted), 100 (diagonal lines) and 10 (straight lines) µg/mL; and the controls LPS (black spotted), CC (black squared).

The induced level of IL-1ra was observed to be higher in 3D vs. 2D from day 1 for the microspheres. More specific, the amounts of IL-1ra were between 1500-15000 pg/mL in 3D vs. 1-1400 pg/mL in 2D. The soluble alginates induced higher levels of IL-1ra in 2D from day 5. SA was observed to induce the highest amounts of IL-1ra compared to UPLVG and LVM, on day 5 and 8, by ranging from 3400-12500 vs. 3600-10000 pg/mL. SA showed a similar picture in 3D, 4000-6000 vs. 900-5000 pg/mL. CC induced higher amounts of IL-1ra in 3D, for example on day 5, 7000 vs. 50 pg/mL.

Overall, the measured concentration for most cytokines induced by the microspheres was observed to be higher in 3D. AP showed a prominent induction in 3D compared to the other microspheres for the pro-inflammatory cytokines TNF, IL-1β, and IL-6, as well as, the growth factors M-CSF and GRO-α. For MCP-1, SA was observed to induce the highest levels. In most cases, the soluble alginates induced the highest levels of cytokines in 2D. For some cytokines, the measured level was observed to be in a concentration-dependent manner. For example, the induction of MCP-1 by SA increased with decreasing concentration, both in 2D and 3D. Induction by LPS and CC showed in many cases to be more or less similar in 2D and 3D. However, induction of MCP-1 in 2D and 3D showed some differences, where induction was highest in 3D, and CC was observed to induce levels like SA.

3.1.4 Experiment 4

Experiment 4 was conducted as experiment 3. The only difference was use of donor. Figures 3.1.30 to 3.1.37 show a comparison of the induced concentration (pg/mL) of selected cytokines in 2D and 3D. The plotted data are given in Table C.1.33 to Table C.1.48 in Appendix C on page xxx. Induced levels of IL-8 were in most cases measured out of range above the standard curve, so the cytokine is not presented in results, but is shown in Figure A.2.11 in Appendix A on page ix.

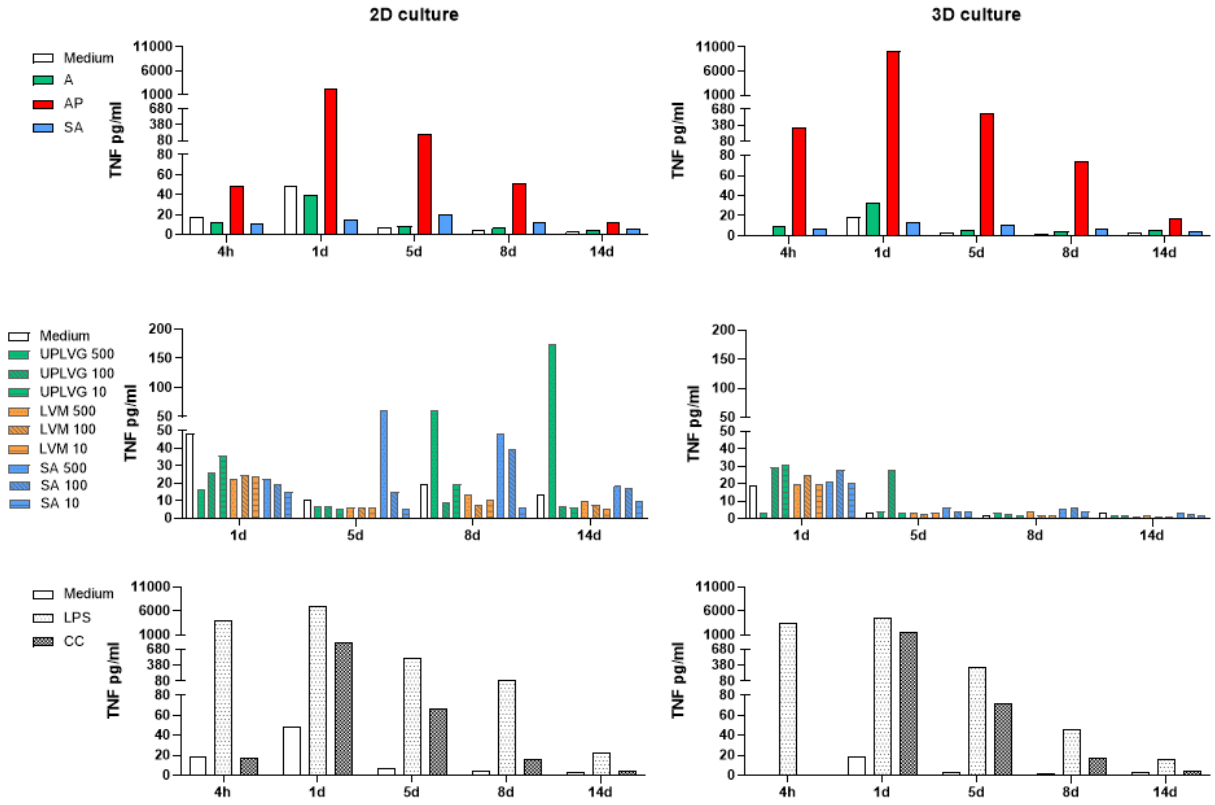

Figure 3.1.30: Comparison of the secretion of TNF in 2D and 3D culturing induced by the microspheres A (green), AP (red), and SA (blue); the soluble alginates UPLVG (G-rich alginate) (green), LVM (M-rich alginate) (orange), SA (sulfated alginate) (blue), with concentrations of 500 (spotted), 100 (diagonal lines) and 10 (straight lines) µg/mL; and the controls LPS (black spotted), CC (black squared).

The induction of TNF was observed to be higher in the 3D culture model as compared to the 2D culture for AP by inducing amounts between 15-4500 pg/mL in 3d vs. 10-2100 pg/mL in 2D. A and SA induced comparable levels between 4-35 pg/mL in 3D and 4-40 pg/mL in 2D. The soluble alginates induced higher levels of TNF in 2D vs. 3D. Except from som outliers, the measured amounts were between 5-60 pg/mL in 2D and 1-30 pg/mL in 3D. CC and LPS induced comparable amounts of TNF in 2D and 3D.

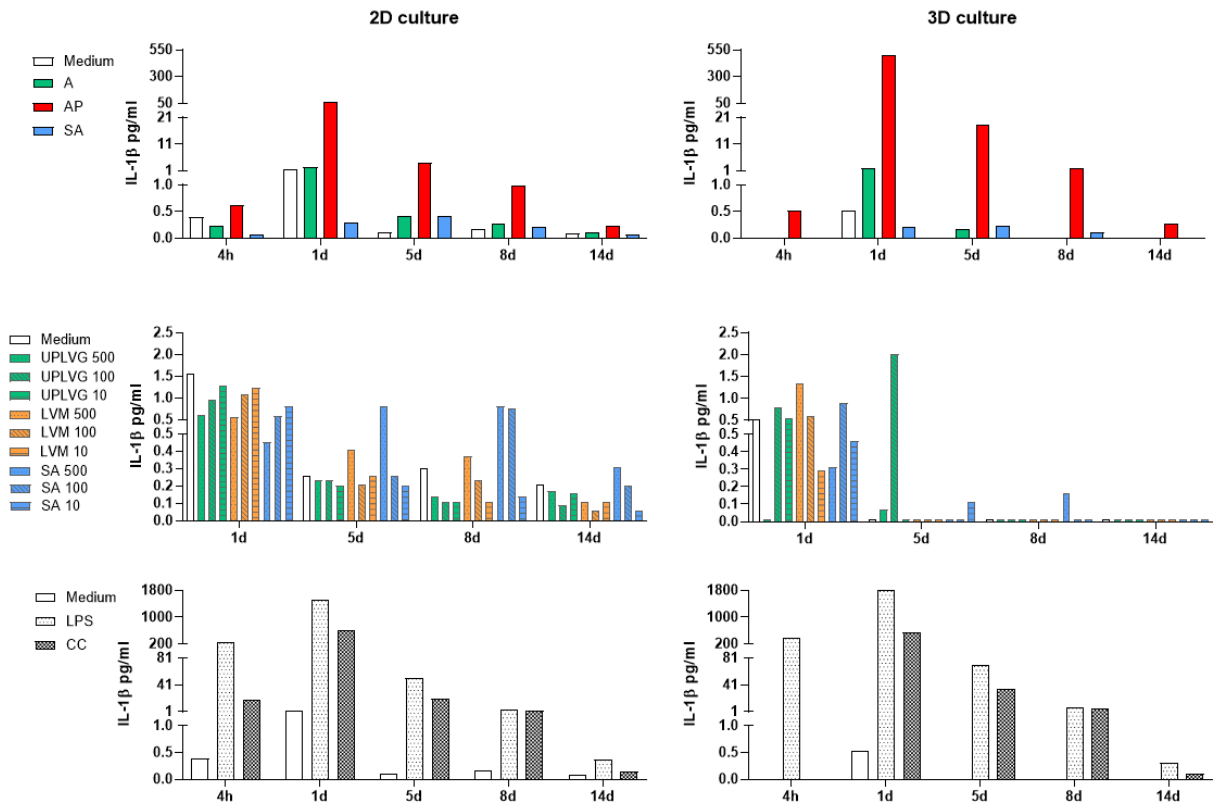

Figure 3.1.31: Comparison of the secretion of IL-1β in 2D and 3D culturing induced by the microspheres A (green), AP (red), and SA (blue); the soluble alginates UPLVG (G-rich alginate) (green), LVM (M-rich alginate) (orange), SA (sulfated alginate) (blue), with concentrations of 500 (spotted), 100 (diagonal lines) and 10 (straight lines) µg/mL; and the controls LPS (black spotted), CC (black squared).

The induction of IL-1β was higher in 3D vs. 2D for AP, ranging between 0.2-60 pg/mL in 2D and 0.3-500 pg/mL in 3D. A and SA induced partial higher amounts of IL-1β in 2D. Of note, in general, low amounts were measured, making the differences of small significance. The Soluble alginates induced higher amounts of IL-1β in 2D. From day 5, the level induced by the soluble alginates were in most cases, out of range below the standard curve in 3D. From day 1, CC and LPS induced comparable amounts of IL-1β in 2D and 3D.

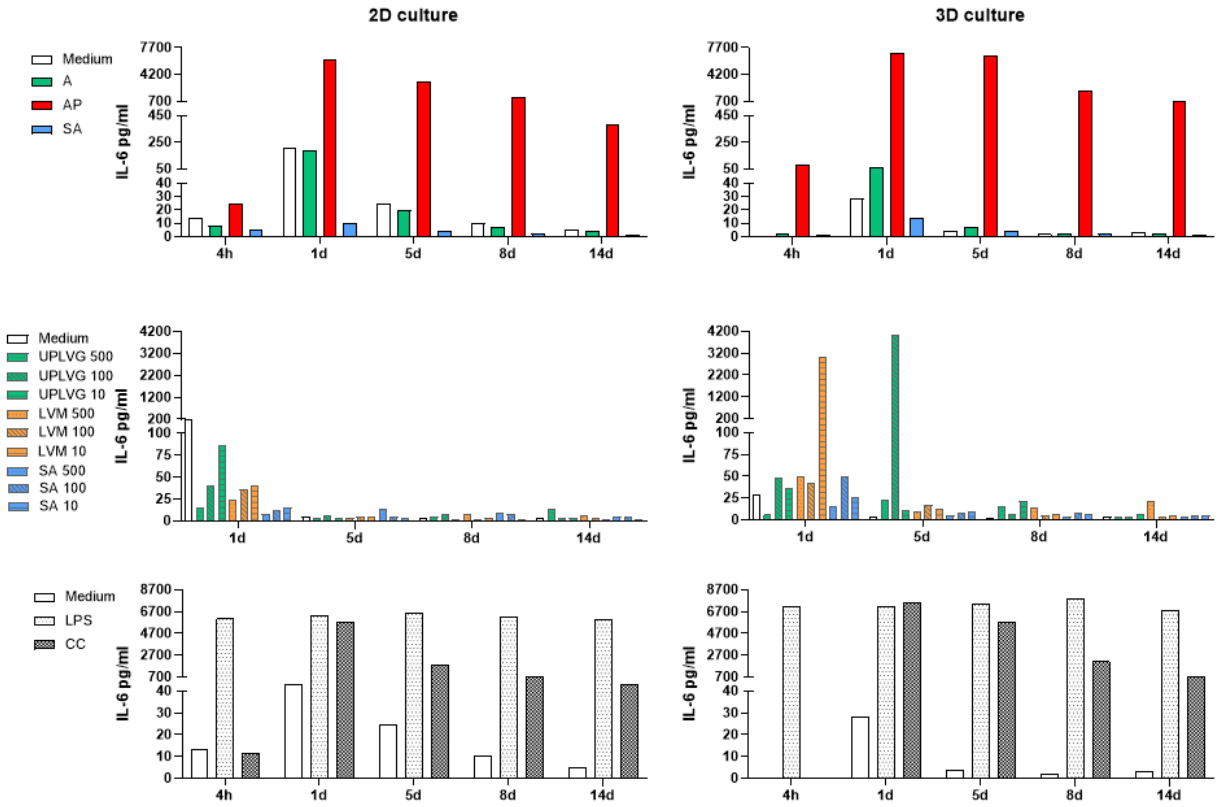

Figure 3.1.32: Comparison of the secretion of IL-6 in 2D and 3D culturing induced by the microspheres A (green), AP (red), and SA (blue); the soluble alginates UPLVG (G-rich alginate) (green), LVM (M-rich alginate) (orange), SA (sulfated alginate) (blue), with concentrations of 500 (spotted), 100 (diagonal lines) and 10 (straight lines) µg/mL; and the controls LPS (black spotted), CC (black squared).

The induction of IL-6 showed a similar picture in 2D vs. 3D for the microspheres by increasing towards day 1 before decreasing. The soluble alginates induced similar levels in 2D vs. 3D, except for a couple outliers of LVM and UPLVG in 3D on day 1 and day 5. CC and LPS induced comparable amounts of IL-6 in 2D vs. 3D. LPS was stabilized on the same level from 4 hours towards day 14, while CC peaked at day 1 before decreasing.

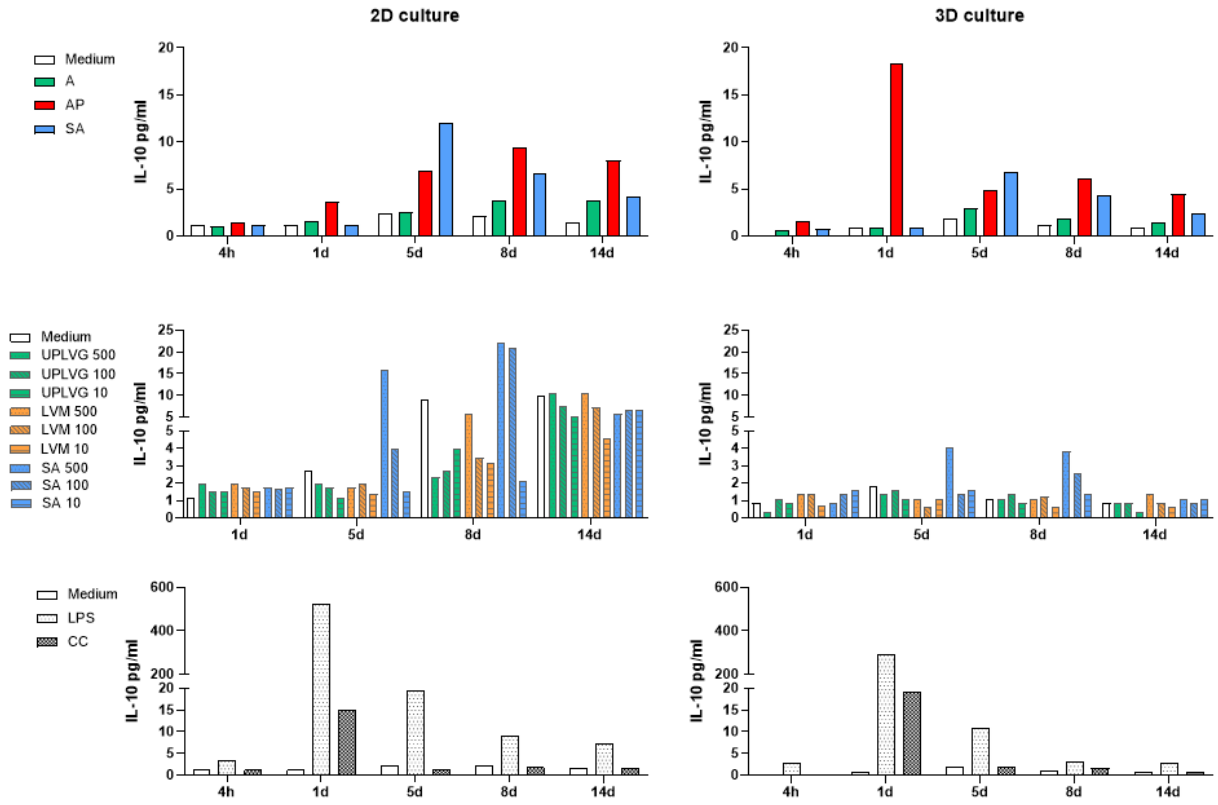

Figure 3.1.33: Comparison of the secretion of IL-10 in 2D and 3D culturing induced by the microspheres A (green), AP (red), and SA (blue); the soluble alginates UPLVG (G-rich alginate) (green), LVM (M-rich alginate) (orange), SA (sulfated alginate) (blue), with concentrations of 500 (spotted), 100 (diagonal lines) and 10 (straight lines) µg/mL; and the controls LPS (black spotted), CC (black squared).

The induction of IL-10 was higher in 2D vs. 3D for the microspheres, except for AP on day 1 in 3D. In 2D, the amounts ranged from 1-10 pg/mL in 2D vs. 0.6-7 pg/mL (without AP on day 1) in 3D. The soluble alginates induced higher amounts of IL-10 in 2D vs. 3D. In most cases, the soluble alginates follow the induced level by the medium control (or below). SA 500 and SA 100 induced higher levels of IL-10 than the medium control on day 5 and 8: 16 vs. 3 pg/mL on day 5 and 21-22 vs. 9 pg/mL on day 8. The overall induced concentration of IL-10 was lower in 3D, but the same pattern could be seen for SA on day 5 and day 8. The induction of IL-10 by CC peaked on day 1 and was comparable in 2D vs. 3D. LPS peaked at day 1, and induced higher amounts of IL-10 in 2D.

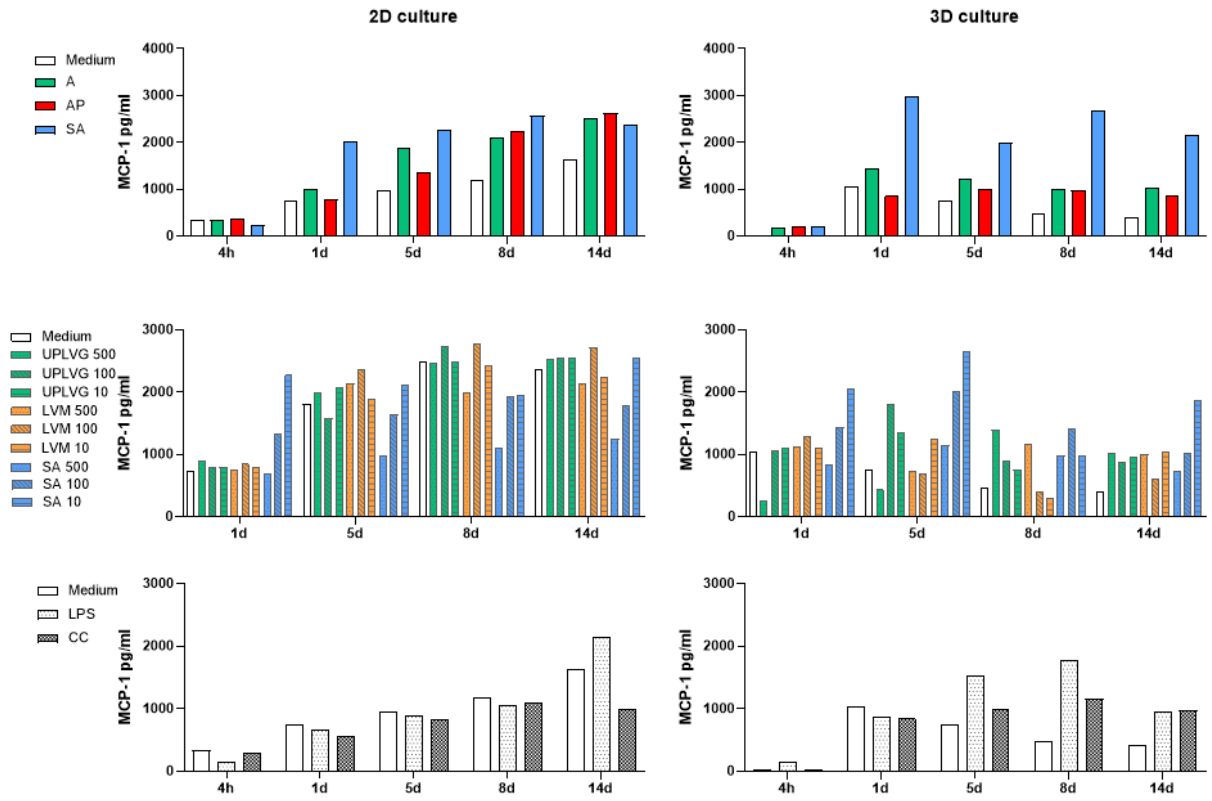

Figure 3.1.34: Comparison of the secretion of MCP-1 in 2D and 3D culturing induced by the microspheres A (green), AP (red), and SA (blue); the soluble alginates UPLVG (G-rich alginate) (green), LVM (M-rich alginate) (orange), SA (sulfated alginate) (blue), with concentrations of 500 (spotted), 100 (diagonal lines) and 10 (straight lines) µg/mL; and the controls LPS (black spotted), CC (black squared).

The induction of MCP-1 was higher in 2D vs. 3D for the microspheres A and AP with values between 350-2600 pg/mL in 2D and 180-1400 pg/mL in 3D. SA was more comparable in 2D vs. 3D by ranging from 200-2600 pg/mL in 2D and 200-3000 pg/mL in 3D. In 2D, the induced levels increase towards day 14 for the medium control and microspheres. In 3D, the induced levels increased towards day 1 before stabilizing or partial decreasing. The soluble alginates induced higher MCP-1 amounts in 2D. UPLVG and LVM induced secretion of MCP-1, similar to the level of medium control. SA showed a concentration-dependent induction with increasing MCP-1 amounts with decreasing SA concentration, where the lowest concentration of SA induced similar MCP-1 amounts like the medium control. The concentration-dependence of SA was also observed in 3D on day 1, day 5, and day 14. CC and LPS induced MCP-1 similar to the medium control and increased towards day 14 in 2D. In 3D, LPS increased towards day 8 before decreasing. CC showed a stabilization from day 1.

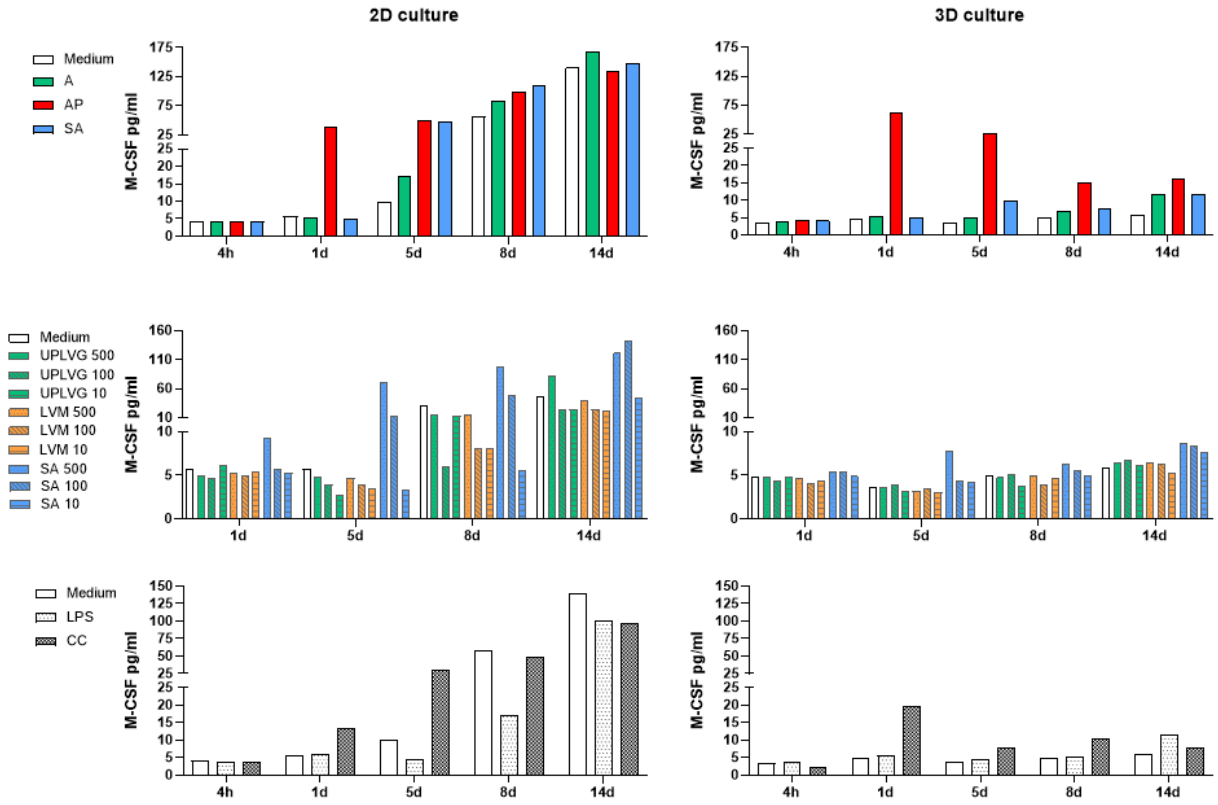

Figure 3.1.35: Comparison of the secretion of M-CSF in 2D and 3D culturing induced by the microspheres A (green), AP (red), and SA (blue); the soluble alginates UPLVG (G-rich alginate) (green), LVM (M-rich alginate) (orange), SA (sulfated alginate) (blue), with concentrations of 500 (spotted), 100 (diagonal lines) and 10 (straight lines) µg/mL; and the controls LPS (black spotted), CC (black squared).

The induction of M-CSF was higher in 2D vs. 3D from day 5 for the microspheres. From 4 hours to day 1 the amounts of M-CSF was comparable 4-40 pg/mL vs. 4-60 pg/mL. From day 5 to day 14 the amounts of induced M-CSF are more different: 15-170 pg/mL vs. 5-30 pg/mL. The levels increased from day 5 towards day 14 in 2D. In 3D, the levels were approximately stabilized (except AP). The soluble alginates induced higher amounts of M-CSF in 2D vs. 3D. The difference was most prominent from day 8: 6-100 pg/mL vs. 3-6 pg/mL. CC and LPS induced amounts of M-CSF increasing from towards day 14, ranging from 4-100 pg/mL in 2D. In 3D, the levels was more stabilized, ranging from 2-20 pg/mL.

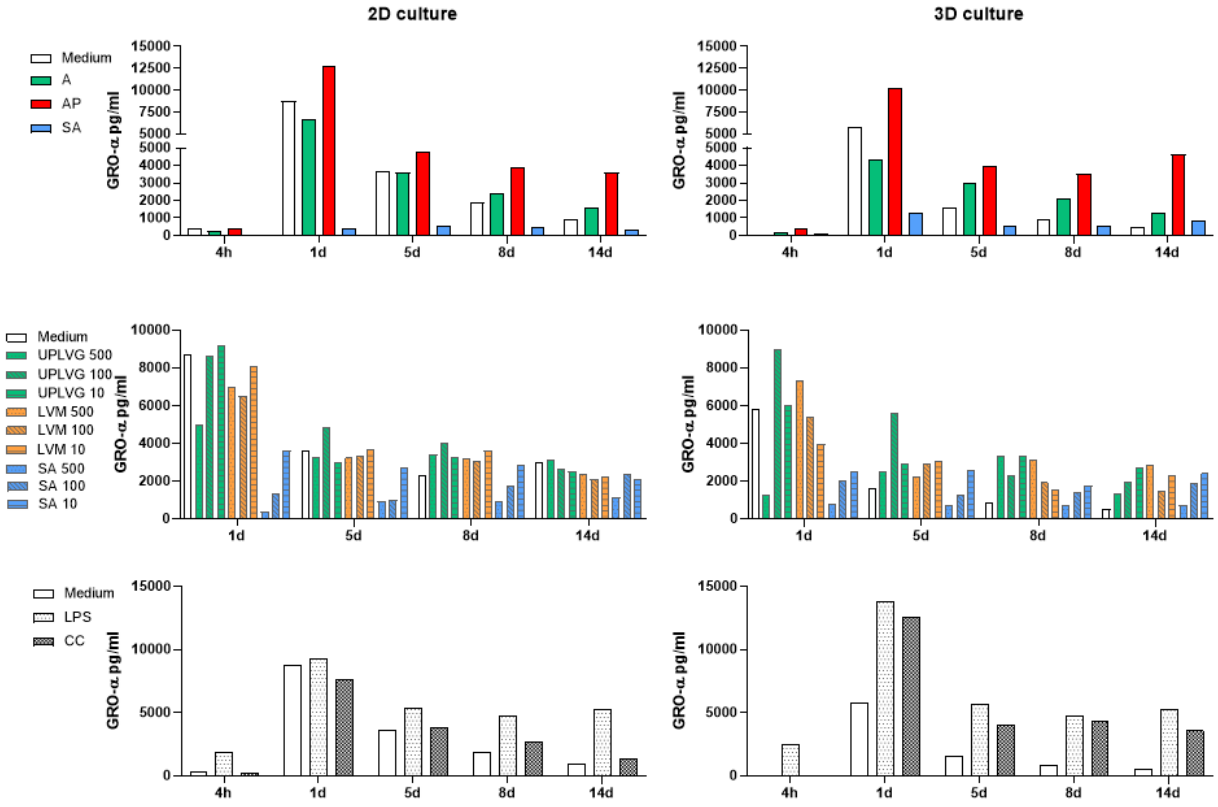

Figure 3.1.36: Comparison of the secretion of GRO-α in 2D and 3D culturing induced by the microspheres A (green), AP (red), and SA (blue); the soluble alginates UPLVG (G-rich alginate) (green), LVM (M-rich alginate) (orange), SA (sulfated alginate) (blue), with concentrations of 500 (spotted), 100 (diagonal lines) and 10 (straight lines) µg/mL; and the controls LPS (black spotted), CC (black squared).

The induction of GRO-α showed an overall comparable picture in 2D and 3D induced by the microspheres, with a partial higher induction in 2D. Several of the conditions induced increased amounts towards day 1 before decreasing. The soluble alginates induced similar levels in 2D and 3D. In 2D, the soluble alginates induced more or less similar levels like the medium control. In 3D, the difference between the medium control and the soluble alginates was more prominent from day 5, where UPLVG, in most cases, induced the highest amounts of GRO-α. A concentration-dependence pattern of SA was seen in both 2D and 3D, where the secretion increased with decreasing SA concentration. LPS and CC induced highest amounts of GRO-α in 3D on day 1: 7600-9200 pg/mL in 2D vs. 12600-13800 pg/mL in 3D. The other time points showed similar amounts in 2D and 3D.

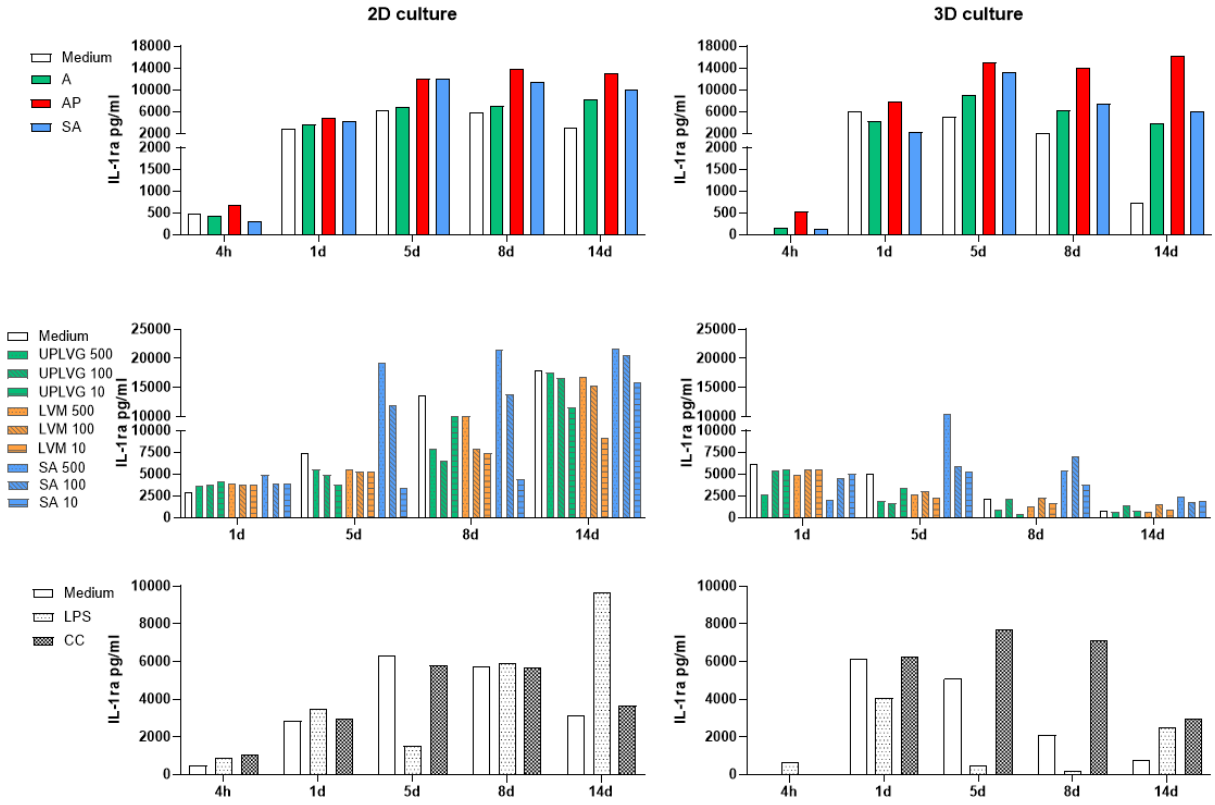

Figure 3.1.37: Comparison of the secretion of IL-1ra in 2D and 3D culturing induced by the microspheres A (green), AP (red), and SA (blue); the soluble alginates UPLVG (G-rich alginate) (green), LVM (M-rich alginate) (orange), SA (sulfated alginate) (blue), with concentrations of 500 (spotted), 100 (diagonal lines) and 10 (straight lines) µg/mL; and the controls LPS (black spotted), CC (black squared).

The induction of IL-1ra was highest in 3D vs. 2D for AP by inducing amounts 7800-16200 vs. 4800-13700 pg/mL from day 1 and onwards. A and SA induced more comparable amounts: 3500-12000 pg/mL vs. 2300-13000 pg/mL. The soluble alginates induced the highest levels of IL-1ra in 2D and increased from day 1 towards day 14. In 3D, an opposite pattern was seen, where the induction decreased from day 1 towards day 14. In comparison, the measured amounts on day 14 in 2D was from 9000-20500 pg/mL, while in 3D from 600-2500 pg/mL. For day 5, 8, and 14, SA showed a concentration-dependent induction of GRO-α in both 2D and 3D. CC induced highest levels in 3D from day 1 to day 14. LPS induced the highest levels in 2D.

Overall, AP showed a prominent induction in 3D compared to the other microspheres for the pro-inflammatory cytokines TNF, IL-1β, and IL-6, as well as, the growth factors M-CSF and GRO-α. SA was observed to induce the highest levels of MCP-1, both in 2D and 3D. In most cases, the soluble alginates induced the highest levels of cytokines in 2D. For some cytokines, the measured level showed patterns of concentration-dependence. For example, the induction of MCP-1 and GRO-α by SA increased with decreasing concentration, both in 2D and 3D. Induction by LPS and CC was observed to be more or less similar in 2D and 3D.

3.2 Trained immunity

Trained immunity has been described as the innate immunity's ability of adaption when exposed to infections. The adaption results in up-regulation of cell function over time that provides broad non-specific protection upon reinfection. The phenomenon has also been investigated as a possible contributor to the pathogenesis of several diseases, among other things, fibrosis[75]. To explore if alginate and cholesterol crystals (CC) can induce a training effect, human monocytes were incubated with different types of soluble alginate and CC in culture medium under 2D conditions. The training was conducted as 24 hours incubation with the selected stimuli before washed out and thereafter, resting for 5 days. A restimulation was performed with LPS for 24 hours before the secretion of selected cytokines were measured. Training of monocytes was tested by three experiments in total, with the same types of alginate and β-glucan as a positive control. Experiment 1 and 2 were conducted with identical experimental designs using heat-inactivated human serum (10%). Experiment 3 was conducted with a change in the serum conditions using heat-inactivated human serum (8%) and non-treated human serum (2%) in order to include the effects of complement opsonization and co-stimulation with the anaphylatoxins. In addition, as a stimulus, LPS was added as control of tolerance induction. Figure 3.2.1 shows an overall experimental procedure of (a) Experiment 1 and 2, and (b) Experiment 3. Figures 3.2.2 to 3.2.6 show the concentration (pg/mL) of induced cytokines. The plotted data are given in Tables C.2.1 to C.2.5 in Appendix C on page xxxviii. Induced levels of IL-8 were in most cases measured out of range above the standard curve, so the cytokine is not presented in results, but is shown in Figure A.3.1 in Appendix A on page x

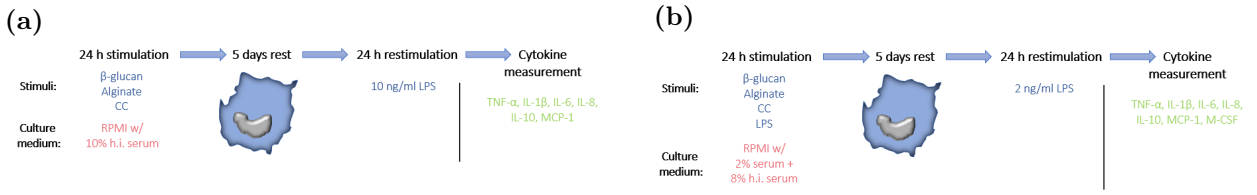

Figure 3.2.1: Experimental procedure used for training of monocytes in experiment 1 and 2 (a) and experiment 3 (b). Monocytes were stimulated for 24 hours in indicated culture medium and washed, before resting for 5 days. On day 6, cells were restimulated with LPS for 24 hours and supernatant was harvested and further analyzed selected cytokines.

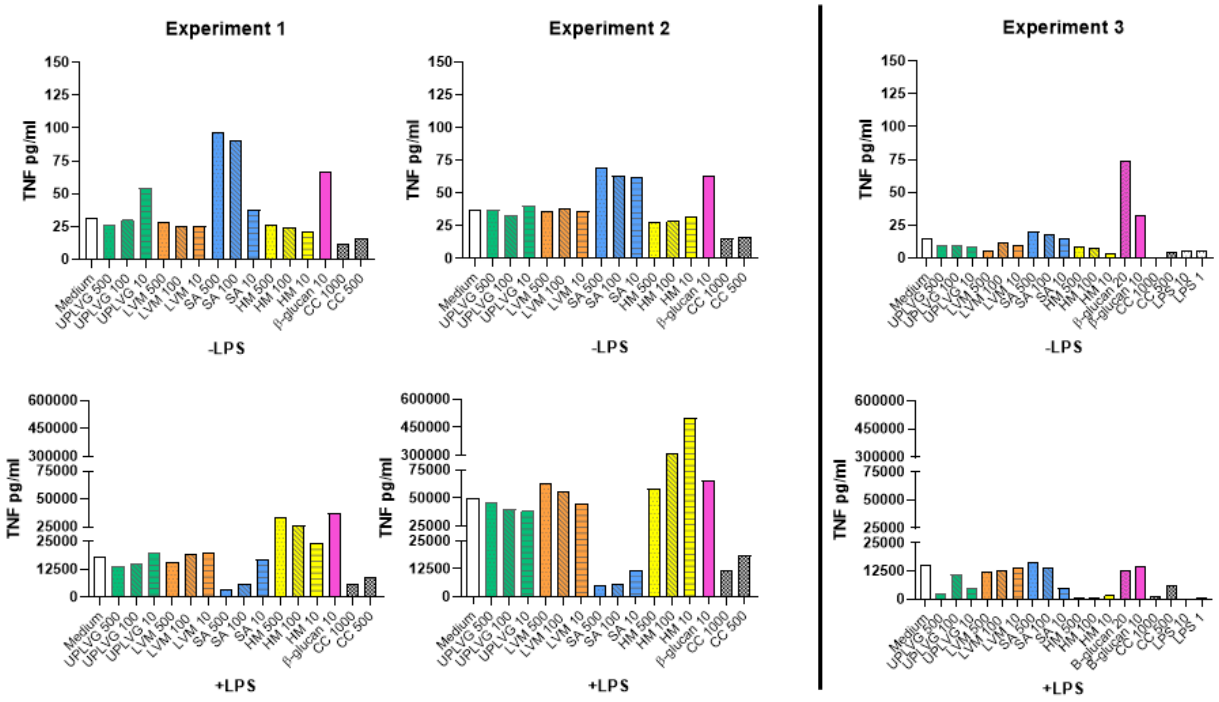

Figure 3.2.2: Comparison of the secretion of TNF by monocytes of three different donors after 24 hours of training, and 5 days of rest before measurement of cytokines either following addition of medion alone (-LPS) of following stimulation of the unrelated stimuli (+LPS). The Following stimuli were tested for training effects: the alginates UPLVG (G-rich alginate) (green), LVM (M-rich alginate) (orange), SA (sulfated alginate) (blue), HM (High-M alginate, 94% M) (yellow) with concentrations of 500 (spotted), 100 (diagonal lines) and 10 (straight lines) µg/mL; β-glucan (purple) with concentrations of 20 and 10 µg/mL; cholesterol crystals (CC) (black squared) with concentrations of 1000 and 500 µg/mL; and LPS (black spotted) with concentrations of 10 and 1 ng/mL. Experiment 1 and 2 follows the same experimental procedure. Experiment 3 is experimental different by change of culture medium and addition of LPS as experimental condition.

The induction of TNF is shown in Figure 3.2.2. Experiment 1 and 2 showed a comparable TNF respone with and without LPS stimulation, although the levels of induction were different for the two donors. After the five-days resting period, the SA and β-glucan were observed to induce cytokine secretion above medium control without LPS restimulation (only addition of medium). Upon restimulation with LPS, β-glucan and some concentrations of HM augmented the production of TNF above the medium control, indicating a possible tolerance effect. In experiment 3, the TNF induction after stimulation with HM showed an opposite response after LPS stimulation to what was observed in experiment 1 and 2, with lower TNF induction compared to the medium control. Of note, neither the β-glucan nor the CC induced more TNF as compared to the medium control upon restimulation with LPS.

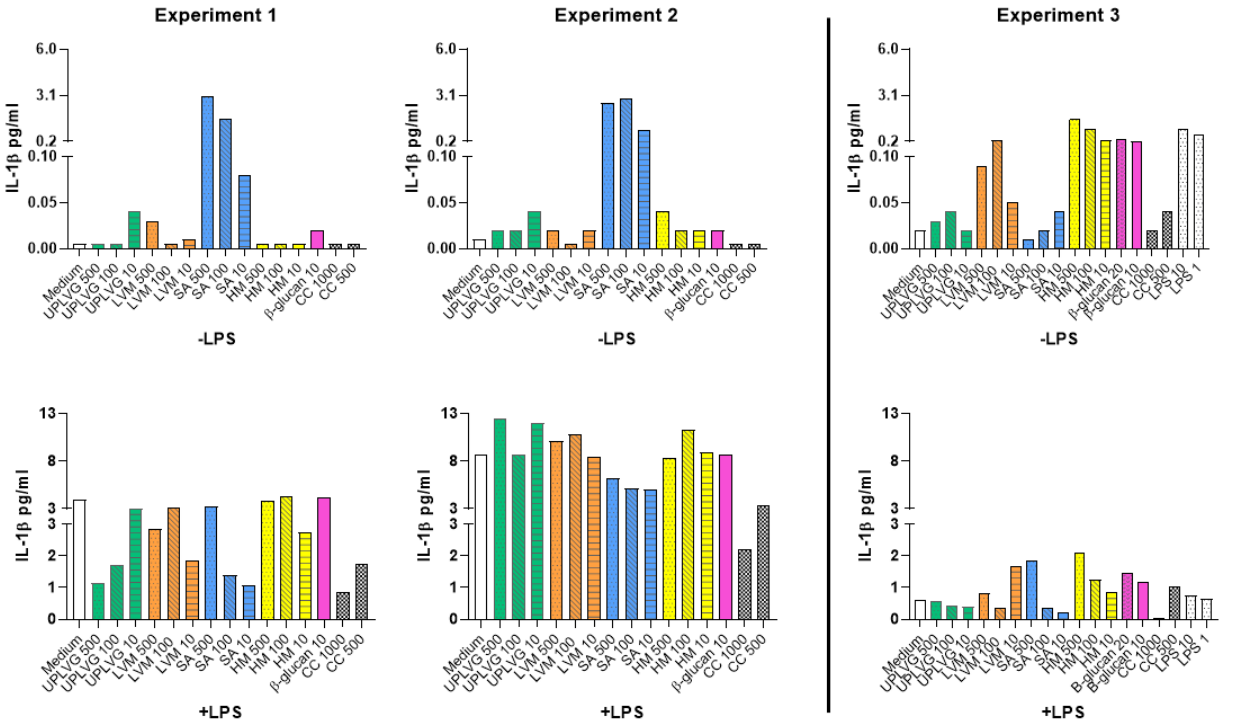

Figure 3.2.3: Comparison of the secretion of IL-1β by monocytes of three different donors after 24 hours of training, and 5 days of rest before measurement of cytokines either following addition of medion alone (-LPS) of following stimulation of the unrelated stimuli (+LPS). The Following stimuli were tested for training effects: the alginates UPLVG (G-rich alginate) (green), LVM (M-rich alginate) (orange), SA (sulfated alginate) (blue), HM (High-M alginate, 94% M) (yellow) with concentrations of 500 (spotted), 100 (diagonal lines) and 10 (straight lines) µg/mL; β-glucan (purple) with concentrations of 20 and 10 µg/mL; cholesterol crystals (CC) (black squared) with concentrations of 1000 and 500 µg/mL; and LPS (black spotted) with concentrations of 10 and 1 ng/mL. Experiment 1 and 2 follows the same experimental procedure. Experiment 3 is experimental different by change of culture medium and addition of LPS as experimental condition.

The induction of IL-1β is shown in Figure 3.2.3. In experiment 1 and 2, SA induced higher levels when restimulated with medium only (-LPS) compared to the other stimuli and medium control. After LPS-restimulation, several of the conditions induced levels compared to medium control, while SA tended for both cases to be lower than the medium control. However, it should be emphasized that the measured cytokine concentrations overall was low. In experiment 3, which also included active serum components, a different stimulation pattern of IL-1β was observed. Upon restimulation with medium only, the LVM and HM alginates, β-glucan and LPS induced elevated IL-1β as compared to the control. The other stimuli, including the SA, did not induce elevated amounts. Upon restimulation with LPS, a stimulatory effect could be found for LVM at the lowest dose, and for HM, SA, and β-glucan at the highest dose. LPS did not induce elevated amounts as compared to the medium control. The effect of CC was minor, with at most a doubling of IL-1β to the medium control.

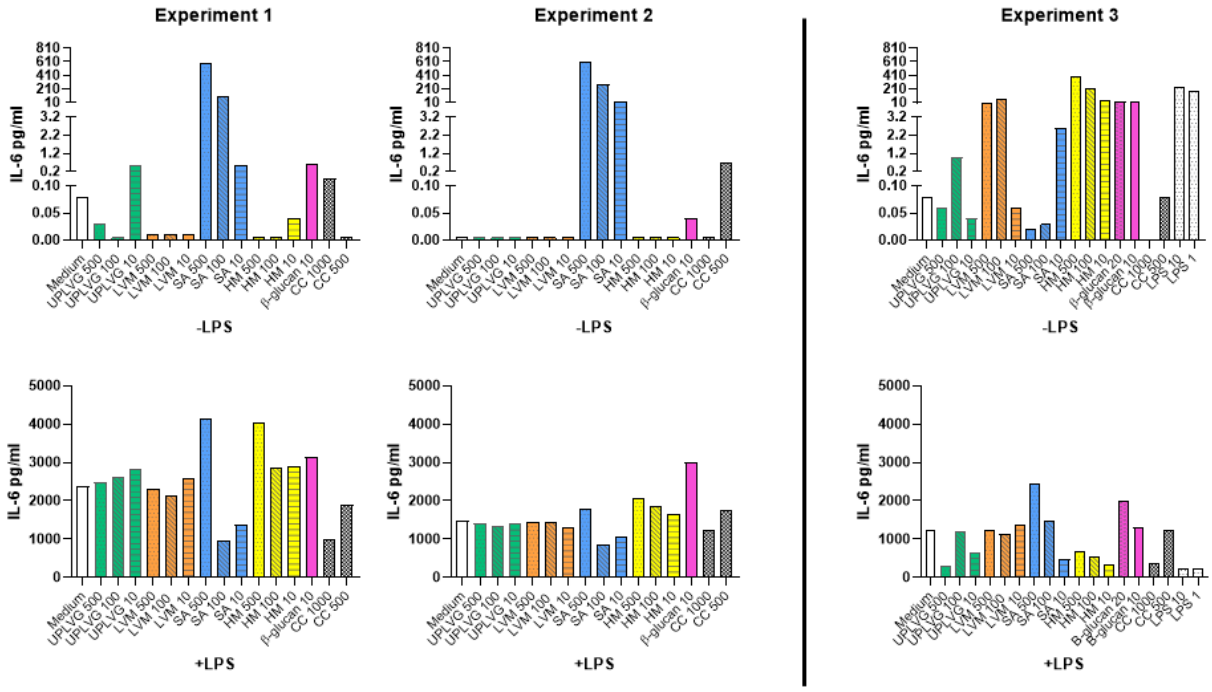

Figure 3.2.4: Comparison of the secretion of IL-6 by monocytes of three different donors after 24 hours of training, and 5 days of rest before measurement of cytokines either following addition of medion alone (-LPS) of following stimulation of the unrelated stimuli (+LPS). The Following stimuli were tested for training effects: the alginates UPLVG (G-rich alginate) (green), LVM (M-rich alginate) (orange), SA (sulfated alginate) (blue), HM (High-M alginate, 94% M) (yellow) with concentrations of 500 (spotted), 100 (diagonal lines) and 10 (straight lines) µg/mL; β-glucan (purple) with concentrations of 20 and 10 µg/mL; cholesterol crystals (CC) (black squared) with concentrations of 1000 and 500 µg/mL; and LPS (black spotted) with concentrations of 10 and 1 ng/mL. Experiment 1 and 2 follows the same experimental procedure. Experiment 3 is experimental different by change of culture medium and addition of LPS as experimental condition.

The outcome of training in experiments upon IL-6 secretion is shown in Figure 3.2.4. In experiment 1 and 2, SA induced a prominent IL-6 induction by the highest dose of SA as compared to the other conditions upon restimulation with medium only. After restimulation with LPS, a dose-dependent effect was observed were the lowest doses tended to lower the induction compared to the medium control. This effect might indicate a tolerance effect induced by SA. However, SA 500 showed a higher induction in both cases (with medium and LPS restimulation). HM was not observed to induce higher levels of IL-6 compared to the medium control upon restimulation with medium. However, after restimulation with LPS, HM showed a higher induction than medium control, with especially HM 500 with a prominent induction. CC induced IL-6 higher than medium control upon restimulation with medium only. After LPS restimulation, CC induced IL-6 around the level of the medium control or below. In experiment 3, both LVM and HM induced higher levels than the medium control upon restimulation with medium only. This was also found upon stimulation with the lowest dose of SA and for the β-glucans and LPS. While the highest dose of CC induced lower IL-6 than the medium control, the lower dose tended to be similar to the medium control, an effect that was also seen upon LPS-restimulation. After restimulation with LPS, HM and LPS showed a lower induction potential than the medium control, which could indicate a tolerance effect. On the opposite side, the highest dose

of SA tended to be a slightly inductor of IL-6 as compared to the medium control. The β-glucan induced similarly a slightly elevated response.

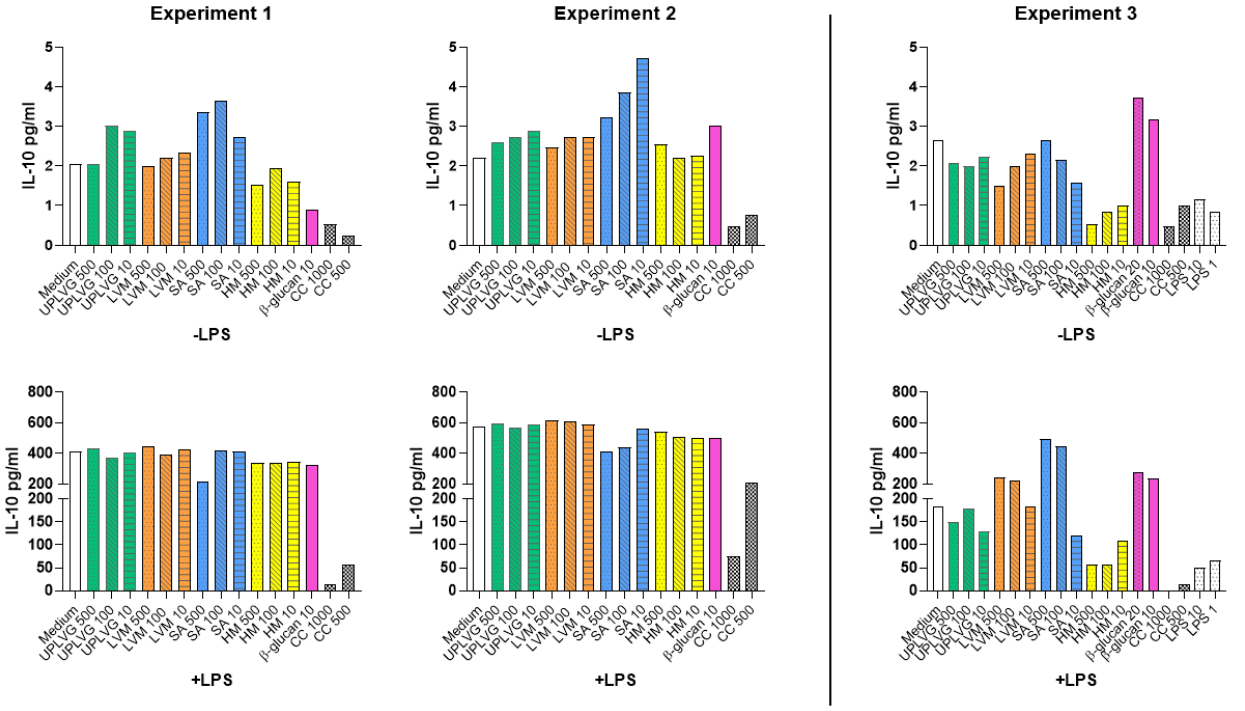

Figure 3.2.5: Comparison of the secretion of IL-10 by monocytes of three different donors after 24 hours of training, and 5 days of rest before measurement of cytokines either following addition of medion alone (-LPS) of following stimulation of the unrelated stimuli (+LPS). The Following stimuli were tested for training effects: the alginates UPLVG (G-rich alginate) (green), LVM (M-rich alginate) (orange), SA (sulfated alginate) (blue), HM (High-M alginate, 94% M) (yellow) with concentrations of 500 (spotted), 100 (diagonal lines) and 10 (straight lines) µg/mL; β-glucan (purple) with concentrations of 20 and 10 µg/mL; cholesterol crystals (CC) (black squared) with concentrations of 1000 and 500 µg/mL; and LPS (black spotted) with concentrations of 10 and 1 ng/mL. Experiment 1 and 2 follows the same experimental procedure. Experiment 3 is experimental different by change of culture medium and addition of LPS as experimental condition.

The induction of IL-10 is given in Figure 3.2.5. In experiment 1 and 2, the induction of IL-10 was augmented by SA upon restimulation with medium after five days of wash-out and resting. CC was observed to induce lower amounts of IL-10 as compared to the medium control. After restimulation with LPS, all alginates were observed to induce a similar level like medium control, while CC still induced IL-10 amounts below the medium control. In experiment 3, HM, CC, and LPS induced less IL-10 amounts than medium, while the rest of the alginates induced IL-10 amounts at a similar level as the medium control after restimulation with medium only. β-glucan was the only added stimuli that induced IL-10 amounts above the medium control. After restimulation with LPS, a doubling of IL-10 was observed for the highest doses of SA. The β-glucans did also show a tendency of inducing elevated IL-10. HM showed a tendency to lower the IL-10 induction, as was the case for CC and LPS.

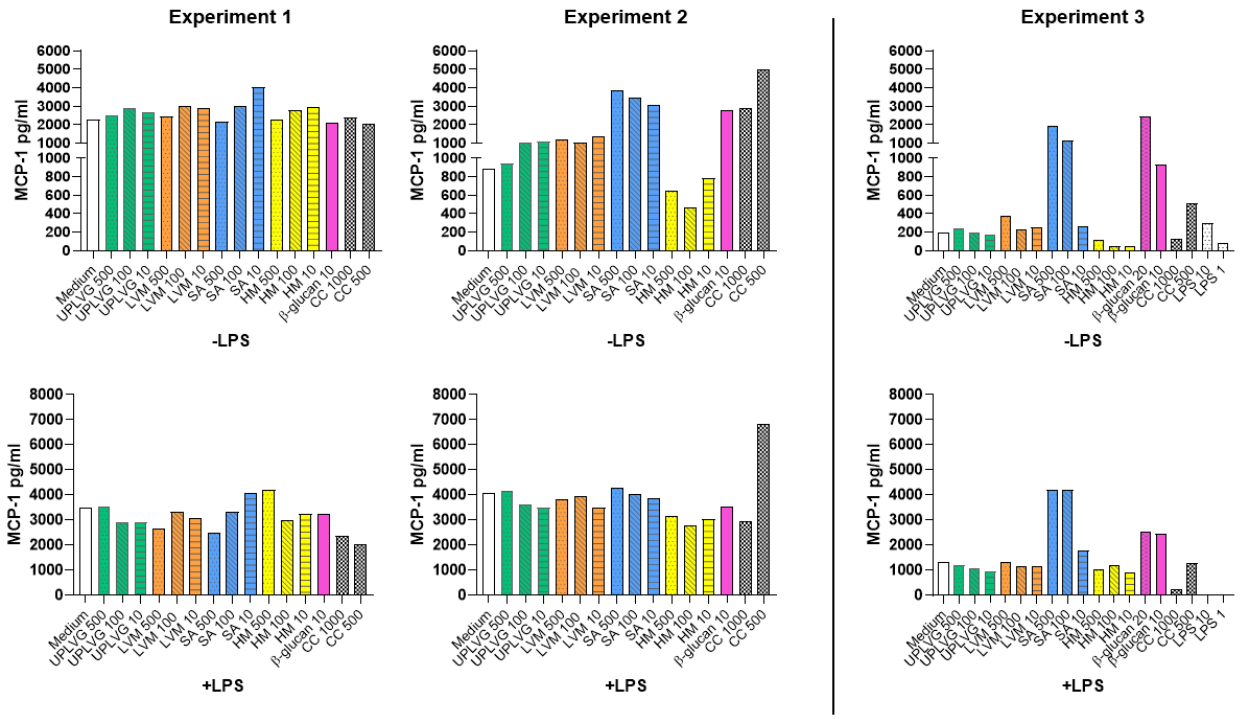

Figure 3.2.6: Comparison of the secretion of MCP-1 by monocytes of three different donors after 24 hours of training, and 5 days of rest before measurement of cytokines either following addition of medion alone (-LPS) of following stimulation of the unrelated stimuli (+LPS). The Following stimuli were tested for training effects: the alginates UPLVG (G-rich alginate) (green), LVM (M-rich alginate) (orange), SA (sulfated alginate) (blue), HM (High-M alginate, 94% M) (yellow) with concentrations of 500 (spotted), 100 (diagonal lines) and 10 (straight lines) µg/mL; β-glucan (purple) with concentrations of 20 and 10 µg/mL; cholesterol crystals (CC) (black squared) with concentrations of 1000 and 500 µg/mL; and LPS (black spotted) with concentrations of 10 and 1 ng/mL. Experiment 1 and 2 follows the same experimental procedure. Experiment 3 is experimental different by change of culture medium and addition of LPS as experimental condition.

The induction of MCP-1 is shown in Figure 3.2.6. Overall, the induction of MCP-1 in experiment 1 and 2 following the various stimuli was minor. All conditions induced a similar level like the medium control for donor 1. For donor 2, SA and CC augmented the production of MCP-1 compared to medium (and UPLVG and LVM), while HM induced a lower production. The overall strongest inductor of MCP-1 was after addition of CC for experiment 1 and 2. After stimulation with LPS, almost all conditions, in both experiments, were observed at the same level as the medium control. One exception from this was CC at the lowest dose (500 µg/mL). Induction of MCP-1 by all conditions showed a comparable picture between restimulation with medium and LPS in experiment 3. SA and β-glucan induced higher levels than medium, while UPLVG, LVM, HM, and CC were observed to lie around the medium control's induction. LPS induced MCP-1 more or less like the medium control upon restimulation with medium. After restimulation with LPS, the measured level was less than 1 pg/mL, suggesting an LPS-tolerance.

Overall, SA induced the highest levels of several cytokines when restimulated with medium in experiment 1 and 2. Upon restimulation with LPS, an opposite effect was observed for the same cytokines, which might indicate an effect of tolerance. β-glucan, used as a positive control, was observed in many cases to induce a

similar level of cytokines like medium control. Cytokine concentration of CC showed in many cases to be like medium or below. In experiment 3, the presence of complement seemed to affect SA and HM by inducing opposite cytokine levels, especially for TNF, IL-1β, and IL-6 compared to experiment 1 and 2.

4 Discussion

The human whole blood model is valuable in the prediction of microspheres' initial inflammatory potential. However, essential knowledge about their ability to trigger an immune response is missed between 4 hours of incubation *in vitro* and several weeks of implantation *in vivo* that eventually results in fibrotic overgrowth of the microspheres. In the search for a better bio(in)compatibility understanding and a predictive *in vitro* model for evaluation of biomaterials, microspheres and different types of soluble alginate were investigated in two distinct procedures to illuminate alternative explanations that cause fibrosis. Incubation of microspheres in the long-term *in vitro* experimental model of peripheral blood mononuclear cells (PBMCs) and monocytes in 2D and 3D was able to induce trends of selected cytokines observed in the human whole blood model (at 4h incubation). Soluble alginate of SA was observed to activate relatively high levels (compared to the others) of cytokines central in the foreign body response. However, in implantation studies, the SA-bead does not cause fibrosis, suggesting that SA also initiates anti-inflammatory responses that hamper the foreign body response. Comparison between induction of cytokines in 2D and 3D showed that microspheres caused, in most cases, highest induction of pro-inflammatory cytokines in 3D, while soluble alginates caused, in most cases, the highest induction in 2D. The possibility for cell adherence and further macrophage differentiation could be a determining factor for this observation. In the investigation of soluble alginate's ability to induce trained immunity, SA and HM were observed to be active molecules and were affected by the presence of complement during incubation. None of the tested alginates were observed to induce a prominent effect of cytokine release connected to training. However, the positive control, β-glucan, did neither, meaning that the setup could be improved before alginate is excluded as a stimulus for training of monocytes.

4.1 Long-term *in vitro* experimental model

Factors contributing to the fibrotic overgrowth of biomaterials are still an unexplored field, and development of a model that can better predict biomaterials' potential in causing fibrosis is needed. Using models in 2D and 3D can be useful, both for comparison, and because the whole blood (WB) model is conducted in 3D. The long-term *in vitro* experimental (L-IVE) model may work as an extension of the WB model to predict inflammatory properties using knowledge obtained from the WB model. For example, research based on the WB model has shown that complement plays a role in leukocyte activation and cytokine release[34], and should, therefore, be included in the L-IVE model. However, to avoid additional activation through reactive culture plates, the model was conducted in heat-inactivated (h.i.) serum, but with microspheres opsonized in active serum for the inclusion of protein-opsonization, including complement. As an approach to get a more comprehensive and understandable picture of inflammatory responses induced by microspheres over a longer period of time, opsonized alginate microspheres and different types of soluble alginate were incubated with PBMCs for 14 days in h.i. serum, while the level of cytokines was measured at specific time points.

4.1.1 Microspheres

The induction of the pro-inflammatory cytokines TNF, IL-1β, and IL-6 in experiment 2-4 showed that AP stood out compared to A and SA, and displays the effect of opsonization of microspheres in active serum for 24 hours before incubation. The purpose of opsonization before long-term incubation was to mimic an *in vivo* situation and recreate some of the effects observed in the human whole blood model, so that specific

conditions of incubation in the models are comparable. Of note, 24-hour opsonization in active serum will be different from the one in whole blood due to, among other things, the presence of cells in whole blood and the incubation time of 4 hours. Protein adsorption is also a dynamic process[105], opening up the possibility for the microspheres to be of different protein-adsorbed character when comparing 4 hours and 24 hours of opsonization. Thereby, the results of the L-IVE model can, in theory, show different trends than those from the WB model. However, data from a whole blood experiment based on the same microspheres presented in Figure 1.4.1 on page 19, show the same trends observed for A, AP, and SA in experiment 2-4, meaning that the L-IVE model is able to regenerate trends observed in the WB model. This strengthens the L-IVE model's reliability to produce valuable results in the further search of the connection between microspheres' inflammatory potential and development of fibrosis.

Microspheres' surface properties are essential in the initial activation of the immune response. AP differs from A and SA, among other things, by having a poly-L-lysine coat around the alginate core, making this capsule positively charged and becomes a determining factor for its susceptibility for opsonization. Ørning et al. have shown that a microsphere's potential of activating the complement system is connected to the release of pro-inflammatory cytokines[34]. Active serum contains complement proteins, and activation of the system results in deposition of C3b and iC3b, which are important ligands for leukocyte adhesion through the receptor CD11b/CD18 (CR3). This binding contributes to leukocyte activation and is an important mechanism for the release of cytokines, such as TNF, IL-1β, and IL-6[34]. At physiological pH, complement proteins, such as C3 and C3b/iC3b, are negatively charged, making AP's positively charged surface susceptible to deposition, further leading to cytokine release[11]. The fact that complement is a driver behind the release of some cytokines can be observed in most cases for the measured level of TNF, IL-1β, and IL-6 induced by AP for all experiments.

MCP-1 has also shown to be induced in a complement-dependent manner, where blockage of C3 completely inhibited the secretion of MCP-1[12]. However, blockage of CD11b or CD18 did not reduce the secretion of MCP-1, but rather increased it, which suggests that induction of MCP-1 depends on another mechanism related to complement than cell-adhesion[34]. The induced level of MCP-1 by SA and AP can partly confirm this, especially in the 3D model. In several cases, SA induces a higher level than AP, first seen from day 1 and onward, contributing to the fact that induction of MCP-1 is not caused by cell-adhesion through deposited iC3b and CR3(CD11b/CD18). Lappegård et al. observed the effect of complement inhibition through heparin-coating and suggested that secretion of MCP-1 was driven by both complement-dependent and complement-independent mechanisms, due to complete inhibition by heparin-coating, and only partial inhibition with C5a blockage[106]. Sulfation of alginate seems to increase the binding of factor H, an inhibitory complement protein[21], due to factor H's affinity of binding glucosaminoglucans, such as heparin[107]. Sulfated alginate work probably as a glucosaminoglycan analog, causing more binding of factor H, which explains low activation of cytokines by SA related to cell-adhesion through complement proteins. The high levels of MCP-1 induced by SA in several of these experiments support Lappegård et al.'s suggestion of MCP-1 being driven by complement-independent mechanisms, but which mechanisms that drive the induction of MCP-1 by SA is yet to be investigated.

4.1.2 Soluble alginates

Different types of soluble alginates were added as experimental conditions in experiment 2-4 to observe if a potential leakage from the microspheres could induce cytokine release. In several cases, the level induced was not so different from the medium control, meaning that leakage from microspheres does not necessarily affect the induction of selected cytokines. However, observation of some cytokines showed that soluble alginate has an effect on the induction in a concentration-dependent manner. First of all, the induction of MCP-1 showed a clear image of increased induction with a decreasing concentration of SA. The relation was observed in all experiments in Figures 3.1.18, 3.1.26 and 3.1.34 in both 2D and 3D, which strengthens the reliability of this observation. The measured concentration is admittedly not higher than medium in 2D like it is in 3D. Although, this may be explained by background activation caused by the polystyrene plate itself, which causes a relatively high induction by the medium control. Leakage from microspheres is probably in smaller concentrations, and the results suggest that small concentrations may be enough to induce relatively high cytokine levels that are a contributing factor in the development of fibrosis. MCP-1 attracts monocytes to the site of inflammation and has been shown to play an important role in macrophage fusion into FBGCs during the foreign body response[108]. The leakage of SA from the microbead may induce MCP-1 and thereby be a contributing factor during the early phase in the development of the fibrotic capsule around the biomaterial, which eventually will hamper its function.

Induction of M-CSF by soluble alginates is shown in Figures 3.1.19, 3.1.27 and 3.1.35. The measured level of the soluble alginates was, in many cases, at the same level as medium, but SA was often observed to lie at an overall higher level. M-CSF is an important inflammatory mediator that stimulates macrophage growth, differentiation, and survival through the colony-stimulating factor 1 receptor (CSF1R). The receptor has been investigated in its role in the development of fibrosis and has found to be crucial in the foreign body reaction in response to transplantation of biomaterials in rodents and non-human primates[43]. Inhibition of CSF1R by macrophage depletion caused a loss of fibrosis, while other macrophage functions like wound healing and phagocytosis were preserved[43]. Induction of M-CSF caused by leakage of SA may, therefore, be an explanation if fibrosis is observed around the SA microbead.

Soluble alginate of SA seems to activate cytokines important for monocyte recruitment and differentiation central in the foreign body response. However, from unpublished data, microbeads of the same alginate do not display fibrotic overgrowth after implantation in rodents after several weeks (2-14), suggesting that there are effects *in vivo* that prevent SA to initiate a foreign body reaction. SA (both microbead and soluble alginate) is probably not perceived as inert by the body based on the observed results but may be of an anti-inflammatory character that causes a lack of fibrosis. Observation of induced levels of IL-10 and IL-1ra in 3D shown in Figures 3.1.25, 3.1.29, 3.1.33 and 3.1.37 from experiment 3 and 4 may indicate that SA also has an inhibiting effect on the inflammatory response after implantation. IL-10 and IL-1ra are anti-inflammatory cytokines and promote wound-healing. As IL-1ra works as an inhibiting competitor to IL-1β, IL-10 down-regulates activity of cells stimulated by IL-1β, and is one of the most important mediators connected to resolution of inflammation[55]. IL-10 is also a stimulator of macrophage differentiation towards a wound-healing phenotype, in particular, a subset of M2 called M2c. Further, M2c secrete IL-10 and TGF-β contributing to suppression of immune responses[109]. M1 macrophages perform a phenotypic switch to the M2 subset Ma in response to IL-4, which is crucial in the formation of FBGCs starting the

foreign body reaction[48, 110]. IL-10 has shown to enhance the expression of IL-4 receptor on macrophages making macrophages display a more anti-fibrotic and anti-inflammatory phenotype of M2a[111, 112]. The M2c subset has been transcriptomic analyzed, and findings of up-regulated genes may suggest that this subset contributes in the early stages of wound-healing before M2a[113]. Somehow, SA may induce higher levels of IL-10, causing macrophage differentiation towards M2c, which responds by producing more anti-inflammatory mediators. This can create an anti-inflammatory milieu and hampering the initiation of the foreign body reaction caused by M2a macrophages. However, macrophage polarization is not a two-sided occurrence. In response to various mediators in the microenvironment, macrophage polarization can be shaped into specific phenotypes somewhere on the broad spectrum between M1 and M2, providing both pro-inflammatory and anti-inflammatory traits.

4.1.3 2D model vs. 3D model

The L-IVE model was conducted in two different experimental models: 2D and 3D. As the 3D model gives a better representation of the cell environment found *in vivo* by, among other things, providing cell-to-cell interaction and a more realistic nutrient access, 2D is still used in the majority of cell research due to cost and existence of comparative literature. However, 3D modeling is more and more used within tissue engineering but has not been applied to any great extent within immunological research (besides the whole blood model). By conducting the experiments in both 2D and 3D, experimental differences and similarities could be provided, like an observation of specific patterns.

Results of culturing microspheres in 2D and 3D were fluctuating. The pro-inflammatory cytokines were observed to be highest induced in 3D in most cases. Again, the importance of opsonization is displayed, but also the effect of suspension culturing in non-adherent materials. When PBMCs are incubated with opsonized microspheres in vials not promoting cell adherence, the cells will bind to microspheres via deposited iC3b (or C3b) and the receptor CR3, further leading to release of pro-inflammatory cytokines in a complement-dependent manner, as earlier described. When PBMCs are incubated with opsonized microspheres in 2D with polystyrene plates, some cells may rather bind to the plate surface as unstimulated to produce cytokines induced by complement, and "reduce" the possible amount of cells that can bind to the surface of microspheres and induce the release of cytokines. Thereby, the absence of other materials that promote adherence can be a contributing factor to this observation. The chemokine GRO-α showed a similar picture like the pro-inflammatory cytokines and was, in several cases, observed to be induced in higher amounts in 3D. TNF has been shown to induce release of GRO-α in human endothelial cells *in vitro*[114]. It is not unlikely that TNF may also induce the release of GRO-α in human monocytes, thereby explaining the induction of the chemokine.

The induced level of M-CSF by microspheres showed to be partly higher in 2D, where the secretion seemed to increase over time. This was an effect observed both for medium and microspheres, and the microspheres did not induce higher levels than medium in many cases. The response may be following macrophage differentiation via cell-adhesion to the polystyrene plates. This creates a background activation, where the secretion of M-CSF is somewhat explained by the polystyrene plates and not through stimuli caused by the microspheres. The theory of background activation can also be justified by looking at the induction by LPS and CC, which also follows the induced level of medium. A partly similar picture may be seen in 3D, but only

A and SA induced concentrations around the level of medium. AP, on the other hand, induced higher levels, which suggest that AP promotes an activation that is not induced by A and SA. Further, this activation was more prominent in 3D than in 2D, and can be due to lack of surfaces other than the microspheres, that promote cell adhesion.

Generally, the measured level of cytokines induced by soluble alginates was higher in 2D than in 3D, and this elevation was also observed for the medium control in the 2D setup. This may indicate that the polystyrene plate itself stimulates cytokine release and thereby provide some background activation in addition to the stimulating conditions of soluble alginates. One explanation can be the degree of differentiation from monocytes to macrophages. Adherence is an important mechanism for blood monocytes to differentiate into macrophages[115]. Polystyrene culturing plates are made hydrophilic to promote cell adhesion through promoting first protein adsorption. The possibility of the cells to adhere further promotes cell differentiation[116]. The polypropylene vials have a low protein binding capacity, and do not promote cell adhesion like polystyrene. Cell culturing in polypropylene will probably result in less differentiation of blood monocytes into macrophages unless they have a surface that promotes attachment. Soluble alginate will not promote such an attachment. However, it can promote activation through pattern recognition receptors (PRRs), like Toll-like receptors (TLRs). A study by Schutte et al. showed that macrophages differentiated from monocytes secrete higher levels of selected cytokines compared to unactivated and activated monocytes in tissue culture polystyrene plates[117]. This applied for several of the cytokines emphasized in this study: TNF, IL-1β, IL-6, IL-8, MCP-1, IL-10, and IL-1ra. The higher induction of cytokines observed in 2D for soluble alginates may, therefore, be a result of more extensive differentiation into macrophages due to adherence. However, LPS, an important stimulus for activation of monocytes through TLR2/CD14, did not show distinct differences between 2D and 3D. This may suggest that it is not only polystyrene plates promoting adherence that result in higher induced levels in 2D. Soluble alginate and polystyrene plates may together cause better conditions in 2D, which LPS and polystyrene cannot do, so that the induced levels are higher than in 3D.

4.2 Trained immunity

Different kinds of stimuli, such as β-glucan, have shown to induce epigenetic changes of histones resulting in the up-regulation of cell function and a long-term pro-inflammatory phenotype. The phenomenon may play a role in fibrosis development, a major obstacle in cell encapsulation therapy with microspheres of alginate. Monocytes were exposed to different kinds of soluble alginate to explore their ability to induce trained immunity by measuring the induced level of selected cytokines that have been revealed as a trait of the pro-inflammatory phenotype.

SA and HM displayed some specific patterns observed in the induction of TNF, IL-1β, and IL-6. In experiment 1 and 2, SA seemed to induce some sort of tolerance after restimulation with unrelated stimuli, LPS. Endotoxin tolerance is induced by persistent TLR stimulation and result in a phenotype switch from pro-inflammatory to anti-inflammatory by reducing the production of TNF and IL-6 and increasing the production of IL-10 and TGF-β[118]. As LPS induce cytokine release through TLR2 and TLR4, the observed tolerance might suggest that SA works as a ligand for the same TLRs, thereby causing a tolerance effect when the macrophages are stimulated with LPS. A study by Prechel et al. showed that specific platelet

factor 4 (PF4) and heparin complexes were able to cause a TLR4-mediated response by mimicking pathogen-associated molecular patterns (PAMPs)[119]. As sulfated alginate may work as a heparin analog, SA could induce activation through TLR4 by resembling PAMPs, thereby causing a tolerance effect when cells are restimulated with LPS. However, HM has been shown to activate monocytes and induce cytokine release by the involvement of TLR2 and TLR4[89] like LPS, meaning that such a tolerance effect should in theory also have been observed for HM. But, of note, the results are based on few replicates, and donor differences will be more prominent. Results based on several replicates will provide a more specific and reliable image.

The presence of complement did also seem to affect the induction of the pro-inflammatory cytokines IL-1β and IL-6. For the cells added medium five days after stimuli wash-out, high levels were induced by SA and low levels by HM without complement. The presence of complement showed an opposite pattern by low induction by SA, and high induction by HM. This suggests that complement has an impact on cytokine release induced by SA and HM. SA's ability to bind the inhibiting factor H can be a contributing factor to lower the response of cytokines secreted in a complement-dependent manner. Further, HM's ability to induce cytokine release via TLR2 and TLR4 became more prominent when complement proteins were present, which can be a result of crosstalk between TLRs and the complement system. For example, it was established that C5aR and C3aR, receptors of the anaphylatoxins C5a and C3a (and protein fragments of the complement proteins C3 and C5), had a regulatory effect on cytokine production, including TNF, IL-1β and IL-6, induced by TLR4 in mice[120], suggesting that presence of complement enhance a TLR4-mediated response. Therefore, culture media supplemented with active serum may explain the induced levels of IL-1β and IL-6 by HM.

The most essential with these experiments was to observe a possible training effect on monocytes induced by alginate. Overall, none of the soluble alginate types tested showed any prominent effect of training in human monocytes. However, the positive control used, β-glucan, did not either. By observations of results presented by Bekkering et al.[60, 74], the effect of β-glucan training, after restimulation with LPS, should be more prominent. For example, training 24 hours of training and 6 days of resting induced approximately a 6 fold and 10 fold change to RPMI training for IL-6 and TNF, respectively[60]. For the same cytokines, it was observed approximately a 1.5 fold change to RPMI training, proposing that the experiments were not successful. The type of β-glucan may be a crucial factor contributing to the observed results. The one used in these experiments was from *Saccharomyces Cerevisiae* (S. Cerevisiae), which on molecular level contained linear β1,3-glucan with a small number of β1,6-glucan branches, while Bekkering et al. used β1,3-(D)-glucan, a β-glucan without branches. However, dectin-1 have been identified as a PRR that recognizes both β1,3-linked and β1,6-linked glucans, including *S. Cerevisiae*. The lack of training can rather be connected to the size of the β-glucan. Elder et al. have reported that the size of beta-glucan particulates controls the innate immune response mediated by dectin-1 in human monocyte-derived dendritic cells[121]. This applied for, among other things, IL-1β and IL-6, where larger particles of β-glucan induced higher levels of the cytokines. They concluded with phagocytosis being a determining factor. Small particles get phagocytosed, which results in loss of dectin-1 expression on the surface and lower the induction of IL-1β. Bigger particles that cannot be phagocytosed will rather stimulate immune response through dectin-1, resulting in induced cytokine release. The β-glucan solution used in this study could be of smaller particles, thereby be phagocytosed rather than stimulate epigenetic reprogramming through dectin-1, further leading to

increased cytokine response when stimulated with unrelated stimuli. The results are based on few replicates also contributing to lack of statistics and thereby less reliable data. This must also be taking into account when comparing data with Bekkering et al. and searching for a training effect induced by the soluble alginates, CC, and β-glucan.

4.3 Future Perspectives

The differentiation of macrophages induced by biomaterials is still an unexplored area. Further work of the L-IVE model can focus on monocytes' maturing to macrophages induced by the microspheres. First of all, a broader cytokine measurement can be included for better prediction of macrophage differentiation. For example, measurement of induced IL-4 and IL-13 can supplement a hypothesis of differentiation towards M2 subsets. Receptors of monocytes and macrophages can be mapped by flow cytometry for prediction of maturation degree caused by microspheres as monocytes and macrophages express a differential degree of receptors during maturation. For example, monocytes express receptors like CD14 and CD64, while macrophages express more of the receptors CSF-1R, CD68, and MHCII[122, 123], making these receptors useful for mapping the level of maturation of monocytes to macrophages. Further, gene expression panels can be employed to investigate the transcriptome of the monocytes/macrophages. For example, using nCounter® technology from NanoString gives a direct detection of gene and protein expression profiling[124]. This can provide information on which genes that is up-regulated and thereby an understanding of what kind of macrophage polarization the different microspheres and soluble alginates induce. This kind of information will be beneficial in predicting factors contributing or inhibiting the pathogenesis of fibrosis and will further be valuable for development and selection of the best microsphere candidates for transplantation studies in animals.

In the trained immunity experiments, it was challenging to decide whether a training effect was observed or not, both for the soluble alginates and the positive control, β-glucan. The protocol of this setup should be further developed before a conclusion related to alginate and CC inducing trained immunity or not is drawn. The fact that the positive control did not show prominent induction of the cytokines relevant for trained immunity suggests that the setup can be improved. Methyltransferases causing histone methylation is known to be essential for the epigenetic reprogramming induced by β-glucan. As trained immunity experiments are conducted, a control setup containing a methyltransferase, such as 5'-thioadenosine, can be performed. A comparison between the setups can tell if training is observed, first of all, for β-glucan, and confirm or decline that the developed protocol is functional. As 3D culturing is a better approximation of *in vivo* conditions, developing a 3D model for training could be of interest. Of note, no literature of training in 3D was found, perhaps being an unexplored area. If alginate is confirmed as an inducer of training, further investigation of macrophage polarization can be performed, like for the long-term model. For example, β-glucan from *Candida albicans* differentiate human monocytes into a specific subset of macrophages somewhere in between M1 and M2 and further prevents apoptosis in the absence of M-CSF[77]. Does soluble alginate also cause such an effect? Findings of macrophage differentiation from the L-IVE model and trained immunity can be compared and contribute with a more comprehensive understanding of the development of fibrosis.

5 Conclusion

By using knowledge obtained from the whole blood model, a long-term *in vitro* experimental model of PBMCs was established as an intention for a broader understanding of biomaterials' ability to develop or avoid fibrosis. Three alginate microspheres, four types of soluble alginate, and cholesterol crystals (CC) were used as materials for the study. The cultivation conditions were compared in 2D and 3D by secretion patterns of selected cytokines. Soluble alginate and CC were also investigated as possible inducers of trained immunity.

Incubation of the alginate microspheres in the long-term *in vitro* model in 2D and 3D was able to induce trends of cytokine release observed in the whole blood model, showing that the developed model can work as an extension of the whole blood model in inflammatory evaluation. Opsonization of microspheres before incubation was an essential step for using the whole blood model as a comparison, as well as protein adsorption to the biomaterial is a fundamental process after transplantation. Microspheres' surface properties become essential during opsonization, and AP was here confirmed as a microcapsule with complement-binding properties and thereby resulted in a prominent release of pro-inflammatory cytokines in a complement-dependent manner.

The level of cytokines induced by the soluble alginates was, in most cases, not so different from medium control. For some cytokines, like MCP-1, the induction was observed to be in a concentration-dependent manner.

Both microbead SA and soluble SA activated cytokines important for monocyte recruitment (MCP-1) and differentiation (M-CSF), central in the foreign body response. As the SA microbead does not display fibrotic overgrowth after implantation in rodents, SA may also induce an anti-inflammatory response, reducing the foreign body response initiated via MCP-1 and M-CSF. This could partly be confirmed by induced levels of IL-10 and IL-1ra by soluble SA.

Incubation in 2D and 3D showed some various responses. The microspheres showed the highest induction in 3D for the pro-inflammatory cytokines and GRO-α. Soluble alginates induced the highest levels of cytokines in 2D. Polystyrene promotes cell adherence and, thereby, macrophage differentiation, which can increase the production of cytokines.

The trained immunity experiments did not show a specific training effect on human monocytes by the soluble alginates or CC. However, the positive control β-glucan did neither. SA and HM showed to be active molecules by showing opposite patterns depending on the presence of complement in the culture medium. SA was also observed to induce a tolerance effect for the cytokines TNF, IL-1β, and IL-6 upon restimulation with LPS.

Further studies should focus on optimizing the protocol of the long-term *in vitro* model, as well as the maturing of monocytes to macrophages for the determination of macrophage polarization. The trained immunity protocol should also be optimized for further studies before a concluding whether soluble alginates and CC are able to induce training of human monocytes.

References

[1] Mirjana Pavlovic. "What Are Biomaterials?" In: *Bioengineering*. Springer International Publishing, Sept. 2014, pp. 229–244. DOI: 10.1007/978-3-319-10798-1_18. URL: https://doi.org/10.1007/978-3-319-10798-1_18.

[2] *WHO | Transplantation*. https://www.who.int/topics/transplantation/en/. (Accessed on 12/02/2019).

[3] Grace J. Lim et al. "Cell Microencapsulation". In: *Advances in Experimental Medicine and Biology*. Springer New York, 2010, pp. 126–136. DOI: 10.1007/978-1-4419-5786-3_11. URL: https://doi.org/10.1007/978-1-4419-5786-3_11.

[4] T Vial. "Immunosuppressive drugs and cancer". In: *Toxicology* 185.3 (Apr. 2003), pp. 229–240. DOI: 10.1016/s0300-483x(02)00612-1. URL: https://doi.org/10.1016/s0300-483x(02)00612-1.

[5] Khalid Shah. "Genetically Engineered Mesenchymal Stem Cells". In: *Mesenchymal Stem Cells in Cancer Therapy*. Elsevier, 2014, pp. 1–36. DOI: 10.1016/b978-0-12-416606-6.00001-5. URL: https://doi.org/10.1016/b978-0-12-416606-6.00001-5.

[6] Catherine Tomaro-Duchesneau et al. "Microencapsulation for the Therapeutic Delivery of Drugs, Live Mammalian and Bacterial Cells, and Other Biopharmaceutics: Current Status and Future Directions". In: *Journal of Pharmaceutics* 2013 (2013), pp. 1–19. DOI: 10.1155/2013/103527. URL: https://doi.org/10.1155/2013/103527.

[7] Franklin Lim and Anthony M. Sun. "Microencapsulated Islets as Bioartificial Endocrine Pancreas". In: *Science* 210.4472 (1980), pp. 908–10. URL: www.jstor.org/stable/1684447.

[8] Anne Mari Rokstad et al. "Advances in biocompatibility and physico-chemical characterization of microspheres for cell encapsulation". In: *Advanced Drug Delivery Reviews* 67-68 (Apr. 2014), pp. 111–130. DOI: 10.1016/j.addr.2013.07.010. URL: https://doi.org/10.1016/j.addr.2013.07.010.

[9] Buddy D. Ratner. "The Biocompatibility Manifesto: Biocompatibility for the Twenty-first Century". In: *Journal of Cardiovascular Translational Research* 4.5 (June 2011), pp. 523–527. DOI: 10.1007/s12265-011-9287-x. URL: https://doi.org/10.1007/s12265-011-9287-x.

[10] Anne Mari Rokstad et al. "Biocompatibility and Biotolerability Assessment of Microspheres Using a Whole Blood Model". In: *Micro and Nanosystems* 5.3 (July 2013), pp. 177–185. DOI: 10.2174/1876402911305030005. URL: https://doi.org/10.2174/1876402911305030005.

[11] Anne Mari Rokstad et al. "Alginate microbeads are complement compatible, in contrast to polycation containing microcapsules, as revealed in a human whole blood model". In: *Acta Biomaterialia* 7.6 (June 2011), pp. 2566–2578. DOI: 10.1016/j.actbio.2011.03.011. URL: https://doi.org/10.1016/j.actbio.2011.03.011.

[12] Anne Mari Rokstad et al. "The induction of cytokines by polycation containing microspheres by a complement dependent mechanism". In: *Biomaterials* 34.3 (Jan. 2013), pp. 621–630. DOI: 10.1016/j.biomaterials.2012.10.012. URL: https://doi.org/10.1016/j.biomaterials.2012.10.012.

[13] Aileen King et al. "Improvement of the biocompatibility of alginate/poly-L-lysine/alginate microcapsules by the use of epimerized alginate as a coating". In: *Journal of Biomedical Materials Research Part A* 64A.3 (Feb. 2003), pp. 533–539. DOI: 10.1002/jbm.a.10276. URL: https://doi.org/10.1002/jbm.a.10276.

[14] Matthew A. Bochenek et al. "Alginate encapsulation as long-term immune protection of allogeneic pancreatic islet cells transplanted into the omental bursa of macaques". In: *Nature Biomedical Engineering* 2.11 (Aug. 2018), pp. 810–821. DOI: 10.1038/s41551-018-0275-1. URL: https://doi.org/10.1038/s41551-018-0275-1.

[15] Edorta Santos et al. "Biomaterials in Cell Microencapsulation". In: *Advances in Experimental Medicine and Biology*. Springer New York, 2010, pp. 5–21. DOI: 10.1007/978-1-4419-5786-3_2. URL: https://doi.org/10.1007/978-1-4419-5786-3_2.

[16] Bo Nilsson et al. "Can cells and biomaterials in therapeutic medicine be shielded from innate immune recognition?" In: *Trends in Immunology* 31.1 (Jan. 2010), pp. 32–38. DOI: 10.1016/j.it.2009.09.005. URL: https://doi.org/10.1016/j.it.2009.09.005.

[17] Jenni Punt et al. *Kuby Immunology*. 8th ed. W. H. Freeman and Company, 2019.

[18] Abul K. Abbas and Andrew H. Lichtman. *Basic immunology: functions and disorders of the immune system*. 3rd ed., updated. Elsevier, Saunders, 2011. ISBN: 9781416055693.

[19] Sandra Franz et al. "Immune responses to implants – A review of the implications for the design of immunomodulatory biomaterials". In: *Biomaterials* 32.28 (Oct. 2011), pp. 6692–6709. DOI: 10.1016/j.biomaterials.2011.05.078. URL: https://doi.org/10.1016/j.biomaterials.2011.05.078.

[20] Daniel Ricklin et al. "Complement: a key system for immune surveillance and homeostasis". In: *Nature Immunology* 11.9 (Aug. 2010), pp. 785–797. DOI: 10.1038/ni.1923. URL: https://doi.org/10.1038/ni.1923.

[21] Øystein Arlov, Gudmund Skjåk-Bræk, and Anne Mari Rokstad. "Sulfated alginate microspheres associate with factor H and dampen the inflammatory cytokine response". In: *Acta Biomaterialia* 42 (Sept. 2016), pp. 180–188. DOI: 10.1016/j.actbio.2016.06.015. URL: https://doi.org/10.1016/j.actbio.2016.06.015.

[22] Maud B. Gorbet and Michael V. Sefton. "Biomaterial-associated thrombosis: roles of coagulation factors, complement, platelets and leukocytes". In: *Biomaterials* 25.26 (Nov. 2004), pp. 5681–5703. DOI: 10.1016/j.biomaterials.2004.01.023. URL: https://doi.org/10.1016/j.biomaterials.2004.01.023.

[23] Massimo Cugno and Alberto Tedeschi. "Coagulation Factor Autoantibodies". In: *Autoantibodies*. Elsevier, 2014, pp. 499–509. DOI: 10.1016/b978-0-444-56378-1.00059-9. URL: https://doi.org/10.1016/b978-0-444-56378-1.00059-9.

[24] C. T. ESMON, J. XU, and F. LUPU. "Innate immunity and coagulation". In: *Journal of Thrombosis and Haemostasis* 9 (July 2011), pp. 182–188. DOI: 10.1111/j.1538-7836.2011.04323.x. URL: https://doi.org/10.1111/j.1538-7836.2011.04323.x.

[25] Steven P. Grover and Nigel Mackman. "Intrinsic Pathway of Coagulation and Thrombosis". In: *Arteriosclerosis, Thrombosis, and Vascular Biology* 39.3 (Mar. 2019), pp. 331–338. DOI: 10.1161/atvbaha.118.312130. URL: https://doi.org/10.1161/atvbaha.118.312130.

[26] Saulius Butenas, Thomas Orfeo, and Kenneth G. Mann. "Tissue Factor in Coagulation". In: *Arteriosclerosis, Thrombosis, and Vascular Biology* 29.12 (Dec. 2009), pp. 1989–1996. DOI: 10.1161/atvbaha.108.177402. URL: https://doi.org/10.1161/atvbaha.108.177402.

[27] Maria I Bokarewa, James H Morrissey, and Andrej Tarkowski. In: *Arthritis Research* 4.3 (2002), p. 190. DOI: 10.1186/ar405. URL: https://doi.org/10.1186/ar405.

[28] Bo Nilsson et al. "The role of complement in biomaterial-induced inflammation". In: *Molecular Immunology* 44.1-3 (Jan. 2007), pp. 82–94. DOI: 10.1016/j.molimm.2006.06.020. URL: https://doi.org/10.1016/j.molimm.2006.06.020.

[29] Kristina N. Ekdahl et al. "Innate immunity activation on biomaterial surfaces: A mechanistic model and coping strategies". In: *Advanced Drug Delivery Reviews* 63.12 (Sept. 2011), pp. 1042–1050. DOI: 10.1016/j.addr.2011.06.012. URL: https://doi.org/10.1016/j.addr.2011.06.012.

[30] Jürgen Strasser et al. "Unraveling the Macromolecular Pathways of IgG Oligomerization and Complement Activation on Antigenic Surfaces". In: *Nano Letters* 19.7 (June 2019), pp. 4787–4796. DOI: 10.1021/acs.nanolett.9b02220. URL: https://doi.org/10.1021/acs.nanolett.9b02220.

[31] Kei Ikeda et al. "C5a Induces Tissue Factor Activity on Endothelial Cells". In: *Thrombosis and Haemostasis* 77.02 (1997), pp. 394–398. DOI: 10.1055/s-0038-1655974. URL: https://doi.org/10.1055/s-0038-1655974.

[32] Konstantinos Ritis et al. "A Novel C5a Receptor-Tissue Factor Cross-Talk in Neutrophils Links Innate Immunity to Coagulation Pathways". In: *The Journal of Immunology* 177.7 (Sept. 2006), pp. 4794–4802. DOI: 10.4049/jimmunol.177.7.4794. URL: https://doi.org/10.4049/jimmunol.177.7.4794.

[33] Ewelina M. Golebiewska and Alastair W. Poole. "Platelet secretion: From haemostasis to wound healing and beyond". In: *Blood Reviews* 29.3 (May 2015), pp. 153–162. DOI: 10.1016/j.blre.2014.10.003. URL: https://doi.org/10.1016/j.blre.2014.10.003.

[34] Pontus Ørning et al. "Alginate microsphere compositions dictate different mechanisms of complement activation with consequences for cytokine release and leukocyte activation". In: *Journal of Controlled Release* 229 (May 2016), pp. 58–69. DOI: 10.1016/j.jconrel.2016.03.021. URL: https://doi.org/10.1016/j.jconrel.2016.03.021.

[35] Analiz Rodriguez, Howard Meyerson, and James M. Anderson. "Quantitativein vivo cytokine analysis at synthetic biomaterial implant sites". In: *Journal of Biomedical Materials Research Part A* (2008). DOI: 10.1002/jbm.a.31939. URL: https://doi.org/10.1002/jbm.a.31939.

[36] Jun-Ming Zhang and Jianxiong An. "Cytokines, Inflammation, and Pain". In: *International Anesthesiology Clinics* 45.2 (2007), pp. 27–37. DOI: 10.1097/aia.0b013e318034194e. URL: https://doi.org/10.1097/aia.0b013e318034194e.

[37] Hacer Sahin and Hermann E. Wasmuth. "Chemokines in tissue fibrosis". In: *Biochimica et Biophysica Acta (BBA) - Molecular Basis of Disease* 1832.7 (July 2013), pp. 1041–1048. DOI: 10.1016/j.bbadis.2012.11.004. URL: https://doi.org/10.1016/j.bbadis.2012.11.004.

[38] Zlatko Dembic. "Cytokines of the Immune System". In: *The Cytokines of the Immune System*. Elsevier, 2015, pp. 241–262. DOI: 10.1016/b978-0-12-419998-9.00007-9. URL: https://doi.org/10.1016/b978-0-12-419998-9.00007-9.

[39] Shankar Subramanian Iyer and Gehong Cheng. "Role of Interleukin 10 Transcriptional Regulation in Inflammation and Autoimmune Disease". In: *Critical Reviews^{TM} in Immunology* 32.1 (2012), pp. 23–63. DOI: 10.1615/critrevimmunol.v32.i1.30. URL: https://doi.org/10.1615/critrevimmunol.v32.i1.30.

[40] Kian Fan Chung. "Cytokines". In: *Asthma and COPD*. Elsevier, 2009, pp. 327–341. DOI: 10.1016/b978-0-12-374001-4.00027-4. URL: https://doi.org/10.1016/b978-0-12-374001-4.00027-4.

[41] Iain B. McInnes. "Cytokines". In: *Kelley and Firestein's Textbook of Rheumatology*. Elsevier, 2017, pp. 396–407. DOI: 10.1016/b978-0-323-31696-5.00026-7. URL: https://doi.org/10.1016/b978-0-323-31696-5.00026-7.

[42] J. G. Conway et al. "Inhibition of colony-stimulating-factor-1 signaling in vivo with the orally bioavailable cFMS kinase inhibitor GW2580". In: *Proceedings of the National Academy of Sciences* 102.44 (Oct. 2005), pp. 16078–16083. DOI: 10.1073/pnas.0502000102. URL: https://doi.org/10.1073/pnas.0502000102.

[43] Joshua C. Doloff et al. "Colony stimulating factor-1 receptor is a central component of the foreign body response to biomaterial implants in rodents and non-human primates". In: *Nature Materials* 16.6 (Mar. 2017), pp. 671–680. DOI: 10.1038/nmat4866. URL: https://doi.org/10.1038/nmat4866.

[44] Marius Raica and Anca Maria Cimpean. "Platelet-Derived Growth Factor (PDGF)/PDGF Receptors (PDGFR) Axis as Target for Antitumor and Antiangiogenic Therapy". In: *Pharmaceuticals* 3.3 (Mar. 2010), pp. 572–599. DOI: 10.3390/ph3030572. URL: https://doi.org/10.3390/ph3030572.

[45] N Iida and G R Grotendorst. "Cloning and sequencing of a new gro transcript from activated human monocytes: expression in leukocytes and wound tissue." In: *Molecular and Cellular Biology* 10.10 (Oct. 1990), pp. 5596–5599. DOI: 10.1128/mcb.10.10.5596. URL: https://doi.org/10.1128/mcb.10.10.5596.

[46] Laura Beth Moore and Themis R. Kyriakides. "Molecular Characterization of Macrophage-Biomaterial Interactions". In: *Advances in Experimental Medicine and Biology*. Springer International Publishing, 2015, pp. 109–122. DOI: 10.1007/978-3-319-18603-0_7. URL: https://doi.org/10.1007/978-3-319-18603-0_7.

[47] Bryan N. Brown and Stephen F. Badylak. "The Role of the Host Immune Response in Tissue Engineering and Regenerative Medicine". In: *Principles of Tissue Engineering*. Elsevier, 2014, pp. 497–509. DOI: 10.1016/b978-0-12-398358-9.00025-2. URL: https://doi.org/10.1016/b978-0-12-398358-9.00025-2.

[48] James M. Anderson, Analiz Rodriguez, and David T. Chang. "Foreign body reaction to biomaterials". In: *Seminars in Immunology* 20.2 (Apr. 2008), pp. 86–100. DOI: 10.1016/j.smim.2007.11.004. URL: https://doi.org/10.1016/j.smim.2007.11.004.

[49] Martin Guilliams, Alexander Mildner, and Simon Yona. "Developmental and Functional Heterogeneity of Monocytes". In: *Immunity* 49.4 (Oct. 2018), pp. 595–613. DOI: 10.1016/j.immuni.2018.10.005. URL: https://doi.org/10.1016/j.immuni.2018.10.005.

[50] Claire E. Olingy et al. "Non-classical monocytes are biased progenitors of wound healing macrophages during soft tissue injury". In: *Scientific Reports* 7.1 (Mar. 2017). DOI: 10.1038/s41598-017-00477-1. URL: https://doi.org/10.1038/s41598-017-00477-1.

[51] Toby Lawrence and Gioacchino Natoli. "Transcriptional regulation of macrophage polarization: enabling diversity with identity". In: *Nature Reviews Immunology* 11.11 (Oct. 2011), pp. 750–761. DOI: 10.1038/nri3088. URL: https://doi.org/10.1038/nri3088.

[52] Christopher J. Ferrante and Samuel Joseph Leibovich. "Regulation of Macrophage Polarization and Wound Healing". In: *Advances in Wound Care* 1.1 (Feb. 2012), pp. 10–16. DOI: 10.1089/wound.2011.0307. URL: https://doi.org/10.1089/wound.2011.0307.

[53] Lionel B. Ivashkiv. "Epigenetic regulation of macrophage polarization and function". In: *Trends in Immunology* 34.5 (May 2013), pp. 216–223. DOI: 10.1016/j.it.2012.11.001. URL: https://doi.org/10.1016/j.it.2012.11.001.

[54] Chao Zhong et al. "Trained Immunity: An Underlying Driver of Inflammatory Atherosclerosis". In: *Frontiers in Immunology* 11 (Feb. 2020). DOI: 10.3389/fimmu.2020.00284. URL: https://doi.org/10.3389/fimmu.2020.00284.

[55] Carl Nathan and Aihao Ding. "Nonresolving Inflammation". In: *Cell* 140.6 (Mar. 2010), pp. 871–882. DOI: 10.1016/j.cell.2010.02.029. URL: https://doi.org/10.1016/j.cell.2010.02.029.

[56] Arturo J Vegas et al. "Combinatorial hydrogel library enables identification of materials that mitigate the foreign body response in primates". In: *Nature Biotechnology* 34.3 (Jan. 2016), pp. 345–352. DOI: 10.1038/nbt.3462. URL: https://doi.org/10.1038/nbt.3462.

[57] Jos W.M. van der Meer et al. "Trained immunity: A smart way to enhance innate immune defence". In: *Molecular Immunology* 68.1 (Nov. 2015), pp. 40–44. DOI: 10.1016/j.molimm.2015.06.019. URL: https://doi.org/10.1016/j.molimm.2015.06.019.

[58] Mihai G. Netea and Jos W.M. van der Meer. "Trained Immunity: An Ancient Way of Remembering". In: *Cell Host & Microbe* 21.3 (Mar. 2017), pp. 297–300. DOI: 10.1016/j.chom.2017.02.003. URL: https://doi.org/10.1016/j.chom.2017.02.003.

[59] Joachim Kurtz. "Specific memory within innate immune systems". In: *Trends in Immunology* 26.4 (Apr. 2005), pp. 186–192. DOI: 10.1016/j.it.2005.02.001. URL: https://doi.org/10.1016/j.it.2005.02.001.

[60] Siroon Bekkering et al. "In VitroExperimental Model of Trained Innate Immunity in Human Primary Monocytes". In: *Clinical and Vaccine Immunology* 23.12 (Oct. 2016). Ed. by H. F. Rosenberg, pp. 926–933. DOI: 10.1128/cvi.00349-16. URL: https://doi.org/10.1128/cvi.00349-16.

[61] Rob J. W. Arts, Leo A. B. Joosten, and Mihai G. Netea. "The Potential Role of Trained Immunity in Autoimmune and Autoinflammatory Disorders". In: *Frontiers in Immunology* 9 (Feb. 2018). DOI: 10.3389/fimmu.2018.00298. URL: https://doi.org/10.3389/fimmu.2018.00298.

[62] Daniela C. Ifrim et al. "Trained Immunity or Tolerance: Opposing Functional Programs Induced in Human Monocytes after Engagement of Various Pattern Recognition Receptors". In: *Clinical and Vaccine Immunology* 21.4 (Feb. 2014). Ed. by C. J. Papasian, pp. 534–545. DOI: 10.1128/cvi.00688-13. URL: https://doi.org/10.1128/cvi.00688-13.

[63] Julia van Tuijl et al. "Immunometabolism orchestrates training of innate immunity in atherosclerosis". In: *Cardiovascular Research* 115.9 (May 2019), pp. 1416–1424. DOI: 10.1093/cvr/cvz107. URL: https://doi.org/10.1093/cvr/cvz107.

[64] M. G. Netea et al. "Trained immunity: A program of innate immune memory in health and disease". In: *Science* 352.6284 (Apr. 2016), aaf1098–aaf1098. DOI: 10.1126/science.aaf1098. URL: https://doi.org/10.1126/science.aaf1098.

[65] Bilal Alaskhar Alhamwe et al. "Histone modifications and their role in epigenetics of atopy and allergic diseases". In: *Allergy, Asthma & Clinical Immunology* 14.1 (May 2018). DOI: 10.1186/s13223-018-0259-4. URL: https://doi.org/10.1186/s13223-018-0259-4.

[66] S.-C. Cheng et al. "mTOR- and HIF-1 -mediated aerobic glycolysis as metabolic basis for trained immunity". In: *Science* 345.6204 (Sept. 2014), pp. 1250684–1250684. DOI: 10.1126/science.1250684. URL: https://doi.org/10.1126/science.1250684.

[67] May-Lill Garly et al. "BCG scar and positive tuberculin reaction associated with reduced child mortality in West Africa". In: *Vaccine* 21.21-22 (June 2003), pp. 2782–2790. DOI: 10.1016/s0264-410x(03)00181-6. URL: https://doi.org/10.1016/s0264-410x(03)00181-6.

[68] J. W. WOUT, R. POELL, and R. FURTH. "The Role of BCG/PPD-Activated Macrophages in Resistance against Systemic Candidiasis in Mice". In: *Scandinavian Journal of Immunology* 36.5 (Nov. 1992), pp. 713–720. DOI: 10.1111/j.1365-3083.1992.tb03132.x. URL: https://doi.org/10.1111/j.1365-3083.1992.tb03132.x.

[69] J. Tribouley, J. Tribouley-Duret, and M. Appriou. "Effect of Bacillus Calmette Guerin (BCG) on the receptiviy of nude mice to Schistooma mansoni". In: *Comptes Rendus des Seances de la Societe de Biologie et de ses Filiales* 172 (1978), pp. 902–904.

[70] F Bistoni et al. "Evidence for macrophage-mediated protection against lethal Candida albicans infection." In: *Infection and Immunity* 51.2 (1986), pp. 668–674. DOI: 10.1128/iai.51.2.668-674.1986. URL: https://doi.org/10.1128/iai.51.2.668-674.1986.

[71] F. Bistoni et al. "Immunomodulation by a low-virulence, agerminative variant ofCandida albicans. Further evidence for macrophage activation as one of the effector mechanisms of nonspecific anti-infectious protection". In: *Medical Mycology* 26.5 (Jan. 1988), pp. 285–299. DOI: 10.1080/02681218880000401. URL: https://doi.org/10.1080/02681218880000401.

[72] Jessica Quintin et al. "Candida albicans Infection Affords Protection against Reinfection via Functional Reprogramming of Monocytes". In: *Cell Host & Microbe* 12.2 (Aug. 2012), pp. 223–232. DOI: 10.1016/j.chom.2012.06.006. URL: https://doi.org/10.1016/j.chom.2012.06.006.

[73] Harald Arnesen. *Aterosklerose*. 2018. URL: http://sml.snl.no/aterosklerose.

[74] Siroon Bekkering et al. "Oxidized Low-Density Lipoprotein Induces Long-Term Proinflammatory Cytokine Production and Foam Cell Formation via Epigenetic Reprogramming of Monocytes". In: *Arteriosclerosis, Thrombosis, and Vascular Biology* 34.8 (Aug. 2014), pp. 1731–1738. DOI: 10.1161/atvbaha.114.303887. URL: https://doi.org/10.1161/atvbaha.114.303887.

[75] Mohamed Jeljeli et al. "Trained immunity modulates inflammation-induced fibrosis". In: *Nature Communications* 10.1 (Dec. 2019). DOI: 10.1038/s41467-019-13636-x. URL: https://doi.org/10.1038/s41467-019-13636-x.

[76] Subha Karumuthil-Melethil et al. "Fungal β-Glucan, a Dectin-1 Ligand, Promotes Protection from Type 1 Diabetes by Inducing Regulatory Innate Immune Response". In: *The Journal of Immunology* 193.7 (Aug. 2014), pp. 3308–3321. DOI: 10.4049/jimmunol.1400186. URL: https://doi.org/10.4049/jimmunol.1400186.

[77] Julia Leonhardt et al. "Candida albicans β-Glucan Differentiates Human Monocytes Into a Specific Subset of Macrophages". In: *Frontiers in Immunology* 9 (Nov. 2018). DOI: 10.3389/fimmu.2018.02818. URL: https://doi.org/10.3389/fimmu.2018.02818.

[78] C Zhao et al. "The CD14(+/low)CD16+ monocyte subset is more susceptible to spontaneous and oxidant-induced apoptosis than the CD14+CD16- subset". In: *Cell Death & Disease* 1.11 (Nov. 2010), e95–e95. DOI: 10.1038/cddis.2010.69. URL: https://doi.org/10.1038/cddis.2010.69.

[79] Jinchen Sun and Huaping Tan. "Alginate-Based Biomaterials for Regenerative Medicine Applications". In: *Materials* 6.4 (Mar. 2013), pp. 1285–1309. DOI: 10.3390/ma6041285. URL: https://doi.org/10.3390/ma6041285.

[80] Marguerite Rinaudo. "Biomaterials based on a natural polysaccharide: alginate". In: *TIP* 17.1 (June 2014), pp. 92–96. DOI: 10.1016/s1405-888x(14)70322-5. URL: https://doi.org/10.1016/s1405-888x(14)70322-5.

[81] Kuen Yong Lee and David J. Mooney. "Alginate: Properties and biomedical applications". In: *Progress in Polymer Science* 37.1 (Jan. 2012), pp. 106–126. DOI: 10.1016/j.progpolymsci.2011.06.003. URL: https://doi.org/10.1016/j.progpolymsci.2011.06.003.

[82] Ivan Donati et al. "New Hypothesis on the Role of Alternating Sequences in Calcium-Alginate Gels". In: *Biomacromolecules* 6.2 (Mar. 2005), pp. 1031–1040. DOI: 10.1021/bm049306e. URL: https://doi.org/10.1021/bm049306e.

[83] Ýrr A. Mørch, Ivan Donati, and Berit L. Strand. "Effect of Ca2+, Ba2+, and Sr2+ on Alginate Microbeads". In: *Biomacromolecules* 7.5 (May 2006), pp. 1471–1480. DOI: 10.1021/bm060010d. URL: https://doi.org/10.1021/bm060010d.

[84] Thomas A. Davis et al. "Metal Selectivity of Sargassum spp. and Their Alginates in Relation to Their α-l-Guluronic Acid Content and Conformation". In: *Environmental Science & Technology* 37.2 (Jan. 2003), pp. 261–267. DOI: 10.1021/es025781d. URL: https://doi.org/10.1021/es025781d.

[85] Berit L. Strand, Abba E. Coron, and Gudmund Skjåk-Bræk. "Current and Future Perspectives on Alginate Encapsulated Pancreatic Islet". In: *STEM CELLS Translational Medicine* 6.4 (Feb. 2017), pp. 1053–1058. DOI: 10.1002/sctm.16-0116. URL: https://doi.org/10.1002/sctm.16-0116.

[86] Yrr A. Mørch et al. "Binding and leakage of barium in alginate microbeads". In: *Journal of Biomedical Materials Research Part A* 100A.11 (June 2012), pp. 2939–2947. DOI: 10.1002/jbm.a.34237. URL: https://doi.org/10.1002/jbm.a.34237.

[87] Ji-Sheng Yang, Ying-Jian Xie, and Wen He. "Research progress on chemical modification of alginate: A review". In: *Carbohydrate Polymers* 84.1 (Feb. 2011), pp. 33–39. DOI: 10.1016/j.carbpol.2010.11.048. URL: https://doi.org/10.1016/j.carbpol.2010.11.048.

[88] M. Otterlei et al. "Similar Mechanisms of Action of Defined Polysaccharides and Lipopolysaccharides: Characterization of Binding and Tumor Necrosis Factor Alpha Induction". In: *Infection and Immunity* 61.5 (May 1993), pp. 1917–1925. URL: https://iai.asm.org/content/iai/61/5/1917.full.pdf.

[89] Trude H. Flo et al. "Involvement of Toll-like Receptor (TLR) 2 and TLR4 in Cell Activation by Mannuronic Acid Polymers". In: *Journal of Biological Chemistry* 277.38 (June 2002), pp. 35489–35495. DOI: 10.1074/jbc.m201366200. URL: https://doi.org/10.1074/jbc.m201366200.

[90] Yoshiko YAMAMOTO et al. "Induction of Multiple Cytokine Secretion from RAW264.7 Cells by Alginate Oligosaccharides". In: *Bioscience, Biotechnology, and Biochemistry* 71.1 (Jan. 2007), pp. 238–241. DOI: 10.1271/bbb.60416. URL: https://doi.org/10.1271/bbb.60416.

[91] Birger Svihus. *Kolesterol*. (Accessed on 06/26/2020). 2020. URL: https://sml.snl.no/kolesterol.

[92] Alena Grebe and Eicke Latz. "Cholesterol Crystals and Inflammation". In: *Current Rheumatology Reports* 15.3 (Feb. 2013). DOI: 10.1007/s11926-012-0313-z. URL: https://doi.org/10.1007/s11926-012-0313-z.

[93] Eivind O. Samstad et al. "Cholesterol Crystals Induce Complement-Dependent Inflammasome Activation and Cytokine Release". In: *The Journal of Immunology* 192.6 (Feb. 2014), pp. 2837–2845. DOI: 10.4049/jimmunol.1302484. URL: https://doi.org/10.4049/jimmunol.1302484.

[94] Caroline S. Gravastrand et al. "Cholesterol Crystals Induce Coagulation Activation through Complement-Dependent Expression of Monocytic Tissue Factor". In: *The Journal of Immunology* 203.4 (July 2019), pp. 853–863. DOI: 10.4049/jimmunol.1900503. URL: https://doi.org/10.4049/jimmunol.1900503.

[95] Tom Eirik Mollnes et al. "Essential role of the C5a receptor in E coli–induced oxidative burst and phagocytosis revealed by a novel lepirudin-based human whole blood model of inflammation". In: *Blood* (2002), pp. 1869–1877. URL: https://ashpublications.org/blood/article/100/5/1869/106360/Essential-role-of-the-C5a-receptor-in-E-coli.

[96] Onur Uysal et al. "Cell and Tissue Culture". In: *Omics Technologies and Bio-Engineering*. Elsevier, 2018, pp. 391–429. DOI: 10.1016/b978-0-12-804659-3.00017-8. URL: https://doi.org/10.1016/b978-0-12-804659-3.00017-8.

[97] Kayla Duval et al. "Modeling Physiological Events in 2D vs. 3D Cell Culture". In: *Physiology* 32.4 (July 2017), pp. 266–277. DOI: 10.1152/physiol.00036.2016. URL: https://doi.org/10.1152/physiol.00036.2016.

[98] Marta Kapałczyńska et al. "2D and 3D cell cultures – a comparison of different types of cancer cell cultures". In: *Archives of Medical Science* (2016). DOI: 10.5114/aoms.2016.63743. URL: https://doi.org/10.5114/aoms.2016.63743.

[99] Sigma Aldrich. *3D Scaffolds - 3D Cell Culture Products | Sigma-Aldrich*. https://www.sigmaaldrich.com/labware/labware-products.html?TablePage=110533206. (Accessed on 06/27/2020).

[100] Rasheena Edmondson et al. "Three-Dimensional Cell Culture Systems and Their Applications in Drug Discovery and Cell-Based Biosensors". In: *ASSAY and Drug Development Technologies* 12.4 (May 2014), pp. 207–218. DOI: 10.1089/adt.2014.573. URL: https://doi.org/10.1089/adt.2014.573.

[101] Berit L. Strand et al. "Visualization of alginate-poly-L-lysine-alginate microcapsules by confocal laser scanning microscopy". In: *Biotechnology and Bioengineering* 82.4 (Mar. 2003), pp. 386–394. DOI: 10.1002/bit.10577. URL: https://doi.org/10.1002/bit.10577.

[102] Gudmund Skjåk-Bræk, Hans Grasdalen, and Bjørn Larsen. "Monomer sequence and acetylation pattern in some bacterial alginates". In: *Carbohydrate Research* 154.1 (Oct. 1986), pp. 239–250. DOI: 10.1016/s0008-6215(00)90036-3. URL: https://doi.org/10.1016/s0008-6215(00)90036-3.

[103] Farid Bensebaa. "Biomedical". In: *Interface Science and Technology*. Elsevier, 2013, pp. 385–427. DOI: 10.1016/b978-0-12-369550-5.00006-9. URL: https://doi.org/10.1016/b978-0-12-369550-5.00006-9.

[104] Bio-Rad Laboratories Inc. *Bio-Plex Pro Human Cytokine, Instruction Manual*. http://www.bio-rad.com/webroot/web/pdf/lsr/literature/10000092045.pdf. (Accessed on 12/08/2019).

[105] David Richard Schmidt, Heather Waldeck, and Weiyuan John Kao. "Protein Adsorption to Biomaterials". In: *Biological Interactions on Materials Surfaces*. Springer US, 2009, pp. 1–18. DOI: 10.1007/978-0-387-98161-1_1. URL: https://doi.org/10.1007/978-0-387-98161-1_1.

[106] Knut Tore Lappegård et al. "Artificial surface-induced cytokine synthesis: effect of heparin coating and complement inhibition". In: *The Annals of Thoracic Surgery* 78.1 (July 2004), pp. 38–44. DOI:

10.1016/j.athoracsur.2004.02.005. URL: https://doi.org/10.1016/j.athoracsur.2004.02.005.

[107] Øystein Arlov and Gudmund Skjåk-Bræk. "Sulfated Alginates as Heparin Analogues: A Review of Chemical and Functional Properties". In: *Molecules* 22.5 (May 2017), p. 778. DOI: 10.3390/molecules22050778. URL: https://doi.org/10.3390/molecules22050778.

[108] Themis R. Kyriakides et al. "The CC Chemokine Ligand, CCL2/MCP1, Participates in Macrophage Fusion and Foreign Body Giant Cell Formation". In: *The American Journal of Pathology* 165.6 (Dec. 2004), pp. 2157–2166. DOI: 10.1016/s0002-9440(10)63265-8. URL: https://doi.org/10.1016/s0002-9440(10)63265-8.

[109] Nihal Engin Vrana. *Biomaterials and immune response: complications, mechanisms and immunomodulation*. Devices, circuits, and systems. Taylor & Francis, 2018. ISBN: 9781138506374.

[110] Alexander N. Orekhov et al. "Monocyte differentiation and macrophage polarization". In: *Vessel Plus* 2019 (Mar. 2019). DOI: 10.20517/2574-1209.2019.04. URL: https://doi.org/10.20517/2574-1209.2019.04.

[111] Roland Lang et al. "Shaping Gene Expression in Activated and Resting Primary Macrophages by IL-10". In: *The Journal of Immunology* 169.5 (Sept. 2002), pp. 2253–2263. DOI: 10.4049/jimmunol.169.5.2253. URL: https://doi.org/10.4049/jimmunol.169.5.2253.

[112] Thomas A. Wynn and Kevin M. Vannella. "Macrophages in Tissue Repair, Regeneration, and Fibrosis". In: *Immunity* 44.3 (Mar. 2016), pp. 450–462. DOI: 10.1016/j.immuni.2016.02.015. URL: https://doi.org/10.1016/j.immuni.2016.02.015.

[113] Emily B. Lurier et al. "Transcriptome analysis of IL-10-stimulated (M2c) macrophages by next-generation sequencing". In: *Immunobiology* 222.7 (July 2017), pp. 847–856. DOI: 10.1016/j.imbio.2017.02.006. URL: https://doi.org/10.1016/j.imbio.2017.02.006.

[114] Huey-ming Lo et al. "TNF-α induces CXCL1 chemokine expression and release in human vascular endothelial cells in vitro via two distinct signaling pathways". In: *Acta Pharmacologica Sinica* 35.3 (Feb. 2014), pp. 339–350. DOI: 10.1038/aps.2013.182. URL: https://doi.org/10.1038/aps.2013.182.

[115] Anindita Bhattacharya et al. "3D micro-environment regulates NF-κβ dependent adhesion to induce monocyte differentiation". In: *Cell Death & Disease* 9.9 (Sept. 2018). DOI: 10.1038/s41419-018-0993-z. URL: https://doi.org/10.1038/s41419-018-0993-z.

[116] PerkinElmer. *Plate Treatments, Coatings and Applications | Application Support Knowledgebase | Lab Products & Services | PerkinElmer*. https://www.perkinelmer.com/no/lab-products-and-services/application-support-knowledgebase/microplates/plate-treatments.html. (Accessed on 06/30/2020).

[117] Robert J. Schutte, Andreina Parisi-Amon, and W. Monty Reichert. "Cytokine profiling using monocytes/macrophages cultured on common biomaterials with a range of surface chemistries". In: *Journal of Biomedical Materials Research Part A* 88A.1 (Jan. 2009), pp. 128–139. DOI: 10.1002/jbm.a.31863. URL: https://doi.org/10.1002/jbm.a.31863.

[118] Eleni Vergadi, Katerina Vaporidi, and Christos Tsatsanis. "Regulation of Endotoxin Tolerance and Compensatory Anti-inflammatory Response Syndrome by Non-coding RNAs". In: *Frontiers in Im-*

munology 9 (Nov. 2018). DOI: 10.3389/fimmu.2018.02705. URL: https://doi.org/10.3389/fimmu.2018.02705.

[119] M. M. Prechel and J. M. Walenga. "Complexes of platelet factor 4 and heparin activate Toll-like receptor 4". In: *Journal of Thrombosis and Haemostasis* 13.4 (Feb. 2015), pp. 665–670. DOI: 10.1111/jth.12847. URL: https://doi.org/10.1111/jth.12847.

[120] Wen-Chao Song. "Crosstalk between Complement and Toll-Like Receptors". In: *Toxicologic Pathology* 40.2 (Nov. 2011), pp. 174–182. DOI: 10.1177/0192623311428478. URL: https://doi.org/10.1177/0192623311428478.

[121] Matthew J. Elder et al. "β-Glucan Size Controls Dectin-1-Mediated Immune Responses in Human Dendritic Cells by Regulating IL-1β Production". In: *Frontiers in Immunology* 8 (July 2017). DOI: 10.3389/fimmu.2017.00791. URL: https://doi.org/10.3389/fimmu.2017.00791.

[122] BioLegend. *Essential Markers for Phenotyping*. https://www.biolegend.com/en-us/essential-markers. (Accessed on 06/24/2020).

[123] Bio-Rad. *Major Histocompatibility Complex | Bio-Rad*. https://www.bio-rad-antibodies.com/mhc-hla-h-2-rt1-markers-antibodies.html. (Accessed on 06/24/2020).

[124] NanoString. *Direct Digital Detection with nCounter® Technology*. https://www.nanostring.com/scientific-content/technology-overview/ncounter-technology. (Accessed on 06/24/2020).

A Supplementary data

A.1 Platelet experiment

The SA bead tested in the human whole blood induced surprisingly high amounts of VEGF and prothrombin. This was further explored in a platelet experiment based on the experimental procedure of the whole blood model described in [11]. The microspheres were incubated in human whole blood, platelet-rich plasma (PRP), or platelet-free plasma (PFP) for 4 hours before EDTA was added to stop the activation. The experiment was performed three times with blood from three donors. Figure A.1.1 show the results of PDGF-BB, RANTES, and VEGF. VEGF induced lower amounts in this experiment compared to the A and AP, and the one conducted in autumn 2019. The amounts of VEGF in PRP and PFP were to low to be measured. A theory is that the new batch of VEGF-beads used in the multiplex system for this experiment was less sensitive than those used in 2019. It has been partially confirmed by conducting multiplex with VEGF-beads from the same kit used in autumn 2019 and the VEGF-beads used on this experiment on the same sample supernatants. VEGF-beads used in autumn 2019 showed to be more sensitive, but due to lack of time and response from the manufacturer, the experiment was set on hold.

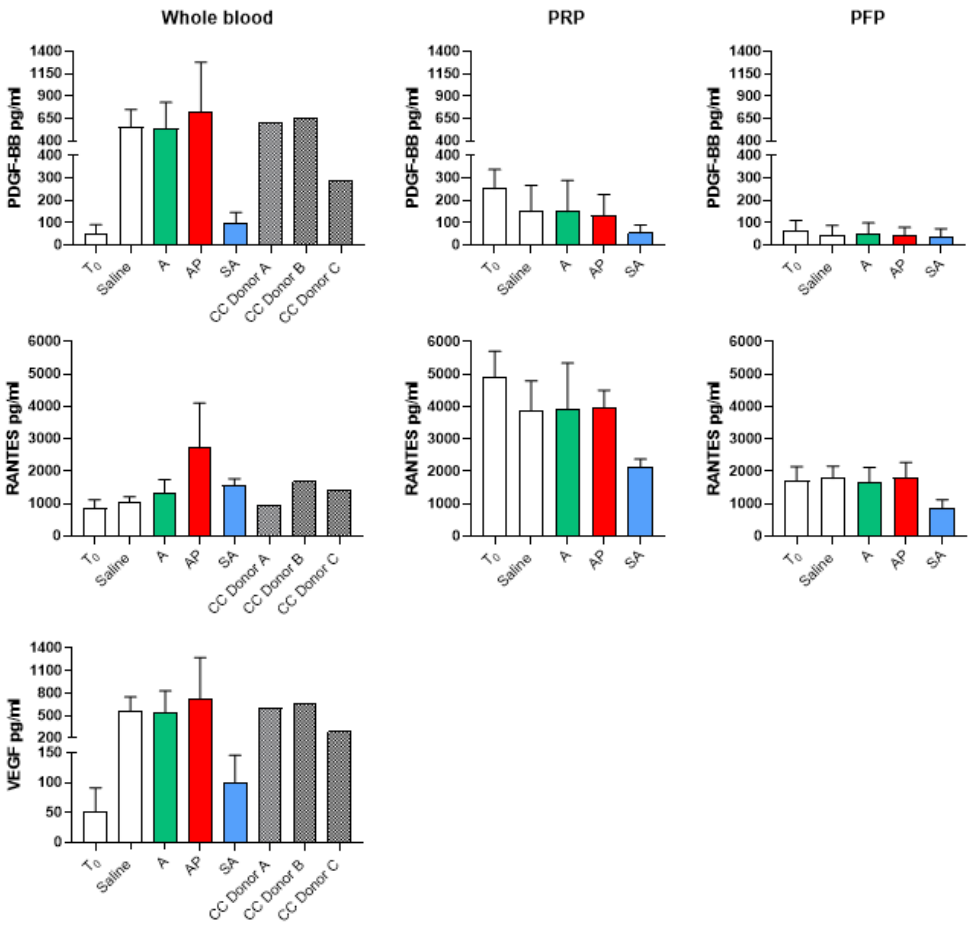

Figure A.1.1: PDGF-BB, RANTES and VEGF in plasma from anticoagulated whole blood, platelet-rich plasma (PRP) and platelet-free plasma (PFP) after 240 minutes of incubation of alginate microspheres. Induced by T_0 and negative control saline (white); negative control bead A (green); SA-bead (blue); positive control microcapsule (red); and cholesterol crystals (CC) (black spotted) with different concentrations and incubation interval for each donor: Donor A 400 µg/mL 4 h, Donor B 2000 µg/mL 4 h, Donor C 2000 µg/mL 1h.

A.2 Long-term *in vitro* experimental model

A.2.1 Experiment 1

In experiment 1, several cytokines relevant for fibrosis were measured. Plasma samples were analyzed using the multiplex assay Bio-plex^{TM} Pro Human Cytokine Assay (Bio-Rad Laboratories, Inc.), where beads from single kits were combined to conduct the assay: IFN-γ(171B5019M), IP-10 (171B5020M), MIP-1α (171B5022M), IL-17A (171B5014M), VEGF (171B5027M), IL-13 (171B5012M). TGF-β1, TGF-β2, and TGF-β3 was from measured by a 3-plex assay (171W4001M). These cytokines were not chosen to be measured in further experiments, and the induced cytokine levels measured in experiment 1 are therefore shown in supplementary data in Figures A.2.1 to A.2.9.

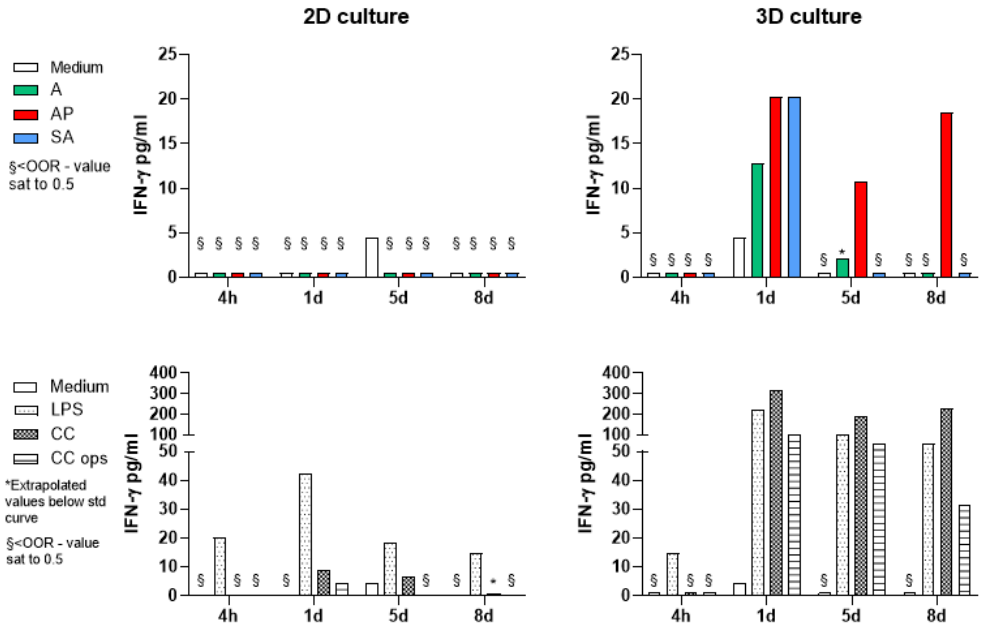

Figure A.2.1: Comparison of the secretion of IFN-γ in 2D and 3D culturing induced by the microspheres A (green), AP (red), and SA (blue); and the controls LPS (black spotted), CC (black squared) and opsonized CC (black striped). * indicates values extrapolated beyond the the range of the standard curve. § indicates valuesout of range.

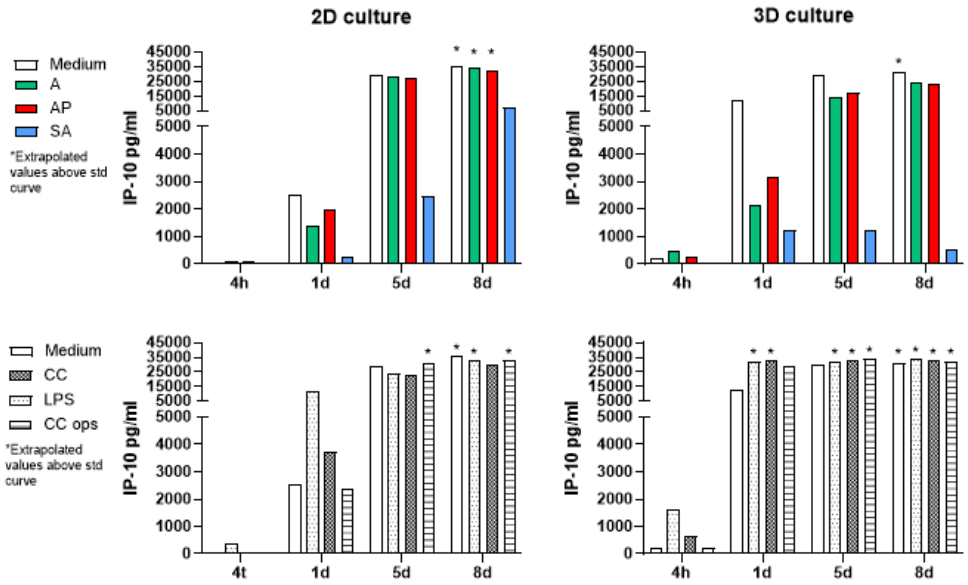

Figure A.2.2: Comparison of the secretion of IP-10 in 2D and 3D culturing induced by the microspheres A (green), AP (red), and SA (blue); and the controls LPS (black spotted), CC (black squared) and opsonized CC (black striped). * indicates values extrapolated beyond the the range of the standard curve. § indicates valuesout of range.

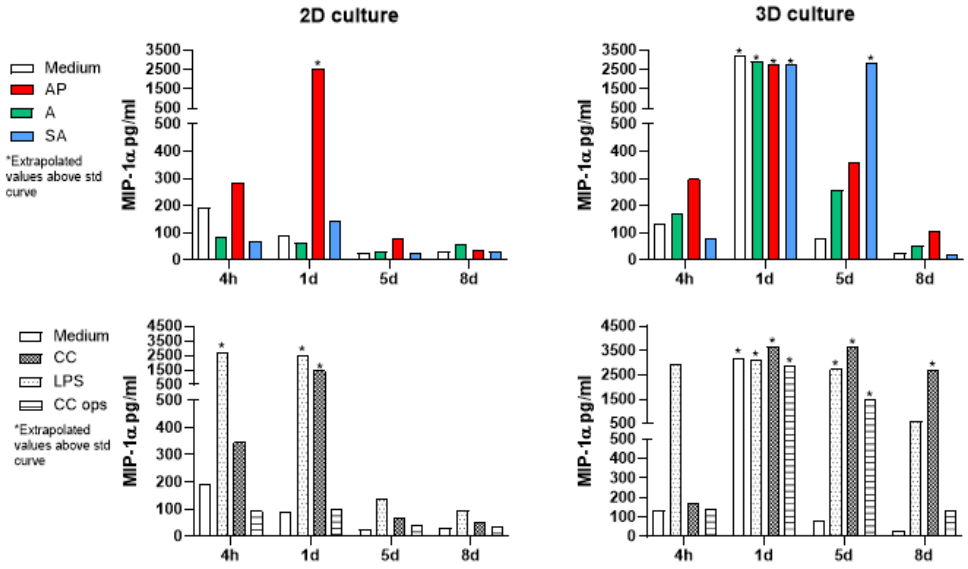

Figure A.2.3: Comparison of the secretion of MIP-1α in 2D and 3D culturing induced by the microspheres A (green), AP (red), and SA (blue); and the controls LPS (black spotted), CC (black squared) and opsonized CC (black striped). * indicates values extrapolated beyond the the range of the standard curve. § indicates valuesout of range.

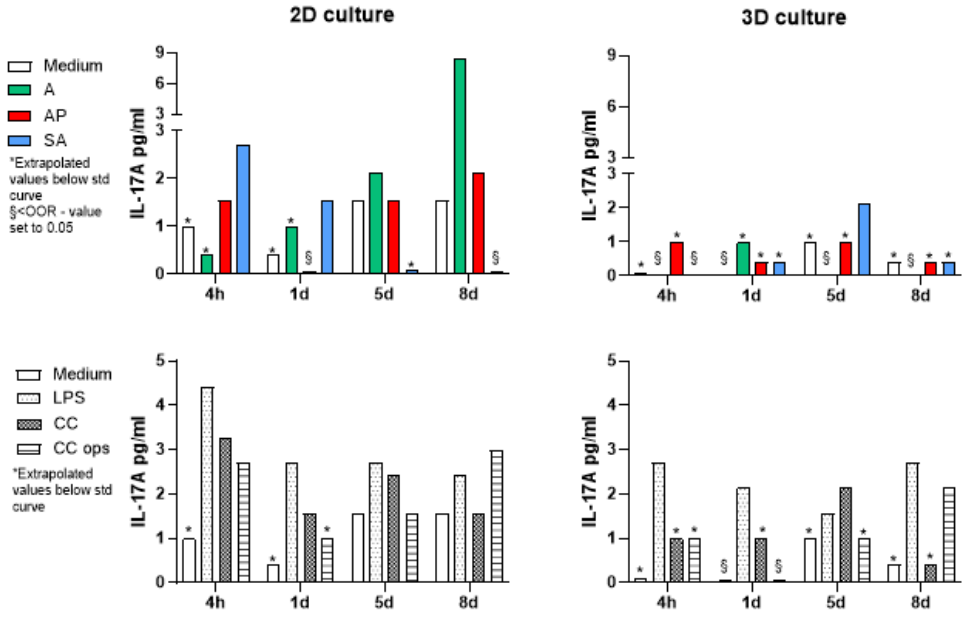

Figure A.2.4: Comparison of the secretion of IL-17A in 2D and 3D culturing induced by the microspheres A (green), AP (red), and SA (blue); and the controls LPS (black spotted), CC (black squared) and opsonized CC (black striped). * indicates values extrapolated beyond the the range of the standard curve. § indicates valuesout of range.

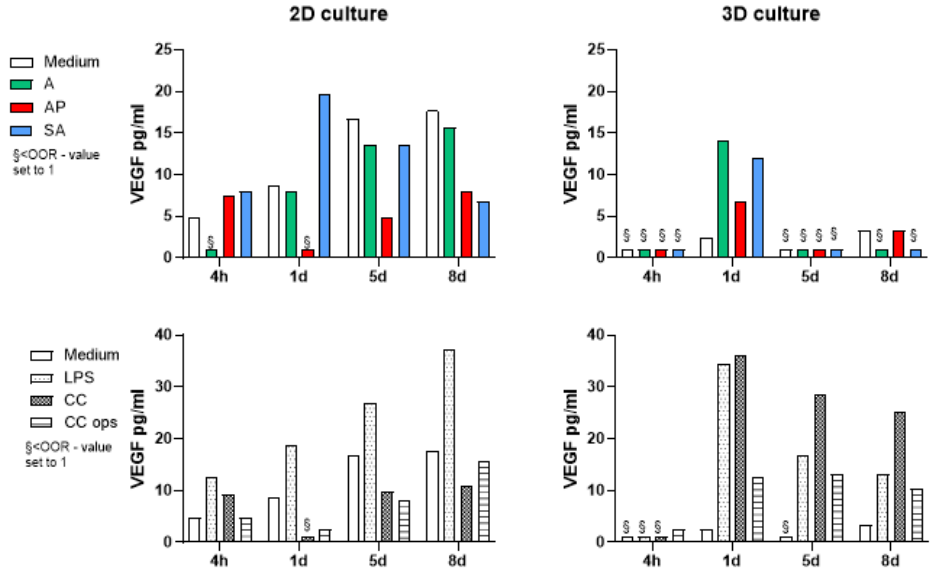

Figure A.2.5: Comparison of the secretion of VEGF in 2D and 3D culturing induced by the microspheres A (green), AP (red), and SA (blue); and the controls LPS (black spotted), CC (black squared) and opsonized CC (black striped). * indicates values extrapolated beyond the the range of the standard curve. § indicates valuesout of range.

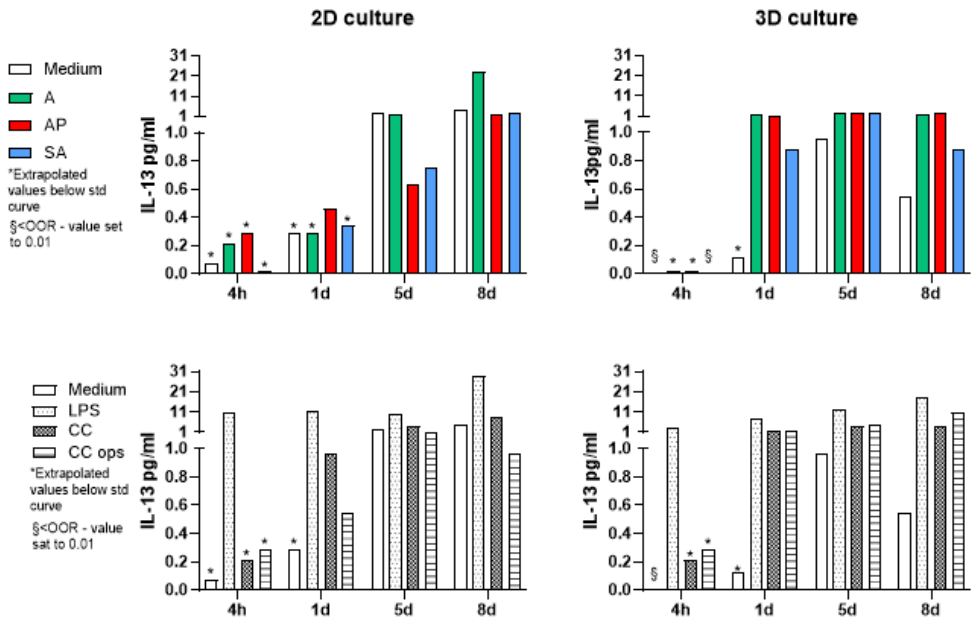

Figure A.2.6: Comparison of the secretion of IL-13 in 2D and 3D culturing induced by the microspheres A (green), AP (red), and SA (blue); and the controls LPS (black spotted), CC (black squared) and opsonized CC (black striped). * indicates values extrapolated beyond the the range of the standard curve. § indicates valuesout of range.

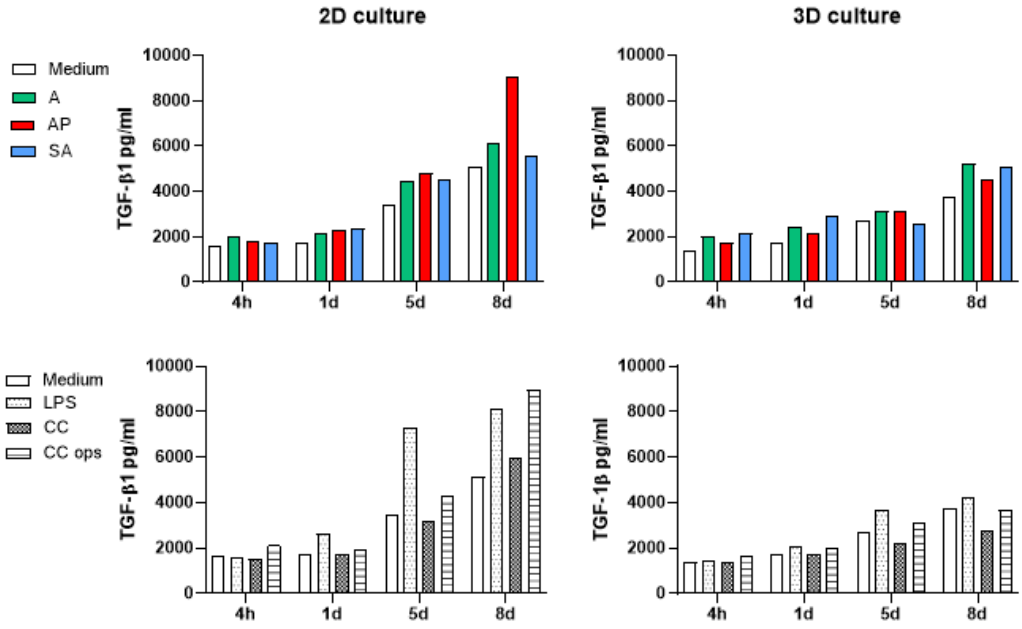

Figure A.2.7: Comparison of the secretion of TGF-β1 in 2D and 3D culturing induced by the microspheres A (green), AP (red), and SA (blue); and the controls LPS (black spotted), CC (black squared) and opsonized CC (black striped).

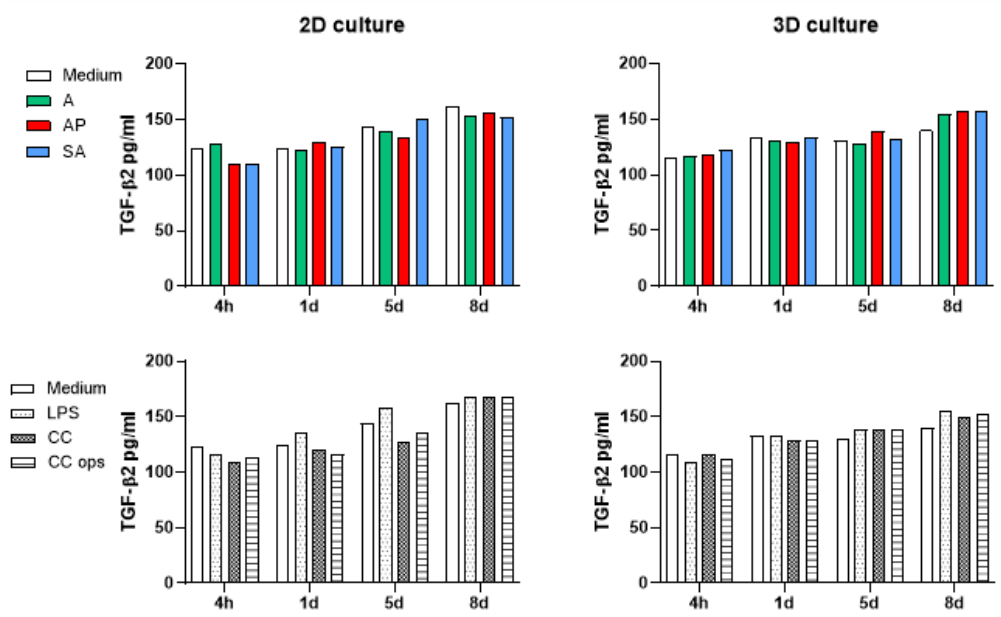

Figure A.2.8: Comparison of the secretion of TGF-β2 in 2D and 3D culturing induced by the microspheres A (green), AP (red), and SA (blue); and the controls LPS (black spotted), CC (black squared) and opsonized CC (black striped).

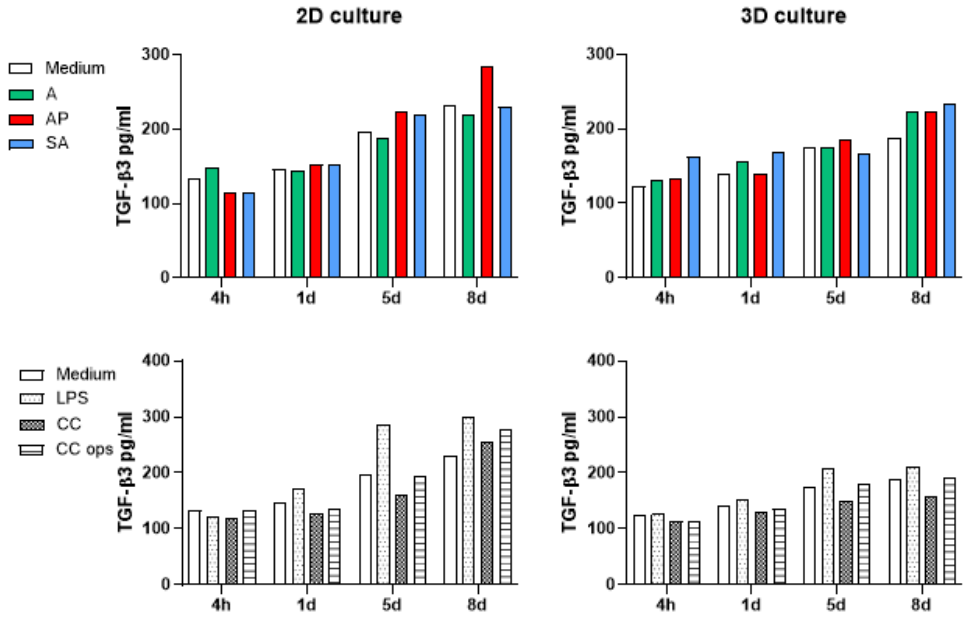

Figure A.2.9: Comparison of the secretion of TGF-β3 in 2D and 3D culturing induced by the microspheres A (green), AP (red), and SA (blue); and the controls LPS (black spotted), CC (black squared) and opsonized CC (black striped).

A.2.2 Experiment 3

Figure A.2.10 show the induced level of IL-8.

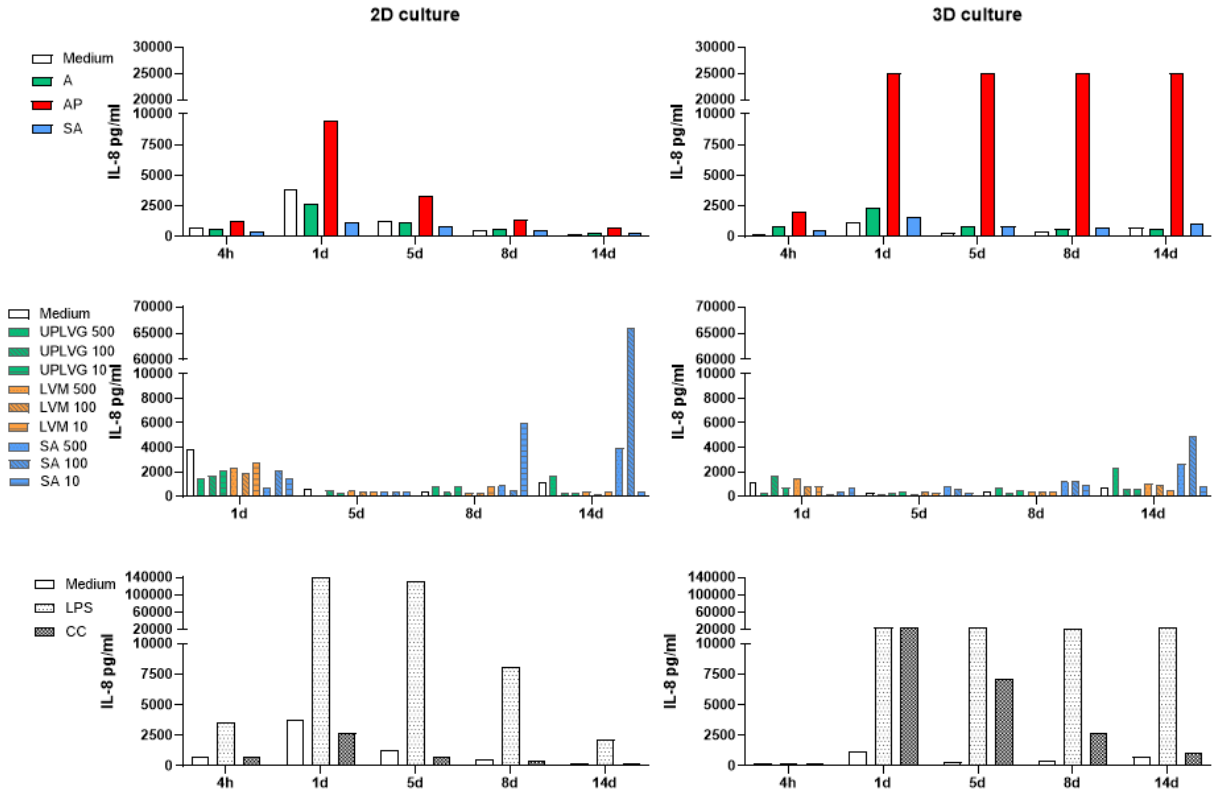

Figure A.2.10: Comparison of the secretion of IL-8 in 2D and 3D culturing induced by the microspheres A (green), AP (red), and SA (blue); the soluble alginates UPLVG (G-rich alginate) (green), LVM (M-rich alginate) (orange), SA (sulfated alginate) (blue), with concentrations of 500 (spotted), 100 (diagonal lines) and 10 (straight lines) µg/mL; and the controls LPS (black spotted), CC (black squared).

A.2.3 Experiment 4

Figure A.2.11 show the induced level of IL-8.

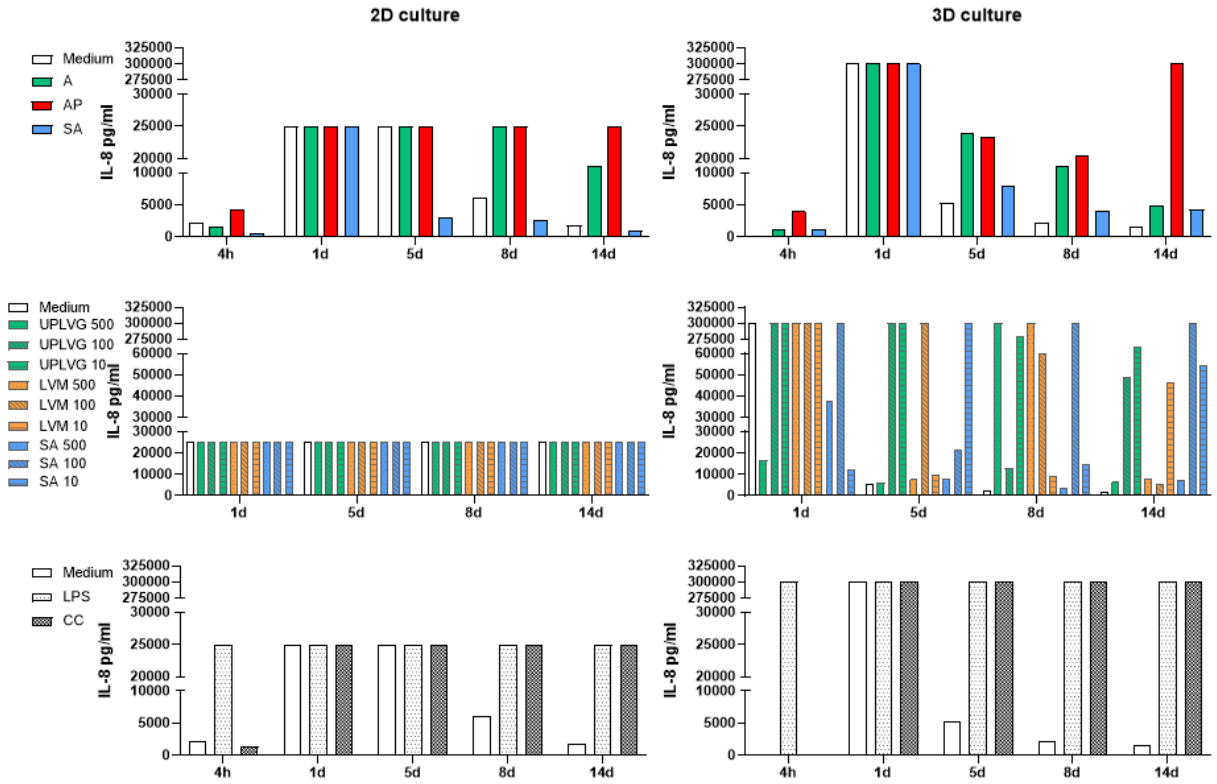

Figure A.2.11: Comparison of the secretion of IL-8 in 2D and 3D culturing induced by the microspheres A (green), AP (red), and SA (blue); the soluble alginates UPLVG (G-rich alginate) (green), LVM (M-rich alginate) (orange), SA (sulfated alginate) (blue), with concentrations of 500 (spotted), 100 (diagonal lines) and 10 (straight lines) µg/mL; and the controls LPS (black spotted), CC (black squared).

A.3 Trained immunity

Figure A.3.1 show the induced level of IL-8.

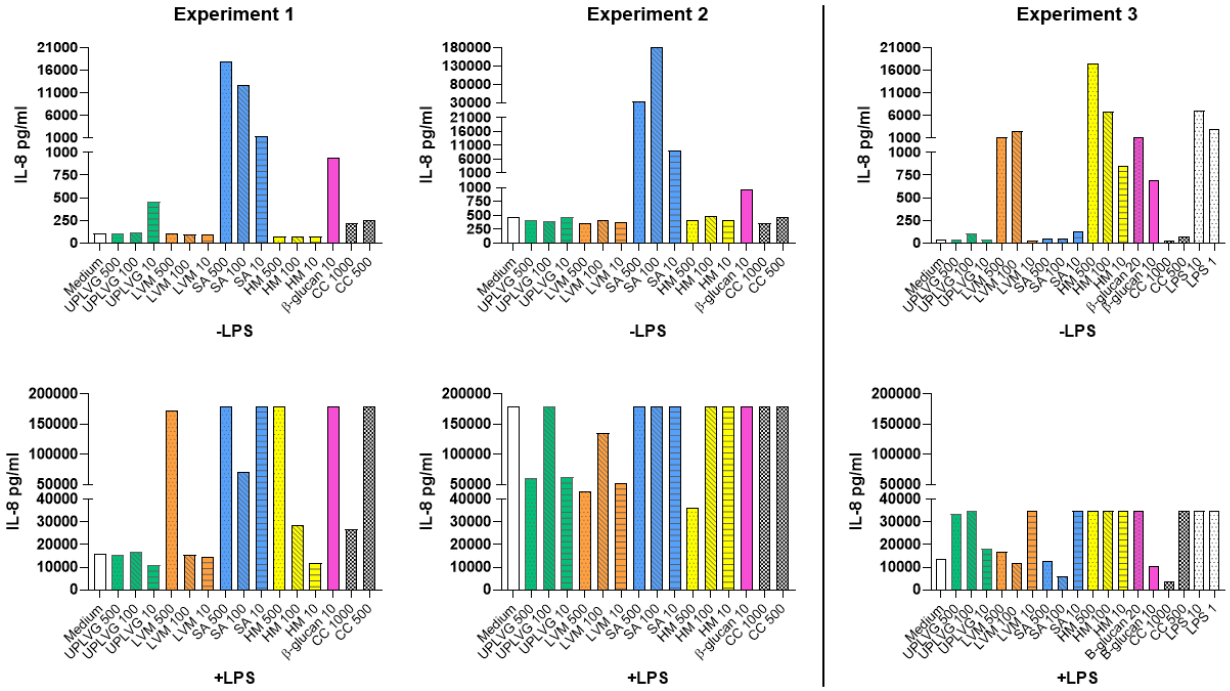

Figure A.3.1: Comparison of the secretion of IL-8 by macrophages of three different donors after 24 hours of training, and 5 days of rest before restimulation with RPMI (-LPS) or unrelated stimuli (+LPS). Induced by: the alginates UPLVG (G-rich alginate) (green), LVM (M-rich alginate) (orange), SA (sulfated alginate) (blue), HM (High-M alginate, 94% M) (yellow) with concentrations of 500 (spotted), 100 (diagonal lines) and 10 (straight lines) µg/mL; β-glucan (purple) with concentrations of 20 and 10 µg/mL; cholesterol crystals (CC) (black squared) with concentrations of 1000 and 500 µg/mL; and LPS (black spotted) with concentrations of 10 and 1 ng/mL. Experiment 1 and 2 follows the same experimental procedure. Experiment 3 is experimental different by change of culture medium and addition of LPS as experimental condition.

B Experimental setup

B.1 Experiment 1

Figure B.3.1 show the experimental set up of experiment 1 in 2D and 3D. Supernatants in 2D were harvested from the same well for all time points. Supernatants in 3D were harvested from a new vial at each time point. Both were incubated with continuous shaking.

Plate

	1	2	3	4	
	5	6	7	8	

Vials

Day 1												
			1	2	3	4	5	6	7	8		
Day 5												
			1	2	3	4	5	6	7	8		
Day 8			1	2	3	4	5	6	7	8		
Day 14			1	2	3	4	5	6	7	8		

Figure B.1.1: Simple overview of the setup in 2D and 3D for experiment 1. Condition 1-8 were harvested from the same well in 2D each time point. Condition 1-8 were harvested from a vial in 3D for each time point).

B.2 Experiment 2

Figure B.3.1 show the experimental set up of experiment 2 in 2D and 3D. Supernatants in 2D were harvested from the same well for all time points. Supernatants in 3D were harvested from a new vial at each time point. Both were incubated with continuous shaking.

Plate

1	2	3	4	5	6
7	8	9	10	11	12
13	14	15	14	15	

Vials

Day 1	1	2	3	4	5	6	7	8	9	10	11	12
										13	14	15
Day 5	1	2	3	4	5	6	7	8	9	10	11	12
										13	14	15
Day 8	1	2	3	4	5	6	7	8	9	10	11	12
										13	14	15
Day 14	1	2	3	4	5	6	7	8	9	10	11	12
										13	14	15

Figure B.2.1: Simple overview of the setup in 2D and 3D for experiment 2. Condition 1-15 were harvested from the same well in 2D each time point. Condition 1-15 were harvested from a vial in 3D for each time point).

B.3 Expriment 3 and 4

Figure B.3.1 show the experimental set up of experiment 3 and 4 in 2D and 3D. The conditions of 2D were distributed on 3 different plates. In 2D, supernatants from condition 1-6 (medium, LPS, CC, A, SA, AP) were harvested from the same well. 7-15 (soluble alginates) were harvested from a new well for each time point. Plate 1 was placed on continuous shaking while incubated. A=day 1, B= day 5, C= day 8, D= day 14, H= HBSS. The conditions of 3D were distributed on one plate for all vials. Supernatants from condition 1-6 were harvested from the same well at each time point. 7-15 were harvested from a new vial for each time point. 3D conditions were placed on continuous shaking while incubated.

Plate 1

H	1	2	3	4	H
H	5	6	7A	8A	H
H	9A	10A	11A	12A	H
H	13A	14A	15A	H	H

Plate 2

H	1	7B	8B	9B	H
10B	11B	12B	13B	14B	15B
7C	8C	9C	10C	11C	H
H	12C	13C	14C	15C	H

Plate 3

H	H	1	7D	H	H
H	8D	9D	10D	11D	H
H	12D	13D	14D	15D	H
H	H	H	H	H	H

Vials

Day 1	1	2	3	4	5	6	7	8	9	10	11	12
										13	14	15
Day 5							7	8	9	10	11	12
										13	14	15
Day 8							7	8	9	10	11	12
										13	14	15
Day 14							7	8	9	10	11	12
										13	14	15

Figure B.3.1: Simple overview of the setup in 2D and 3D for experiment 3 and 4. Condition 1-6 (medium, LPS, CC, A, SA, AP) were harvested from the same well/vial for each time point. 7-15 (soluble alginates) were harvested from a new well/vial for each time point). A=day 1, B= day 5, C= day 8, D= day 14, H= HBSS

C Bio-plex data

Bio-plex was used to measure induced cytokine levels at selected time points by microspheres and soluble alginates in two different experimental procedures.

C.1 Long-term *in vitro* experimental model

Cytokine levels measured at selected time points during 14 days of incubation of microspheres and soluble alginates with PBMCs is shown in Table C.1.1 to Table C.1.46.

C.1.1 Experiment 1

Table C.1.1: Concentration (pg/mL) of TNF in 2D and 3D culturing measured at selected time points.

	2D culture				**3D culture**			
	4h	**1d**	**5d**	**8d**	**4h**	**1d**	**5d**	**8d**
Medium	96.10	53.55	18.67	50.88	75.72	1215.90	64.29	50.29
A	43.80	24.07	18.95	67.29	98.54	3656.05	209.79	270.33
AP	121.02	236.08	27.22	29.81	118.55	5497.47	513.88	456.99
SA	29.52	47.63	15.30	5.97	50.29	1914.80	811.65	296.04
LPS	9593.78	5547.76	614.41	478.60	7287.78	10314.81	5679.66	4093.19
CC	152.18	221.95	53.55	39.99	138.43	7589.89	1115.12	734.81
CC ops	53.55	78.75	48.22	50.59	96.40	7591.41	873.15	342.96

Table C.1.2: Concentration (pg/mL) of IL-1β in 2D and 3D culturing measured at selected time points.

	2D culture				**3D culture**			
	4h	**1d**	**5d**	**8d**	**4h**	**1d**	**5d**	**8d**
Medium	8.91	6.79	2.44	2.95	5.48	29.52	10.90	6.65
A	4.76	5.10	2.41	3.27	8.87	637.61	90.15	151.36
AP	10.64	14.99	6.03	4.29	13.09	352.68	126.91	233.91
SA	3.86	5.97	1.78	1.24	7.42	298.13	775.65	226.62
LPS	603.39	525.98	305.46	212.73	1271.27	4394.72	2062.17	1509.33
CC	58.74	139.75	74.26	45.11	105.00	1263.04	428.35	185.50
CC ops	24.04	34.82	18.78	12.38	41.80	877.49	587.38	193.99

Table C.1.3: Concentration (pg/mL) of IL-6 in 2D and 3D culturing measured at selected time points. * indicates values extrapolated beyond the linear range of the standard curve.

	2D culture				3D culture			
	4h	**1d**	**5d**	**8d**	**4h**	**1d**	**5d**	**8d**
Medium	45.69	35.42	4.74	6.10	22.58	67.98	33.80	21.81
A	24.10	31.17	4.77	7.34	30.67	8353.21	698.93	4210.08
AP	53.72	62.56	7.16	5.31	43.66	1598.19	1443.09	2650.35
SA	21.73	23.44	3.06	3.54	11.39	11464.08	*30945.40	26229.34
LPS	3294.06	28531.60	*31600.03	30811.75	11373.05	*31335.54	*34057.23	*34932.37
CC	55.98	58.80	11.77	9.05	23.03	1954.89	2565.36	3467.11
CC ops	28.28	20.35	5.81	6.90	23.85	2673.10	5046.50	2536.03

Table C.1.4: Concentration (pg/mL) of IL-8 in 2D and 3D culturing measured at selected time points. * indicates values extrapolated beyond the linear range of the standard curve.

	2D culture				3D culture			
	4h	**1d**	**5d**	**8d**	**4h**	**1d**	**5d**	**8d**
Medium	1264.07	3201.42	723.31	2230.52	658.76	27009.24	16280.38	11611.53
A	584.45	1290.45	508.44	3238.93	750.60	13860.85	27874.68	32038.91
AP	2019.72	17112.35	30836.03	17527.50	1890.17	25419.03	*42757.26	*342597.00
SA	339.41	2148.19	807.38	393.80	242.30	15797.50	24171.21	27481.78
LPS	7564.95	18741.23	*41488.42	*114656.70	6276.38	20838.42	23126.32	23779.06
CC	2223.89	4679.60	9747.02	10606.80	1377.08	12650.52	*42815.00	34039.18
CC ops	906.45	2131.41	4693.38	5164.21	1372.52	18268.34	23289.98	*61419.55

Table C.1.5: Concentration (pg/mL) of IL-10 in 2D and 3D culturing measured at selected time points. * indicates values extrapolated beyond the linear range of the standard curve. Blue indicates values out of range below the lowest observed value and was set to 0.10 for 3D.

	2D culture				3D culture			
	4h	**1d**	**5d**	**8d**	**4h**	**1d**	**5d**	**8d**
Medium	1.22	0.54	1.54	4.83	0.72	0.78	0.97	1.67
A	0.78	0.54	1.41	7.15	0.66	1.29	0.72	2.57
AP	1.35	1.03	3.35	5.36	0.97	1.29	2.54	1.06
SA	0.66	0.60	*0.39	2.87	0.10	0.97	1.13	1.06
LPS	7.11	17.29	7.97	12.05	4.76	97.01	32.73	25.47
CC	1.54	1.16	1.35	1.41	1.10	1.48	1.94	3.70
CC ops	1.41	1.29	1.16	1.29	0.94	1.22	2.30	3.84

Table C.1.6: Concentration (pg/mL) of MCP-1 in 2D and 3D culturing measured at selected time points.

	2D culture				3D culture			
	4h	**1d**	**5d**	**8d**	**4h**	**1d**	**5d**	**8d**
Medium	144.36	70.48	103.43	718.40	161.29	521.02	166.66	64.11
A	64.11	67.67	56.81	1175.82	351.99	745.53	700.04	1113.88
AP	321.32	703.52	176.75	114.60	436.18	781.21	808.35	1399.72
SA	73.25	1762.40	38.77	158.16	212.66	3737.02	2744.38	1470.82
LPS	671.23	777.27	813.27	1165.90	664.09	806.81	1584.21	1913.21
CC	416.81	608.94	678.11	1265.14	364.98	666.95	896.85	1936.25
CC ops	243.98	625.11	660.96	1190.82	413.67	732.51	1009.40	1495.85

Table C.1.7: Concentration (pg/mL) of M-CSF in 2D and 3D culturing measured at selected time points.

	2D culture				3D culture			
	4h	**1d**	**5d**	**8d**	**4h**	**1d**	**5d**	**8d**
Medium	-	-	-	-	0.36	72.55	63.84	53.28
A	0.51	2.31	1.92	27.49	0.42	97.95	85.52	74.97
AP	1.16	50.80	23.99	25.10	0.60	99.26	81.64	58.51
SA	0.54	6.33	2.47	13.65	0.48	50.54	70.74	50.80
LPS	-	-	-	-	0.42	36.60	68.34	57.24
CC	-	-	-	-	0.54	84.49	104.52	112.93
CC ops	-	-	-	-	0.67	93.52	91.60	92.64

Table C.1.8: Concentration (pg/mL) of GRO-α in 2D and 3D culturing measured at selected time points. * indicates values extrapolated beyond the linear range of the standard curve. Red indicates values out of range above the highest observed value and was set to 100000.00 for 2D.

	2D culture				3D culture			
	4h	**1d**	**5d**	**8d**	**4h**	**1d**	**5d**	**8d**
Medium	97.10	78.39	46.94	54.60	30.23	628.57	842.85	434.28
A	78.39	117.24	45.49	72.41	146.38	8370.63	7666.01	18760.45
AP	319.29	1675.32	2385.56	947.16	291.03	7159.50	11487.22	18715.80
SA	27.86	128.03	226.00	313.95	39.02	3052.09	10561.64	9481.45
LPS	420.82	20553.01	99223.54	100000.00	329.66	16512.97	*55764.14	*37110.60
CC	136.84	276.69	441.53	513.84	84.10	3711.34	12113.89	16267.83
CC ops	96.73	119.87	169.26	191.76	153.91	5528.53	12585.51	15399.37

C.1.2 Experiment 2

Table C.1.9: Concentration (pg/mL) of TNF in 2D and 3D culturing measured at selected time points.

	2D culture	**3D culture**			
Conc. [µg/mL]	**1d**	**4h**	**1d**	**8d**	**14d**
Medium	52.32	45.30	120.64	5.64	2.63
A	11.21	13.95	53.18	2.91	1.50
AP	27.22	203.52	8036.06	265.84	78.95
SA	13.30	12.78	120.77	5.51	7.52
LPS	2578.02	4408.86	4580.93	153.46	36.11
CC	32.19	86.48	1035.93	23.68	5.10
UPLVG 1500	7.92	8.32	72.51	5.37	3.19
UPLVG 750	9.11	33.62	129.91	5.10	2.35
UPLVG 375	14.34	43.44	162.71	8.05	2.35
LVM 1500	4.56	36.36	60.05	9.90	2.07
LVM 750	10.43	39.35	143.49	11.21	2.35
LVM 375	9.90	52.20	175.67	9.38	2.49
SA 1500	5.10	13.17	24.82	2.91	1.21
SA 750	14.73	17.69	24.19	3.87	2.35
SA 375	8.45	17.82	38.85	2.91	2.07

Table C.1.10: Concentration (pg/mL) of IL-1β in 2D and 3D culturing measured at selected time points. * indicates values extrapolated beyond the linear range of the standard curve. Blue indicates values out of range below the lowest observed value and was set to 0.004 for 3D.

	2D culture	**3D culture**			
Conc. [µg/mL]	**1d**	**4h**	**1d**	**8d**	**14d**
Medium	10.090	1.100	5.410	0.160	0.004
A	2.870	0.230	2.740	0.160	0.004
AP	6.610	4.730	1258.740	31.770	1.130
SA	1.590	*0.030	42.570	0.490	0.004
LPS	926.920	1241.750	1672.160	61.640	1.570
CC	135.120	6.500	430.270	17.600	0.390
UPLVG 1500	1.040	0.120	2.440	*0.090	*0.010
UPLVG 750	1.920	0.840	12.720	0.360	0.004
UPLVG 375	2.740	1.310	8.950	0.640	0.004
LVM 1500	0.640	0.950	2.010	0.920	*0.010
LVM 750	1.720	1.250	12.080	1.780	*0.010
LVM 375	3.400	1.310	8.950	0.640	0.004
SA 1500	0.190	0.120	0.230	*0.010	*0.010
SA 750	0.290	0.640	0.860	*0.050	*0.010
SA 375	0.290	0.640	0.390	*0.050	0.004

Table C.1.11: Concentration (pg/mL) of IL-6 in 2D and 3D culturing measured at selected time points.

	2D culture	**3D culture**			
Conc. [µg/mL]	**1d**	**4h**	**1d**	**8d**	**14d**
Medium	23.86	7.81	61.41	6.34	3.18
A	16.88	1.34	15.13	4.46	4.41
AP	76.86	52.62	8867.63	5155.76	4058.66
SA	18.97	1.57	1230.50	90.06	24.81
LPS	7200.39	5318.79	7718.19	6751.11	7422.71
CC	214.03	16.12	1768.57	417.19	41.74
UPLVG 1500	1.86	1.11	15.71	1.92	14.58
UPLVG 750	6.45	5.54	103.59	8.04	2.03
UPLVG 375	12.75	7.17	58.14	17.38	7.30
LVM 1500	1.23	6.13	17.53	38.08	2.68
LVM 750	9.84	6.85	148.94	65.81	5.54
LVM 375	9.26	9.08	112.16	29.54	4.24
SA 1500	1.34	1.34	1.63	0.72	0.63
SA 750	1.57	2.37	1.05	1.14	0.87
SA 375	1.40	3.26	3.53	0.63	1.17

Table C.1.12: Concentration (pg/mL) of IL-8 in 2D and 3D culturing measured at selected time points. * indicates values extrapolated beyond the linear range of the standard curve. Red indicates values out of range above the highest observed value and was set to 65000.00 for 3D.

	2D culture	**3D culture**			
Conc. [µg/mL]	**1d**	**4h**	**1d**	**8d**	**14d**
Medium	3825.36	421.63	3394.45	1219.92	689.89
A	2238.58	171.79	2242.47	1131.57	923.84
AP	8470.09	1340.98	16498.57	65000.00	65000.00
SA	2646.06	146.72	5425.02	65000.00	*50543.12
LPS	29732.90	11363.59	9864.17	65000.00	65000.00
CC	3547.37	585.22	*63297.82	65000.00	34946.05
UPLVG 1500	641.99	120.97	1518.97	908.19	2108.82
UPLVG 750	1065.11	419.56	2818.37	1030.15	604.44
UPLVG 375	1442.56	667.18	2654.89	2338.82	887.13
LVM 1500	413.49	449.31	1636.41	3887.59	834.10
LVM 750	1094.91	534.19	4329.31	2929.30	937.92
LVM 375	1233.87	709.55	2828.17	2265.98	753.42
SA 1500	57.44	22.91	80.50	333.80	1582.64
SA 750	318.16	58.76	56.25	547.87	1527.74
SA 375	259.20	110.87	319.49	289.95	1289.01

Table C.1.13: Concentration (pg/mL) of IL-10 in 2D and 3D culturing measured at selected time points. * indicates values extrapolated beyond the linear range of the standard curve.

	2D culture	**3D culture**			
Conc. [µg/mL]	**1d**	**4h**	**1d**	**8d**	**14d**
Medium	0.81	1.16	1.02	0.54	*0.47
A	1.23	0.84	0.91	0.60	*0.47
AP	1.02	1.70	42.17	2.14	2.47
SA	1.23	0.95	1.95	1.09	1.16
LPS	266.80	6.69	332.86	9.61	4.37
CC	2.40	1.02	4.14	1.52	0.88
UPLVG 1500	1.16	1.02	1.09	0.57	0.74
UPLVG 750	0.88	1.16	1.02	0.60	0.60
UPLVG 375	0.95	1.27	1.23	0.84	*0.40
LVM 1500	1.45	1.30	0.98	0.81	0.54
LVM 750	0.88	1.16	1.09	0.88	0.60
LVM 375	0.95	1.02	1.52	1.02	0.54
SA 1500	0.81	1.09	0.95	1.02	1.02
SA 750	0.74	1.09	0.74	1.30	1.23
SA 375	0.88	1.23	1.23	1.23	0.67

Table C.1.14: Concentration (pg/mL) of MCP-1 in 2D and 3D culturing measured at selected time points.

	2D culture	**3D culture**			
Conc. [µg/mL]	**1d**	**4h**	**1d**	**8d**	**14d**
Medium	855.37	126.17	983.48	69.85	308.74
A	1054.24	112.39	647.58	103.68	247.69
AP	926.00	278.61	1181.42	695.40	591.52
SA	1916.24	132.71	2137.96	394.77	1196.97
LPS	781.57	183.50	779.65	266.58	832.07
CC	813.10	275.67	857.95	819.57	848.90
UPLVG 1500	775.59	170.04	1083.83	363.85	1111.47
UPLVG 750	735.34	220.35	861.38	114.22	381.12
UPLVG 375	773.23	220.78	807.17	146.96	383.35
LVM 1500	757.74	258.03	1057.37	586.82	772.60
LVM 750	592.45	233.20	877.17	411.14	361.60
LVM 375	700.93	227.24	1044.98	162.49	342.56
SA 1500	592.45	125.18	528.17	796.51	880.82
SA 750	808.43	220.44	115.64	931.30	1146.86
SA 375	1254.70	366.68	758.19	1416.01	1241.09

Table C.1.15: Concentration (pg/mL) of M-CSF in 2D and 3D culturing measured at selected time points.

	2D culture	**3D culture**			
Conc. [µg/mL]	**1d**	**4h**	**1d**	**8d**	**14d**
Medium	2.15	1.60	2.50	1.95	2.79
A	1.16	1.54	1.79	2.05	3.94
AP	1.86	1.48	20.94	22.64	8.84
SA	1.73	1.54	2.57	2.31	4.93
LPS	1.67	1.67	1.73	2.05	2.76
CC	3.61	1.48	9.52	2.44	3.87
UPLVG 1500	1.10	1.35	2.24	1.60	2.57
UPLVG 750	1.10	1.41	2.44	1.54	2.31
UPLVG 375	1.22	1.38	3.18	1.79	2.50
LVM 1500	0.91	1.35	2.05	1.54	2.63
LVM 750	1.29	1.32	2.57	1.67	2.02
LVM 375	1.16	1.29	3.61	1.51	2.18
SA 1500	1.48	1.60	2.34	2.57	3.02
SA 750	2.18	1.60	2.08	3.02	3.54
SA 375	1.29	1.51	4.07	2.11	3.35

Table C.1.16: Concentration (pg/mL) of GRO-α in 2D and 3D culturing measured at selected time points. * indicates values extrapolated beyond the linear range of the standard curve. Blue indicates values out of range below the lowest observed value and was set to 1.00.

	2D culture	**3D culture**			
Conc. [µg/mL]	**1d**	**4h**	**1d**	**8d**	**14d**
Medium	2094.89	108.48	2138.36	404.47	146.97
A	2038.42	36.02	1325.50	474.13	443.22
AP	8865.81	240.33	15136.77	17369.93	*30554.53
SA	453.12	24.48	1504.28	1838.10	4460.70
LPS	11400.11	1556.62	12601.13	17748.41	*31096.47
CC	1531.66	146.38	9692.66	7928.73	1690.54
UPLVG 1500	258.12	21.71	1073.05	103.59	624.37
UPLVG 750	945.36	80.66	3358.62	416.02	169.12
UPLVG 375	1291.88	148.72	2773.53	1245.92	433.09
LVM 1500	219.48	80.66	1099.45	1165.23	194.20
LVM 750	872.46	114.75	4024.29	2438.86	538.44
LVM 375	1085.32	196.24	3345.97	1753.43	291.03
SA 1500	1.00	1.00	1.00	1.00	33.57
SA 750	20.74	1.00	*2.66	11.23	41.25
SA 375	47.80	9.64	19.73	12.67	29.46

C.1.3 Experiment 3

Table C.1.17: Concentration (pg/mL) of TNF in 2D and 3D culturing measured at selected time points. * indicates values extrapolated beyond the linear range of the standard curve.

	2D culture					3D culture				
	4h	**1d**	**5d**	**8d**	**14d**	**4h**	**1d**	**5d**	**8d**	**14d**
Medium	6.42	8.31	4.71	1.03	1.03	*2.54	14.60	3.14	4.60	4.31
A	5.85	6.80	3.17	2.20	0.63	15.45	21.33	8.93	6.63	4.89
AP	14.86	37.49	10.94	3.36	1.03	62.46	4538.16	176.42	31.05	6.05
SA	5.66	7.55	3.75	1.81	1.03	6.05	10.07	10.07	8.35	3.43
LPS	1309.02	2578.02	142.81	24.48	2.78	62.19	4421.18	169.57	27.45	7.20
CC	6.99	32.19	3.36	1.42	1.42	3.72	57.58	7.78	3.72	*1.35

Table C.1.18: Concentration (pg/mL) of TNF in 2D and 3D culturing measured at selected time points. * indicates values extrapolated beyond the linear range of the standard curve.

	2D culture				3D culture			
Conc. [µg/mL]	**1d**	**5d**	**8d**	**14d**	**1d**	**5d**	**8d**	**14d**
Medium	8.31	10.75	16.54	12.62	14.60	3.14	4.60	4.31
UPLVG 500	7.55	7.55	13.93	15.05	4.89	*2.54	*2.54	7.20
UPLVG 100	5.28	4.90	7.37	9.06	28.56	3.14	6.05	*2.84
UPLVG 10	6.80	5.66	9.82	9.06	9.21	6.63	4.89	3.14
LVM 500	6.61	8.12	8.69	10.38	20.22	*2.54	*1.95	*1.35
LVM 100	10.94	5.09	3.36	6.04	8.64	6.05	4.89	3.72
LVM 10	5.66	5.28	10.57	8.69	11.77	3.14	5.18	3.72
SA 500	6.42	25.59	23.93	30.36	3.43	6.63	10.07	3.72
SA 100	10.94	17.83	22.82	81.66	4.31	4.89	5.47	5.47
SA 10	7.18	5.66	16.35	10.19	11.77	6.34	10.07	4.89

Table C.1.19: Concentration (pg/mL) of IL-1β in 2D and 3D culturing measured at selected time points. * indicates values extrapolated beyond the linear range of the standard curve. Blue indicates values out of range below the lowest observed value and was set to 0.01 for 2D and 0.004 for 3D.

	2D culture					3D culture				
	4h	**1d**	**5d**	**8d**	**14d**	**4h**	**1d**	**5d**	**8d**	**14d**
Medium	0.070	0.390	*0.004	*0.004	*0.040	0.010	*0.210	*0.030	*0.090	*0.060
A	*0.040	0.220	*0.040	0.001	*0.040	*0.090	*0.210	*0.030	0.010	*0.030
AP	0.340	2.360	0.070	*0.040	*0.040	0.630	119.570	3.270	0.480	*0.090
SA	*0.040	0.340	0.070	0.001	*0.004	0.010	*0.150	*0.150	*0.120	*0.010
LPS	48.900	363.000	4.910	0.340	0.020	5.310	510.170	8.710	0.630	*0.210
CC	1.790	19.600	0.190	*0.004	*0.004	0.010	21.330	0.730	*0.090	*0.030

Table C.1.20: Concentration (pg/mL) of IL-1β in 2D and 3D culturing measured at selected time points. * indicates values extrapolated beyond the linear range of the standard curve. Blue indicates values out of range below the lowest observed value and was set to 0.01 for 3D.

	2D culture				3D culture			
Conc. [µg/mL]	**1d**	**5d**	**8d**	**14d**	**1d**	**5d**	**8d**	**14d**
Medium	0.390	0.140	*0.050	0.070	*0.210	*0.030	*0.090	*0.060
UPLVG 500	0.310	0.070	0.070	0.070	*0.030	0.010	*0.150	0.010
UPLVG 100	0.240	*0.004	*0.004	*0.040	1.550	*0.030	*0.090	*0.030
UPLVG 10	0.240	0.070	*0.040	0.100	*0.150	*0.090	0*.030	0.010
LVM 500	0.240	*0.040	0.070	*0.040	0.430	*0.030	*0.150	0.010
LVM 100	0.440	0.050	*0.040	*0.050	*0.090	0.010	*0.030	0.010
LVM 10	0.340	0.070	0.070	0.070	*0.090	*0.030	*0.030	*0.030
SA 500	0.270	0.170	0.170	0.480	0.010	*0.090	*0.090	*0.030
SA 100	0.510	0.070	0.120	0.870	*0.030	*0.090	*0.090	*0.030
SA 10	0.290	0.090	0.070	*0.004	0.320	*0.060	*0.030	*0.030

Table C.1.21: Concentration (pg/mL) of IL-6 in 2D and 3D culturing measured at selected time points. * indicates values extrapolated beyond the linear range of the standard curve.

	2D culture					3D culture				
	4h	**1d**	**5d**	**8d**	**14d**	**4h**	**1d**	**5d**	**8d**	**14d**
Medium	2.16	50.29	18.07	6.94	3.40	0.47	6.81	1.26	0.92	1.14
A	1.49	36.69	14.70	7.78	4.17	2.49	4.49	2.21	1.43	1.01
AP	6.18	189.60	47.38	20.49	8.13	9.94	5062.71	1072.42	419.64	176.80
SA	1.53	25.35	5.65	2.54	1.58	1.01	2.17	1.97	1.52	1.01
LPS	1032.24	5658.39	2837.41	1324.34	496.63	17.43	*7031.92	5662.01	3153.55	1397.58
CC	2.35	164.01	40.35	15.76	6.63	0.56	252.43	44.20	12.75	4.79

Table C.1.22: Concentration (pg/mL) of IL-6 in 2D and 3D culturing measured at selected time points.

	2D culture				3D culture			
Conc. [µg/mL]	**1d**	**5d**	**8d**	**14d**	**1d**	**5d**	**8d**	**14d**
Medium	50.29	1.63	2.16	3.98	6.81	1.26	0.92	1.14
UPLVG 500	8.61	1.00	3.52	7.06	1.60	0.92	7.71	2.33
UPLVG 100	14.12	1.05	1.24	4.70	17.23	1.43	1.52	1.43
UPLVG 10	6.61	0.81	1.41	4.67	4.79	1.93	1.52	1.60
LVM 500	9.14	0.76	1.24	7.85	4.64	0.96	1.35	1.09
LVM 100	14.12	0.95	0.52	2.69	4.42	1.52	1.43	2.17
LVM 10	23.94	1.05	1.53	4.22	5.38	1.60	1.43	2.05
SA 500	9.47	1.77	10.05	274.08	1.09	0.88	1.68	1.22
SA 100	31.31	1.00	2.66	1201.12	1.43	0.83	1.01	1.09
SA 10	22.72	1.10	169.67	6.13	2.77	1.52	1.18	1.18

Table C.1.23: Concentration (pg/mL) of IL-10 in 2D and 3D culturing measured at selected time points. * indicates values extrapolated beyond the linear range of the standard curve. Blue indicates values out of range below the lowest observed value and was set to 0.01 for 2D.

	2D culture					3D culture				
	4h	**1d**	**5d**	**8d**	**14d**	**4h**	**1d**	**5d**	**8d**	**14d**
Medium	*0.10	*0.10	*0.10	0.01	0.01	0.44	0.74	1.05	1.36	1.05
A	*0.36	0.01	0.01	0.01	0.01	0.74	0.74	1.99	1.67	1.05
AP	*0.10	0.01	*0.10	0.01	0.01	1.36	6.62	4.94	5.44	2.31
SA	*0.36	*0.36	*0.10	0.01	0.01	0.44	0.74	2.96	2.96	1.99
LPS	6.52	127.95	4.10	*0.63	0.01	0.44	197.87	6.28	2.96	1.20
CC	*0.10	*1.17	0.01	0.01	0.01	0.44	0.74	1.99	1.99	1.05

Table C.1.24: Concentration (pg/mL) of IL-10 in 2D and 3D culturing measured at selected time points. * indicates values extrapolated beyond the linear range of the standard curve.

	2D culture				3D culture			
Conc. [µg/mL]	**1d**	**5d**	**8d**	**14d**	**1d**	**5d**	**8d**	**14d**
Medium	*0.10	2.27	4.80	6.23	0.74	1.05	1.36	1.05
UPLVG 500	*0.36	*1.17	3.96	7.95	0.44	1.05	1.05	0.44
UPLVG 100	*0.10	*0.90	2.83	12.31	1.05	1.67	1.67	1.05
UPLVG 10	*0.36	*0.90	2.27	14.65	0.44	1.67	1.05	0.74
LVM 500	*0.10	*1.17	2.83	16.42	0.74	0.44	1.20	0.44
LVM 100	*0.63	*0.36	*0.63	8.82	0.74	1.36	1.05	0.74
LVM 10	*0.10	*0.90	3.39	13.19	0.74	1.05	1.36	1.36
SA 500	*0.36	5.66	2.83	4.52	0.74	2.79	2.96	1.36
SA 100	*0.36	2.00	4.80	7.23	1.05	2.31	2.31	1.05
SA 10	*0.36	*0.90	4.24	11.72	1.36	1.99	1.67	1.67

Table C.1.25: Concentration (pg/mL) of MCP-1 in 2D and 3D culturing measured at selected time points.

	2D culture					3D culture				
	4h	**1d**	**5d**	**8d**	**14d**	**4h**	**1d**	**5d**	**8d**	**14d**
Medium	67.86	702.30	589.80	341.70	161.70	28.77	897.89	462.01	831.83	671.31
A	58.22	662.34	493.89	396.84	248.16	188.04	1088.20	918.13	1165.04	1136.69
AP	58.37	724.82	1104.36	793.22	449.09	238.85	972.50	1178.74	1185.92	1106.75
SA	49.98	318.72	394.78	312.78	218.01	162.91	2014.92	1774.43	2132.04	1665.12
LPS	36.07	620.79	746.96	1064.53	525.87	30.28	996.40	1454.16	1353.25	1228.31
CC	50.06	449.15	184.48	122.34	78.61	31.36	1011.15	1614.73	1780.09	1192.87

Table C.1.26: Concentration (pg/mL) of MCP-1 in 2D and 3D culturing measured at selected time points. * indicates values extrapolated beyond the linear range of the standard curve.

	2D culture				3D culture			
Conc. [µg/mL]	**1d**	**5d**	**8d**	**14d**	**1d**	**5d**	**8d**	**14d**
Medium	702.3	1139.68	2222.96	2333.64	897.89	462.01	831.83	671.31
UPLVG 500	592.67	1258.79	2060.93	1958.13	112.87	397.84	935.11	1244.63
UPLVG 100	657.14	943.72	2391.57	2260.65	1031.63	338.64	761.13	977.27
UPLVG 10	739.29	867.12	2034.99	*2783.60	388.60	622.44	823.04	823.72
LVM 500	661.31	1067.85	2007.65	*2591.60	462.37	323.74	909.37	1542.53
LVM 100	693.04	1037.92	1196.66	*2622.56	464.22	443.17	697.82	1039.9
LVM 10	712.03	903.28	*2802.96	*3145.3	614.71	289.42	589.11	981.45
SA 500	660.69	838.67	966.64	1039.06	724.29	1174.25	1106.51	920.77
SA 100	1057.67	1415.89	1417.65	1699.31	1430.77	1702.24	1679.32	1228.79
SA 10	960.81	1100.64	2226.89	2436.38	1808.07	2076.92	2059.67	1571.04

Table C.1.27: Concentration (pg/mL) of M-CSF in 2D and 3D culturing measured at selected time points.

	2D culture					**3D culture**				
	4h	**1d**	**5d**	**8d**	**14d**	**4h**	**1d**	**5d**	**8d**	**14d**
Medium	6.39	7.61	10.75	12.44	18.04	4.74	5.86	6.76	9.06	15.96
A	5.63	5.93	8.68	12.13	17.12	5.05	7.67	10.65	15.76	24.87
AP	5.02	6.47	16.43	14.13	14.74	5.25	68.05	123.17	66.10	29.37
SA	6.08	6.54	13.13	11.29	12.67	4.23	6.76	11.64	11.84	21.98
LPS	4.94	6.39	8.23	14.66	16.97	4.44	6.87	5.25	7.07	12.63
CC	4.71	6.85	9.14	10.22	14.51	4.54	14.3	11.05	9.06	9.36

Table C.1.28: Concentration (pg/mL) of M-CSF in 2D and 3D culturing measured at selected time points.

	2D culture				**3D culture**			
Conc. [µg/mL]	**1d**	**5d**	**8d**	**14d**	**1d**	**5d**	**8d**	**14d**
Medium	7.61	11.37	92.78	41.02	5.86	6.76	9.06	15.96
UPLVG 500	6.16	8.68	43.03	86.59	5.15	5.25	8.27	14.39
UPLVG 100	6.39	4.25	37.00	63.04	6.06	5.66	8.87	14.49
UPLVG 10	6.24	4.71	29.74	94.11	5.05	6.26	10.26	14.69
LVM 500	6.39	5.93	39.47	80.65	5.66	4.84	9.66	15.18
LVM 100	5.93	5.32	11.75	37.62	5.86	5.86	11.25	16.45
LVM 10	6.08	4.86	42.88	100.85	5.05	5.45	9.66	14.59
SA 500	6.54	68.80	138.23	128.89	5.96	12.82	18.78	18.49
SA 100	6.93	40.25	83.39	149.34	6.06	8.87	11.34	18.10
SA 10	6.39	4.56	9.45	154.90	5.66	7.87	8.77	22.17

Table C.1.29: Concentration (pg/mL) of GRO-α in 2D and 3D culturing measured at selected time points. Red indicates values out of range above the highest observed value and was set to 7000.00 for 3D.

	2D culture					3D culture				
	4h	**1d**	**5d**	**8d**	**14d**	**4h**	**1d**	**5d**	**8d**	**14d**
Medium	73.32	1600.19	522.82	158.59	47.30	52.67	453.97	112.02	83.65	64.73
A	69.98	560.43	250.84	122.70	52.94	60.99	619.66	253.76	145.75	77.88
AP	98.70	1473.36	588.87	265.10	93.62	166.81	7000.00	7000.00	2477.72	2137.13
SA	30.59	76.53	75.27	65.75	47.30	36.64	195.48	116.05	132.64	160.58
LPS	428.79	3811.24	3628.71	1628.68	430.37	47.95	7000.00	7000.00	2800.29	2318.82
CC	82.60	520.09	138.68	62.78	30.59	36.64	2682.05	1721.28	863.89	314.26

Table C.1.30: Concentration (pg/mL) of GRO-α in 2D and 3D culturing measured at selected time points. Blue indicates values out of range below the lowest observed value and was set to 1 for 3D.

	2D culture				3D culture			
Conc. [µg/mL]	**1d**	**5d**	**8d**	**14d**	**1d**	**5d**	**8d**	**14d**
Medium	1600.19	431.42	353.20	692.54	453.97	112.02	83.65	64.73
UPLVG 500	543.63	278.51	647.33	993.80	60.99	60.99	213.60	130.90
UPLVG 100	568.49	363.75	315.04	397.36	863.89	69.96	90.33	71.62
UPLVG 10	909.10	216.32	556.21	454.32	219.80	139.35	105.67	71.62
LVM 500	1028.50	234.93	222.68	502.92	452.53	42.68	68.27	94.10
LVM 100	801.35	337.25	193.76	331.08	210.42	94.10	82.24	118.01
LVM 10	1157.92	261.70	601.72	501.87	253.76	74.81	52.67	89.03
SA 500	145.02	147.08	251.05	1190.72	1.00	64.73	105.67	79.36
SA 100	370.05	77.16	228.66	3294.78	59.02	77.88	100.06	153.35
SA 10	550.65	305.00	3663.07	418.93	150.36	109.95	100.6	107.83

Table C.1.31: Concentration (pg/mL) of IL-1ra in 2D and 3D culturing measured at selected time points. Blue indicates values out of range below the lowest observed value and was set to 1.00.

	2D culture					3D culture				
	4h	**1d**	**5d**	**8d**	**14d**	**4h**	**1d**	**5d**	**8d**	**14d**
Medium	219.01	305.79	140.07	16.16	1.00	26.79	3090.69	3418.20	2557.74	358.88
A	202.74	169.94	189.08	93.88	1.00	153.20	3227.06	6743.43	4616.17	1866.69
AP	251.90	399.67	1407.15	111.65	16.16	276.52	4320.39	15356.74	14077.43	4731.00
SA	208.91	238.60	779.51	64.00	24.03	116.30	1545.75	7481.06	6642.45	2158.57
LPS	418.02	585.96	364.71	605.53	1.00	26.79	2586.52	171.18	109.73	571.21
CC	228.41	268.56	50.83	*1.55	1.00	32.62	3674.45	6993.04	5492.92	651.51

Table C.1.32: Concentration (pg/mL) of IL-1ra in 2D and 3D culturing measured at selected time points.

	2D culture				3D culture			
Conc. [µg/mL]	**1d**	**5d**	**8d**	**14d**	**1d**	**5d**	**8d**	**14d**
Medium	305.79	7601.92	11362.54	11093.36	3090.69	3418.20	2557.74	358.88
UPLVG 500	480.28	6013.82	7813.58	13313.71	1389.30	927.86	911.06	32.62
UPLVG 100	466.57	3671.16	6788.84	10527.08	3200.74	2223.08	2881.36	448.38
UPLVG 10	413.08	3740.46	7006.36	11398.63	3186.92	4928.71	2119.71	299.77
LVM 500	600.58	4676.34	6924.17	11296.18	2242.28	1018.84	1422.97	77.13
LVM 100	432.70	3798.38	4207.84	8585.08	2753.92	3653.04	2595.69	773.60
LVM 10	309.23	4092.55	9978.56	11291.72	3449.72	2325.07	1940.08	1097.78
SA 500	362.30	12454.67	12562.16	10739.09	458.16	6957.40	5441.08	1172.18
SA 100	655.31	11214.44	11313.17	12292.93	893.45	7027.76	4544.87	2914.96
SA 10	457.09	3393.58	4762.47	12022.27	1753.20	6000.83	3995.50	3497.73

C.1.4 Experiment 4

Table C.1.33: Concentration (pg/mL) of TNF in 2D and 3D culturing measured at selected time points. * indicates values extrapolated beyond the linear range of the standard curve.

	2D culture					3D culture				
	4h	**1d**	**5d**	**8d**	**14d**	**4h**	**1d**	**5d**	**8d**	**14d**
Medium	18.17	48.35	6.76	4.03	2.54	0.71	18.88	3.27	1.88	3.00
A	11.84	39.38	8.40	6.47	4.52	8.83	33.12	6.23	4.36	4.90
AP	48.71	2167.76	195.65	51.72	12.03	325.53	10206.21	611.98	73.78	16.65
SA	10.60	14.88	19.76	12.79	5.89	6.49	13.66	11.26	6.49	4.09
LPS	4076.95	7078.31	522.23	111.75	22.75	3553.27	4509.50	341.46	46.51	16.16
CC	17.51	957.35	67.25	15.82	3.93	*0.08	1676.05	72.20	17.03	4.36

Table C.1.34: Concentration (pg/mL) of TNF in 2D and 3D culturing measured at selected time points. * indicates values extrapolated beyond the linear range of the standard curve.

	2D culture				3D culture			
Conc. [µg/mL]	**1d**	**5d**	**8d**	**14d**	**1d**	**5d**	**8d**	**14d**
Medium	48.35	10.89	19.01	13.74	18.88	3.27	1.88	3.00
UPLVG 500	16.67	7.05	61.81	173.42	3.14	3.82	3.27	2.16
UPLVG 100	26.01	6.66	8.98	7.05	29.30	27.86	2.44	1.45
UPLVG 10	35.71	5.11	19.39	6.08	31.09	3.00	1.59	1.16
LVM 500	22.19	6.28	13.74	10.03	19.37	3.00	4.23	2.16
LVM 100	24.80	6.28	7.34	7.44	24.85	2.72	1.74	1.31
LVM 10	23.59	5.89	10.41	5.01	19.37	3.27	2.16	1.01
SA 500	22.19	60.09	48.16	18.36	21.33	6.23	5.70	3.00
SA 100	19.29	15.06	39.75	17.51	27.86	4.09	6.23	2.44
SA 10	15.06	5.50	5.69	9.55	20.35	4.09	4.09	2.16

Table C.1.35: Concentration (pg/mL) of IL-1β in 2D and 3D culturing measured at selected time points. * indicates values extrapolated beyond the linear range of the standard curve. Blue indicates values out of range below the lowest observed value and was set to 0.01 for 3D.

	2D culture					3D culture				
	4h	**1d**	**5d**	**8d**	**14d**	**4h**	**1d**	**5d**	**8d**	**14d**
Medium	0.39	1.56	0.11	0.17	0.09	0.01	0.52	0.01	0.01	0.01
A	0.23	2.28	0.42	0.26	0.11	0.01	1.82	*0.16	0.01	0.01
AP	0.61	60.16	3.90	0.99	0.23	0.51	494.46	18.04	1.94	0.27
SA	*0.06	0.28	0.42	*0.20	*0.06	0.01	0.20	*0.23	0.11	0.01
LPS	241.34	1510.20	50.97	4.43	0.37	375.59	1796.45	69.88	6.98	0.31
CC	19.31	618.86	19.67	2.00	0.14	0.01	536.51	34.66	4.85	*0.11

Table C.1.36: Concentration (pg/mL) of IL-1β in 2D and 3D culturing measured at selected time points. * indicates values extrapolated beyond the linear range of the standard curve. Blue indicates values out of range below the lowest observed value and was set to 0.01.

	2D culture				3D culture			
Conc. [µg/mL]	**1d**	**5d**	**8d**	**14d**	**1d**	**5d**	**8d**	**14d**
Medium	1.56	0.26	0.30	0.21	0.52	0.01	0.01	0.01
UPLVG 500	0.60	0.23	0.14	0.17	0.01	*0.07	0.01	0.01
UPLVG 100	0.96	0.23	0.11	0.09	0.79	2.01	0.01	0.01
UPLVG 10	1.28	0.20	0.11	0.16	0.54	0.01	0.01	0.01
LVM 500	0.56	0.41	0.37	0.11	1.34	0.01	0.01	0.01
LVM 100	1.07	0.21	0.23	*0.06	0.59	0.01	0.01	0.01
LVM 10	1.23	0.26	0.11	0.11	0.29	0.01	0.01	0.01
SA 500	0.45	0.80	0.80	0.31	0.31	0.01	*0.16	0.01
SA 100	0.59	0.26	0.75	0.20	0.89	0.01	0.01	0.01
SA 10	0.80	0.20	0.14	*0.06	0.46	0.11	0.01	0.01

Table C.1.37: Concentration (pg/mL) of IL-6 in 2D and 3D culturing measured at selected time points. * indicates values extrapolated beyond the linear range of the standard curve. Blue indicates values out of range below the lowest observed value and was set to 0.01 for 3D.

	2D culture					3D culture				
	4h	**1d**	**5d**	**8d**	**14d**	**4h**	**1d**	**5d**	**8d**	**14d**
Medium	13.62	204.22	24.93	10.33	4.94	*0.08	28.29	3.66	1.82	3.34
A	8.15	186.35	19.91	7.34	4.26	2.49	60.41	6.67	2.56	2.29
AP	24.5	6215.97	3311.21	1176.96	378.10	82.03	*7045.64	6691.98	2006.14	785.67
SA	4.94	10.19	4.33	2.44	1.19	1.26	14.25	4.35	2.42	1.40
LPS	6052.34	6284.07	6529.77	6254.48	5968.32	*7189.80	*7164.94	*7370.75	*7881.79	*6834.61
CC	11.35	5748.83	1840.41	759.08	336.50	0.01	*7530.27	5713.78	2126.00	704.52

Table C.1.38: Concentration (pg/mL) of IL-6 in 2D and 3D culturing measured at selected time points.

	2D culture				3D culture			
Conc. [µg/mL]	**1d**	**5d**	**8d**	**14d**	**1d**	**5d**	**8d**	**14d**
Medium	204.22	5.06	3.51	3.81	28.29	3.66	1.82	3.34
UPLVG 500	15.39	3.3	4.89	14.2	5.92	23.59	15.84	3.34
UPLVG 100	40.42	6.81	8.29	3.58	48.03	4039.51	6.16	4.29
UPLVG 10	86.83	3.34	2.49	3.15	36.88	11.68	21.6	5.77
LVM 500	24.64	3.2	8.43	6.01	50.22	8.68	14.73	22.06
LVM 100	36.29	4.85	2.44	2.68	42.87	17.28	5.16	3.72
LVM 10	40.9	5.13	3.39	2.25	3039	12.02	6.31	5.16
SA 500	7.46	13.35	8.99	4.89	15.79	5.22	3.27	3.15
SA 100	12.77	5.03	7.71	4.96	50.35	7.62	7.45	4.35
SA 10	14.97	3.63	2.37	2.42	26.62	10.25	6.19	5.22

Table C.1.39: Concentration (pg/mL) of IL-10 in 2D and 3D culturing measured at selected time points. * indicates values extrapolated beyond the linear range of the standard curve.

	2D culture					3D culture				
	4h	**1d**	**5d**	**8d**	**14d**	**4h**	**1d**	**5d**	**8d**	**14d**
Medium	*1.17	*1.17	2.34	2.14	1.45	*0.11	0.85	1.84	1.10	0.85
A	*0.98	1.55	2.54	3.76	3.76	0.60	0.85	2.96	1.84	1.35
AP	1.36	3.66	6.92	9.42	8.00	1.59	18.39	4.82	6.06	4.45
SA	*1.17	*1.17	11.97	6.71	4.17	0.73	0.85	6.81	4.32	2.34
LPS	3.35	523.25	19.51	9.09	7.13	2.83	290.59	10.82	3.08	2.83
CC	*1.17	14.91	1.36	1.75	1.55	0.11	19.15	1.84	1.59	0.85

Table C.1.40: Concentration (pg/mL) of IL-10 in 2D and 3D culturing measured at selected time points. * indicates values extrapolated beyond the linear range of the standard curve.

	2D culture				3D culture			
Conc. [µg/mL]	**1d**	**5d**	**8d**	**14d**	**1d**	**5d**	**8d**	**14d**
Medium	1.17	2.74	9.09	9.97	0.85	1.84	1.10	0.85
UPLVG 500	1.94	1.94	2.34	10.41	0.36	1.35	1.10	0.85
UPLVG 100	1.55	1.75	2.74	7.57	1.10	1.59	1.35	0.85
UPLVG 10	1.55	*1.17	3.96	5.22	0.85	1.10	0.85	0.36
LVM 500	1.94	1.75	5.75	10.41	1.35	1.10	1.10	1.35
LVM 100	1.75	1.94	3.45	7.24	1.35	0.60	1.22	0.85
LVM 10	1.55	1.36	3.14	4.59	0.73	1.10	0.60	0.60
SA 500	1.75	15.82	22.20	5.64	0.85	4.07	3.82	1.10
SA 100	1.65	3.96	21.03	6.71	1.35	1.35	2.58	0.85
SA 10	1.75	1.55	2.14	6.49	1.59	1.59	1.35	1.10

Table C.1.41: Concentration (pg/mL) of MCP-1 in 2D and 3D culturing measured at selected time points. * indicates values extrapolated beyond the linear range of the standard curve.

	2D culture					3D culture				
	4h	**1d**	**5d**	**8d**	**14d**	**4h**	**1d**	**5d**	**8d**	**14d**
Medium	333.19	739.06	958.08	1183.24	1625.76	23.10	1042.01	748.41	467.86	405.36
A	345.69	987.58	1868.70	2102.95	2515.93	181.05	1438.64	1227.70	1005.52	1025.11
AP	366.87	782.36	1358.21	2246.38	*2626.32	209.56	849.72	991.48	973.30	849.83
SA	232.35	2029.37	2276.35	*2569.12	2380.78	195.34	*2971.80	1992.81	*2669.70	2140.25
LPS	146.13	657.08	878.74	1047.83	2142.46	154.54	877.02	1528.31	1768.33	945.69
CC	300.08	559.25	821.96	1103.71	991.87	19.10	838.07	982.46	1155.93	971.54

Table C.1.42: Concentration (pg/mL) of MCP-1 in 2D and 3D culturing measured at selected time points. * indicates values extrapolated beyond the linear range of the standard curve.

	2D culture				3D culture			
Conc. [µg/mL]	**1d**	**5d**	**8d**	**14d**	**1d**	**5d**	**8d**	**14d**
Medium	739.06	1802.73	2484.16	2366.10	1042.01	748.41	467.86	405.36
UPLVG 500	904.03	1999.29	2473.84	*2535.46	260.85	433.26	1393.51	1023.23
UPLVG 100	802.12	1577.99	*2742.98	*2558.47	1067.14	1801.87	894.66	882.76
UPLVG 10	797.19	2073.31	2493.71	*2558.04	1105.70	1344.02	755.23	949.63
LVM 500	750.89	2138.49	1996.90	2128.95	1119.33	721.86	1162.18	998.09
LVM 100	845.11	2359.97	*2772.68	*2718.06	1297.61	683.32	409.31	608.77
LVM 10	797.38	1878.91	2432.03	2247.45	1110.87	1256.48	289.61	1052.26
SA 500	698.24	986.74	1109.14	1253.80	828.40	1145.83	981.60	737.77
SA 100	1321.65	1638.20	1935.18	1792.72	1432.68	2016.45	1412.80	1025.63
SA 10	2272.18	2122.08	1958.34	*2558.47	2058.13	*2660.64	976.34	1875.68

Table C.1.43: Concentration (pg/mL) of M-CSF in 2D and 3D culturing measured at selected time points.

	2D culture					3D culture				
	4h	**1d**	**5d**	**8d**	**14d**	**4h**	**1d**	**5d**	**8d**	**14d**
Medium	4.20	5.76	9.94	57.12	140.40	3.36	4.76	3.67	4.91	5.82
A	4.02	5.40	17.07	84.45	168.96	4.06	5.37	5.22	7.02	11.83
AP	4.32	39.39	50.61	99.65	135.21	4.29	63.35	27.07	14.96	16.08
SA	4.14	5.04	47.89	109.27	148.79	4.14	4.91	9.81	7.76	11.55
LPS	3.96	5.88	4.68	16.95	101.51	3.67	5.59	4.60	5.37	11.69
CC	3.84	13.51	30.18	49.31	97.31	2.40	19.69	7.76	10.54	7.91

Table C.1.44: Concentration (pg/mL) of M-CSF in 2D and 3D culturing measured at selected time points.

	2D culture				3D culture			
Conc. [µg/mL]	**1d**	**5d**	**8d**	**14d**	**1d**	**5d**	**8d**	**14d**
Medium	5.76	5.70	31.48	45.41	4.76	3.67	4.91	5.82
UPLVG 500	4.92	4.80	16.35	81.82	4.76	3.67	4.76	6.42
UPLVG 100	4.68	3.96	6.00	23.98	4.45	3.98	5.06	6.8
UPLVG 10	6.12	2.75	13.03	24.04	4.76	3.20	3.83	6.12
LVM 500	5.28	4.68	14.28	39.98	4.6	3.20	4.91	6.42
LVM 100	4.92	3.96	8.16	24.28	4.14	3.52	3.98	6.27
LVM 10	5.40	3.42	8.16	21.38	4.45	3.04	4.60	5.22
SA 500	9.35	70.34	98.21	121.41	5.37	7.76	6.27	8.65
SA 100	5.76	13.63	49.67	142.66	5.37	4.45	5.52	8.35
SA 10	5.28	3.36	5.52	43.76	4.91	4.29	4.91	7.62

Table C.1.45: Concentration (pg/mL) of GRO-α in 2D and 3D culturing measured at selected time points. Blue indicates values out of range below the lowest observed value and was set to 1.00 for 3D.

	2D culture					3D culture				
	4h	**1d**	**5d**	**8d**	**14d**	**4h**	**1d**	**5d**	**8d**	**14d**
Medium	363.21	8727.16	3641.10	1905.52	911.18	1	5790.37	1595.25	879.36	499.22
A	268.91	6722.53	3592.87	2388.46	1618.63	168.64	4311.38	3029.75	2076.90	1277.74
AP	417.32	12790.80	4747.32	3870.15	3585.04	369.33	10296.96	3932.53	3517.82	4636.70
SA	36.76	366.12	504.67	445.54	291.20	132.68	1266.89	567.67	555.05	819.39
LPS	1911.33	9296.82	5330.26	4726.96	5291.41	2516.46	13781.27	5676.08	4787.36	5260.63
CC	229.27	7647.97	3850.00	2720.07	1389.01	1.00	12604.07	4044.33	4305.33	3576.87

Table C.1.46: Concentration (pg/mL) of GRO-α in 2D and 3D culturing measured at selected time points.

	2D culture				3D culture			
Conc. [µg/mL]	**1d**	**5d**	**8d**	**14d**	**1d**	**5d**	**8d**	**14d**
Medium	8727.16	3590.84	2294.83	3003.17	5790.37	1595.25	879.36	499.22
UPLVG 500	4953.32	3252.59	3409.34	3115.55	1275.03	2541.51	3303.53	1315.65
UPLVG 100	8603.51	4878.81	4053.63	2611.57	9000.10	5619.46	2329.17	1935.23
UPLVG 10	9176.05	3006.83	3230.43	2524.62	6037.59	2937.40	3361.06	2731.54
LVM 500	7013.63	3235.04	3221.97	2347.95	7300.71	2223.46	3111.66	2870.97
LVM 100	6516.83	3302.20	3090.10	2097.99	5369.10	2890.79	1931.46	1491.31
LVM 10	8100.52	3643.19	3608.63	2213.51	3956.00	3048.05	1562.63	2282.53
SA 500	369.45	918.27	944.91	1136.98	785.34	732.52	736.03	721.24
SA 100	1346.91	989.67	1766.10	2334.66	2049.94	1275.18	1391.96	1910.61
SA 10	3618.91	2706.34	2848.99	2114.93	2480.99	2565.42	1745.68	2415.31

Table C.1.47: Concentration (pg/mL) of IL-1ra in 2D and 3D culturing measured at selected time points. Blue indicates values out of range below the lowest observed value and was set to 2.00 for 3D.

	2D culture					3D culture				
	4h	**1d**	**5d**	**8d**	**14d**	**4h**	**1d**	**5d**	**8d**	**14d**
Medium	470.08	2844.65	6314.39	5752.21	3114.98	2.00	6113.42	5072.77	2113.86	735.77
A	439.48	3597.02	6834.14	7097.51	8187.40	153.11	4260.18	8960.60	6153.34	3751.80
AP	668.99	4860.01	12063.24	13708.59	13059.91	535.58	7708.30	15041.50	13942.65	16236.54
SA	296.20	4248.03	11988.97	11347.59	9952.14	118.43	2310.01	13247.10	7494.01	6059.79
LPS	869.76	3492.02	1515.73	5893.06	9653.82	668.70	4063.86	497.27	205.94	2484.35
CC	1044.75	2988.19	5807.71	5654.76	3653.28	2.00	6248.65	7681.01	7105.69	2989.95

Table C.1.48: Concentration (pg/mL) of IL-1ra in 2D and 3D culturing measured at selected time points.

	2D culture				3D culture			
Conc. [µg/mL]	**1d**	**5d**	**8d**	**14d**	**1d**	**5d**	**8d**	**14d**
Medium	2844.65	7450.60	13557.32	17840.21	6113.42	5072.77	2113.86	735.77
UPLVG 500	3689.42	5554.76	7837.98	17562.44	2699.36	1876.62	867.46	641.15
UPLVG 100	3722.32	4921.83	6516.28	16587.00	5376.92	1610.18	2192.58	1439.23
UPLVG 10	4183.30	3772.24	10091.87	11557.94	5562.59	3343.29	435.00	762.31
LVM 500	3960.17	5531.64	10077.48	16758.90	4952.77	2681.57	1305.67	646.01
LVM 100	3816.99	5265.19	7948.65	15256.27	5460.07	3030.87	2285.87	1571.49
LVM 10	3741.85	5315.22	7416.05	9169.17	5557.15	2222.98	1686.40	839.05
SA 500	4875.42	19318.82	21564.62	21708.11	2089.08	10432.80	5451.01	2426.37
SA 100	3854.45	11852.55	13776.48	20464.71	4476.20	5903.09	6981.96	1734.02
SA 10	3954.65	3351.45	4399.70	15921.50	5008.27	5250.18	3758.40	1942.46

C.2 Trained immunity

Cytokine levels in supernatant were measured after monocytes were trained for 24 hours by indicated stimuli, 5 days of rest, and restimulated with RPMI or LPS for 24 hours. The induced levels are shown in Tables C.2.1 to C.2.5

Table C.2.1: Concentration (pg/mL) of TNF in experiment 1, 2 and 3. -LPS indicates restimulation with RPMI. +LPS indicates restimulation with LPS. * indicates values extrapolated beyond the linear range of the standard curve. Red indicates values out of range above the highest observed value and was set to 500000.00 for experiment 2.

	Experiment 1		**Experiment 2**		**Experiment 3**	
Conc.[µg/mL]	**-LPS**	**+LPS**	**-LPS**	**+LPS**	**-LPS**	**+LPS**
Medium	31.76	18454.35	37.32	*49464.13	14.99	15328.86
UPLVG 500	26.97	13981.45	37.32	46393.15	9.51	2285.15
UPLVG 100	30.12	14952.15	33.52	39970.49	9.95	10968.79
UPLVG 10	54.31	19741.63	40.48	38308.13	9.37	4910.29
LVM 500	28.35	15836.25	35.80	*62548.24	5.28	11964.42
LVM 100	25.71	19656.73	38.58	*55564.03	11.72	12639.54
LVM 10	25.46	19720.33	36.05	45087.83	9.81	14157.31
SA 500	96.49	3452.80	69.86	5302.79	20.36	16396.95
SA 100	90.46	6139.61	63.22	5968.20	18.27	14060.35
SA 10	37.82	16844.28	62.08	11890.34	14.54	4888.20
HM 500	26.09	33424.22	27.47	*58361.57	8.48	571.34
HM 100	24.45	26385.78	28.48	*308979.50	7.61	745.49
HM 10	21.44	24171.48	31.51	500000.00	3.55	1669.74
β-glucan 20					74.05	12913.77
β-glucan 10	67.05	37293.38	63.73	*65549.29	32.43	14551.41
CC 1000	12.44	6175.41	15.56	11574.41	0.44	1097.28
CC 500	16.43	9265.96	16.43	118463.62	4.41	5941.98
LPS 10 ng/mL					5.57	108.84
LPS 1 ng/mL					5.28	477.59

Table C.2.2: Concentration (pg/mL) of IL-1β in experiment 1, 2 and 3. -LPS indicates restimulation with RPMI. +LPS indicates restimulation with LPS. * indicates values extrapolated beyond the linear range of the standard curve. Blue indicates values out of range below the lowest observed value and was set to 0.005 for experiment 1 and 2, and 0.01 for experiment 3.

	Experiment 1		**Experiment 2**		**Experiment 3**	
Conc.[µg/mL]	**-LPS**	**+LPS**	**-LPS**	**+LPS**	**-LPS**	**+LPS**
Medium	0.005	3.93	*0.01	8.73	*0.02	0.61
UPLVG 500	0.005	1.15	0.02	12.45	*0.03	0.57
UPLVG 100	0.005	1.72	0.02	8.73	*0.04	0.42
UPLVG 10	0.04	3.05	0.04	11.97	*0.02	0.39
LVM 500	0.03	2.85	0.02	10.11	0.09	0.83
LVM 100	0.005	3.16	0.005	10.8	0.28	0.37
LVM 10	*0.01	1.85	0.02	8.49	*0.05	1.69
SA 500	3.01	3.25	2.6	6.17	0.01	1.84
SA 100	1.58	1.39	2.88	5.14	*0.02	0.37
SA 10	0.08	1.07	0.94	5.05	*0.04	0.21
HM 500	0.005	3.81	0.04	8.29	1.58	2.11
HM 100	0.005	4.27	0.02	11.28	0.98	1.25
HM 10	0.005	2.74	0.02	8.91	0.25	0.85
β-glucan 20					0.33	1.45
β-glucan 10	0.02	4.23	0.02	8.64	0.21	1.16
CC 1000	0.005	0.84	0.005	2.19	*0.02	*0.05
CC 500	0.005	1.73	0.005	3.32	*0.04	1.02
LPS 10 ng/mL					0.96	0.75
LPS 1 ng/mL					0.65	0.64

Table C.2.3: Concentration (pg/mL) of IL-6 in experiment 1, 2 and 3. -LPS indicates restimulation with RPMI. +LPS indicates restimulation with LPS. * indicates values extrapolated beyond the linear range of the standard curve. Blue indicates values out of range below the lowest observed value and was set to 0.005 for experiment 1 and 2, and 0.001 for experiment 3.

	Experiment 1		**Experiment 2**		**Experiment 3**	
Conc.[µg/mL]	**-LPS**	**+LPS**	**-LPS**	**+LPS**	**-LPS**	**+LPS**
Medium	*0.08	2368.45	0.005	1471.20	*0.08	1252.35
UPLVG 500	*0.03	2477.99	0.005	1410.29	*0.06	306.46
UPLVG 100	0.005	2618.78	0.005	1356.28	0.98	1188.39
UPLVG 10	0.56	2839.51	0.005	1392.89	*0.04	648.12
LVM 500	*0.01	2300.68	0.005	1456.10	10.96	1226.66
LVM 100	*0.01	2120.99	0.005	1456.55	69.78	1135.21
LVM 10	*0.01	2598.29	0.005	1297.35	*0.06	1391.2
SA 500	593.97	4128.23	601.88	1772.77	*0.02	2448.03
SA 100	93.19	967.71	272.87	851.08	*0.03	1484.74
SA 10	0.52	1376.55	22.77	1072.52	2.58	474.20
HM 500	0.005	4040.35	0.005	2078.42	383.97	677.63
HM 100	0.005	2847.68	0.005	1845.67	208.71	532.67
HM 10	*0.04	2903.16	0.005	1643.31	37.26	329.04
β-glucan 20					19.56	2007.69
β-glucan 10	0.63	3141.55	*0.04	3000.38	14.08	1297.07
CC 1000	0.12	987.87	0.005	1249.27	0.001	358.20
CC 500	0.005	1887.31	0.71	1741.24	*0.08	1237.74
LPS 10 ng/mL					235.11	219.84
LPS 1 ng/mL					174.76	243.30

Table C.2.4: Concentration (pg/mL) of IL-10 in experiment 1, 2 and 3. -LPS indicates restimulation with RPMI. +LPS indicates restimulation with LPS. * indicates values extrapolated beyond the linear range of the standard curve.

	Experiment 1		**Experiment 2**		**Experiment 3**	
Conc.[µg/mL]	**-LPS**	**+LPS**	**-LPS**	**+LPS**	**-LPS**	**+LPS**
Medium	2.06	408.92	2.20	572.31	2.66	183.75
UPLVG 500	2.06	430.95	2.60	592.55	2.07	149.51
UPLVG 100	3.02	375.08	2.74	565.00	1.99	179.20
UPLVG 10	2.88	406.80	2.88	589.72	2.24	128.42
LVM 500	2.00	447.15	2.47	616.02	1.49	242.04
LVM 100	2.0	393.58	2.74	611.33	1.99	219.02
LVM 10	2.33	424.48	2.74	590.60	2.32	184.44
SA 500	3.37	212.65	3.23	412.86	2.66	494.61
SA 100	3.65	420.80	3.86	439.64	2.15	447.87
SA 10	2.74	411.34	4.72	564.13	1.57	120.32
HM 500	1.53	337.65	2.54	541.97	0.54	56.84
HM 100	1.93	336.10	2.20	510.21	0.85	56.03
HM 10	1.60	345.74	2.26	502.44	1.00	109.78
β-glucan 20					3.71	277.63
β-glucan 10	0.90	321.81	3.02	499.65	3.18	236.35
CC 1000	0.53	12.65	0.47	75.08	0.47	1.41
CC 500	*0.24	56.42	0.77	208.23	1.00	13.18
LPS 10 ng/mL					1.16	49.41
LPS 1 ng/mL					0.85	66.15

Table C.2.5: Concentration (pg/mL) of MCP-1 in experiment 1, 2 and 3. -LPS indicates restimulation with RPMI. +LPS indicates restimulation with LPS. * indicates values extrapolated beyond the linear range of the standard curve.

	Experiment 1		**Experiment 2**		**Experiment 3**	
Conc.[µg/mL]	**-LPS**	**+LPS**	**-LPS**	**+LPS**	**-LPS**	**+LPS**
Medium	2284.35	3507.74	883.41	4059.59	191.03	1301.46
UPLVG 500	2514.81	3546.93	941.00	4141.83	235.04	1187.91
UPLVG 100	2881.69	2899.89	1058.78	3614.06	191.93	1089.31
UPLVG 10	2682.15	2921.77	1090.48	3498.61	176.84	947.61
LVM 500	2446.98	2659.08	1187.27	3821.55	372.38	1329.94
LVM 100	2982.78	3320.79	1035.33	3930.52	223.63	1177.90
LVM 10	2880.94	3089.98	1359.22	3499.14	249.34	1143.99
SA 500	2158.06	2479.05	3850.82	4272.83	1914.67	4204.25
SA 100	2995.66	3324.20	3444.18	4021.71	1145.94	4201.75
SA 10	4019.63	4085.23	3049.86	3870.14	259.01	1795.04
HM 500	2290.41	4204.47	642.44	3141.15	112.51	1015.49
HM 100	2786.90	2986.79	464.00	2768.19	48.43	1207.75
HM 10	2929.51	3236.12	785.20	3024.18	50.85	907.01
β-glucan 20					2452.50	2521.48
β-glucan 10	2131.77	3231.48	2765.38	3535.41	929.66	2447.43
CC 1000	2377.09	2377.09	2921.77	2932.23	125.77	249.74
CC 500	2033.39	2033.39	5016.09	*6811.97	515.97	1292.17
LPS 10 ng/mL					294.29	0.29
LPS 1 ng/mL					86.47	0.56

Fredrikke Kjærnsmo

Explorations of *in vitro* models for new understanding of the host-material response

NTNU
Norwegian University of
Science and Technology